EFFECT OF VARIABLE ENVIRONMENTAL CONDITIONS ON FATE AND TRANSPORT OF EXPLOSIVE-RELATED CHEMICALS NEAR SOIL-ATMOSPHERIC SURFACE

by

ANGEL A. ANAYA A.

A thesis submitted in partial fulfillment of the requirements for the degree of

MASTER OF SCIENCE
in
CIVIL ENGINEERING

UNIVERSITY OF PUERTO RICO
MAYAGÜEZ CAMPUS
2009

Approved by:

_____   _____
Ingrid Y. Padilla, Ph.D .   Date
President, Graduate Committee

_____
Sangchul Hwang, Ph.D.   _____
Member, Graduate Committee   Date

_____   _____
Eric Harmsen, Ph.D.   Date
Member, Graduate Committee

_____   _____
Victor Huerfano, Ph.D.   Date
Representative of Graduate Studies

_____   _____
Ismael Pagán, MS   Date
Chairperson of the Department

ABSTRACT

Landmines and other buried explosive devices (BEDs) pose an immense threat to military personnel, civilian population, and the environment in many places of the world, requiring large efforts on detection. Chemical detection of explosive-related chemicals (ERCs) near BEDs, including chemical, biological, canine, and infrared (IR) detections, relies on the presence of ERCs near the soil-atmospheric surface. ERCs distribution near this surface and their relation to the location of explosive devices are controlled by the fate and transport processes.

A three-dimensional laboratory-scale SoilBed system was designed and developed to assess the influence of environmental parameters on the flow patterns and transport of TNT, DNT and related chemicals. Experimental work to determine the effect of visible light, temperature, and rainfall conditions indicated that the mobility and persistence of water, TNT, DNT and others related chemicals are highly influenced by interrelated environmental and boundary conditions.

Experimental results indicate that rainfall events and low system temperatures induce higher water contents and retention. The presence of radiation and high system-temperatures induce water drainage and low water saturation in sandy soils. Advective and dispersive transport dominates mobility under high soil saturation. High water contents induce higher TNT and DNT source dissolution, higher advective transport, lower sorption, and increases spatial and

temporal detection and concentration distribution. Higher rainfall intensity, thus, results in higher detection and concentration distribution. Lower water flux, higher potential for sorption and degradation, and greater volatilization contribute to lower detection and concentration at low soil water contents. Higher temperatures tend to induce higher source dissolution rates, but enhance water drainage and lower water contents and limits TNT and DNT detection. At low temperatures, detection is enhanced by higher water contents and lower sorption, degradation and volatilization losses. The effect of temperature on DNT and TNT detection is highly variable and is influenced by interrelated factors. Solar radiation influences soil temperature and heat fluxes, and enhance TNT/DNT dissolution, transport, and degradation. It significantly enhances DNT detection.

A generalized linear mixed statistical model has been applied to quantify the temporal and spatial effect of environmental conditions on ERC detection and concentrations. The statistical analysis indicated that rainfall events and related water contents were the most influential factors affecting the presence and concentrations of ERCs in the aqueous and gaseous phase. Solar radiation, and related heat flux, is the second most influential parameter. Although atmospheric temperature influences the presence and concentration of ERCs in soils, it is the least influential parameter.

.

RESUMEN

Minas y otros artefactos explosivos enterrados representan un gran peligro para el personal militar, la población civil y el ambiente además de requerir un esfuerzo grande para su detección. La detección química de químicos explosivos cerca de los artefactos explosivos depende de la presencia de estos químicos cerca de la interfase suelo-atmosfera. La distribución de químicos explosivos cerca de esta interfase y su relación con la localización de artefactos explosivos esta controlado por procesos de transporte y destino en el suelo.

Un modelo físico tridimensional de suelo a escala de laboratorio fue diseñado y desarrollado para evaluar la influencia de parámetros ambientales en los patrones de flujo y transporte de 2,4,6 trinitrotolueno (TNT), 2,4 dinitrotolueno (DNT) y otros químicos relacionados. El trabajo experimental realizado a fin de determinar el efecto de la luz visible, la temperatura y la lluvia, indican que el movilidad y persistencia de agua., TNT, DNT y otros químicos relacionados es altamente influenciada por condiciones ambientales interrelacionadas.

Resultados experimentales indican que eventos de lluvia y temperaturas bajas del sistema inducen drenaje y saturaciones de agua bajas en suelos arenosos. El transporte advectivo y dispersivo demuestran la movilidad bajo condiciones de saturación de agua. Estas saturación de agua induce una disolución mas alta de la fuente de TNT, DNT, transporte advectivo más alto y menos absorción y aumenta la detección y distribución de concentración espacial y temporal. Por lo tanto, intensidades de lluvias más altas reclutan en mayor detección y

distribución de contracciones. Flujo de agua bajos, mayor potencial de adsorción, degradación y volatilización a contenidos de agua bajo contribuyen a detección y concentración bajos en el sistema. Temperaturas altas tienden a inducir mayor taza de disolución, pero aumenta el drenaje, baja el contenido de agua y limita la detección de TNT y DNT. A bajas temperaturas la detección es mejorada debido a contenidos de agua mas altos, menores perdidas por adsorción, degradaron y volatilización. El efecto de temperaturas es altamente variable y esta influenciado por otros factores interrelacionados. La radiación solar influye en la temperatura y el flujo de calor en el suelo, aumenta la disolución, transporte y degradación de TNT/DNT. La radiación mejora significativamente la detección de DNT.

Un modelo estadístico lineal mixto generalizado se ha aplicado para cuantificar el efecto temporal y espacial de las condiciones ambientales en la detección y concentraciones de químicos explosivos. El análisis estadístico indica que la lluvia y los acontecimientos relacionados con el contenido de agua son los factores más influyentes que afectan a la presencia y las concentraciones de ERCs en la fase acuosa y gaseosa. La radiación solar y el flujo de calor relacionado a esta, es el segundo parámetro de mayor influencia. Aunque la temperatura atmosférica influencia la presencia y concentración de quimos explosivos en el suelo, este es el parámetro de menor influencia.

To my family . . .

ACKNOWLEDGEMENTS

During the development of my graduate studies in the University of Puerto Rico, several people and institutions collaborated directly and indirectly for my research. Without their support it would be impossible for me to finish my work.

I want to start expressing a sincere acknowledgement to my advisor, Dr. Ingrid Padilla, because she gave me the research opportunity under her guidance and supervision. I received motivation, encouragement and support form her during all my studies. With her, I have learned writing papers for conferences and sharing my ideas to the public. I also want to thank the examples, motivation, inspiration, and support I received from Dr. Sangchul Hwang. From these two persons, I am completely grateful. Special thanks are extended to the Environmental laboratory team for the opportunity of researching under their support, guidance, and transmitted knowledge for the completion of my work.

At last, but the most importantly, I would like to thank my family, for their unconditional support, inspiration, and love.

Table of Contents

List of Tables

xiii

List of Figures

List of Symbols and Abbreviations

B_d	-	Soil bulk density (ML-2T-2)
C^*	-	Concentration of the solute phase bound to the
C	-	Concentration (M/L^3)
C_A	-	Concentration of the compounds in the air
C_{im}	-	Solute concentration in the immobile water
C_G	-	Vapor concentration
C_m	-	Solute concentration in the mobile water
C_S	-	Concentration sorbed on the solid phase
C_W	-	Concentration of the compounds in the water
D^*	-	Effective molecular diffusion coefficient (L^2/T)
D_i	-	Hydrodynamic dispersion coefficient (L^2/T) in the
D_L	-	Longitudinal hydrodynamic dispersion coefficient (L^2/T)
D_m	-	Molecular diffusion in the bulk fluid
D_{sm}	-	Soil moisture dispersion coefficient for the mobile water
D_s	-	Hydrodynamic dispersion coefficient. Its a function of
dC/dx	-	Concentration gradient $(M/L^3/L)$
D_T	-	Transversal hydrodynamic dispersion coefficient (L^2/T)
e	-	Random error
$E_u(Y_{ij})$	-	Marginal mean of Y_{ij}
F_D	-	Dispersive mass flux of solute (M/TL^2)
f_{OM}	-	Mass of organic matter/mass of soil
f_{OC}	-	Weight fraction of organic carbon in the soil
F_{ZA}	-	Advective mass flux (M/TL^2)
g	-	Link function
H	-	Hydraulic head (L)
h_b	-	Bubbling pressure
h_p	-	Pressure head in unsaturated soil
J	-	Total mass of solute $(M/TL2)$
K	-	Hydraulic conductivity (L/T)
K_D	-	Soil-water partitioning coefficient
K_D'	-	Soil-air partitioning coefficient
K_H	-	Henry's law constant
K_{OC}	-	Organic carbon distribution coefficient
K_{OM}	-	Organic-matter distribution coefficient
L	-	Van Genuchten parameter
M_S	-	Mass of dry soil particles

MW	-	Molecular weight
n	-	Porosity (dimensionless)
n_m	-	Number of moles
P_c	-	Soil-water pressure, capillary pressure (MLT^{-2}/L^2)
q	-	Convective soil moisture flux = to qvz (M/TL2)
R_g	-	Constant gas
r	-	Radius of liquid
R	-	Retardation factor
R_m	-	Retardation factor for the mobile water
R_{im}	-	Retardation factor for the immobile water
S	-	Aqueous solubility
Se	-	Effective saturation
T	-	Temperature
V	-	Average soil-moisture velocity (L/T)
v^*	-	Variance function
$Var_u(Y_{ij})$	-	Marginal variance of Y_{ij}
V_A	-	Volume of air
VP	-	Vapor pressure
Vt	-	Volume of soil
V_X	-	Advecting velocity
V_z	-	Empirical value accounting for pore tortuosity connectivity
W	-	Tortuosity factor
Y_a	-	Expected value
α	-	Parameters estimated from soil-water retention curve (cm^{-1})
α_L	-	Longitudinal dynamic dispersivity coefficient (L)
α_T	-	Transversal dynamic dispersivity coefficient (L)
$\alpha_L V_i$	-	Longitudinal Mechanic dispersivity (L^2/T)
$\alpha_T V_i$	-	Transversal Mechanic dispersivity (L^2/T)
ε	-	Residual error
ρ_σ	-	Soil particle density
θ	-	Volumetric water content
θ_s	-	Water content the soil is saturated at atmospheric pressure
θ_r	-	Water content corresponding to a matric potential of -15000 cm
θ'	-	Scale factor
θC	-	Dissolved solute mass
θ_m	-	Volumetric mobile water content
θ_{im}	-	Volumetric immobile water content
φ	-	Contact angle
σ	-	Surface tension liquid-gas interface (MLT^{-2}/L^2)
u'_i		GLMM statistical model parameter
μ_A	-	Treatment mean
BEDs	-	Buried explosives devices

BTC	-	Breakthrough curve
DNT	-	2,4 dinitrotoluene
ECD	-	Electron capture detector
ERCs	-	Explosive related chemicals
GC	-	Gas chromatography
GMML	-	Generelalized linear mixed model
HPLC	-	High pressure liquid chromatography
mg/L	-	Miligram(s) per liter
mL	-	Milliliter(s)
mM	-	Milimolar
ppm	-	Part per million
ppb	-	Part per billion
SPE	-	Solid phase extraction
SWCC	-	Soil water characteristic curve
SS	-	Stainless steel
TNT	-	2,4,6 trinitrotoluene
TSD	-	Thermionic specific detector
UXO	-	Unexploded ordnance
ug/L	-	Microgram(s) per liter

1 INTRODUCTION

Landmines and other buried explosive devices (BEDs) pose an immense threat to military personnel, civilian population, and the environment in many places of the world, requiring large efforts on detection and neutralization of these objects. The detection of landmines and explosive related chemicals (ERCs), is a challenging field of great importance to national security, military branches, and many civil operations. The widespread production and use of ERCs have caused severe contamination of soils and underground environments. The toxicity and mutagenic effects of explosives and its degradation products pose an environmental threat in soils, especially in connection to shooting ranges, military bases and former munitions manufacturing plants (Hawari et. al., 2000; Spain, 1995).

Chemical detection of ERCs near BEDs, including chemical, biological, canine, and infrared (IR) detections, relies on the presence of ERCs near the soil-atmospheric surface. ERCs distribution near this surface and their relation to the location of explosive devices are controlled by the fate and transport processes.

Fate and transport processes of ERC in soils, including advection, dispersion, surface reactions, and transformations, are interrelated each other (e.g., degradation depends on advection) and are influenced by soil and environmental factors. These factors, which include rainfall (intensity, duration), temperature, atmospheric pressure, relative humidity, solar radiation, soil properties and conditions, soil-water content infiltration, and evapotranspiration, are dynamic and interrelated (i.e., not independent variables). Rainfall,

2

temperature gradients, and solar radiation, for instance, vary spatially and temporally. They influence infiltration and evapotranspiration rates, soil hydraulic conditions, and advective, dispersive and transformation processes near the soil surface. Accurate detection of ERCs near the soil-atmospheric surface must, therefore, consider the variability of ERC concentration distributions near the soil surface as affected by fate and transport processes controlled by the interrelated environmental factors.

Although studies have been conducted to assess and quantify the effect of environmental factors on the transport behavior of ERCs near soil surfaces (Comfort et al., 1995; Hawari et al., 2000; Pennington and Patrick, 1990; Phelan et al. 2000; Ravikrishna et al., 2002), most of the experimental work has focused on simple one-dimensional systems and completely-mixed reactors. The effect of variable environmental conditions and interrelated (i.e., not-independent) factors that vary in space and time, have been mostly addressed in numerical studies (Webb et al., 1998 and 1999), but have not been validated with data.

A need, thus, exists, to develop a physical experimental system that will generate accurate data and information on the effect of spatially and temporally variable environmental factors on the fate, transport and detection of ERCs near soil surfaces. To fulfill this need, it is necessary to conduct experimental work in a multidimensional soil-atmospheric physical system, which can simulate the fate and transport behavior of ERCs near partially-saturated soil surfaces under variable environmental conditions.

1.1 Objectives

The main goal of the proposed work is to determine and quantify the effect of spatially and temporally variable environmental factors on fate and transport of TNT and DNT near soil-atmospheric surfaces. Specifically, this work:

• Develops a three-dimensional soil-atmospheric system (3D SoilBed System), which can simulate and monitor the fate and transport behavior of ERCs near soil surfaces when exposed to variable precipitation, temperature, and radiation (visible and UV) conditions.

• Simulates experimentally the fate and transport behavior of 2, 4, 6 trinitrotoluene (TNT) and 2, 4 dinitrotoluene (DNT) and related chemicals under the variable environmental conditions in the SoilBed system.

• Determine the effect of variable and interrelated environmental processes and conditions (precipitation, infiltration, evaporation, water content, temperature, solar radiation) on the fate and transport processes and spatial and temporal detection and concentrations distribution of TNT and DNT in a sandy soil.

1.2 Thesis organization

This thesis integrates the work conducted to determine and quantify the effect of spatially and temporally variable environmental factors on fate and transport of TNT and DNT near soil-atmospheric surfaces. The work integrates the design and development of a experimental 3D SoilBed system and experimental methodology; performing fate and transport

experiments; assessment and integration of the results; and the development of models to advance our knowledge and understanding of the environmental factors affecting the mobility and presence of ERCS near soil-atmospheric surfaces. The knowledge gained applies directly to the development of enhancing detection techniques, and remedial alternatives.

This thesis is organized in several chapters. Chapter 2 develops necessary background theory and discusses the state of the knowledge on ERC sources, detection, fate and transport processes, environmental variables affecting transport processes, and statistical analysis of variable data. Chapter 3 describes the material, methods developed and used in the physical model, experimental set up, and data analysis. The fourth Chapter presents and discusses the experimental result and statistical analysis of the data. The results are integrated in Chapter 5, which leads to the conclusions developed in the study and summarized in Chapter 6. Chapter 7 provides recommendations to further assess the effect of environmental conditions on fate, transport, and detection of ERCs, and enhance detection capabilities.

2 THEORETICAL BACKGROUND

The production and use of conventional weapons, such as BEDs, in military conflicts and training results in the release of weapon – related chemicals into the environment. Some of these chemicals pose detrimental effect to the environment and public health (U.S. EPA, 2002). Landmines and other BEDs pose an immense threat to military personnel, civilian population, and the environment in many places of the world, requiring large efforts on detection and neutralization of these objects. There are thousands of landmines and unexploded ordinance (UXO)s through the world, leading to mine casualties in many regions of the world (Landmine monitor report, 2006). In the United States, there are millions of acres potentially containing UXOs, including military base installations (Brannon et al. 1999).

Many of the available detection techniques (McDonald et al., 2003), including chemical, biological, canine, and IR detections, require the presence of ERCs near the soil-atmospheric surface. However, the presence of ERCs near this surface and their relation to the location of BEDs, depends on the fate and transport processes that affect their mobility and persistence in soils.

The fate and transport of ERCs in soils are influenced by advection, dispersion, sorption, precipitation, mass transfer and transformation reactions (Brannon et al., 1999; Burlinson, 1980; Cattaneo et al., 2000; Comfort et al., 1995; Costanza and Brusseau, 2000; Dillert et al., 1995; Erikson and Skyllberg, 2001; Hawari et al., 2000; Hwang et al., 2000; Hwang et al.,

2005; Kaplan and Kaplan, 1982; Pennington and Patrick, 1990; Pennington et al., 2003; Phelan and Webb, 2002; Ravikrishna et al., 2002).These transport processes are interrelated with each other (e.g., degradation depends on advection) and are influenced by soil and environmental conditions, including rainfall (intensity and duration), temperature, atmospheric pressure, relative humidity, solar radiation, soil hydraulic conditions, soil water content infiltration, and evapotranspiration. Near the soil-atmospheric surfaces, where most BEDs are located, these conditions are dynamic and interrelated (i.e., not independent variables). Rainfall, temperature gradients, and solar radiation, for instance, vary spatially and temporally. They influence infiltration and evapotranspiration rates, soil hydraulic conditions, and advective, dispersive, and transformation processes near the soil surface.

This chapter presents necessary background and state-of the-art knowledge on landmines as ERC sources, fate and transport processes, environmental variables affecting transport presence, and statistical analysis of variable data. This background and knowledge have been applied for the design of experimental setup and methods, data analysis, and result interpretation.

2.1 Explosive Devices and Landmines

Landmines are explosive devices designed to explode when triggered by pressure, tripwire, or remote detonation. There are also smart mines, which automatically de-activate themselves after a certain amount of time. These devices are typically found on or just below

the surface of the ground. They are generally used by armed forces to disable any person or vehicle that comes into contact with it by an explosion or fragments released at high speeds.

There are more than 100-million landmines located in 70 countries around the world, according to One World International (Landmine monitor report, 2006). Since 1975, landmines have killed or maimed more than 1-million people, which has led to a worldwide effort to ban further landmine use and clear away existing landmines (Yoshikawa et al., 2002).

2.1.1 Landmines Types

While more than 350 varieties of mines exist, they can be broken into two categories (Bonsor, 2001):

- Anti-personnel (AP) mines
- Anti-tank (AT) mines

The basic function of both of these types of landmines is the same, but there are a couple of key differences between them. Anti-personnel landmines (Figure 2-1) are designed specifically to reroute or push back foot soldiers from a given geographic area. Anti-tank mines (Figure 2-2) are typically larger and contain several times more explosive material than anti-personnel mines. There is enough explosive in an anti-tank mines to destroy a tank or truck, as well as kill people in or around the vehicle. Additionally, more pressure is

usually required for an anti-tank mine to detonate (Bonsor, 2001). Most of these mines are found on roads, bridges, and large clearances where tanks may travel. Most antitank mines require an applied pressure of 348.33 pounds (158 kg) to 745.16 pounds (338 kg) in order to detonate. Most tanks and other military vehicles apply that kind of pressure.

Figure 2-1 PMA-2 Anti-personnel mine and fuse. Source: Phelan and Webb, 2002
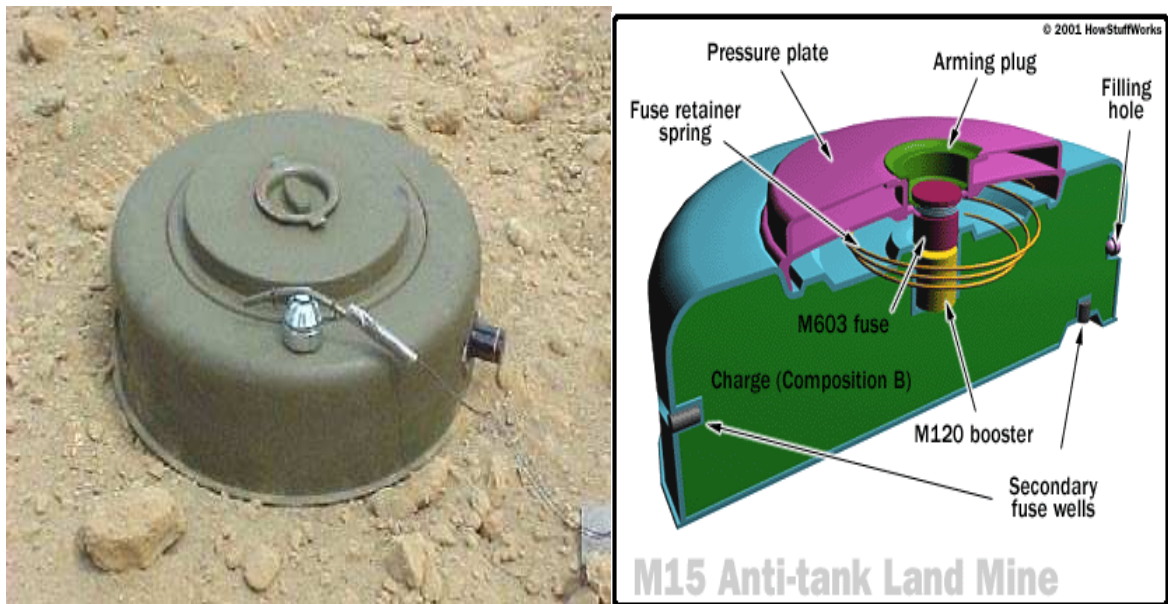
Figure 2-2 M15 Pressure-operated blast mine and schematic. Source: Bonsor, 2001.

Mainly landmines components include (Bonsor, 2001):

1. Trigger device: A device that triggers the detonation of the mine. It is generally comprised of a pressure plate (e.g., metal disc) placed on top of the mine, which depresses and triggers the mine when stepped on. Some mines can also be activated by tripwire or remote detonation.

2. Detonator: It's a small amount of explosive used to ignite larger amounts of explosive. The igniter is a metal rod that is projected from the ground, triggering the mine when has been activated by the trigger device.

3. Main charge: It's the large amount of explosive in the mine that causes it to explode.

4. Casing: landmines can be encapsulated in plastic or metal (steel) cages.

When the trigger device is activated, the detonator ignites the main charge of explosives. Destruction effects are enhanced by a propelling charge (a small among of explosive placed at the bottom of landmine to propel it into the air) and the presence of projectiles, metal balls or glass fragments placed in the mine to cause greater injuries to victims (the mine's metal casing can also become projectiles after the mine explodes).

The main charge contains explosive-related chemicals (ERCs), such as TNT (2, 4, 6-trinitrotuluene) and RDX (hexahydro 1, 3, 5- trinitro – 1, 3, 5 triazine), which are used in the greatest quantities (Walsh et al, 1993). TNT and RDX are somewhat mobile in the soil, and

can cause pollution of groundwater and underground systems (Spaulding and Fulton, 1988). Several other organic chemical explosives have also been used in specific munitions formulations, including 2, 4-DNT (2,4 Dinitrotoluene), HMX (octahydro – 1, 3, 5 , 7 – tetranitro – 1, 3, 5, 7 – tetrazocine, m – NT (m – nitrotoluene) and TNB (1, 3, 5 trinitrobencene) (Walsh et al, 1993).

TNT is the most relevant component of landmines, being in approximately 80% landmines manufactured in the world, (Cumming et al. 2001). The most important vapor constituents of military grade TNT are 2, 4, 6, TNT; 2, 4 DNT; 1, 3 DNB (dinitrobenzene) (Phelan and Web, 2002).

TNT is manufactured by nitration of toluene with a nitric acid solution; the toluene is derived from the distillation of crude oil and may have impurities such as benzene (Phelan and Web, 2002). TNT used in explosive formulations may contain chemicals that were impurities in production grade material, including isomers of DNT, 1, 3 dinitrobenzene (DNB), isomers of TNT especially 2, 4, 5 TNT and 2, 3, 4, TNT (Legget et al 1977), and environmental transformation by products (photo degradation and microbial degradation) of major or minor constituents (Phelan and Webb, 2002, Walsh et al, 1993).

2.1.2   *Emissions of ERCs from buried explosive devices*

Emissions of ERCs from BEDs occur mainly through two mechanisms, leakage and permeation (Phelan and Webb, 2002). Leakage occurs thorough openings in the case (e.g., like open joints) and, failures in casing material. Permeation occurs as diffusion through the thickness of casing material. The main factors affect permeation are: type of plastic (polymer) physical state of polymer, nature of penetrating gas or vapor, and environmental conditions (Phelan and web, 2002).

The release of ERCs from landmines has shown to be different when the landmines are exposed to air or water (Legget el l., 2001). Vapor fluxes emanating from mines to air at 20 ^{o}C have ranged from 0.6 to 30.3 ng/cm^2 –day for DNT and from 0.2 to 3.0 ng/cm^2 –day for TNT (Torres, 2008). When submerged in water, emissions form the mines occurred rapidly at the beginning of the experiments and tended toward a constant flux. Fluxes from mines in water are about 3 times higher than in air (Legget el l., 2001).

Measurements of surface concentration on two TMM1 Metal-cased mines prior to burial showed levels of TNT at 10 and 62 ng/cm^2 and DNT at 10 and 20 ng/cm^2. Surface concentrations 472 days after burial only show a trace of TNT below 1 ng/cm^2 (Jenkins et al, 2000). This shows that landmines may contain vapor signature from the paint. Landmine paint can, therefore, serve as a reservoir for explosive chemical signatures that are derived from external sources during manufacturing or storage processes (Bender et al, 1992).

Permeability rates generally increase about 30 to 50% for every 5 ^{0}C (Phelan and Webb, 2002). Mines made with rubber surfaces will permeate larger amounts than PVC or other more dense plastics.

2.1.3   *Landmines Detection*

Landmines and other buried explosives devices (BEDs) pose an immense thread to military personnel, civilian population, and the environment in many places of the world, requiring large efforts on detection and neutralization of these objects. The detection of landmines and ERCs is a challenging field of great importance to national security, military branches, and many civil operations. Several detection technologies have been applied, including: metal detectors, acoustic, seismic, electromagnetic, and Infrared (IR) technologies, mine-sniffing dogs, biological, and chemical sensing (MacDonald et al., 2003; Hussein, 2000). The response of these technologies varies in time and accuracy and may be influenced by environmental conditions. Moreover, chemical, biological, canine, and some of the IR sensing technologies require the presence of chemicals for detection the near the soil-atmospheric surface.

Previous studies have shown that ERCs are transported to the surface of the soil through upward water movement, following evaporation processes (Gutierrez, 2008; Phelan and Webb, 1997), and through molecular diffusion (Torres et al., 2007; Torres, 2008). As the

water evaporates from the soil, the signature compounds are carried out by the water and deposited on the ground surface.

Once on the ground surface, the molecules thermally desorb from the solid soil phase and can be detected by vapor snifters. Detection of ERCs near the soil-atmospheric surface, and their relation to the location of landmines depends on the source characteristics and on fate and transport processes that affect their movement in soils (Figure 2-3). Fate and transport processes are influenced by the physical-chemical properties of the chemical and soil, and the environmental conditions.
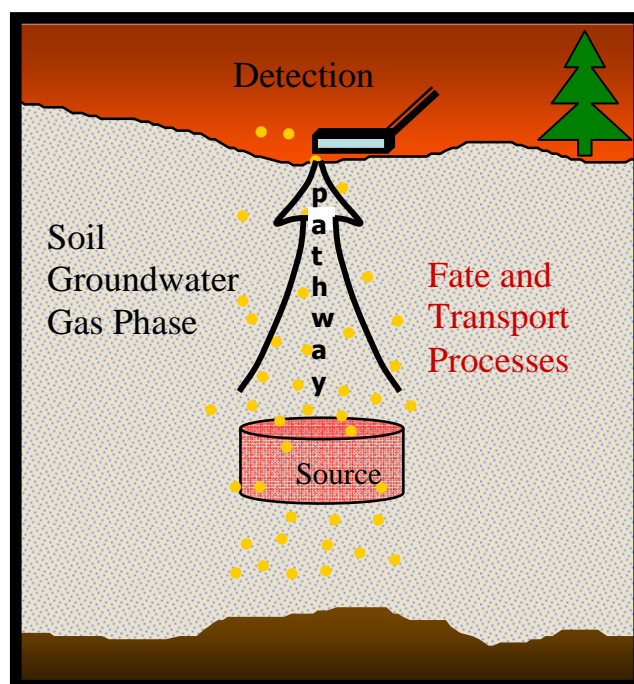
Figure 2-3 Landmine signature compounds movement in subsurface environments.

2.2 Physical and chemical properties of nitro-aromatic ERCs

TNT and DNT are organic nitro-aromatic compounds consisting of toluene and nitro groups in its structure (Figure 2-4). These chemicals are non-polar, but the pressure of the nitrogen and oxygen give slight polarization to the molecules. The principal physical-chemical properties affecting their fate and transport behavior include vapor pressure, water solubility, and air-water (Henry's constant), soil-water, and soil-air partitioning and mass transfer coefficients.
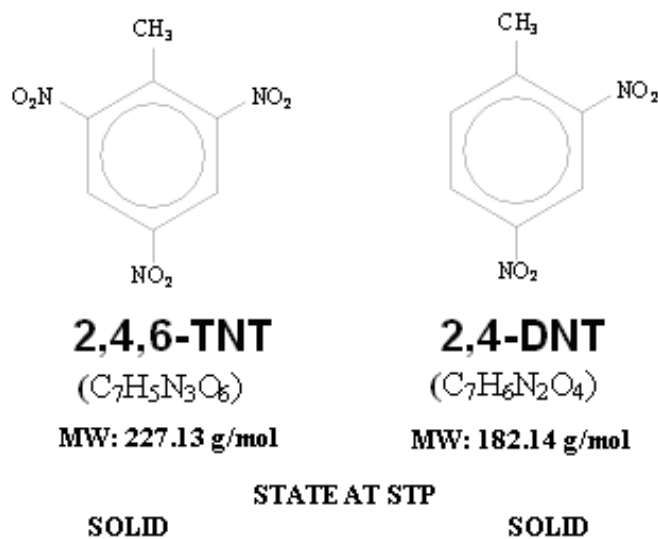
Figure 2-4 Molecular formula of principals ERCs presents in buried landmines

As a group, these chemicals have low vapor densities ad moderately low water solubility. Table 2-1 and 2-2 shows these properties at different temperatures (Phelan and Webb, 1997).

Table 2-1 Physical chemicals properties for TNT (2, 4, 6 - TNT) Source: Phelan and Webb, 1997

TEMP.	VAPOR PRESSURE	VAPOR DENSITY	WATER SOLUBILITY	HENRY'S LAW CONSTANT
^{o}C	Atm.	$\mu g/m^3$	mg/l	$cm^3,a/\ cm^3,w$
10	1.01E-09	9.8	110	8.94E-08
15	2.18E-09	21.0	120	1.75E-07
20	4.61E-09	43.5	130	3.35E-07
25	9.49E-09	88.1	150	5.87E-07
30	1.91E-08	174.3	175	9.96E-07
35	3.75E-08	337.2	225	1.50E-06

Table 2-2 Physical chemicals properties for DNT (2, 4, - DNT) Source: Phelan and Webb, 1997; *Torres, 2008.

TEMP.	VAPOR PRESSURE	VAPOR DENSITY	WATER SOLUBILITY	HENRY'S LAW CONSTANT
^{o}C	Atm.	$\mu g/m^3$	mg/l	$cm^3,a/\ cm^3,w$
10	3.87E-10	30.3	115*	
15	7.98E-09	61.5	138*	
20	1.61E-08	121.8	168*	4.51E-07*
25	3.17E-08	235.6	204*	
30	6.09E-08	445.9	250*	
35	2.12E-07	1501.2	379*	2.34E-05*

2.2.1 Vapor Pressure and Density

The vapor pressure is indicative of the ability of the compound to volatilize to the gas phase. It is the pressure of a compound in the gaseous phase in equilibrium with its condensed phase (Schwarzenbach et al., 2003). High values indicate a high capacity to volatilize, achieve high concentrations, and move in the vapor phase. Although a function of temperature, TNT and DNT have low vapor pressures (Tables 2-1 and 2-2), indicating limited capacity of the compounds to be stored and transported in air.

The highest vapor pressures of 2, 4 DNT than TNT indicate a preferential presence of DNT in the gas phase over that of TNT. Vapor densities are the vapor concentration obtained at equilibrium under given temperatures and pressures: it is directly estimated from the universal gas equation as (Brown et al., 2000):

$$MW\left(\frac{n_m}{V_A}\right) = \frac{VP}{R_g T} \qquad \textbf{2-1}$$

where: MW is the molecular weight, n_m is the number of moles, V_A is the volume of air, VP is the vapor pressure, R_g is the constant gas, and T is temperature. Because of the higher vapor pressures of DNT, vapor densities at given temperature and pressure are higher for DNT than TNT (Figure 2-5). Similar to vapor pressures, vapor densities of TNT and DNT increase with temperature.

2.2.2 Solubility

Solubility (aqueous solubility S) indicates the capacity of a chemical to dissolve in water. Because of high polarity of water, the solubility of non-polar or low-polarity organic compounds is limited in water. DNT and TNT are slightly soluble in water, with aqueous solubility in the mg/l range (Tables 2-1 and 2-2). Reported solubility of DNT at 20 ^{o}C averages 189 mg/L ($\pm$54.60), while for TNT, the average is 106 mg/L ($\pm$20.2) (Torres, 2008). This, difference results in a higher capacity of DNT for aqueous transport when is compared to TNT.

Similarly, higher aqueous solubility at high temperatures (Tables 2-1 and 2-2) results in higher capacity for aqueous transport at higher temperatures. Several studies have reported solubility values for TNT and DNT at different temperatures (Torres, 2008). The data, however, shows some variability and generates some degree of uncertainty in the actual values. Temperature-dependent solubility models for TNT and DNT were, therefore, developed by Torres (2008), and used for this study. The models, which were developed using regression analysis of published data, predict the average solubility of TNT (Eq. 8) and DNT (Eq. 9) as a function of temperature. Estimated solubility values for TNT and DNT at the temperatures used in this study are given in Tables 2-1 and 2-2, respectively. These estimates indicate that DNT is slightly more soluble in water than TNT at all temperatures

$$S_{TNT} = 17.7407 + 31.4089 \cdot (1.0516)^{T(^{\circ}C)} \qquad \textbf{(mg/L)} \qquad \textbf{2-2}$$

$$S_{DNT} = 23.9662 + 58.0766 \cdot (1.0463)^{T(^{\circ}C)} \qquad \textbf{(mg/L)} \qquad \textbf{2-3}$$
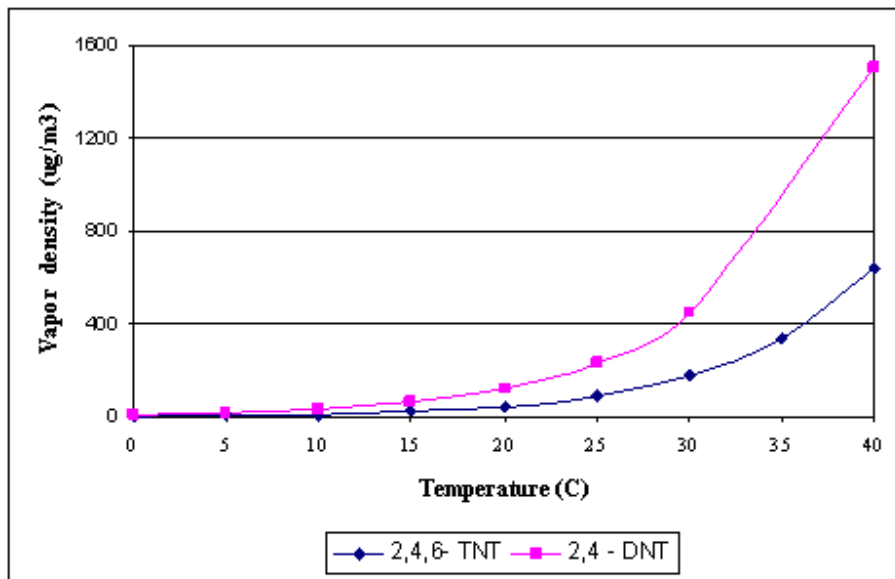
Figure 2-5 Vapor pressure of 2,4,6 TNT and 2,4 DNT

2.2.3 Partitioning Coefficients

Partitioning coefficients are indicative of the partitioning behavior of compounds among different phases (i.e., solid, liquid, gas). The vapor pressure, aqueous solubility, and polarity properties of DNT and TNT allow partitioning into the gas, the aqueous, and soil phases in subsurface environment. This partition controls the fate and extent of mass transfer among the different phases, and influences the fate and transport presences in the soil-surface (Figure 2-6).

19
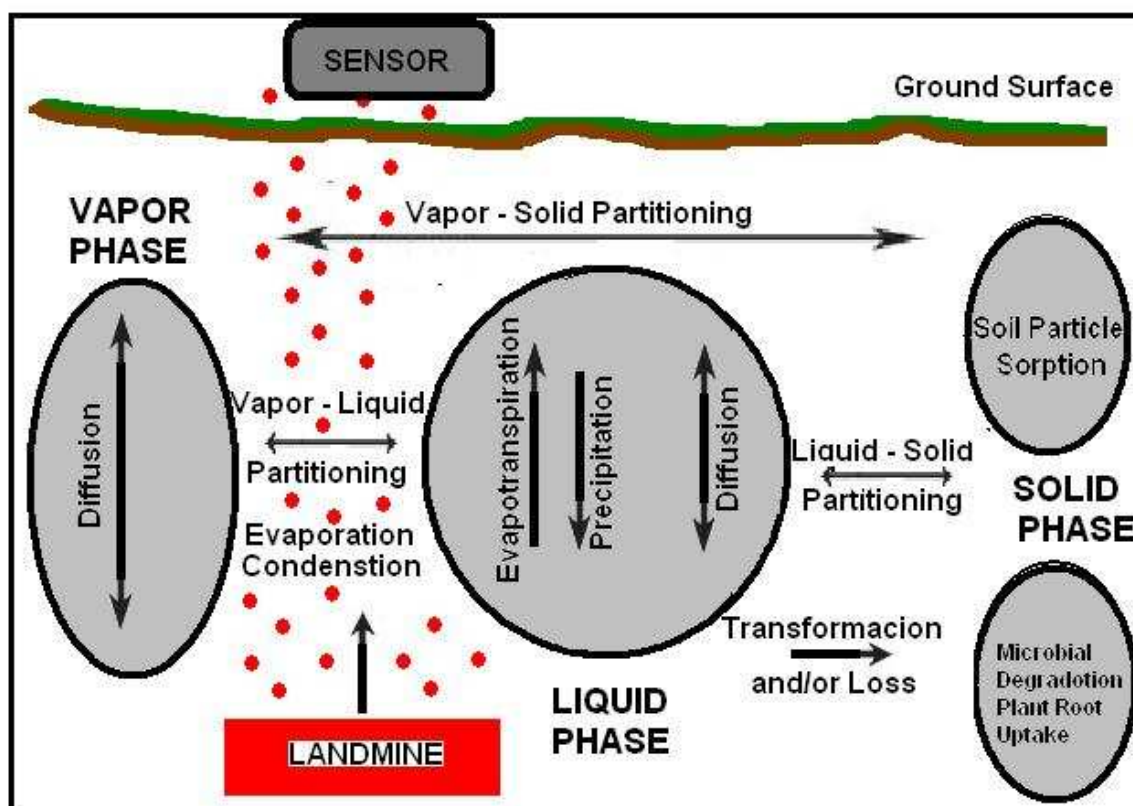
Figure 2-6 Processes affecting ERCs molecules released from a landmine. Source: modified from Woodfin, 2007.

The partitioning behavior of chemicals between the gas and aqueous phases is described by

Henry's Constant (K_H) (Fetter, 1999):

$$K_H = \frac{C_A}{C_W} = \frac{VP}{S} \qquad \text{(dimensionless)} \qquad 2\text{-}4$$

where, C_A and C_w are the concentration of the compounds in the air and water phases

respectively, VP is the vapor pressure, and S is the aqueous solubility of the compound. Low

K_H values ($< 2.5 \times 10^{-5}$) of TNT and DNT (Table 2-1 and 2-2) indicate that these compounds

have higher tendency to get dissolved in water than to volatilize. Although characterized by

low aqueous solubility (mg/l range), at equilibrium a greater fraction of the mass would

consequently be in the water than in the gas phase. Higher values at higher temperature reflect a greater fraction of the compounds in the gas phase at higher temperatures. Higher values of DNT reflect at both temperatures the greater volatility over TNT.

The partitions behavior at equilibrium between the aqueous concentrations (g/cm^3) and the concentration sorbed on the solid phase (g/g of soil) is given by the soil-water partition constant, K_D (cm^3/g) (Schwarzenbach, 2003). The linear soil-water partitioning coefficient is described by,

$$K_D = \frac{C_S}{C_W}$$

2-5

where C_S is the concentration sorbed on the solid phase and C_W is the aqueous concentration. In unsaturated media, DNT and TNT can be sorbed to soil organic matter, the mineral surface, or to the air-water inter phase (Torres, 2008). The degree to which the chemicals are sorbed to each of these compartments depends on the physical-chemical properties of the chemical, the amount and nature of organic matter, soil properties, and the air-water inter phase area (Schwarzenbach, 2003, water content, and other environmental conditions (Torres, 2008; Torres et al, 2007).

Sorption to soil organic matter (OM) is the predominant sorption mechanism for non-ionic organic compounds (Schwarzenbach et al., 2003) in wet soils containing relatively high fraction of organic matter (f_{om} = mass of organic matter/mass of soil > 1%) (Fetter, 1999). It is often quantified using the organic-matter distribution coefficient (K_{OM}) and the organic carbon distribution coefficient (K_{OC}):

$$K_D = f_{OM} K_{OM} \qquad\qquad \textbf{2-6}$$

$$K_D = f_{OC} K_{OC} \qquad\qquad \textbf{2-7}$$

where, f_{oc} is the weight fraction of organic carbon in the soil. Values of K_{OC} are measured or often estimated using linear free energy relationships with solute solubility (S) and the solute distribution constant between octanol and water (K_{OW}):

$$log\ K_{oc} = a\ log\ K_{ow} + b \qquad\qquad \textbf{\textit{2-8}}$$

$$log\ K_{oc} = -c\ log\ S\ + d \qquad\qquad \textbf{\textit{2-9}}$$

where, a, b, c, and d are empirical constants derived to different groups of homologous organic compounds (Schwarzenbach et al., 2003). Considering TNT and DNT homologous to alkylated and chlorinated benzenes, a, b, c, and d are assumed to be 0.74, 0.15, 0.70, and 0.59, respectively. Applying these values to the respective log K_{OW} (2.2 – 2.7 for TNT (ATSDR, 1995), 1.98 for DNT (ATSDR, 1995)), and S values for TNT and DNT yield log K_{OC} values ranging between 1.778 and 2.854 for TNT, and between 1.615 and 2.647 for DNT (Torres, 2008). The estimated values are within reported $log\ K_{OC}$ values for TNT (1.6-2.7; Eriksson and Skyllberg, 2001) and DNT (-0.6 -2.3; Hernandez et al., 2006; Phelan et al., 2000) for various soils. Using calculated Koc values and the fraction of organic carbon in the soil used in this study (f_{oc}=0.07%), the soil-water partitions coefficient (K_D) was estimated from 0.042 to 0.500 L/kg for TNT, and from 0.029 to 0.310 L/kg for DNT (Torres, 2008). These values indicate slightly higher sorption capacity for TNT than DNT.

Sorption to mineral surface can be a dominant mechanism for soils with low foc (Karimi-Loftbad et al., 1996) and low water contents. Under natural conditions, soil particles are preferentially sorbed with water because the polar nature of water and the charge characteristics of most soils (Shoemaker et al., 1990). As a result, the sorption of organic

chemicals to soil, which is mostly through relatively week van deer Waals forces, is limited in the presence of water (Torres, 2008; Petersen et al., 1994).

The equilibrium soil-air partitioning process is described in a similar way as that between soil and water, except that it relates sorbed to any concentration. The soil-air partitioning coefficient ($K_{D'}$) (Fetter, 1999) can be described by:

$$K_D' = \frac{C_S}{C_G} \qquad \qquad 2\text{-}10$$

where C_S is the soil concentration (g/g), C_G is the vapor concentration (g/mL), and $K_{D'}$ has units of mL/g (same as for the soil-water partitioning coefficient, K_D). The amount of DNT and TNT sorbed to soils has been shown to be impacted by the soil water content (Torres, 2008; Petersen et al., 1994, 1995). Generally, soils have a high sorption capacity for organic chemicals when dry, but significantly lower when wet. Sorption constants of gases or vapors (K_D') have been shown to be substantially greater than the solute sorption constants (K_D) (Phelan and Barnett, 2001b). Phelan and Webb [2002] show that K_D' for TNT and DNT increases about 5 orders of magnitude (10^8) as the soil dries from 11 to 1% gravimetric water content.

Estimated values of K_D' for the sandy soil used in this work range between 10^4-10^7 cm^3/g for DNT and 10^5-10^7 cm^3/g for TNT (Torres, 2008), with higher values at lower water contents (Figure 2-7). Higher vales have been reported by Phelan and Barrent (2001) (Figure 2-8). The soil used by Phelan and Barrent (2001b), was also sandy, but air-soil partition had

much higher organic carbon fractions (0.8%). The soil-water partition coefficient (K_D) estimated for the same experiments show much lower values than the soil-air coefficient (K_D'). For instance, estimated K_D values range between 0.4 and 2 cm^3/g for DNT, with higher values at lower water contents. There are estimated values in the literature (0.6-2.3 cm^3/g, Hernandez et al, 2006; Phelan et al., 2000), and show a much greater tendency of DNT to partitions from air onto the soil than from water into the solid.
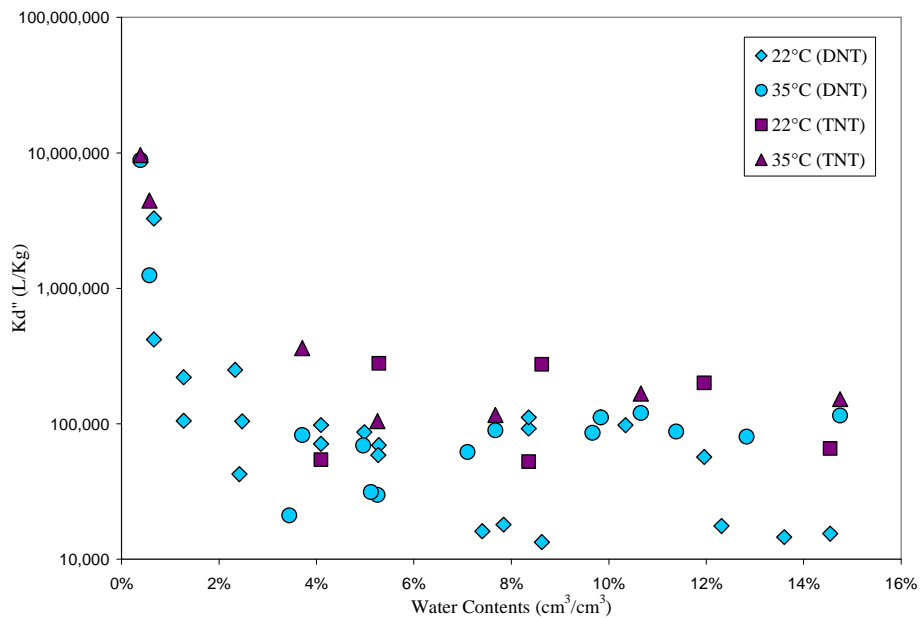
Figure 2-7 K_D' values of DNT and TNT at different temperatures as function of water content. Source: Torres, 2008.

Overall, soil sorption affects the mass fraction of DNT and TNT in soil, water, and air phases in the soil. The fraction of DNT and TNT in the soil solid phase is expected to increase as water content decreases (Figure 2-9).
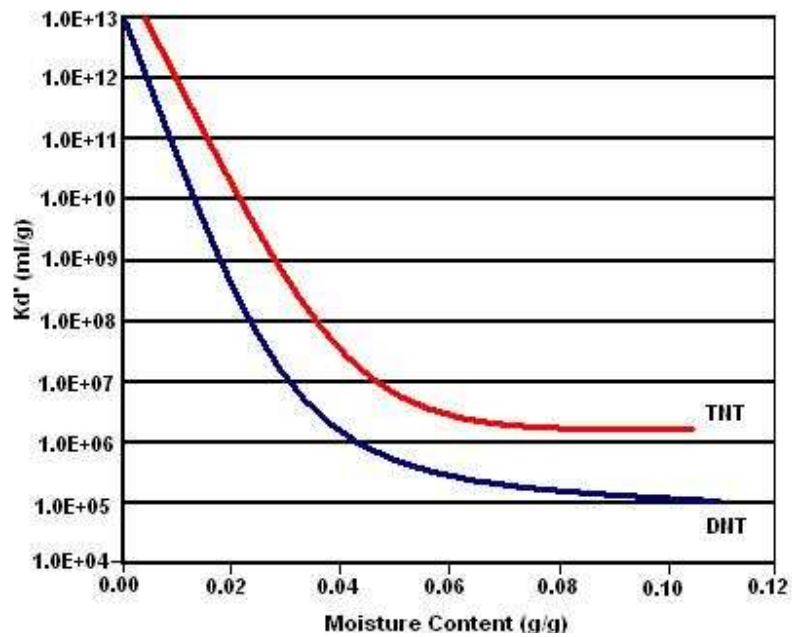
Figure 2-8 Influence of soil water content on K_D'. Source: modified from Phelan and Barnet, 2001.
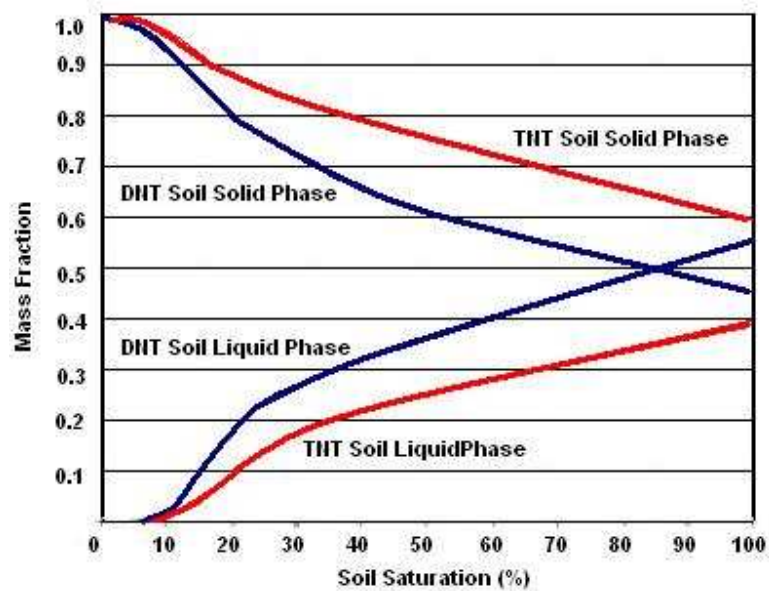
Figure 2-9 Soil solid and liquid phase mass fractions, $K_D = 0.9$. Source: modified from Phelan and Webb, 2002.

The fraction in the soil water is expected to increase as water content increases. Mass fractions in soil vapor (Figure 2-10) are expected to be much lower than in water and soil, but are also expected to vary with water content.
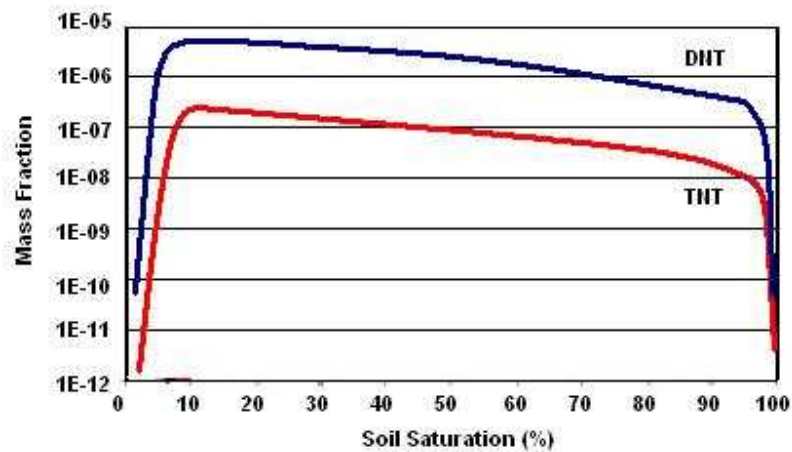
Figure 2-10 Soil vapor mass fraction. Source: modified from Phelan and Webb, 2002.

Rapid increase in vapor concentrations as water content increases up to about 10% saturation is expected due to lower soil sorption at higher water contents. At higher water contents, the vapor mass fraction is expected to decrease, as greater mass is stored in greater volumes of water. Similar behavior, in which vapor concentrations increase to a maximum and then decrease as water content increases, has been also reported by Torres, 2008.

Influence of soil - water partitioning coefficient (K_D) on vapor phase mass fraction can be observed in Figure 2.11. K_D values typically range between 0.5 and 3 mL/g are a typical range for most soils. For three different K_D values fixed at same temperature, high values of soil vapor mass fraction can be expected for the lowest K_D . For all curves at the extremes,

the effect of vapor – solid partitioning (low saturation) and decrease in the soil air porosity (high saturation) becomes important.
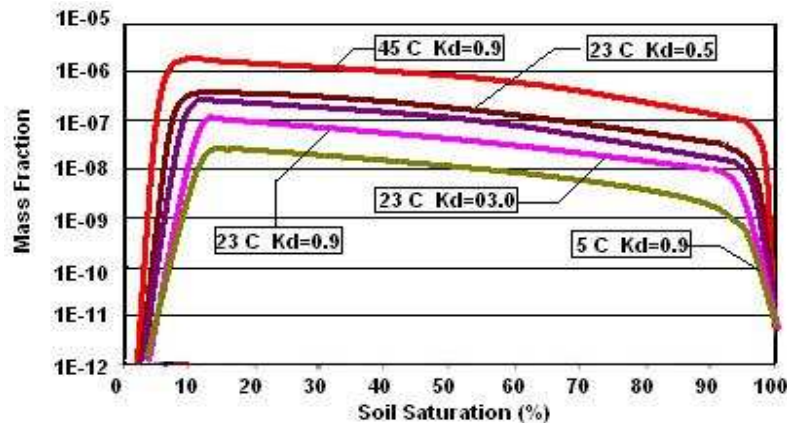
Figure 2-11 Effect of temperature on TNT vapor mass fraction. Source: modified from Phelan and Webb, 2002.

Temperature effects on vapor mass fraction can be observed in Figure 2-11. An increase from 5 to 45 °C involves an increase in the concentration in the vapor phase. The vapor concentration at 23 °C is about 10 times greater than concentrations at 5 °C, and vapor concentration at 45 °C is 5 times greater than concentrations at 23 °C (Phelan and Webb, 2002).

2.3 Fate and Transport Processes

The presence of ERCs near the soil-atmospheric surface and their relation to the location of the source (e.g., landmine) depend on the source characteristics and on the fate and transport processes controlling their persistence and mobility in soils. The fate and transport of ERCs in soils is influenced by advection, dispersion, sorption, precipitation, mass transfer and

transformation reactions (Brannon et al., 1999; Burlinson, 1980; Cattaneo et al., 2000; Comfort et al., 1995; Costanza and Brusseau, 2000; Dillert et al., 1995; Erikson and Skyllberg, 2001; Hawari et al., 2000; Hwang et al., 2000; Hwang et al., 2005; Kaplan and Kaplan, 1982; Pennington and Patrick, 1990; Pennington et al., 2003; Phelan and Webb, 2002; Ravikrishna et al., 2002). These processes are described below.

2.3.1 Advective – Dispersive Transport

Advective and dispersive processes relate to the movement of the chemicals with and within the bulk fluid (water or air). Advection is the transport of a chemical with the flowing fluid (water or air) and results in the bulk movements of the chemical in the direction of the fluid movement. Dispersive transport results in the movement and spreading of chemicals within the fluid from regions of high concentrations to low concentrations. Near soil-atmospheric surfaces, both modes of transport (advective and dispersive) can occur in soil-water and soil-air. It is often assumed that gas advection in soil is negligible and that vapor transport occurs mostly by molecular dispersion or diffusion. This is not necessarily true, especially near soil-atmospheric boundary when changes in local atmospheric pressure and temperature could induce air pressure gradient and flow. Furthermore, water-percolation fronts near the surface may often cause air-phase displacement during infiltration events. Advection and dispersion occur in the soil water as dissolved components move with the water during infiltration, redistribution, and evapotranspiration periods. Advection and dispersion in the water phase dominate transport during wet conditions (Gutierrez, 2008): at low soil-water contents during

28

dry conditions water flow is limited and transport of chemicals occur through water diffusion and/or vapor transport. Volatile and semi-volatile chemicals, such as TNT and DNT, would be subjected to both forms of transport (Torres, 2008; Torres et al., 2007).

2.3.1.1 Advective Transport

Advection is the transport processes by which dissolved solutes of chemical signatures are carried along with the flowing fluid (soil water, air). Mathematically, advection is described as a mass flux. Advective mass flux (F_{ZA}) for transport is described as:

$$F_{ZA} = V_z C \qquad\qquad \textbf{2-11}$$

where
V_z = average linear water velocity (L/T)
C = concentration (M/L^3)
F_{ZA} = advective mass flux (M/TL^2)

The average linear velocity, V_z, of the fluid in porous media depends on hydraulic gradients (dh/dl) and the physical and hydraulic properties and conditions of the soil, including hydraulic conductivities, porosity (n), and the water content (θ). Water flux, V_z, is commonly described with Darcy's Law (Jury and Horton, 2004):

$$V_z = -K(\theta) * \frac{dH}{Dl} = F_{ZA} * n_e \qquad\qquad \textbf{2-12}$$

where

K = hydraulic conductivity (L/T). At 100% soil-water saturation, K=K_{sat}, whereas K=K (θ) at lower saturation.
θ = water content
H = hydraulic head (L) H = z + p (position energy, z, plus pressure energy, P)
l = Length (L)
n_e = Effective porosity

29

In unsaturated soil, soil-water pressure and hydraulic conductivities are a function of water content (Jury and Horton, 2004). The functional relationship between pressure heads and water content is given by the soil-water characteristic curve (Figure 2-12). The most commonly functional forms used to relate water content, hydraulic conductivity, and soil-water pressure, are the van Genuchten (Van Genuchten, 1980) and Brooks and Corey, (Brooks and Corey, 1966) functions. Previous work (Molina, 2008) shows that Van Genuchten function applies well to the water characteristic curves generated for the sandy soil use in these work. It is, therefore, adopted for the analysis presented in this thesis. Van Genuchten relationships between water content, matrix potential and by hydraulic conductivity are expressed in equations 2-14, 2-15 and 2-16.
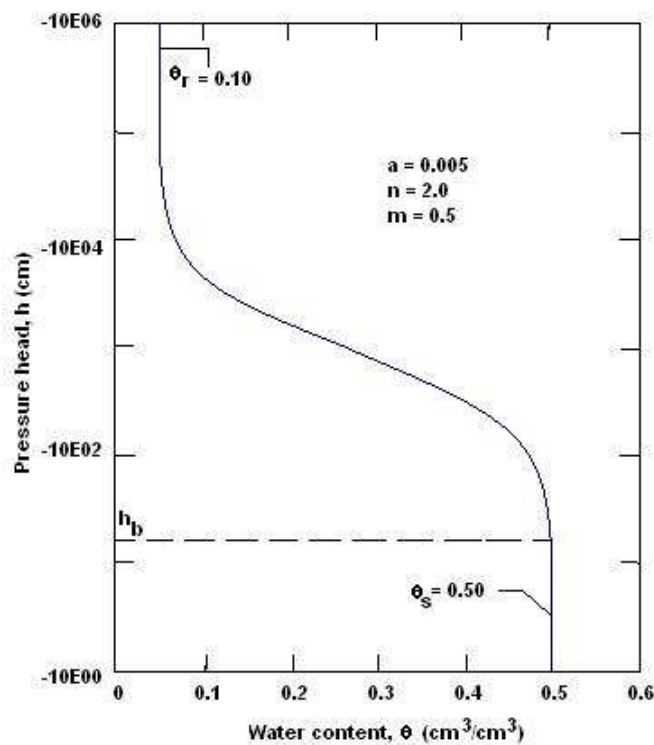
Figure 2-12 Typical soil water retention curve. Source: Modified from Fetter, 1999

Van Genuchten relationships by water content, matric potential (Pore water pressure) and hydraulic conductivity (Fetter, 1999) are expressed by equations 2.7, 2.8 and 2.9.

$$S_e = \frac{\theta - \theta_r}{\theta_s - \theta_r} = \frac{1}{\left[1 + \left(\alpha|h|\right)^n\right]^m} \qquad \textbf{2-13}$$

$$K(\theta) = K_{Sat} S_e^{\ L} \left[1 - \left(1 - S_e^{\frac{1}{m}}\right)^m\right]^2 \qquad \textbf{2-14}$$

$$K(h) = K_{Sat} \frac{\left\{1 - (\alpha h)^{n-1}\left[1 + (\alpha h)^n\right]^{-m}\right\}^2}{\left[1 + (\alpha h)^n\right]^{\frac{m}{2}}} \qquad \textbf{2-15}$$

with:

$$h_p(\theta) = \frac{P_c}{\rho_w g} = \frac{2\sigma_l \cos(\varphi)}{r \rho_w g} \qquad \textbf{2-16}$$

where:

θ_s = water content when the soil is saturated at atmospheric pressure.
θ_r = water content corresponding to a matric potential of -15000 cm.
h_b = bubbling pressure (matric potential when it is negative enough that water can   begin to drain form the soil).
α,m,n = parameters estimated from soil-water retention curve. (cm^{-1}, dimensionless, dimensionless
S_e = effective saturation
$h_p(\theta)$ = pressure head in unsaturated soil, related to the capillary (L)
P_c = Soil-water pressure, capillary pressure (MLT^{-2}/L^2)
φ = contact angle
σ = surface tension liquid-gas interface (MLT^{-2}/L^2); air-water surface tension = 72.7 dynes/cm at standard pressure and water
r   = radius of liquid – gas interface (L)
L   = empirical value accounting for pore tortuosity connectivity. Generally assumed to be 0.5 (Kussogi, 1999), but can be other values

2.3.1.2 Dispersive Transport

Dispersive transport accounts for spreading of the contaminants along and across the main flow direction. In systems having no advective transport, dispersion results as contaminants move from regions of high to low concentrations by molecular diffusion. For systems having advective transport, dispersion also incorporates the effect of velocity variations along flow lines. In this case, the hydrodynamic dispersion is defined as the sum of effective molecular diffusion and mechanical dispersion (Padilla et al., 1999). Mechanical dispersion is attributed to velocity variations caused by velocity differences along pore ratio and in pores of different size, and by differences in flow path lengths. Longitudinal dispersion occurred along the direction of flow, and results in a dilution of solute at the advancing edge. Transverse dispersion occur normal to the main direction of flow, and results in lateral spreading of the solute (Fetter, 1999).

Longitudinal and transverse hydrodynamic dispersion are often described by dispersion coefficients, as shown in equations 2-21 and 2-22:

$$D_L = \alpha_L V_i + D^* \qquad\qquad \textbf{2-17}$$

$$D_T = \alpha_T V_i + D^* \qquad\qquad \textbf{2-18}$$

where

D_L = longitudinal hydrodynamic dispersion coefficient (L^2/T)
D_T = transversal hydrodynamic dispersion coefficient (L^2/T)
α_L = longitudinal dynamic dispersivity coefficient (L)
α_T = transversal dynamic dispersivity coefficient (L)
$\alpha_L V_i$ = longitudinal Mechanic dispersivity (L^2/T)
$\alpha_T V_i$ = transversal Mechanic dispersivity (L^2/T)
D^* = effective molecular diffusion coefficient (L^2/T)

These equations show that hydrodynamic dispersion is expected to increase linearly with velocity by a constant given by the dispersivity coefficient. The dispersivity coefficient generally considered an intrinsic property of porous media under fully saturated conditions. Greater values have been reported for the same media when unsaturated flow conditions are imposed in the system and dispersivity has been shown to vary with degree of water saturation (Padilla, 1999). The effective molecular diffusion coefficient (D*) in porous media is described by:

$$D^* = D_m W \qquad\qquad \textbf{2-19}$$

Where D_m is the molecular diffusion in the bulk fluid (e.g., bulk water, air) and W is the tortuosity factor (Fetter, 1999). The tortuosity factor accounts for tortuous path in the media, results for the presence of the mineral grains. Its values are less than 1.0 and depend on the porous media and the degree of saturation (Jury and Horton, 2004).

In unsaturated porous media, molecular diffusion in the aqueous and vapor phases is controlled by water content (Figure 2-13). At high water contents (low air saturation), aqueous diffusion can be a significant transport mechanism under negligible advection conditions, in sandy soils, such as the one used in this work, water tends to drain rapidly under high water content conditions, and aqueous molecular diffusion may be significant only at low water contents, depending on the solute properties. Although the low vapor pressures of TNT and DNT limit the vapor transport in soils, (Phelan and Webb, 2002), their molecular diffusion coefficient are much higher in the gas phase than the water phase (Table

2-3). Consequently at low water content (high air saturation), vapor diffusion tends to dominate their transport (Grifoll et al., 2005; Phelan and Webb, 2002; Torres et al., 2007).
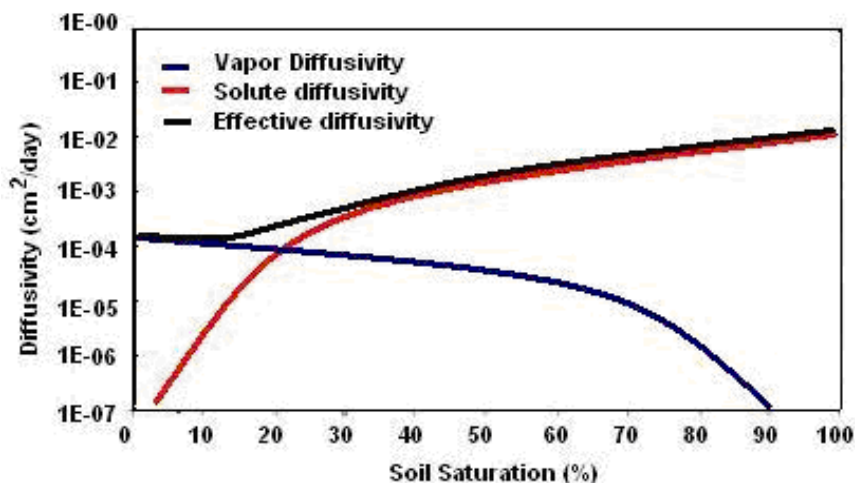
Figure 2-13 TNT vapor, solute, and effective diffusivity. **Source: Modified from Phelan and Webb, 1997**

Table 2-3 Values of the TNT and DNT physicochemical properties used in this study.
Source: Torres, 2008.

	Temperature: 22°C		Temperature: 35°C	
	TNT	**2,4-DNT**	**TNT**	**2,4-DNT**
Water-Molecular Diffusion (cm²/day)	0.5758	0.6063	0.7963	0.8383
Gas-Molecular Diffusion (cm²/day)	5,180	5,461	5,586	5,889
Solubility (mg/L)	112.7	181.2	200.5	307.1
Vapor Pressure (mg/L)	5.911E-05	1.451E-03	3.439E-04	7.188E-03
K_H (-)	5.243E-07	8.011E-06	1.715E-06	2.341E-05
Molecular Weight (g/mol)	227.133	182.1354		

Effective dispersivity (molecular diffusion) describing the total effect of soil-water and vapor diffusivity (Figure 2-13) shows that aqueous (solute) diffusivity dominate diffusive transport at soil air saturation below 20% (soil water saturation are 80%). At lower water contents (i.e., higher air contents), vapor diffusivity dominates the transport of these chemicals. Vapor

molecular diffusion is, thus, the controlling transport mechanism during dry periods. At very low water contents, the effective diffusion is reduced significantly due to direct sorption of TNT and DNT onto the soil particle (Phelan and Webb, 2002; Torres, 2008). As a result, at very dry conditions, there is very limited or no effective transport from BEDs to the surface (Woodfin, 2007). Transport resume as water content increases following rainfall events.

Slightly higher diffusion coefficients for DNT in the gas than aqueous phases (Table 2-3) indicates that molecular diffusivity of DNT is supposed to be slightly higher than TNT under the same conditions and gradients. Table 2-3 also shows that diffusion transport is higher at higher temperatures.

Dispersive transport processes can be described by Fick's first law, equation 2.20 and Fick's second law, equation 2.21:

$$F_D = -D_i \frac{dC}{dX} \qquad \textbf{2-20}$$

$$\frac{\partial C}{\partial t} = D_d \frac{\partial^2 C}{\partial x^2} \qquad \textbf{2-21}$$

where

F_D = dispersive mass flux of solute (M/TL^2)
D_i = hydrodynamic dispersion coefficient (L^2/T) in the longitudinal or transversal (i) direction
C = concentration (M/L^3)
dC/dx = concentration gradient ($M/L^3/L$)

2.3.2   *Reactive Transport*

The fate and transport of ERCs in soils is influenced by reactive processes (Phelan and Webb, 2002). These processes include sorption, precipitation, and transformations. Sorption involves equilibrium and non-equilibrium interactions between ERC solutes and vapors and the soil organic matter, mineral surface, and air-water interfaces (Costanza and Brusseau, 2000; Erikson and Skyllberg, 2001; Ravikrishna et al., 2002; Pennington and Patrick, 1990). Precipitation may occur when solute concentration exceeds solubility limits. This could occur near the soil-surface during evapotranspiration processes. Transformation reactions include biotic and abiotic processes (Brannon et al., 1999; Hawari et al., 2000), and are influenced by sorption, solute availability (Eriksson and Skyllberg, 2001), oxidation conditions (Pennington et al., 1990), residence time, and other environmental factors.

2.3.2.1 Sorption Processes

Sorption involves equilibrium and non-equilibrium interactions between the ERC solutes and vapors and the soil organic matter, mineral surface, and air-water interfaces (Costanza and Brusseau, 2000; Erikson and Skyllberg, 2001; Hwang et al., 2005; Pennington and Patrick, 1990; Ravikrishna et al., 2002). These processes are responsible for delaying the transport or ERCs, and concentration them around landmines (Jenkins et al., 2000; George et al., 1999). The degree and rates of sorption depends on a number of factors, including the concentration and characteristics of the contaminant, the soil type and its composition, the pH value of water, the presence of other water solutes (Schwarzenbach et al., 2003), and environmental

conditions (Torres, 2008). Each of these factors may vary in time and space, resulting in a variation of retardation in the natural environment (Jenkins et al., 2000; George et al., 1999; Spitz and Moreno, 1996).

The rates of sorption are often influenced by transport processes (Torres, 2008). If the sorptive process is slow compared with the rate of contaminant transport in the porous media, sorption will not reach equilibrium and must be described by a kinetic sorption model. On the other hand, if the sorptive process is rapid compared with the contaminant transport, sorption reaches an equilibrium condition and could be described by equilibrium sorption models. Measurements from direct soil phase TNT concentration have showed that equilibrium in the sorbed phase for some soils is not reached because TNT continues to transform, especially under anaerobic conditions (Myers and Townsend, 1996 Price et al., 1995).

2.3.2.2 Transformations Processes

Transformation reactions for TNT and DNT include biotic and abiotic processes (Brannon et al., 1999; Hawari et al., 2000), and are influenced by sorption, solute availability (Eriksson and Skyllberg, 2001; Hwang et al., 2000), oxidation conditions (Cattaneo et al., 2000; Pennington et al., 1990 and 2000), residence time (Hwang et al., 2006), and other environmental factors, such as water content and soil tpe (Phelan and Webb, 2002). Generally, TNT transformations occur by sequential reduction of nitro groups to amino groups (Figure 2-14). Biotransformation (biodegradation) of 2,4,6-trinitrotoluene (TNT) has been reported to form aminometabolites, including 4-amino-2,6-dinitrotoluene (4ADNT)

and 2-amino-4,6-DNT (2ADNT), 2,4-diamino-6-nitrotoluene (2,4-DANT), 2,6-diamino-4-nitrotoluene (2,6-DANT) mostly through reduction of the nitro moieties to amino groups (Cattaneo et al., 2000; Pennington et al., 2003).

Transformation occurs under aerobic and anaerobic conditions, but studies suggest that that the transformation rates are strongly dependent on the redox potential (Eh), with lower Eh values resulting in higher rates (Cattaneo et al., 2000). Reductive degradation of 2,4-DNT have been suggested to form 4-methyl-3-nitroaniline (Pennington et al., 2003). Under aerobic conditions, 2,4- and 2,6-DNTs are reduced to monoamine byproducts. Complete reduction to diamine byproducts occurs under anaerobic conditions (Pennington et al., 2003). Biotransformation of dinitrotoluene (2,4 -and 2,6- DNT) and aminometabolites (4ADNT and 2ADNT) have been suggested to also form nitrate and nitrite (Cattaneo et al., 2000).

Abiotic transformations of TNT through photodecomposition have been reported in sun-lit environments (Burlinson, 1980; Hwang et al., 2000, Larson et al., 2000) and photocatalized systems (Dillert et al., 1995; Schmelling et al., 1996). Hwang et al. (2000) observed in a laboratory study that TNT was degraded rapidly and to a greater extent when exposed to light. Walsh et al. (1993) observed that an oxidized product, 1,3,5-trinitrobenzene (1,3,5-TNB), formed in samples exposed to light and suggested that photo-oxidation predominates in the sun-lit degradation pathway (Figure 2.15).
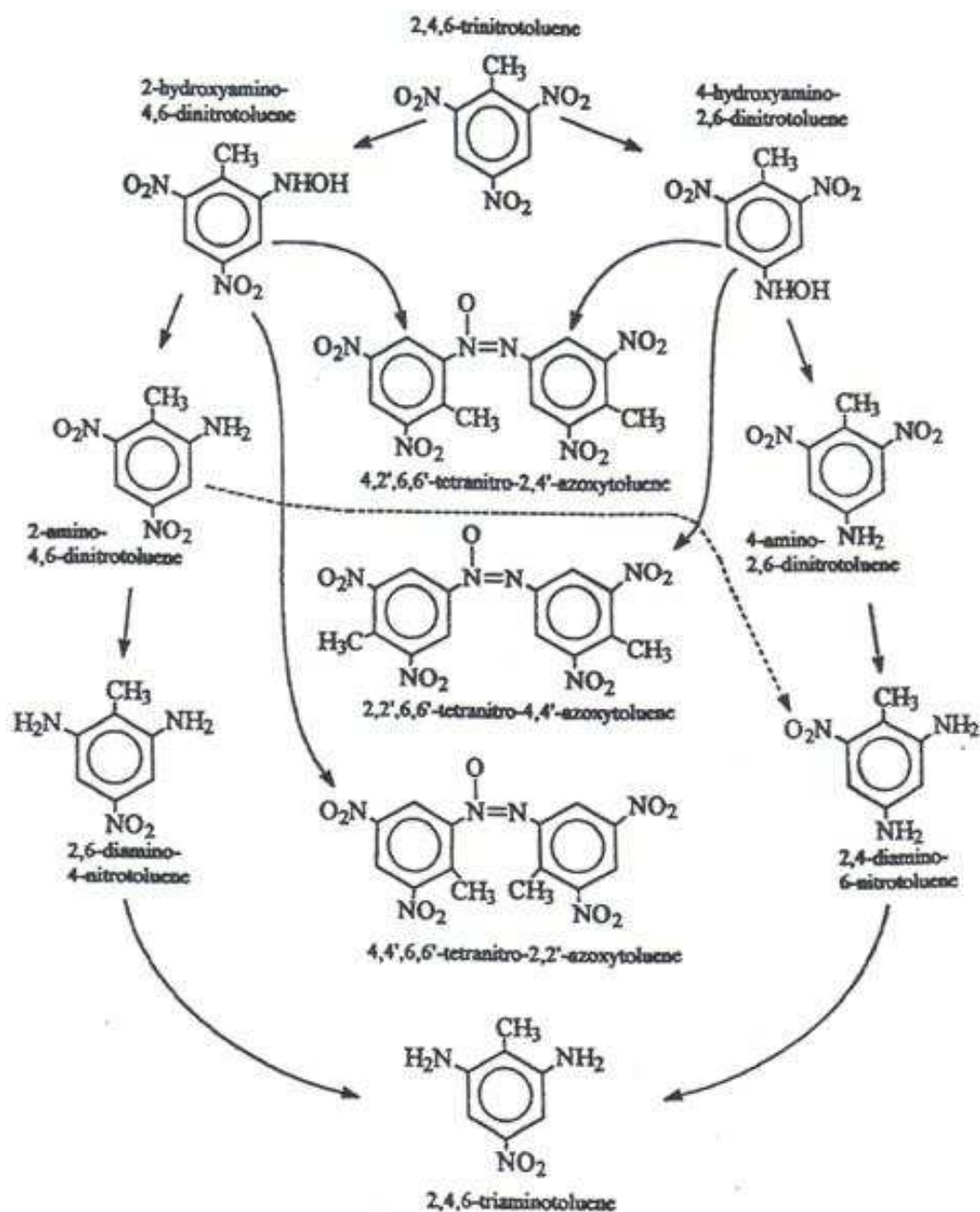
Figure 2-14 Proposed TNT transformation. Source: Brannon and Myers, 1997.

The formation of 1,3,5-TNB has also been reported by Dillert et al. (1995). Greater degradation on TNT in the light exposed samples was attributed to photo-oxidation of TNT and subsequent biodegradation of the photodegradation byproducts.
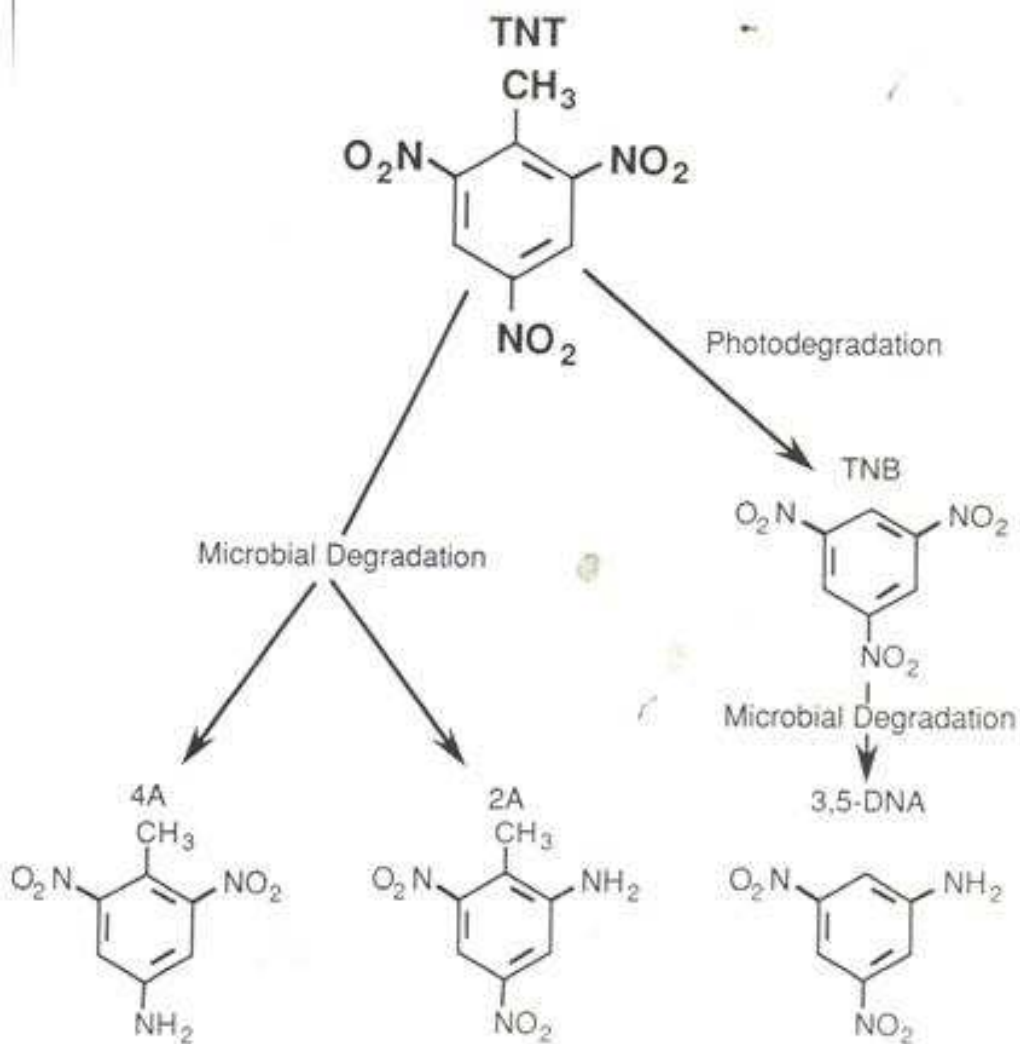
Figure 2-15 Microbial and photodegradation by TNT. Source: Walsh et al 1993.

Enhanced degradation of nitro aromatic compounds have also been attributed to their reactivity when photo chemically excited (Larson et al., 2000). Photodegradation of nitro-aromatic compounds has been shown to be influenced by solution pH, alkalinity, and the presence of surface-active agents (Larson et al., 2000; Schmelling et al., 1996).

2.3.3 Fate and Transport Equations

Mathematically, transport process in unsaturated porous media can be described using the total flux of a solute in a fluid. For one-dimensional transport in soil-water, the flux is given by equation 2-22 (Todd and May, 2005):

$$J = V\theta C - D_S \frac{dC}{dz}$$

2-22

By applying mass balance and the continuity equation, fate and transport can be described by equation 2-23:

$$\frac{\partial C}{\partial t} = D_S \frac{\partial^2 C}{\partial z^2} - v\frac{\partial C}{\partial z} - \frac{B_d}{\theta}\frac{\partial C^*}{\partial t} \pm \frac{\partial C}{\partial t}_{RXN}$$

2-23

where

J	= total mass of solute (M/TL^2)
V	= average soil-moisture velocity (L/T)
C	= solute concentration in the soil moisture (M/L^3)
θ	= volumetric water content
dC/dz	= solute gradient $(M/L^3/L)$
D_S	= hydrodynamic dispersion coefficient. Its a function of θ and V_z (L^2/T)
B_d	= soil bulk density $(ML^{-2}T^{-2})$
C^*	= concentration of the solute phase bound to the soil (M/L^3)
θC	= dissolved solute mass
q	= convective soil moisture flux = to θV_z (M/TL^2)
$\frac{\partial C}{\partial t}_{RXN}$	= others sources and sinks, biological/chemical transformations and precipitations.

ERCs sources include landmines and other BEDs such as plant uptake (Best and Sprecher, 1996), biodegradation, and others transformation reactions remove nutrients and solutes from solution, but may also generates by products (e.g., degradation of TNT may produce DNT).

For equilibrium and linear sorption, equation 2-23 can be expressed as (Fetter, 1999):

41

$$R \frac{\partial C}{\partial t} = D_S \frac{\partial^2 C}{\partial z^2} - v \frac{\partial C}{\partial z} \pm \frac{\partial C}{\partial t}_{RXN}$$
2-24

$$R = 1 + \frac{B_d K_d}{\theta}$$
2-25

R   = Retardation factor

When equilibrium is not reached, the first order rate model for sorption does not materially describe this process well (Van Genuchten et al., 1974). To solve this limitation by non-equilibrium transport, can be model applied assuming both, mobile and immobile phases. Mobile phase refers to water participating actively in flow near the center of saturated pores, whereas immobile water consist of then coating on soil particles and water trapped in unsaturated dead-end pores (Coats and Smith 1964). Solute exchange between mobile and immobile is simulated as 1st order diffusive transport, both phases allowing sorption (Van Genuchten and Wierenga, 1976). The mobile-immobile transport model is described by equations 2-26 and 2-27:

$$\theta_m R_m \frac{\partial C_m}{\partial t} + \theta_{im} R_{im} \frac{\partial C_{im}}{\partial t} = \theta_{im} D_{sim} \frac{\partial^2 C_{im}}{\partial z^2} - \theta_m V_m \frac{\partial C_m}{\partial z}$$
2-26

$$\theta_{im} R_{im} \frac{\partial C_{im}}{\partial t} = \beta(C_m - C_{im})$$
2-27

where

β = first order mass transfer coefficient, describe diffusion between mobile-immobile phases
R_m = retardation factor for the mobile water
R_{im} = retardation factor for the immobile water
C_m = solute concentration in the mobile water
C_{im} = solute concentration in the immobile water

θ_m = volumetric mobile water content
θ_{im} = volumetric immobile water content
D_{sm} = soil moisture dispersion coefficient for the mobile water

The mass transfer coefficient is a function of the soil water flux, soils properties, concentration of ionic solute, properties of the species being transported, the interfacial area between the two regions, volume, and geometry of the immobile water, and velocity (Padilla et al., 1999; Armstrong et al., 1994; Bajracharya and Barry, 1997).

2.4 Environmental Variables Affecting Transport Processes

The dynamics of ERCs movement toward the soil surface is complex, involving multiple, interrelated processes that vary with environmental conditions. These processes include transport processes controlling the direction and magnitude of the movement; and chemical, physical, and biological processes controlling the fate of the chemicals. ERCs enter the soil environment from BEDs through volatilization or dissolution processes. Once in the soil environment, they move as vapors or dissolved constituents. Advection, dispersion, and solute diffusion in the water phase dominate transport during wet conditions, whereas gas-phase diffusion is the major transport process controlling the movement of ERCs to the soil-atmosphere surface at low water contents during dry conditions. Movement of ERCs with infiltrating water in soils diverts transport away from the surface, whereas evapotranspiration tends to convey the chemicals toward the surface. In the gas phase, ERCs may move with advecting air and though diffusion. Bulk movement of air in the soil may result from pressure

43

differential induced by atmospheric phenomena and infiltrating water. Gas-phase diffusion becomes important under negligible water movement at low water contents. While moving within the soil and to the soil surface, ERCs partitions into gas, water, soil, and organic phases, adsorbs onto energetically-favorable surfaces, and may be transformed to more sTable compounds. Near the soil-atmospheric surface, ERCs may be uptaken and accumulated by shallow roots or near-surface vegetation.

Fate and transport processes of ERC in soils are interrelated with each other (e.g., degradation depends on advection) and are influenced by soil and environmental factors. These factors, which include rainfall (intensity and duration), temperature, atmospheric pressure, relative humidity, solar radiation, wind velocity, soil properties and conditions, soil water content, and plants coverage are dynamic and also interrelated (i.e., not independent variables). Rainfall, temperature gradients, and solar radiation, for instance, vary spatially and temporally. They influence infiltration and evapotranspiration rates (Amrhein, 1996), soil hydraulic conditions, and advective, dispersive, and transformation processes near the soil surface. Rainfall intensity, duration and initial water content have shown to influence the mixing zone and subsequent surface or subsurface transport of chemicals located near the soil-atmosphere surface (Havis et al., 1992).

Diurnal and seasonal weather variations, cycles of soil wetting and draining, and fluctuations in water Table have shown to affect the concentration distribution of ERCs and other

chemicals in soils (Gutierrez, 2008; McCarthy and Johnson, 1993; Reichman et al., 2000; Phelan et al., 2001; Webb and Phelan, 2000). Variable flow rates and water contents may induce fingering and preferential flow of solutes (Padilla et al., 1999; Wildenschild and Jensen, 1999).

Different numerical models have been developed (Spangler 1974; Jury et al., 1983 and 1990; Phelan and Webb, 1997; Reichman et al, 2000) to assess the behavior of different chemicals under particular environmental conditions. The predictions from these models are only an indication of expected conditions, but are not intended to predict a definitive concentration distribution in the field (Phelan and Webb, 1997).

2.4.1 *Atmospheric Pressure*

Changes in atmospheric pressure and wind can induce solute advection near soil-atmospheric surface by affecting soil-water hydraulic potential and evaporation processes (Gutierrez, 2008). It may also generate pressure gradient that may enhance downward or upward vapor transport (Phelan and Webb, 2002). Relative large pressure gradients must, however, be established to induce significant vapor transport. Auer et al (1996) observed that changes in vapor transport caused by barometric changes are generally small, compared to other transport processes.

2.4.2 *Weather conditions*

Weather conditions, including rainfall, solar radiation, relative humidity, temperature, and wind, affect fate and transport processes (Phelan and Webb, 1997). Rainfall events tent to cool down temperatures, induce infiltration, and increase soil-water content. Higher water contents reduce diffusive vapor transport, but enhance downward solute transport. Evapotranspiration periods after rainfall events may induce upward solute movement and solute concentration near evaporation surface (Gutierrez, 2008), depending on other weather conditions (solar radiation, temperature, ,wind, relative humidity, water content). At dry conditions, vapor phase transport controls the movement of ERCs. Sorption processes affect transport under very dry conditions. Both, diffusive and sorption processes are influenced by soil temperature. Diurnal and seasonal cycles produced by solar and long-wave radiation induce changes in temperatures near the soil-atmospheric surface, which influence various fate and transport processes (Woodfin, 2007).

 Higher concentrations can be found near the surface in warm summers than in the winter season, due to movement of ERCs by evaporation. Temperatures affect evaporation and degradations. High temperatures increase evaporation processes and the amount of ERCs molecules carried up from the to the soil surface explosive source. Biological degradation increase with temperature and presents greater activity in warm soils (Woodfin, 2007). Photo degradation at the surface may be also enhanced at the soil-atmospheric surface during solar radiation.

2.4.3   *Temperature*

Soil surface temperature is influenced by the solar radiation, atmospheric temperature, and long wave radiation, cloud cover, plant coverage (Phelan and Webb, 2002) and relative humidity (Arya, 1988). Seasonal and daily cycles have a significant control on soil surface temperature and ERCs transport processes. (Woodfin, 2007).

Different physical chemical characteristics including vapor pressure, vapor density, water solubility, and partitioning coefficients (water - air partitioning coefficient (Henry's Law Constant), soil - water partitioning coefficient and soil – vapor partitioning coefficient) are temperature dependent (Phelan and Webb, 2002). High surface temperatures involve high Henry's coefficient and water vapor pressure, and greater transport occur in the vapor phase. Soil-temperature also affect the soil-water temperature, soil-water potential, and hydraulic conductivity (Hopmans and Dane, 1986). Others parameters affecting water flow in the unsaturated zone, including surface tension, capillary tension, and contact angle are also temperature dependent (Hopmans and Dane, 1986; Bachmann et al., 2002; Grant and Salehzadeh, 1996).

2.4.4   *Soil-water content*

Soil-water content is influenced by weather conditions (rainfall, evapotranspiration) and soil properties. The effect of water content on fate and transport has been described in section 2.3. Briefly, water content affect partitioning coefficients among phases, and controls the

advective, diffusive, and reactive transport of ERCs. High water contnts induce downward movement of water and low vapor transport. As water content decreases, advective transport in water is reduced, and vapor transport decrease more significant, at very dry conditions, DNT and TNT tend to sorb strongly to soil surfaces and transport is further reduced.

2.5 Statistical Modeling

Statistical data analysis provide tools to describe and summarize a collection of data (descriptive statistics), and to predict and forecast data-based patterns. Statistical data models are applied to infer patterns in the data in a way that accounts for randomize and uncertainty in the observation (Spiegel, 1997). The models incorporate systematic and random effects (McCullagh and Nelder, 1989). Systematic effects relate the response to all explanatory variables. Random effect describes the nature and magnitude of unexplained and random variables. Linear statistical models describe the response (observation) as the sum of the systematic and the random effects (Litell et al., 2006). The simplest of these model is given by the means linear model,

$$Y_a = \mu_A + e \qquad\qquad \textbf{2-28}$$

where μ_A linear denotes the treatment mean (expected value of Y_A) and is the random variation of error. Linear regression models,

$$Y = a + \beta X \pm \varepsilon \qquad\qquad \textbf{2-29}$$

describe the linear change in response as a function of variation in treatment (X_A).

2.5.1 *Model Types and Data Characteristics*

Several statistical linear models have been developed (Table 2-4). The correct model to apply depend on data characteristics and must take into account the nature of the output and input data, the covariance matrix for random effects, and the link function for the selected model (Cerrito, 2005). Input and output variables can be defined as categorical or interval. Categorical data can be nominal (such as gender) or ordinal, in which categories are ordered from smallest to highest (Cerrito, 2005). Intervals define specific range of data. Binary data can take only one of two possible values, specified either as a series of zeros or ones (Bernoulli form), or aggregated as frequencies of successes out of a certain number of trials (Binomial form) (McCullagh and Nelder, 1989). Input variables can be further classified according to this type of effects: fixed or random. An effect is fixed if the levels (specific treatment) in the study present all possible levels of the factors (condition). Factor effects are random if the levels represent a sample of a larger set of potential level characterized by a probability distribution (Litell et al., 2006). Fixed effects are definitive, and will not change regardless of the sample data collection. Random effects can change when the experiment is replicated.

Linear models with fixed effects only include standard ANOVA and Regression models, Logistic Regression and the General and Generalized liner models (Table 2-4). Mixed models contain both fixed and random effects and include the Mixed Linear and the Generalized Linear Mixed model (Table 2-3). Linear mixed models have two defining

49

features in common: first, the errors and random effects are assumed to be normally distributed; second, the response variable is modeled directly as a linear combination of fixed and random effects. In many practical situations, the variable response of interest may not have a normal distribution. In other cases, there may be restrictions on the range of allowable values for predicTable functions that direct modeling of the response variable cannot address (Littell et al., 2006). One approach to handling non normality is to use various data transformations in conjunction with standard lineal model methods. The more commonly used transformations are discussed in introductory statistical methods texts such as those by Steel and Torrie (1980), Littell et al. (2006), and Snedecor and Cochran (1989). Box and Cox (1964) discuss such transformations in considerable depth. The principal linear models considered (Table 2-4) are briefly discussed below.

Table 2-4 Characteristics of the statistical models

MODEL	OUTPUT VARIABLE	INPUT VARIABLE	ASSUMPTIONS
ANOVA	Interval	Categorical, Fixed Effects only	Normality
REGRESSION	Interval,	Interval, ordinal Fixed Effects only	Normality
LOGISTIC REGRESSION.	Binary	Categorical, Interval, Fixed Effects only	Log-Normal
GLM GENERAL LINEAL MODEL	Interval	Categorical, Interval, Fixed Effects only	Normality
GENMOD GENERALIZED LINEAL MODEL	Categorical, Interval, Binary	Categorical, Interval, Fixed Effects only	Exponential Family
MIXED LINEAL MODEL	Interval	Categorical, Interval, Fixed and Random Effects	Normality
GENERALIZED LINEAL MIXED MODEL	Categorical, Interval, Bynary	Categorical, Interval, Fixed and Random Effects	Exponential Family

2.5.1.1 ANOVA and Regression Model

ANOVA (analysis of variances) models only allow *interval* output variables and categorical input variables with fixed effects and normal distribution. These models must only be used for balanced experimental designs, which require categorical variables of equal size. If there are three treatments, then each treatment should have exactly the same number of observations. Regression models can only use interval or ordinal variables as inputs. In order to include nominal data, dummy variables need to be created. The output data is generated in *interval* and a normal distribution of the data is assumed.

2.5.1.2 Logistic Models

Logistic model has a binary outcome variable rather than an interval outcome. If the outcome is ordinal, the model can also be used, but with a complementary log-log link function instead of the more standard log function. A log normal distribution function is assumed.

Binary data can be specified either as a series of zeros and ones (Bernoulli form), or aggregated as frequencies of successes out of a certain number of trials (Binomial form) (McCullagh and Nelder, 1989). In many longitudinal studies, the researcher is interested in a dichotomous variable as response, for example, presence, or absence of a disease in patients of a clinic treated with different medications, effectiveness of a particular health care service, or presence of symptoms in plants treated with different fungicides. In all these cases, the binary responses are clustered within observational units, and hence, the classical model fails in its independence assumption (i.e. data are taken at several occasions on the same unit). In

this case, it is possible to analyze this type of data using this model with appropriate link function (McCullagh and Nelder, 1989).

The logistic model can place ordinal inputs either as class or as quantitative variables. Consideration of the degrees of freedom and the necessity of post-hoc tests should be made before deciding where to use the ordinal inputs. Frequently, logistic regression is used to divide a population into high risk/low risk. However, this dichotomous outcome is not required (McCullagh and Nelder, 1989). There could just as easily be 5 or 10 categories of risk. It is not necessary to reduce the number of outcomes to 2, just to fit the results into a logistic model. Logistic regression also defines odds ratios for the input variables with its confidence limits.

Odd ratios analysis allows quantification of the change of inputs variables on the predictive variable. That is, a change in an independent variable from one level to another produces an increase or decrease on the probability of validation of statistical hypothesis. Odd-ratio values less than one indicate a decrease in a factor one minus the odd ratio value in the probability of success of the outcome variable. In contrast, odd ratios greater than one indicate an increase in a factor equal to the odd ratio value minus one. The main limitation of the logistic model is that it always increases the results especially if the group sizes are very different and one of the groups represents a rare event.

2.5.1.3 General Linear Models

General Linear model (GLM) expresses the mean of the data in terms of a monotonic transform of a lineal model and the parameters are estimated by maximum likelihood. GLMs are extensions of fixed-effects linear models to cases in which data are independent and standard linear model assumptions are not met (Litell et al., 2006, McCullagh and Nelder, 1989). GLM are, for example, applied when the distribution of the data is not normal, the mean is not linearly related to the model parameters, or when the variances of the data are related to the mean. Originally developed for members of the exponential family of distributions, GLMs have been extended to a much broader range of applications (Litell et al., 2006, McCullagh and Nelder, 1989). Data characteristics condition the model parameters. For instance, it is necessary to know the data characteristics before applying specific parameters (e.g., link function type, type of likehood, type of random matrices) for statistic analysis. A conditional distribution can be specified to circumvent this limitation (Litell et al., 2006).

GLM can use both interval and categorical variables as inputs variables. They contain all of the diagnostic tools provided in regression models, and do not require a balanced design. In addition, this model uses the Type III Sum of Squares to examine multiple types of treatments simultaneously. The main restriction the GLM is that it does not account for random effects. For the general linear model, GLM, the model equation is (Cerrito, 2005):

$$Y = a + \beta X \pm \varepsilon \qquad\qquad \textbf{2-30}$$

In which

$$\hat{y} = X\beta \qquad\qquad \textbf{2-31}$$

where

ε = the residual error. It is assumed normally distributed with mean zero add constant variance.

$\hat{y}$ = estimate

GLM models can be expanded to allow binary outcomes (Cerrito, 2005). This expansion is described as the Generalized Lineal Model (GENMOD) in Table 2-4. In this case, the estimation factor from equation 2-31 is described as:

$$g(\hat{y}) = X\beta \qquad\qquad \textbf{2-32}$$

where

g = link function

If the link function is changed to:

$$g(y) = \log\left(\frac{\hat{y}}{1 - \hat{y}}\right) \qquad\qquad \textbf{2-33}$$

and the outcome is binary, then the model is the special case of a logistic regression model. This link function can change depending on due the characteristics of the data; for count data, the denominator of the above expression can be eliminated, and a Poisson distribution is assumed for residuals (Cerrito, 2005). For interval outcome data, the residuals are assumed to form a gamma distribution. GENMOD doesn't allow random effects.

2.5.1.4 Mixed Linear Models

Mixed model has two components, fixed and random effects (Litell et al., 2006). The equation for Mixed Linear Model (MLM) Its equation is given by:

$$y = \beta X + \gamma Z \pm \varepsilon \qquad \textbf{2-34}$$

where:

γZ = random component. These models assume a normal distribution of the random effects, a mean of zero and a constant variance. If $\gamma=0$, then the mixed model is identical to the general linear model. If $\gamma\neq0$, then there is some randomness in the model and some covariance between inputs. Special cases of the mixed model are repeated measures, nested (hierarchical designs), split plot designs, and clustered designs (Littell et al, 2006).

2.5.1.5 Generalized Linear Mixed Models

Generalized Linear Mixed Models (GLMM), generalize the GENMOD model to include error terms that are not normally distributed (Cerrito, 2005). GLMM also generalize the mixed models to allow for random effects (Demidenko, 2004). However, the random effects must be normal. The importance of including random effects in the models has been studied by many authors, which consider that omitting them could generate a loss of efficiency and, therefore, an increase in the standard errors of parameter estimates (Litell et al., 2006). These models are also referred by some authors as conditional models (Lee and Nelder, 2004), multilevel models (Fitzmaurice and Lard, 1993), or latent variable models, depending on the model formulation.

The estimation factor for GLMM models is related with the systematic and random components given in equation 2-35. It expressed as (Torres, 2004):

$$g(\hat{y}_{ij}) = X_{ij}\beta + Z_{ij}u_i \qquad \textbf{2-35}$$

where,

$\hat{y}_{ij}$ = the conditional mean of Y_{ij}

X_{ij}, Z_{ij_i} = the covariates vector of the fixed, and random effects, respectively.

u_{i} = denotes de random effects.

The mean to variance relationship is given by the following equation (Torres, 2004):

$$Var(Y_i|u_i') = \theta' a_i v^*(\hat{y}_{ij}) \qquad \text{2-36}$$

where,

v^* = is the variance function that relates the conditional means and variances
θ' = is a scale factor (i.e. _ is assumed equal to one for standard binomial, and Poisson models)
a_i = is a prior weight, such as the reciprocal of a binomial denominator
u'_i = has a q-dimensional known distribution function $f_{ui}(ui)$, such as the normal distribution N(0,D), which is used in many cases.

By applying an inverse function to the equation 2-36 the value of $(\hat{y}_{ij})$ can be expressed as:

$$E(Y_{ij}|u_i) = (\hat{y}_{ij}) = g^{-1}(X_{ij}\beta + Z_{ij}u_i) \qquad \textbf{2-37}$$

The random effects in the model can be analyzed by the principal moments of the marginal distribution of Y_{ij}, and its expressions are given by the following equations:

$$E_u(Y_{ij}) = E_{ui}\left[g^{-1}(X_{ij}\beta + Z_{ij}u_i)\right] \qquad \textbf{2-38}$$

$$Var_u(Y_{ij}) = Var\left[g^{-1}(X_{ij}\beta + Z_{ij}u_i)\right] + E\{\theta a_i v(X_{ij}\beta + Z_{ij}u_i)]\}$$ **2-39**

$$Cov_u(Y_{ij}, Y_{ik}) = Cov\left[g^{-1}(X_{ij}\beta + Z_{ij}u_i)\right]\left[g^{-1}(X_{ik}\beta + Z_{ik}u_i)\right]$$ **2-40**

where,

$E_u(Y_{ij})$ = marginal mean of Y_{ij} induced by the random effects

$Var_u(Y_{ij})$ = marginal variance of Y_{ij} induced by the random effects

$Cov_u(Y_{ij}, Y_{ik})$ = marginal covariance, assuming conditional independence of the elements Y_i

Several functions g($\hat{y}$) can be used with GLMM. Most common link functions used with

these models include the logit, probit complementary log-log an log functions (Table 2-5).

Table 2-5 The most common link functions used with GLMM

OUTPUT	LINK FUNCTION	EQUATION MODEL
Binary	Logit	$g(\hat{y}) = \log\left(\dfrac{\hat{y}}{1-\hat{y}}\right)$
Binary	Probit	$g(\hat{y}) = \phi^{-1}(\hat{y})$ ϕ is the s standard normal cumulative distribution
Binary	Complementary log-log	$g(\hat{y}) = \ln(-\ln(1 - g(\hat{y})))$
Count	Log	$\log(g(\hat{y})$

There are others link functions and distributions that can be used with the outcome data.

Output data types can be binary, beta, binomial, exponential, gamma, Gaussian, geometric,

lognormal, multinomial, and others.

2.5.2   *Statistical Software*

There are different software packages to fit data with special characteristics, such as random effects and binary outcomes, to generalized lineal mixed models, These include: SAS, R, S-Plus, EGRET, STATA, and MIXREC (Goldsstein, 2003). These programs offer different tools to analyze binary longitudinal data, but each one of them have theirs limitations (SAS, 2004).

SAS routines have better consistency and demand a lesser processing time than R (Torres 2004). These routines are developed within the GLINMIX procedure. The GLIMMIX procedure fits statistical models to data with correlations or non-constant variability and where the response is not necessarily normal distributed. Like linear mixed models, GLMM, assumes normal (Gaussian) random effects. Conditional on these random effects, data can have any distribution in the exponential family (Cerrito, 2005). The exponential family comprises many of the elementary discrete and continuous distributions. Binary, binomial, Poisson, and negative binomial distributions, for example, are discrete members of this family. The normal, beta, gamma, and chi-square distributions are representatives of the continuous distributions in this family. In the absence of random effects, the GLIMMIX procedure fits generalized linear models (fit by the GENMOD procedure) (Cerrito, 2005).

The GLIMMIX procedure does not fit hierarchical models with non-normal random effects. With the GLIMMIX procedure, researchers select the distribution of the response variable

conditional on normally distributed random effects. Some of the features of the GLIMMIX procedure include (SAS, 2004):

- Fittings GLMMs by a pseudo-likehood and using the procedure Mixed, developed by mixed models.

- Allowing multiple random effects, nested and crossed random effects, and multiple cluster types.

- Permitting covariance structures for random effects and cor-related errors.

- Linearization and use of Taylor series techniques to construct Wald-type test statistics and confidence intervals.

- Fittings logistic regression including the ability to fit random effects. It is also capable of fitting errors that ate distributed differently than normal (e.g., binomial, binary etc). A list of those distributions is given below by the Table 2.6.

Table 2-6 Distributions and link functions provided by GLIMMIX SAS

Outcome	Distribution	Link Function
Beta	Beta	Logit
Binary	Binary	Logit
Binomial	Binomial	Logit
Exponential	Exponential	Log
Gamma	Gamma	Log
Gaussian	Normal	Identity
Geometric	Inverse, Gaussian	Inverse squared
Lognormal	Log-normal	Identity
Multinomial	Multinomial	Cumulative, logit
Negbinomial	Negative binomial	Log
Poisson	Poisson	Log
Tcentral	T	Identity

- Blocking of variables matrices and parameter heterogeneity (SUBJECT= GROUP option)

- Choice of linearization about expected values or expansion about current solutions of best linear unbiased predictors

- Flexible covariance structures for random and residual random effects, including variance components, unstructured, autoregressive, and spatial structures

- CONTRAST, ESTIMATE, LSMEANS and LSMESTIMATE statements, which produce hypothesis tests and estimable linear combinations of effects

- NLOPTIONS statement, which enables researcher to exercise control over the numerical optimization. Researcher can choose techniques, update methods, line search algorithms, convergence criteria, and more. Or, researcher can choose the default optimization strategies selected for the particular class of model been fitting

- Computed variables with SAS programming statements inside of PROC GLIMMIX (except for variables listed in the CLASS statement). These computed variables can appear in the MODEL, RANDOM, WEIGHT, or FREQ statements.

- Grouped data analysis

- User-specified link and variance functions

- Choice of model-based variance-covariance estimators for the fixed effects or empirical (sandwich) estimators to make analysis robust against misspecification of the covariance structure and to adjust for small-sample bias

- Joint modeling for multivariate data. For example, researcher can model binary and

- Normal responses from a subject jointly and use random effects to relate (fuse) the two outcomes. This is the nature of the experiments conduced.

- Multinomial models for ordinal and nominal outcomes

- Univariate and multivariate low-rank smoothing

The standard GLIMMIX procedure code, is given in the following lines (SAS, 2004):

PROC GLIMMIX < options > **;**
BY variables **; CLASS** variables **;**
FREQ variable **; ID** variables **; WEIGHT** variable **;**
PARMS (value-list) . . . < / options > **;**
RANDOM random-effects < / options > **;**
programming statements
MODEL response<(response options)> = < fixed-effects >< /options > **;**
MODEL events/trials = < fixed-effects >< /options > **;**
CONTRAST 'label' effect values < . . . effect values > < /options > **;**
ESTIMATE 'label' effect values < . . . effect values > < /options > **;**
LSMEANS effects < / options > **;**
OUTPUT < **OUT**=SAS-data-set ><keyword<(keyword-options)><=name>> . . .
<keyword<(keyword-options)><=name>>< / options > **;**
The primary assumptions underlying the analyses performed by PROC GLIMMIX are as

follows:

- If the model contains random effects, the distribution of the data conditional on the random effects is known. This distribution is either a member of the exponential family of distributions or one of the supplementary distributions provided by the GLIMMIX procedure. In models without random effects, the unconditional (marginal) distribution is assumed to be known for maximum likelihood estimation, or the first two moments are known in the case of quasilikelihood estimation.

- The conditional expected value of the data takes the form of a linear mixed model after a monotonic transformation is applied.

- The problem of fitting the GLMM can be cast as a singly or doubly iterative optimization problem. The objective function for the optimization is a function of either the actual log likelihood, an approximation to the log likelihood, or the log likelihood of an approximated model.

Once the parameters have been estimated, researchers can perform statistical inferences for the fixed effects and covariance parameters of the model using analysis tools like odds ratios, least squares means statements and least-squares means differences graphs, known as a Diffogram. When based on arithmetic means, this display is also known as a mean-mean scatter plot. The Diffogram displays significant and non-significant differences by rotating the confidence interval for least-squares mean differences. Whenever these lines cross the 45-degree reference line, the least-squares means associated with the center point of the line are not significantly different.

3 MATERIALS AND METHODS

The research objectives were accomplished by conducting solute transport experiments in a geo-environmental system, incorporating a 3D- laboratory-scale SoilBed within a controlled atmospheric environment. The SoilBed was subjected to soil-atmospheric processes, and consist of a soil tank packed with a homogeneous sandy soil from Isabela PR. Transport experiments involved burying a point source of TNT and DNT under the soil surface and applying controlled cyclic rainfall and radiation over the soil surface. Experiments were conducted under different environmental conditions, including different rainfall intensities, atmospheric temperatures, and radiation events. Aqueous and vapor concentrations of TNT and DNT, and other related chemicals were monitored in real time. Spatial and temporal breakthroughs curves were analyzed comparatively and analytically. A Generalized Linear Model, was used to analyzed the numerical data collected from experiments conduced. All the experimental work and analysis were conducted at the Environmental Engineering Laboratory at the Civil Engineering Department at the University of Puerto Rico, Mayaguez. The laboratory is equipped with the physical infrastructure, instrumentation for system control, hydraulic data measurement, chemical analytical equipment, and computational resources necessary for this research.

The developed work involves: designing, constructing, and testing a three-dimensional laboratory-scale soil-atmospheric (SoilBed) system; conducting TNT, DNT, and tracer

(sodium chloride, NaCl) transport experiments in the SoilBed system under variable precipitation, radiation, and atmospheric temperature conditions; sampling and analysis in both aqueous and vapor phases; and analyzing the data collected comparatively and quantitatively.

3.1 Geo-Environmental Physical Model System

Experimental work involved conducting experiments in a geo-environmental physical model designed to simulate chemical transport near soil-atmospheric surfaces. The system incorporates a 3D SoilBed inside an environmental chamber equipped with rainfall and solar radiation simulators, and temperature and relative humidity control settings (Figure 3-1). The rainfall simulator is used to control the intensity and duration of precipitation events. Solar radiation is simulated using lamps at different intensities (visible, uv). The temperature and relative humidity control settings are used to simulate atmospheric temperature and relative humidity conditions.

The soil tank, which is packed with a sandy soil, is capable of simulating flow and transport in multiple dimension subjects to different boundary and initial conditions (Anaya and Padilla, 2006). The soil atmospheric boundary is subjected to free atmospheric conditions involving rainfall, infiltration, evaporation processes under variable radiation and temperature settings. The bottom boundary is subjected to drainage under constant head condition.
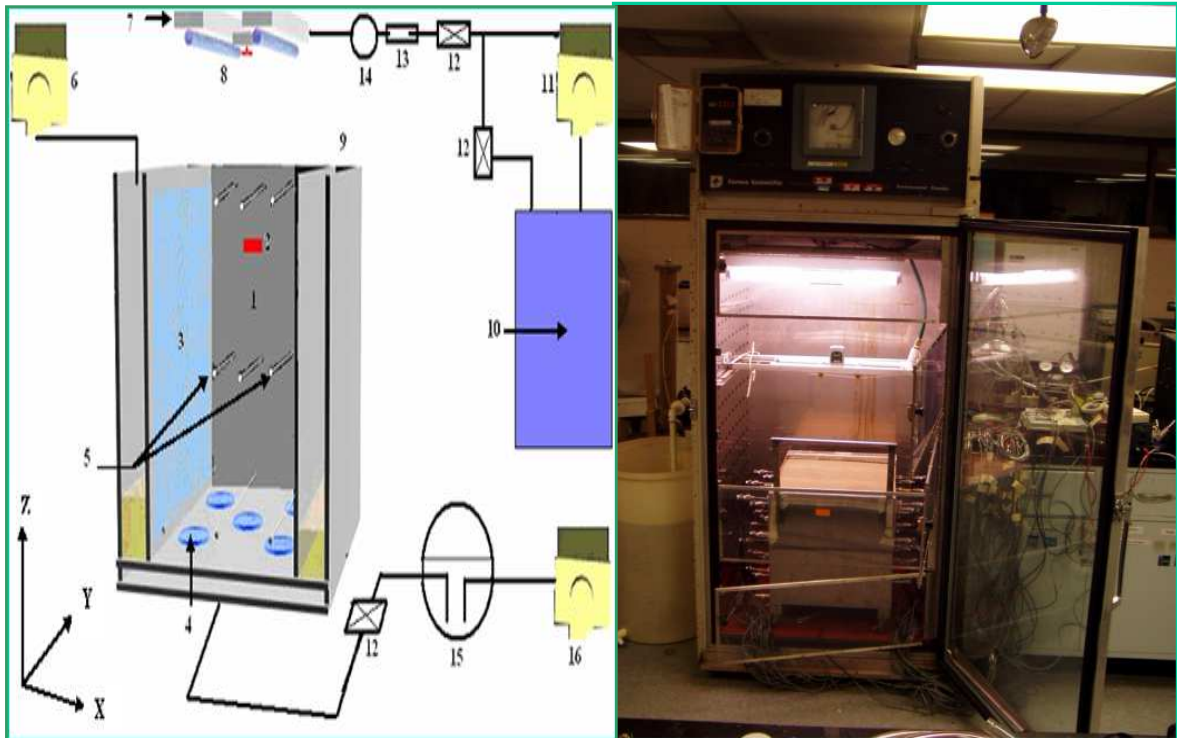
Figure 3-1 Geo-environmental System. 1. 3D scale lab tank, 2. Landmine buried, 3 Lateral pores plate, 4. Bottom pores plate, 5. Sampling probes, 6. Peristaltic pump, 7. System lamps (visible, UV), 8. Rain sprinklers, 9. Boundary conditions, 10. Water reservoir, 11. Volumetric pump, 12 Valves, 13. Flow meter, 14. Pressure indicator, 15. Vacuum reservoir, 16. Peristaltic pump.

3.1.1   The SoilBed System

The SoilBed consists of a stainless steel tank (45 cm deep, 45 cm wide, and 55 cm length), which contains a soil compartment ($45 \times 45 \times 45$ cm^3) and two lateral boundary partitions (Figures 3-1 and 3-2). The soil compartment has a net volume of 91,125 cm^3 and has porous plates (Mott Corp, CT) on the bottom and lateral sides to support the soil and control boundary conditions. The lateral porous plates have an average pore size of 100 μm and could be used to establish atmospheric pressures and/or variable head and flux conditions at

65

any depth in the SoilBed. The bottom porous plates have an average pore size and bubbling pressure of 10 μm and 293 mbar, respectively. It is used to establish water flux conditions under constant or variable heads. A sealed compartment under the porous plate is used to apply bottom boundary conditions. The bottom of the compartment contains sloped panels converging toward an outlet fitting connected to the flow-extraction system (section 3.1.1.4). No flow conditions are imposed on the front and rear panels of the soil compartment. In the Figure 3-2b, red number are the label of each cluster location.

(a) (b)
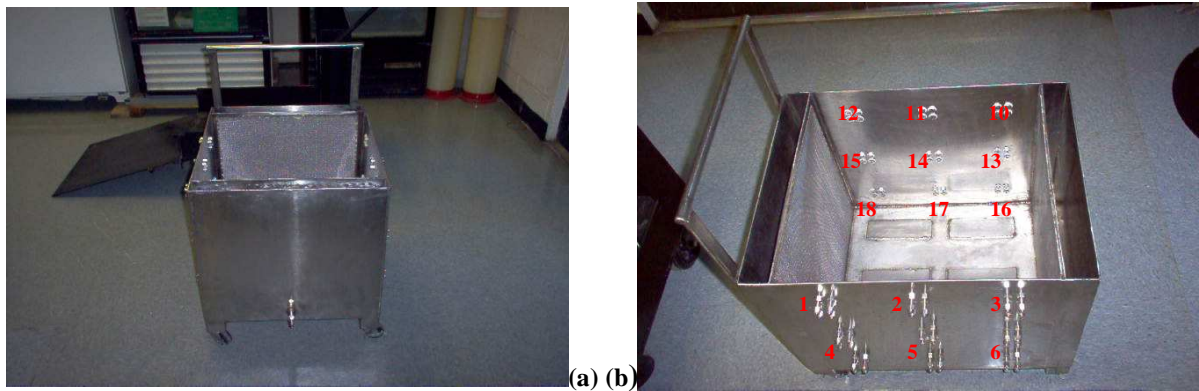
Figure 3-2. 3D-SoilBed System a). Frontal view. b). Aerial view.

The SoilBed Tank has a weight of 53.4 kg when is empty and a total volume of 92125 cm^2. It contains clusters of temperature, concentration, and pressure sampling ports access. Each lateral side of the SoilBed houses nine clusters of four sampling port access holes, which are identified with their sampling ID number in Figure 3-2b. Each cluster has two levels with two holes per level: the upper perforations serve to measure soil-water pressures and water concentration, the lower level perforations were used to measure gas-phase pressures and vapor concentrations. More details on the arrangements of these sampling clusters are given on section 3.1.1.3.

66

3.1.1.1 Soil Properties

The 3D SoilBed tank was filled with beach sand from Isabela, Puerto Rico, the sand is mostly comprised of quartz and calcite (Molina et al, 2006). It is composed of 92.6% sand sizes, and 7.4% of fines (silts and clays) having a particle size distribution (Figure 3-3) characteristic of a fairly homogeneous sand.
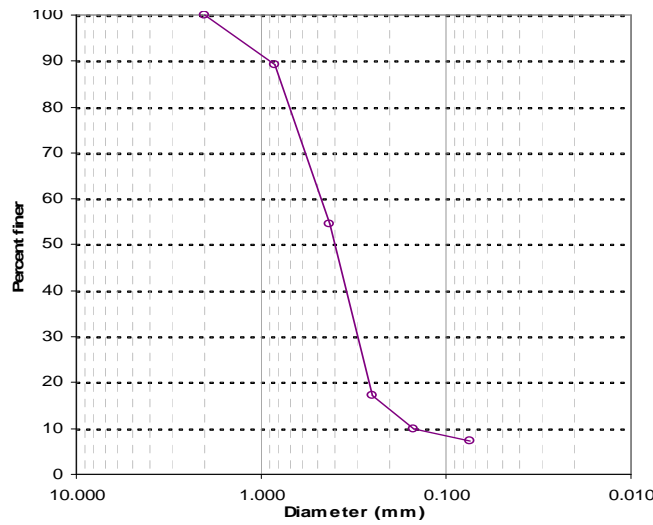
Figure 3-3 Particle size distribution for Isabela sand. Source: Modified from Molina et al. (2006)

The size of particles lower than 60 and 10% of the sample (D_{60}=0.49 and D_{10}=0.16, respectively) yields a coefficient of variation (C_u= 3.06) less than 4, indicating a poorly graded or highly uniform soil (Fetter, 1999). Other physical and chemical properties of the sand are given in Tables 3-1 and 3-2.

Table 3-1 Physical characteristic of Isabela sand. Source: Molina et al., 2006

Soil	USCS Classification	Specific Gravity (g/cm³)	Specific Surface Area m²/g	Mineralogy
Isabela Sand	SP	2.83	1.687	Quartz/calcite

Table 3-2 Chemical characteristic of Isabela sand. Source: Molina et al., 2006

Ca^{+2} (ppm)	Mg^{+2} (ppm)	Na^{+1} (ppm)	HCO_3^- mg/kg	CO_3^- mg/kg	Cl^- (ppm)	FOC %	OM %	TFe mg/kg	TN mg/kg	pH	CEC (mg/100g)
275.00	36.40	36.40	2.00	<1.00	59.00	0.07	0.47	6125.70	<713.00	8.83	2.10

3.1.1.2 Soil Packing

The soil was packed to a bulk density of 1.63 g cm^{-3} and a porosity of 0.42 using a technique developed by Rodriguez et al. (2006). The packing technique is illustrated in Figure 3-4.

(a)   (b)

(c)   (d)
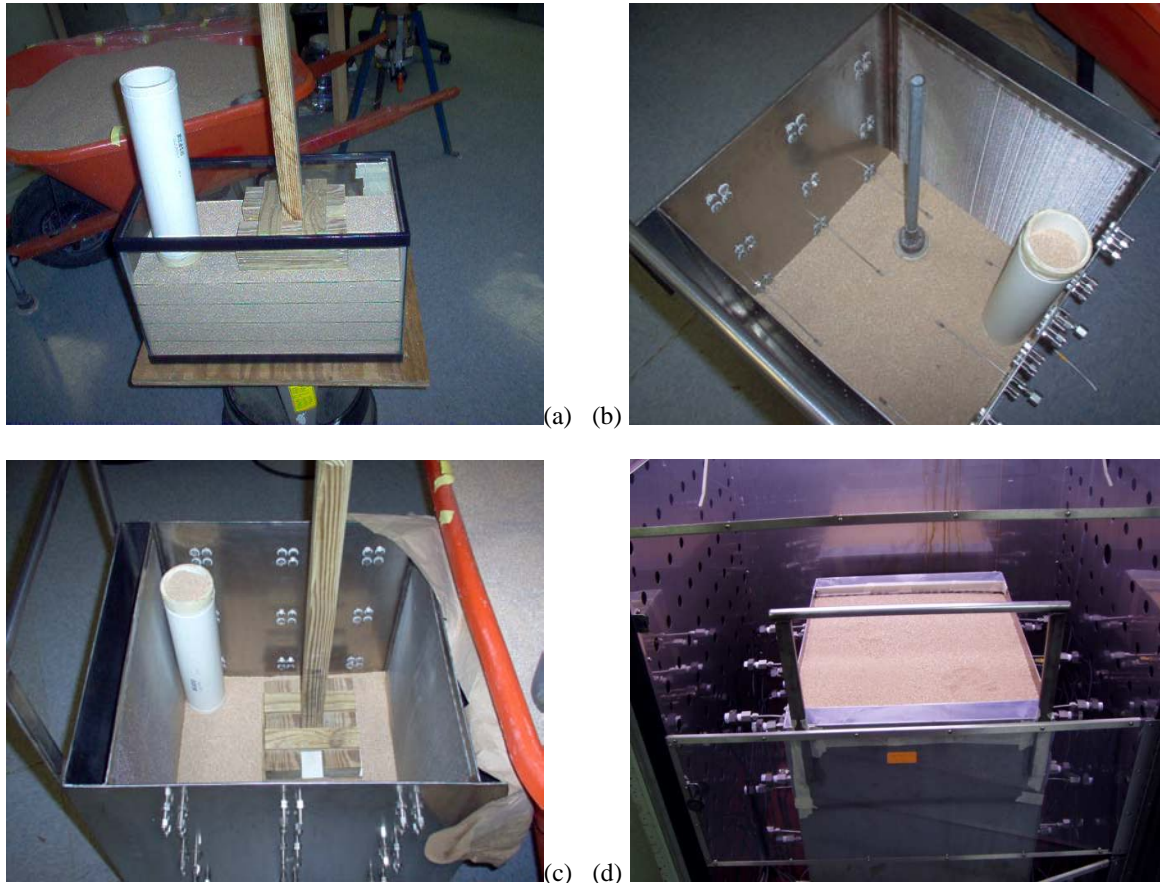
**Figure 3-4 Packing Process. a) Initial test b) Packing near to the porous cup
c) Packing far to the porous cup d) Final Packing process**

Briefly, a 10.2 cm diameter pipe is entirely filled with sand and used to pour the sand over the tank area in intervals of 2.54 cm (1 in) layer thickness. A small separation (1 cm) between the pipe and the tank is use while pouring the sand to avoid size-segregation and obtain homogeneous distributions of particles. The tube is moved horizontally over the area of the tank until the 2.54 cm layer is obtained (when a 10 cm soil drop of observed in the

pouring tube). After laying each layer, the soil was compacted using two different pistons. With this procedure the grains segregation and layers formation is reduced, enhancing the homogeneity of the packed soil. This method allowed to obtain reproducible and consistent bulk densities of 1.63 ($\pm$ 0.2) g/ cm^3 and porosities of 0.42 ($\pm$ 0.2). The bulk density (B$_d$) and media porosity (n) were calculated using the followings equations:

$$B_d = \frac{Ms}{Vt} \qquad \qquad \textbf{3-1}$$

$$n = 1 - \frac{B_d}{\rho_s} \qquad \qquad \textbf{3-2}$$

where M$_s$ is the mass of dry soil particles (g), Vt is the volume of soil (cm^3), and ρ_s is the particle density.

3.1.1.3 Environmental Devices and Samplers

Pressures transducer, and pores samplers were used to monitoring the pressures and concentration in both aqueous and gas phases. As previously described, the SoilBed was equipped with temperatures, pressures, and concentrations sensors and samplers. A thermocouple type J was used to monitor temperature in the soil surface, and was placed at the center of the SoilBed tank above the landmine. The thermocouple was calibrated by immersing it in water with different temperatures and establishing its relationship with the difference of voltage. Clusters of pressure and concentration samplers were used to monitor spatial pressures and concentrations in the aqueous and vapor phases. Pressure and concentration sampling clusters were distributed in three layers located at 9, 24, and 36 cm from the bottom of the SoilBed tank (Figure 3-2 and 3-5). Six gas-phase samplers were also

at the soil surface. Each layer contains 6 clusters located in two rows at 15 and 30 cm from the width origin (Y0), and .5, 23.5, and 38.5 cm from length origin (X0). The samplers consist of stainless steel porous cups (Mott Corporation, CT). Porous cups of 5 (Figure 3-6b) and 100 μm average pore size were used to sample the soil-water and gas phases, respectively. Previous studies (Padilla et al, 2006) have shown that the selected pore sizes were appropriate to selectively sampling water or air, provided that the sampling vacuum did not exceed the bubbling pressure of the porous cup during water sampling. The concentration tubing sampling was connected to stainless steel porous cup (Mott Corporation, CT) attached to 3.175 mm (1/8") stainless steel tubing with different lengths. Concentration samplers are connected to automated sampler valves used to maintain negative water potentials in the samples. The surface – volume of control bordered by porous cup is showed in the Figure 3.5.
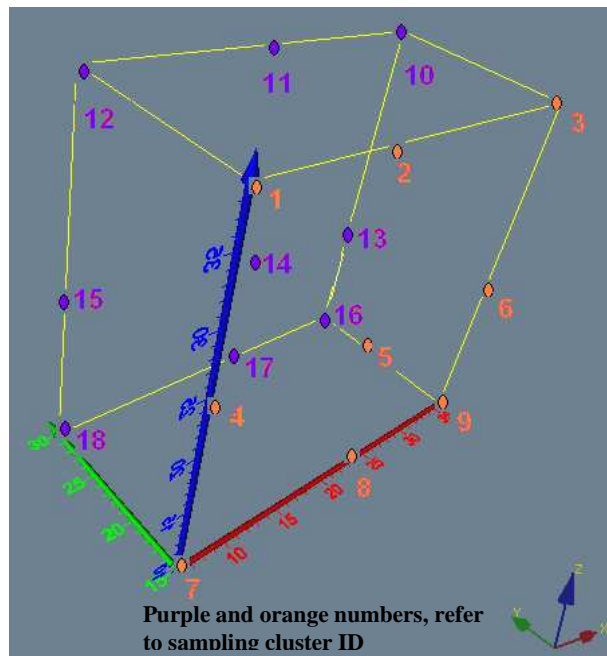
Figure 3-5 Surface and volume of control

Pressure samplers were used to monitor soil-water content and pressures and soil-gas pressure, and determine flow conditions. Pressure samplers were coupled to digital pressure sensors (PC256GW, Honeywell) (Figure 3-6a). The sensors were connected to a relay multiplexer a.m. 16/32 and a data acquisition system controlled by a computer and a data logger (model CR 5000, Campbell Sci., UT). This system recorded the voltage signal of the pressure transducers and allowed real-time monitoring of soil-water and air pressures. The relationship between the voltage signal and pressure transducers was obtained through a calibration process, in which sensors were placed in a stainless steal manifold system that was connected to a vacuum pump (Model 2545B-01, Welch), a pressure regulator (Model 44-50, Siemens), and to a digital manometer (Model 407910, Extech Instruments). Controlled pressures were set in the manifold and changes in voltage signal were recorded for changes in an input pressure. Calibration relationships were highly linear for all sensors. (Figure 3.7). Calibration relationships for all pressure sensors used in this work are given in Table A.1.2 (appendix A).
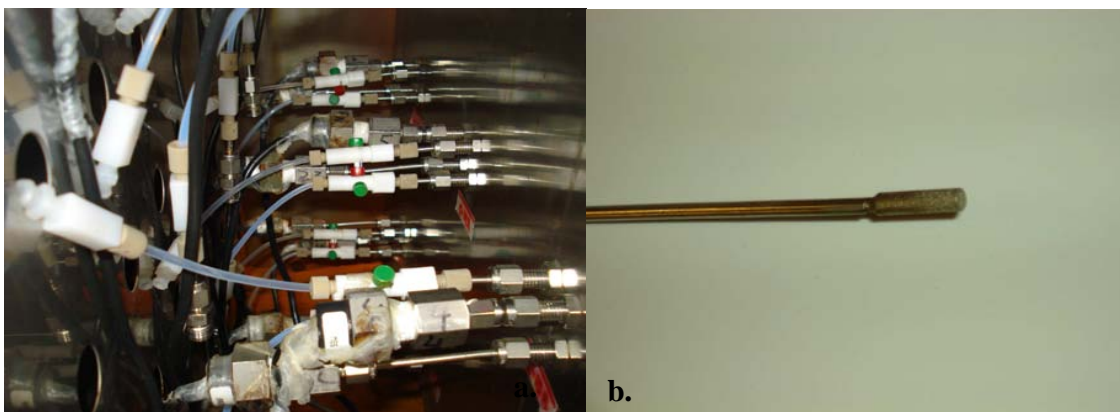
Figure 3-6 Environmental devices and samplers. (a). Pressure transducers (b). Porous cups

71
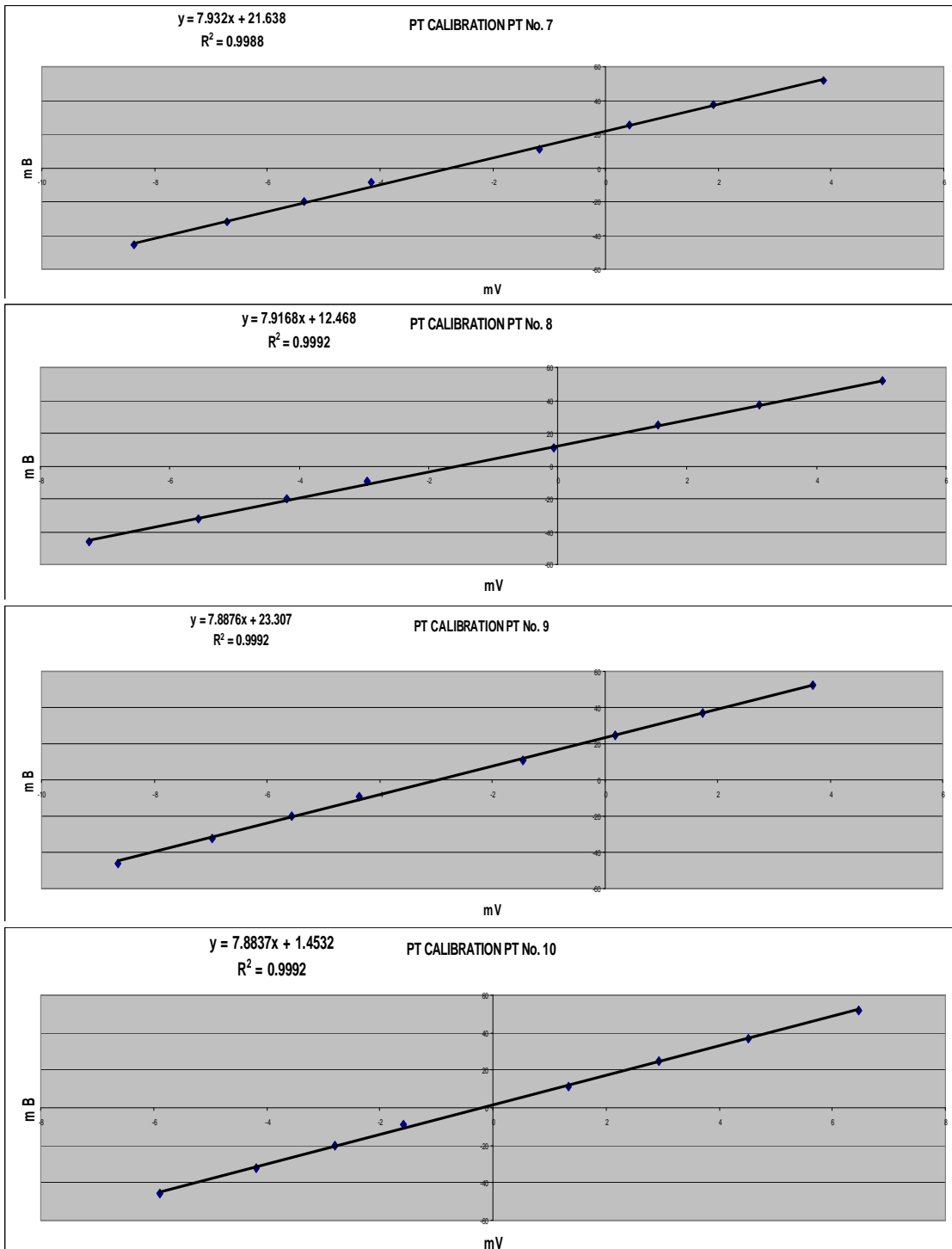
Figure 3-7 Calibration curves for some pressure transducers devices

72

3.1.1.4 Flow Extraction System

A drainage boundary condition was established at the bottom of the SoilBed by applying a negative pressure of 100 mBars through the bottom porous plate. The vacuum was applied using a peristaltic pump (Master flex-Cole Parmer, IL) connected to a sealed compartment under the porous plate (Figure 3-1b). The pump is connected to the compartment with a pressure hoses fitted to a drainage outlet located at the bottom of the tank, which served to monitor the applied vacuum. The hose connection contained a series of valves and two vacuum-sealed water storage containers (Figure 3-1). The 55-gallon tank (Nalgene, NY) stored water drained from the SoilBed and maintained constant vacuum heads. The bottom boundary also allowed bottom-up saturation of the boundary SoilBed and the placements of water table conditions.

3.1.2 Environmental Chamber

The SoilBed was placed within an environmental chamber (Forma Scientific Inc, OH. model 4940; Figure 3-1) designed to control temperature (-30 - 60 ^{0}C) and relative humidity (0-100%). The internal dimensions are 75cm x 90cm x 180cm and its total volume is 1.2 m^3. An external data logger (Extech instruments, MA, model 42270; Figure 3-8) was located into the environmental chamber to record temperature and relative humidity every 60 seconds. The environmental chamber was equipped with rainfall and solar radiation simulators used to control environmental and climatic conditions. The rainfall simulator and visible and UV

lamps are located above the SoilBed in the environmental chamber (Scientific Campbell, UT; Figures 3-1 and 3-8).
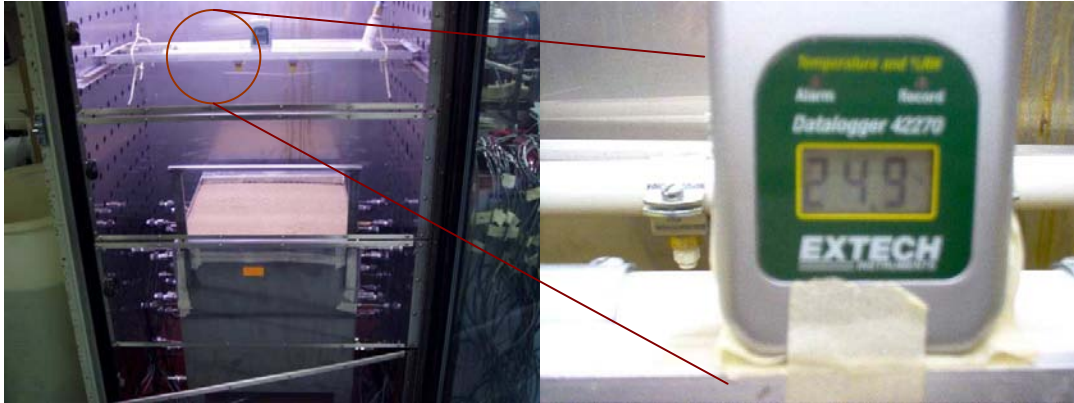
Figure 3-8 External temp-HR data logger

3.1.2.1 Rainfall Simulator

The rainfall simulator is comprised of four Sf-CE2 nozzles (Spraying System co, Wheaton, IL), which distribute the water into a circular surface forming an internal angle of 105 degrees. Water is fed to the simulator using a water delivery system consisting of a 55-gal water reservoir connected to a centrifuge pump (Flotec, WI). Two ball valves control the pressure delivered to the nozzle. A pressure gauge and a flow meter are used to monitor water pressure and the flow in the simulator inlet.

3.1.2.2 Solar Radiation Simulator

A set of lamps simulate solar daylight radiation in the visible (380 – 760 nm) and ultraviolet (320-400 nm) region. Five visible-light bulbs (20 watts cool-white fluorescent lamp, Sylvania GRO-LUX® Wide Spectrum) provide the required photo synthetically active radiation (PAR) over the tank area (26 watts PAR and 3,750 Lumens). The light source for

the UV range is a Raytech Versalume lamp. This lamp has an UV output of 75 watts m^2 and emits at wavelengths of 360 nm.

3.1.3 Sampling System

Both aqueous and gas sample extraction systems were developed to obtain representative ERCs samples, spatially and temporally. The sampling system is generally composed of the porous samplers (Figure 3-6b), on-off valves (mininert, Upchurch Scientific), flexible EFTC tubing and fittings, stainless steal syringe connections, and a glass syringe. The system used for water and vapor sampling are described below.

3.1.3.1 Aqueous Sampling System

Aqueous samples were extracted from the upper row in each sampling cluster. Aqueous samplers integrate the 5 μm samples connected to a luer-lock glass syringe through an on-off valve, EFTC tubing, and 10-32 Teflon union (Upchurch model) and fittings (Figure 3-9).

Figure 3-9 Aqueous sampling system

3.1.3.2 Gas- phase Sampling System

Gas samplers were withdrawn from to the lower row in each cluster. The gas-phase sampling system consist of 100 μm sampler connected to a Solid Phase Extraction (SPE) cartridge, which was packed with XAD-2^{TM} (Supelco, PA) following the procedure established by Acevedo et al. (2007). SPE cartridges for air sampling were assembled in our laboratory. The cartridges consisted of Teflon tubes (4.0 cm long, 0.6 cm ID) packed with XAD-2 resin (Figure 3.12). They contain a PTFE frit at the bottom and glass wool at each end to retain the resin and were packed with approximately 0.10-0.12g of resin to attain a packing density between 0.3-0.4g/cm3. The pore volume of the packed resin was approximately 300μL. The SPE cartridge was fitted with Swagelock® fittings at each end to allow rapid installation and removal from sampling ports, and sample storage. Figures 3-10 and 3-11 show procedure developed by Acevedo et al, (2007).

(a)   (b)
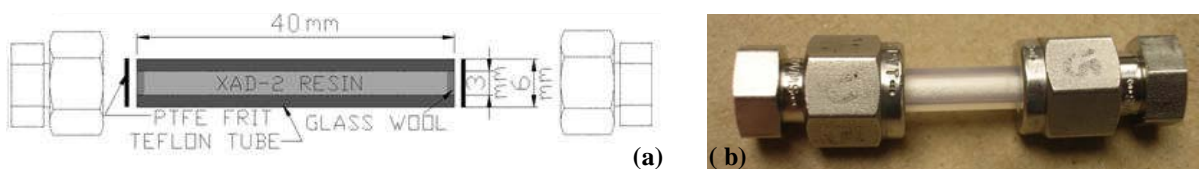
Figure 3-10 Air sampling cartridge a) Design   b) Actual view

Figure 3-11 Typical gas sampling arrangement

3.1.4 Data Acquisition System

All pressure transducers (18 recording water pressure, 18 recording air pressure, and one recording suction pressure at the SoilBed water outlet) and the thermocouple were connected to a data acquisition system consisting of a relay multiplexer a.m. 16/32 (Campbell Sci., UT) interphased to a data logger (model CR 5000, Campbell Sci., UT; Figure 3-12) connected to a computer. The acquisition system was used to monitor and store pressures and temperature in real time. A relay multiplexer, which adds 32 monitoring and recording channels, was used because the limitation of ports available in the data logger (only 20 ports). Thirty-two (32) pressure transducers were connected to the relay multiplexer, and the relay output was connected to the data logger. The remaining 5 transducers and the thermocouple were connected directly to the data logger singles ports.

(a)   (b)
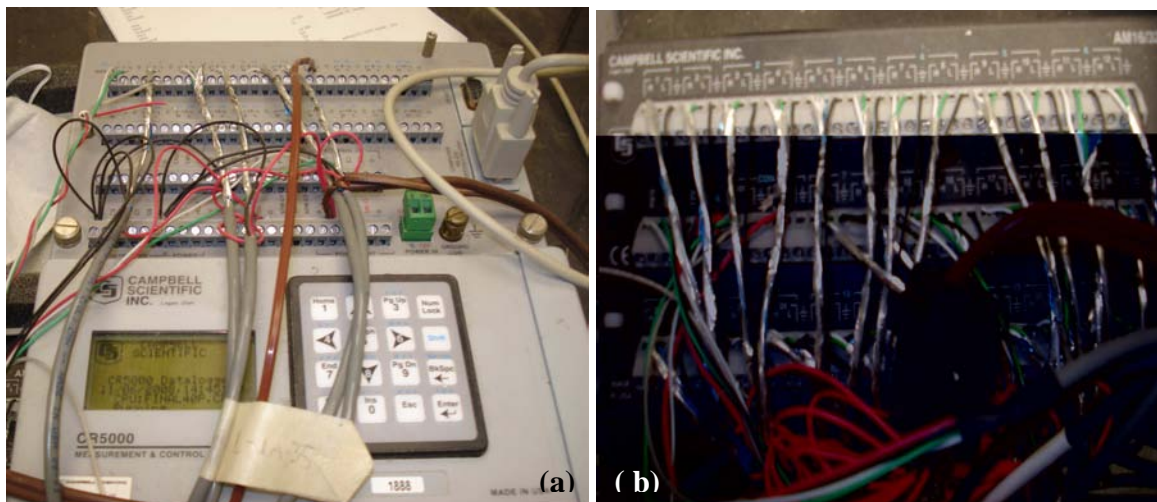
Figure 3-12 Data store system. a) Data Logger CR5000. b) Relay multiplexer 16/32

3.2 Experimental Methods

Different experiments were conduced to analyze the influence of environmental variables in soil water flow, and in the fate and transport of explosive related compounds. Several experiments were conducted to characterize the hydraulic response to different experimental settings in the physical model under atmospheric conditions. Another set of experiments involved burying of a DNT/TNT source under the soil surface, and monitoring their concentrations in the aqueous and vapor phases under different environmental settings.

3.2.1 Soil Hydraulic Properties

Soil hydraulic properties including, hydraulic conductivities, and the soil-water characteristic function parameters were estimated using pedotransfer functions (PTF) that translate basic soil data into hydraulic properties. This research applied PTFs incorporated in the ROSETTA code (Schaap et al., 2001). PTFs generate soil characteristics from other, easily measured and more available soil property data. ROSETTA generates the van Genuchten parameters (α, m, n, θ r; equation (2-13)) from particle-size distribution (Figure 3-3) and dry density (1.63 g/cm^3) data. Estimates of saturation-dependent hydraulic conductivities were generated using the van Genuchten parameters and an estimated saturated hydraulic conductivity (Ks).

3.2.2 *Hydraulic Response Experiments*

A series of experiments were performed to analyze the influence of the rainfall periods, visible radiation, and temperature on the soil hydraulic conditions, water flow, and solute transport. The experiments involved draining and wetting the soil under different light and temperature conditions (Table 3-4). Wetting phases corresponded to periods of rainfall and infiltration conditions. Drainage was imposed under periods of no rainfall and was always started from saturated conditions. Prior to drainage experiments, the soil was slowly saturated from the bottom by pumping 0.7 cm^3/s distilled water into one on the lateral boundary compartments. After saturation, static water levels were set slightly above the soil surface and all water-pressures at sensors were recalibrated were calculated in–situ using the water column height above each sensor. Drainage experiments started at the onset of the vacuum boundary condition at the SoilBed bottom. Boundary conditions in the SoilBed were set at -100 mbars at the bottom, atmospheric pressures on lateral boundaries, and atmospheric boundary with rainfall or evapotranspiration at the top.

After drainage, infiltration experiments were conducted by applying a rainfall intensity of 1.41x 10^{-3} cm s^{-1} (5.01 cm hr^{-1}), which corresponds to rainfall for tropical environments. The radiation conditions were imposed on the top and were set constant (i.e., light or no light) from the beginning of each experimental set. Soil-water and soil-gas pressures, and atmospheric temperature and relative humidity were monitored throughout the experiments. Soil-water and -gas pressures were monitored in 18 pressure transducers located in each of

the sampling clusters. Three set of experiments were conducted (Table 3.3): the first experiment involved drainage and wetting at a constant temperature under no light exposure; the second involved drainage and wetting at a constant temperature with light exposure; and the third one involved drainage and wetting in an open system at room temperature with light exposure. The third experiment included the influx of a NaCl solution during the infiltration processes. This experiment was conducted to characterize advective and dispersive transport of non-reactive solutes.

Table 3-3 Summary hydraulic response conditions

Experiment	Flow Condition	Light[1]	System Condition[2]	Atmospheric Temperature (ºC) (Set)	AVERAGE TEMPERATURES (ºC)	STDEV	Solute
HR-1	Drainage	∅	Closed	24°C Controlled	23.57	2.88	Water
HR-2	Wetting	∅	Closed	24°C Controlled	22.48	1.65	Water
HR-3	Drainage	☼	Closed	24°C Controlled	31.54	3.65	Water
HR-4	Wetting	☼	Closed	24°C Controlled	17.35	1.18	Water
HR-5	Drainage	☼	Open	23°C Room	26.03	2.19	Water
HR-6	Wetting	☼	Open	23°C Room	24.07	2.96	Water, NaCl

A transport experiment was conducted using NaCl as a conservative tracer during the infiltration events in experiment HR-6 (Table 3.3). The experiment was conducted by placing 13.4 grams of NaCl over a soil surface area of 15 cm x 30 cm at the center of the SoilBed. The experiment was designed to assess the dissolution and transport of NaCl with the infiltrating rainfall. Soil solution samples (2 ml) were taken spatially at 15-minute intervals in 10 ports (2, 5, 8, 4, 6, 11, 14, 17, 13, and 15).

NaCl concentrations were analyzed by measuring the specific conductance of the solution using a flow-through conductivity detector (Alltech 550, IL). For each sample, 0.5 ml were injected into a 1 ml min^{-1} flowing stream of distilled water passing through the detector.

3.2.3 Transport Experiments of ERC's

A series of experiments were performed in the 3D SoilBed System to analyze the effect of variable and interrelated environmental processes and conditions (precipitation, infiltration, evaporation, water content, temperature, radiation) on multidimensional advective, dispersive, and reactive processes controlling the fate and transport of TNT, DNT, and other chemicals (NaCl and potential TNT and DNT byproducts) in the sandy soil. The experiments involved burying a point-source chemical (TNT, DNT, and NaCl) in the horizontal center of the tank, near the soil-atmospheric surface (~ 6 cm from the soil surface), and applying different environmental conditions. Sodium chloride was used to evaluate the transport behavior of an un-reactive solute tracer and will serve to determine advective and dispersive physical transport properties of the system under given environmental conditions. NaCl was dissolved in the rainwater to a concentration of 20 mM.

Pressures, temperature, and chemical concentrations in the soil-water and soil–gas phases, and atmosphere above the soil surface were monitored temporally and spatially. TNT and DNT crystals were placed in a round, wire-framed nylon bag with a bubbling pressure of 30 mbar, to simulate a source from a landmine like object (Figure 3-13).
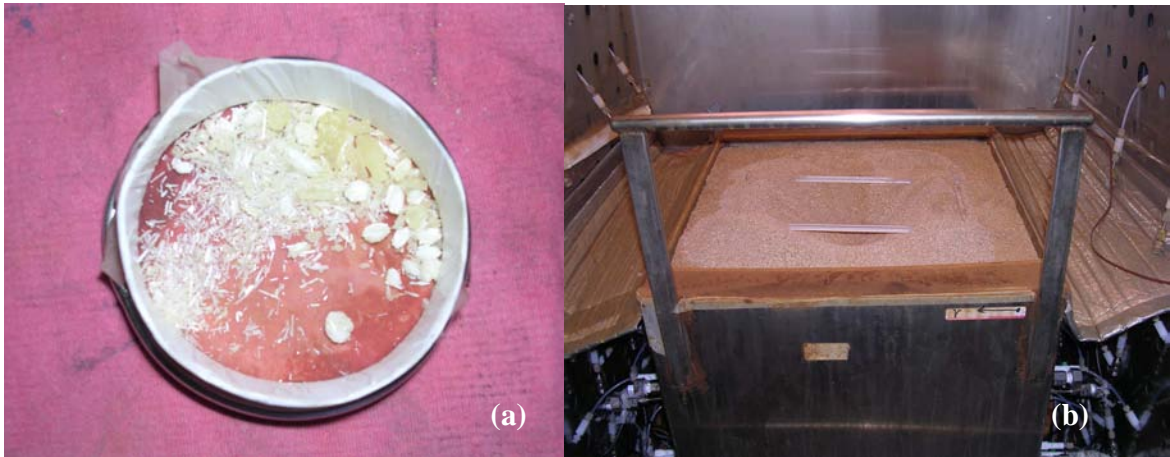
Figure 3-13 Landmine simulation (a). DNT/TNT crystal inside simulated landmine (b). Location inside 3D Tank

Variable environmental conditions in the SoilBed were attained by imposing variable, but controllable environmental settings: precipitation intensity, atmospheric temperature, visible and UV light radiation, and boundary conditions (see Table 3-4 – experimental matrix). These settings affect other environmental processes and conditions in the soil system, including: infiltration, drainage, water content, and soil temperature. The effect, however, depend on the interrelation among all of these environmental conditions.

After burying the chemical point-source in the soil, precipitation was applied at a given intensity for a given period (i.e., duration). Following the precipitation event, the infiltrated water percolated or evaporated through the system according to the conditions imposed in the system. Rainfall and light radiation cycles were applied on a daily basis for a given number of days (Table 3-4). The cycles were configured to represent the tropical environment of the Mayaguez area. Rainfall was applied daily at different rates (Table 3-4) for 2 hours, and was

followed by a period of 22 hr without rainfall. Visible and UV radiation was applied for 12 hours, and was followed by 12 hours of no radiation. The radiation periods (6 am-6 pm) were set to represent a 12-hr cycle in tropical environments. Rainfall periods were applied to coincide with hours 7 to 9 of the daylight period, which represent the period between 1 and 3 pm in Mayaguez, PR. Note that experiment TE-6 (TE-3R) is a replicate of experiment TE-5 (TE-3ERC).

Table 3-4 Experimental matrix transport experiments

Exp.	Chemical	Mass	Intensity and Duration[1]	Duration Cycle[2]	Atmospheric Temp. °C	Exposure Area	Light[3]
TE-1 (1ERC)	TNT- NaCl	600mg-20mM	P1/No P 2/22 Hr	14	25	Landmine Diameter 1in	☐12☼12
TE-2[**] 2ERC)	TNT/DNT- NaCl	750/750mg- 20mM	P1/No P 2/22 Hr	14	25	Landmine Diameter 2in	☐12☼12
TE-3[**] (3ERC)	TNT/DNT- NaCl	750/750mg- 20mM	P1/No P 2/22 Hr	14	35[*]	Landmine Diameter 2in	☐12☼12
TE-3R[**] (3R)	TNT/DNT- NaCl	750/750mg- 20mM	P1/No P 2/22 Hr	14	35[*]	Landmine Diameter 2in [2]	☐12☼12
TE-4 (4ERC)	TNT/DNT- NaCl	750/750mg- 20mM	P1/No P 2/22 Hr	14	15[*]	Landmine Diameter 2in [2]	☐12☼12
TE-5 (5ERC)	TNT/DNT- NaCl	750/750mg- 20mM	P2 /No P 2/22 Hr	14	25[*]	Landmine Diameter 2in [2]	☐12☼12
TE-6 (6ERC)	TNT/DNT- NaCl	750/750mg- 20mM	P1 /No P 2/22 Hr	7	25[*]	Landmine Diameter 2in [2]	☐0☼24

(1) P1 = 2 in/hr;⁻ P2= 0.5 in/hr; No P= period of no precipitation

(2) Number of rainfall/no rainfall cycles per experiment in days

(3) ☼ with light exposure; ☐ no light exposure in hours

(*)   Enabled Soil Surface temperature (thermocouple)

(**) Enabled ERCs Air Samplers

3.2.4 Sampling Methods

A sampling scheme (interval and location) was designed on the basis of the system conditions. Although samples were taken in all sampling ports, the sampling interval varied temporally. A greater number of samples were necessary after the system changes (e.g., precipitation changes), but were reduced as the system tends toward equilibrium. Because samples are taken manually, samplings intervals were of about 30 minutes. Sampling volumes were limited by the water content of the soil, but were lower than 2 ml to minimize any effect on the transport patterns during sampling. Sampling volumes were based on results of experiments conducted by Padilla et al. (2006), which determined the limiting sampling volumes under given water contents. Aqueous samples were directly withdrawn from the liquid sampling ports using a glass syringe. The samples were transferred directly into analytical vials and stored properly for chemical analysis. Gaseous samples were withdrawn through Solid Phase Extraction (SPE). Gas volumes of 1.2 and 1.4 ml were extracted from samples in the soils and on the soil-surface, respectively. After air samplers were taken, cartridges were removed and stored properly for analysis. Cartridges were stored at 4 ^{o}C for less than 3 days prior to solvent extraction with isoamyl acetate (sigma Aldrich, 99.9% purity). Solvent extraction was conducted by injecting a 1.0 pore volume (0.2 ml) of the solvent into the cartridge and eluting it with 2 porous volume after a contact time of 1 hour. Extracted solvent was collected in 2.0 ml GC vials (amber), and stored at 4 ^{o}C prior to analysis. The procedure by air sampling extraction is shown by Figure 3-14.

Figure 3-14 SPE extraction procedure after air sampling

3.3 Chemical Analysis

Experiments were conduced using 2,4,6 TNT and 2,4 DNT as representatives ERCs used in landmines. NaCl (Fischer, NJ) was used as aqueous conservative tracer.

3.3.1   Reagents

The chemical reagents used in the experimental methods are listed in Table 3-5 summarizing each one of this reagents and theirs characteristics. Hydrated TNT and DNT crystals were used for simulation of buried point source. Acetonitrile standards were used for instrument calibration. Isoamil acetate was used as extraction solvent and for preparation of GC standards. Dionized water was used to prepare aqueous solution used in wetting, draining, and transport expedients. It was also used with methanol in the aqueous analysis of TNT, DNT, and related chemical using high-pressure liquid chromatograph (HPLC). XAD-2 was used as the SoilBed phase for SPE sampling. Acetone was used to clan up all the labwork used in the experiments.

Table 3-5 Summary of reagents used in the experiments

Chemical Name	Characteristics	Dealer
2,4,6 TNT	Hydrated (30% minimum water) Crystals with >99% Purity	West Chester, PA
2,4 DNT	Hydrated (30% minimum water) Crystals with >99% Purity	West Chester, PA
2,4,6 TNT	Standards diluted in Acetonitrile	Restek, PA
2,4 DNT	Standards diluted in Acetonitrile	Restek, PA
Isopentyl Acetate anhydrous	>99% Purity	Sigma-Aldrich, MO
Sodium Chloride	Certified by ASC	Fisher Sci, NJ
Methanol	>99% Purity Grade HPLC	Sigma-Aldrich, MO
TNT By products isomers	Standards diluted in Acetonitrile	AcuStandard, MO
XAD-2 resin	Ultra Clean Resin XAD-2	Restek, PA
Deionized water	Type I water	EEL-UPRM
Acetone	>99% Purity	Sigma-Aldrich, MO

3.3.2 Tracer Concentrations

Sodium chloride concentrations were analyzed by measuring the specific conductance (SC) of the samples in a flow-through Conductivity Detector (Model 550, Alltech). The conductivity detector was connected to a high pressure liquid chromatography (HPLC) pump delivering a constant flow of 1.0 mL/min of distillated water. A 0.5 mL of each sample was injected in a high-pressure switching valve (Model 7000, Rheodyne), which introduced the sample into the water stream hawing toward the detector. A Peak Simple Chromatography Data System (Model 203, SRI) was used to obtain the signal from the detector, integrate the pulse response, and determine the electric conductivity. The relationship between NaCl concentration and the area of the peaks were highly lineally. The calibration function was

developed using several NaCl standards: 2, 5, 10, 15, 20, 30, 40 mM. a typical NaCl calibration curve is shown in by the Figure 3-15.

CALIBRATION CURVE (EXPERIMENT 5)

y = 0.4675x - 0.6286
R^2 = 0.9997
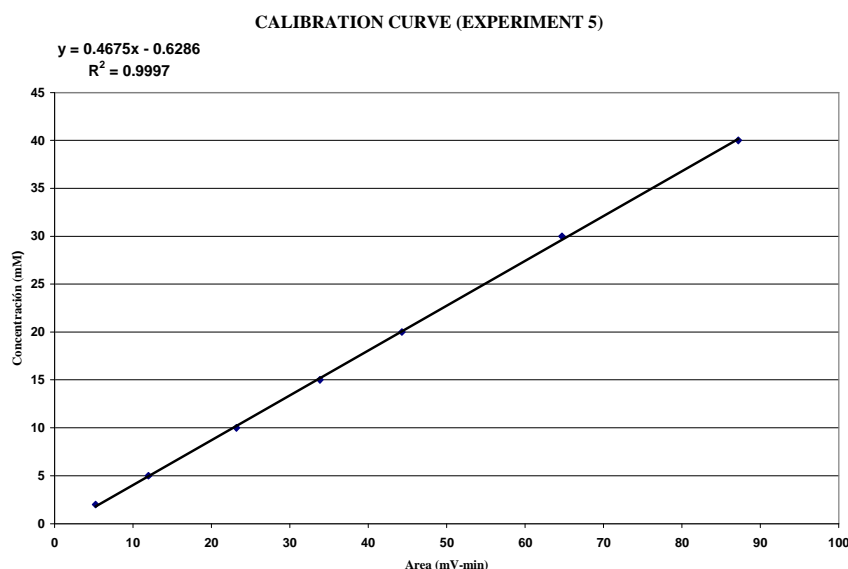
Figure 3-15 Calibration curve for NaCl (TE- 5)

3.3.3   *Aqueous Phase Concentrations of ERC's*

Aqueous TNT, DNT, and potential by-product concentrations were analyzed in a HPLC following the EPA method 8330 (EPA, 1994) and others methods developed in the Environmental Engineering Laboratory at UPRM. Water samples were analyzed in a S200 HPLC (Perking Elmer, CT), equipped with an ultra violet detector with deuterium lights (Figures 3-15). The analytical wave length was set at 254 nm. A 25-cm HPLC column (Supelco®, Ascentis C18) was used to separate the analyses using a 30:70 water: methanol mobile phases at a flow rate of 1 mL/min (Figure 3-16).
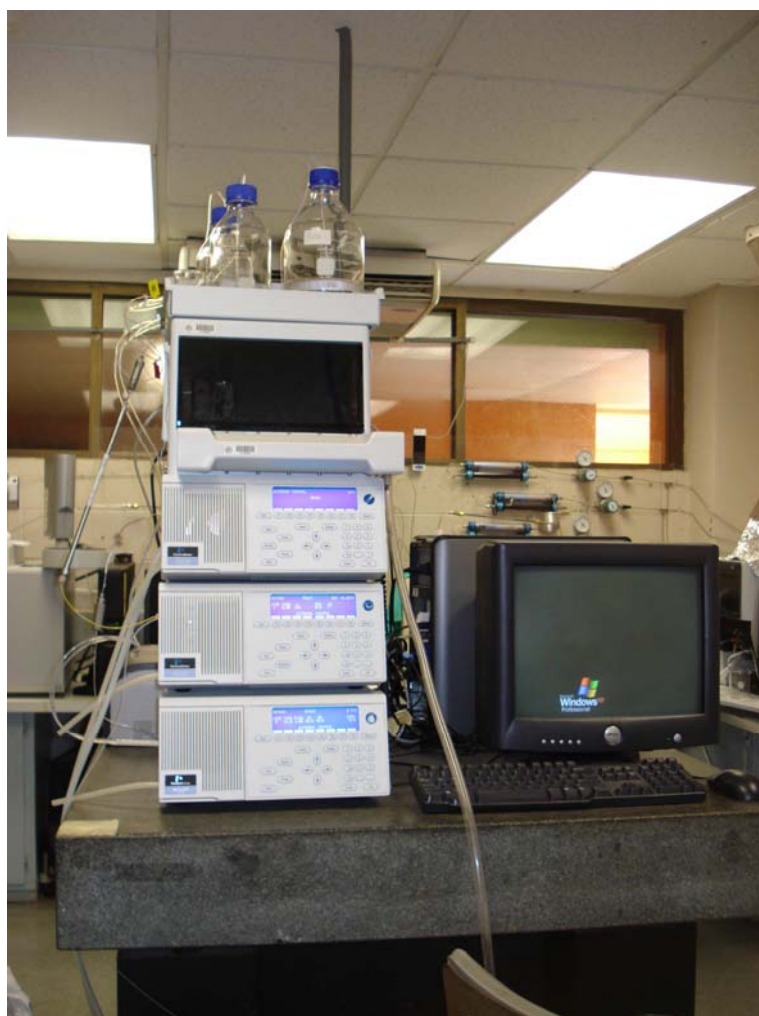
Figure 3-16 HPLC S200 Perkin Elmer

HPLC standards were prepared using Restek and Acustandard reference standards, and were stockpiled in the vial auto sample at 10°C. The calibration curve was constructed with several ERCs aqueous standards: 20, 50, 100, 500, 1000, 2000, and 5000 µg/L. The relationship between TNT and DNT concentrations and the area of the peaks given by the HPLC, were highly linear (Figure 3-17).

Figure 3-17 Calibration function by ERCs (Experiment 5)

3.3.4 Gas- phase Concentrations of ERC's

Gas-phase samples were obtained by withdrawing air samples through SPE sampling cartridges (section 3.1.3.2). the SPE cartridges were extracted with isoamyl acetate (Sigma-Aldrich, MO) (section 3-2-4), and injected into a gas chromatography (GC) equipped with an electron capture detector (ECD) and auto sampler with 100 vial capacity. GC analysis was performed in a Varian (Varian. Inc, CA) CP-3800 GC (Figure 3-18). The analysis was conducted using a 6-m long ATT M-1 (dimethyl polysilicone) column (Alltech, CA) with a 0.53 mm diameter and 1.5 μm film thickness. The detector temperature was se at 300 $^{\circ}$C. the oven was initially set at 100 $^{\circ}$C for 1 minutes, ramped to 150 $^{\circ}$C at 10 $^{\circ}$C / minutes, and

89

ramped again to 200 °C at 20 °C / minutes for a total analysis tie of 11 minutes. The injector was set at 250 °C.

Figure 3-18 CP 3800 Gas Chromatograph

3.4 Data Analysis

Hydraulic response and Transport experiments were analyzed using qualitative and quantitative models and tools. Comparative analysis allows direct assessment of the physical effects due environmental variables. Quantitative analyses allow validates from a physical or mathematical perspective.

3.4.1   *Comparative Analysis*

Comparative analysis involves comparative assessment of environmental variables, time series, breakthrough curve (BTCs), and spatial distribution models. Time series of atmospheric and soil surface temperature and relative humidity (atmospheric) were used to establish a general temporal relationship among climatic variables, such as, rainfall, evaporation, air/water pressure, heads, and radiation on flow and transport processes. NaCl, and ERCs BTCs show temporal and spatial responses of the chemical concentrations for all experiments conduced.

Pressure and total hydraulic heads (pressure + elevation) and NaCl concentrations during the experiments were analyzed spatially and temporally using several interpolation methods provided by Surfer (v. 8.0 Golden Software, CO) The methods evaluated include: Kriging, Radial Basis Function, Median Average, Triangulation with lineal interpolation, and Nearest Neighbor. The best interpolation method for the analysis was selected based on the minimum error obtained between measured and interpolated values at 4 times (30, 60, 90, and 120 minutes) for drainage experiments with and without light under controlled-temperature conditions.

Hydraulic head (energy), NaCl concentration, and ERCs concentrations were analyzed temporally and spatially using the Voxler (v. 1.0 Golden Software, CO) visualization model software. Different interpolation methods were used for each data characteristic. For continuous data (e.g., hydraulic head data), a local polynomial (order 1, power 5) method

was used. For variables with low data or non-continuous spatial data filtering and masking procedures were developed. A color masking filter was developed for the NaCl visualization model using color the Inverse Distance method (isotropy, power 10).

3.4.2   Statistical Analysis

The input and output data in this research is characterized by unequal number of response samples, having fixed and random effects, and binary and distributed components. Consequently, a GLMM statistical model was used to analyze interrelations among the environment variables that were assessed and their dependence with the response variable.

The MIX-SAS procedure was applied using a logit-type link function due to the characteristics of the output data and the distribution model. A diagonal matrix of variances and a maximum likelihood estimation were parameters established for the model. The model yielded statistical fits, odds ratio estimates, parameter estimates, Type III Tests of Fixed Effects, least squares mean analysis, test of effects slices, least means and significance graphs.

4 RESULTS AND DISCUSSION

This research addressees the effect of environmental variables on flow, fate, transport, and detection of ERCs near soil-atmospheric environments. Transport experiments were conducted in the geo-environmental system to characterize and quantify the effect of variable rainfall rates, atmospheric temperatures, and solar radiation patterns on the transport behavior of TNT, DNT and related chemical. Data collected from the experiments are given in **Table 4-1**. Data and results are presented in this chapter.

Table 4-1 Data characteristics

DATA	DATA CHARACTERISTICS
Soil-water and gas pressure	(Continuous) – spatial and temporal
Soil temperature	(Continuous) – temporal
Solute (NaCl, TNT, DNT, and others ERCs) and Vapor Concentrations	(Discrete, unequal number of samples) – spatial and temporal
Atmospheric temperature and relative humidity	(Continuous) – temporal

Data analysis involved spatial and temporal assessment of soil-water and gas pressures, hydraulic heads, soil-water content, soil temperature, and solute and vapor concentrations. Soil hydraulic properties and water contents were assessed and evaluated using pedo-transfer functions. Spatial interpolation and visualization models were developed using Surfer^{TM} and Voxler^{TM}. Breakthrough curves (BTCs) were used to analyze temporal concentrations distributions of solutes along particular sampling clusters. Temporal variation on environmental measurements (atmospheric temperature and relative humidity) were analyzed and related to environmental conditions. A generalized linear mixed statistical model (GLMM) was used to quantify the effect of environmental conditions on transport processes.

4.1   Soil Hydraulic Properties

The saturated hydraulic conductivity calculated by ROSETTA was 390 cm/d (0.27cm/min), this values is within the range estimated on others studies for the same soil (Gutierrez, 2008; Molina, 2008) and for other well sorted sands (Fetter, 2001). The Van Genuchten parameters (equations 2-13, 2-14, and 2-15) generated by ROSETTA for the Isabella sand are given in Table 4-2. These values are very similar to those reported by Gutierrez (2008) and Molina (2008). The values of L, however gave a better fit with a value of (-0.89) instead of the typically assumed value of 0.5. Kusogi (1999) and Schaap et al (2001) have previously reported values of L different from 0.5 and with negative values.

Table 4-2 Soil hydraulic parameters obtained by Rosetta

PARAMETER	VALUE	UNIT
θ_r	0.05	
θ_s	0.349	
α	0.033	
N	2.88	
K_s	390.03	cm/day
K_o	21.38	cm/day
L	-0.89	
m	0.65	

ROSETTA-estimated saturated water content (thus porosity) was lower (16%) than the estimated with equation 3-2. It is suspected that the sand particle density (ρ_s) may be lower than measured. If a value of ρ_s =2.6 (commonly used for sandy soils; Myers et al., 1998) is used with a bulk density of 1.63 g/cm^3 to estimate porosity from equation 3-2, a porosity value of 37% would be estimated. This would be closer to the value given by ROSETTA.

Gutierrez (2008) found similar results, and concluded that NaCl breakthrough curves were described better if n=0.36.

The Van Genuchten parameters (Table 4-2) were used to describe the relationships between volumetric water content, soil-water suction, and unsaturated hydraulic conductivities. These relationships are shown in the Figure 4-1, Figure 4-2, and Figure 4-3.
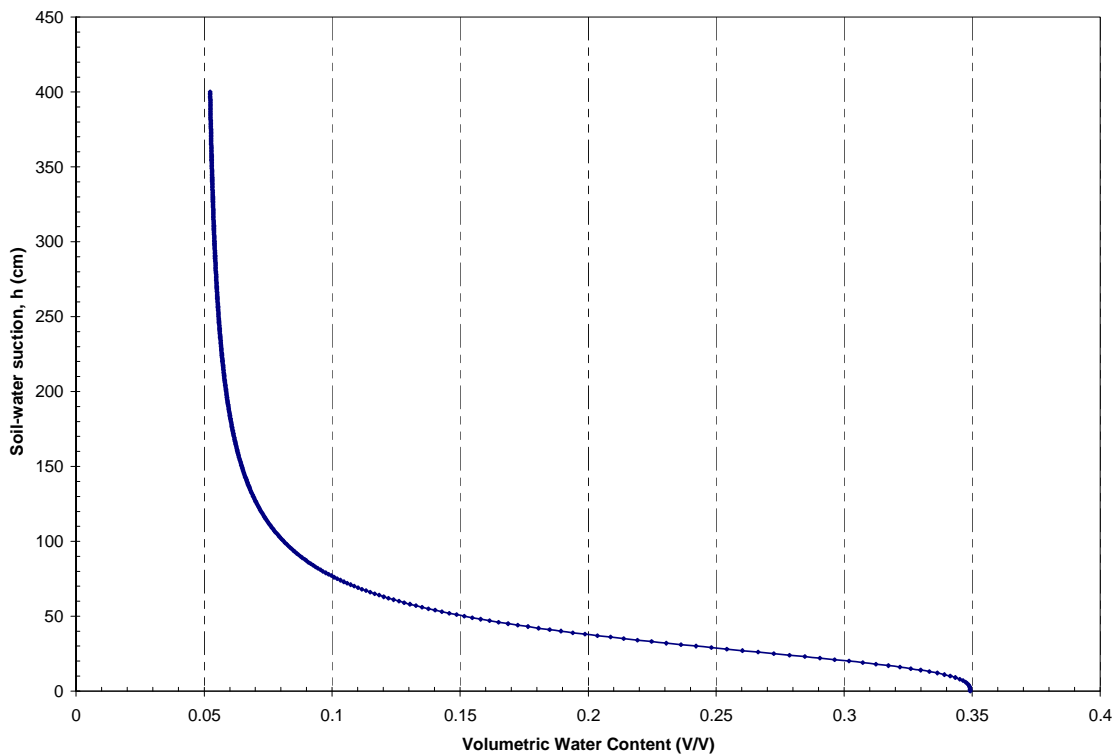
Figure 4-1 Water characteristic curve for Isabela sand
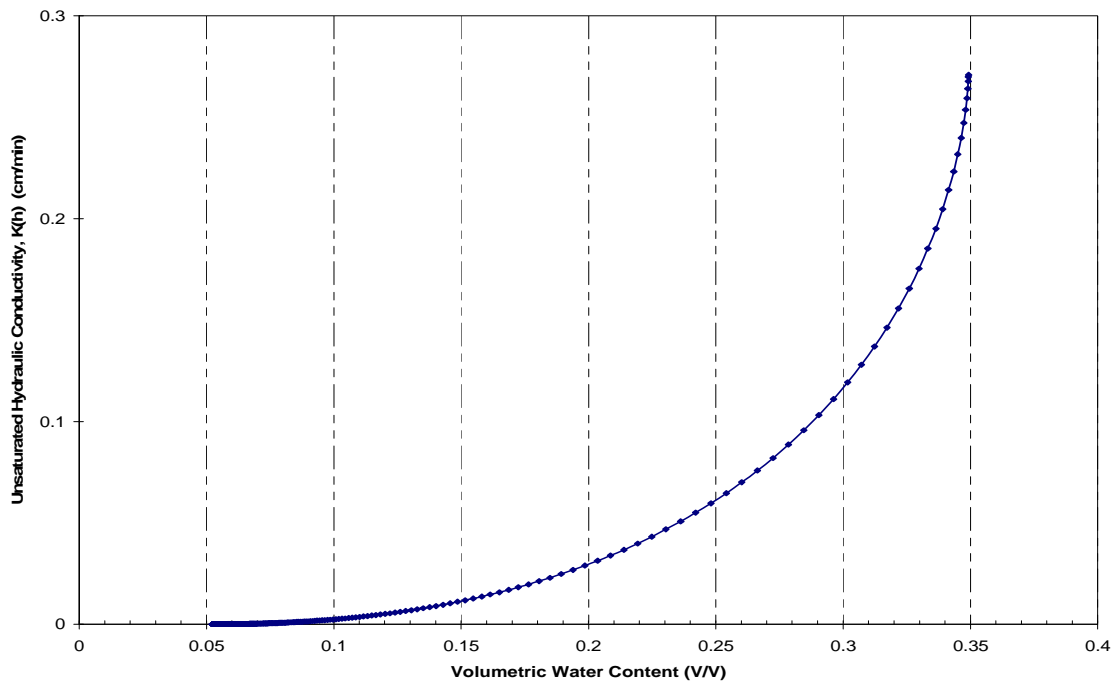
Figure 4-2 Volumetric water content vs. unsaturated hydraulic conductivity for Isabela sand
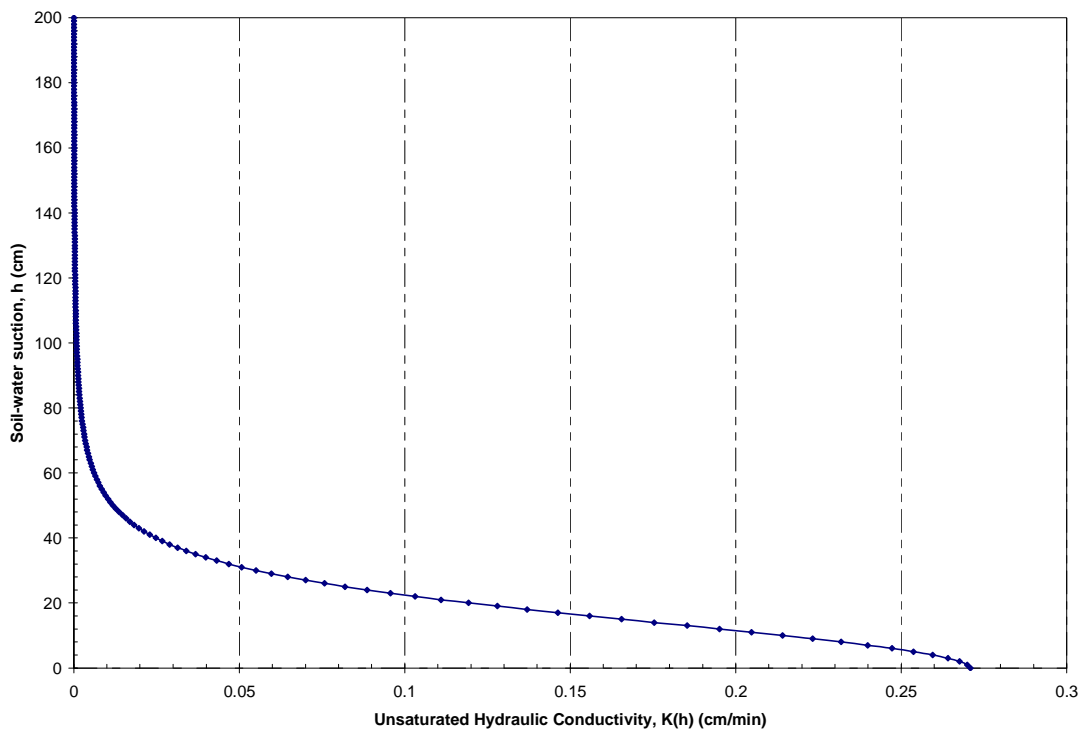
Figure 4-3 Unsaturated conductivity vs. soil-water for Isabela sand

4.2 Soil-Water Pressure and Hydraulic Head

Soil-water pressures $h_p(\theta)$ collected during the experiments were used to determine total hydraulic heads (H) and soil-water contents. The total hydraulic head refers to the energy available in the system and it is the sum of the pressure and elevation (Z) heads (datum is at bottom of the SoilBed). Spatial modeling of hydraulic heads at given time intervals is used to infer water flow patterns and advective transport processes under given environmental conditions. Spatial models of hydraulic were developed using several interpolation methods provided by Surfer^{TM} and Voxler^{TM} (Golden Software, CO). The kriging interpolation method minimized the mean squared errors over all other geo-statistical methods used and was, therefore, selected for all interpolation analysis. Based on this analysis, the spatial behavior of total hydraulic heads and NaCl concentrations were plotted in several two-dimensional planes, YZ, XY, XZ at different times to evaluate the effect of rainfall, temperature, and radiation on the transport of water and solute in unsaturated soils.

4.2.1   Draining experiments

Total hydraulic heads for drainage experiments with and without light exposure under controlled (closed) temperature conditions are shown in Figure 4-4 and Figure 4-5. Total hydraulic heads at the onset of the drainage experiments are around 43 cm of water throughout the SoilBed, reflecting static flow (no-flow) conditions. As water is drained from the system, total heads decrease through time reflecting the lower soil-water pressure (higher suctions) heads. At early times, the total heads for the drainage experiments exposed to light under controlled (closed) temperature conditions show slightly hydraulic heads than those for

the dark (no light) conditions. This is possibly caused by differences in initial temperatures. At later times, total hydraulic heads are lower for the drainage conditions exposed to light (Figure 4-4), suggesting enhanced water drainage under these conditions. Lower heads and greater drainage at later times result from decreasing pressure heads at higher temperatures. Soil-water in unsaturated soils is under negative pressure due to capillary forces, which are a function of the air-water interfacial tension (σ), the contacte angle (ϕ), are the effective pore-radius (see equation 2-16). Higher temperature decreases σ (Bachmann et al., 2002), thus decreasing soil-water tension. This decrease must be accompanied by soil-water drainage.
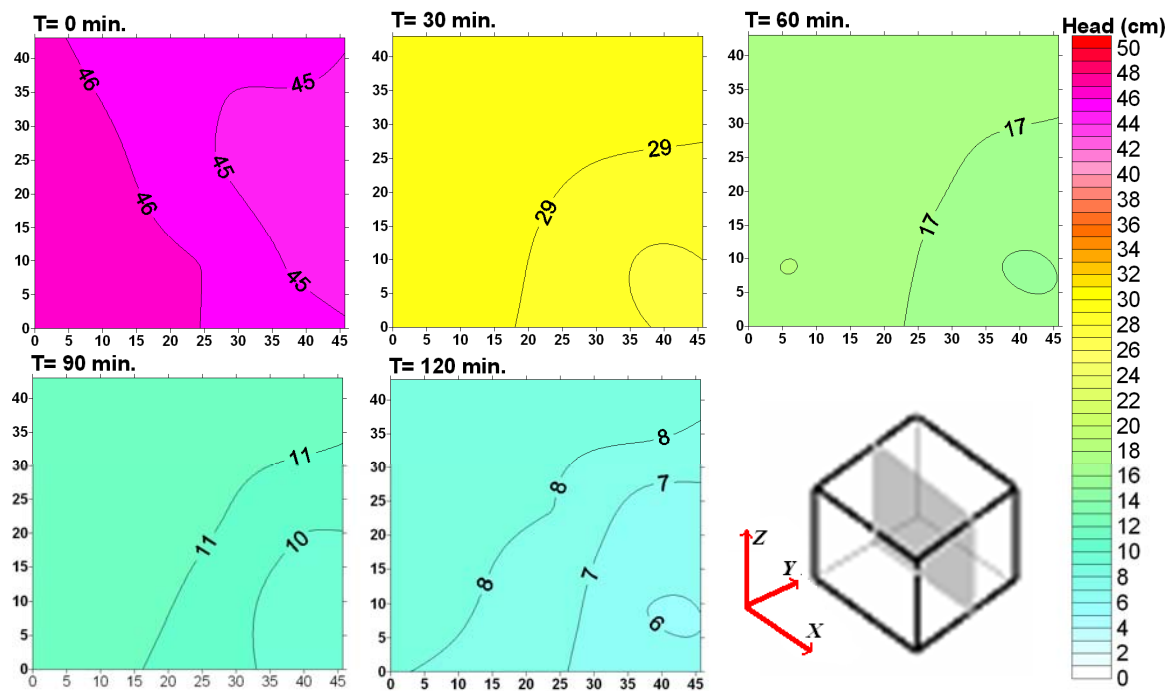
Figure 4-4 Spatial distribution of total hydraulic heads in a XZ plane for drainage experiments under controlled temperature (closed system) with light at 0, 30, 60, 90, and 120 minutes after the beginning of the experiment.

98
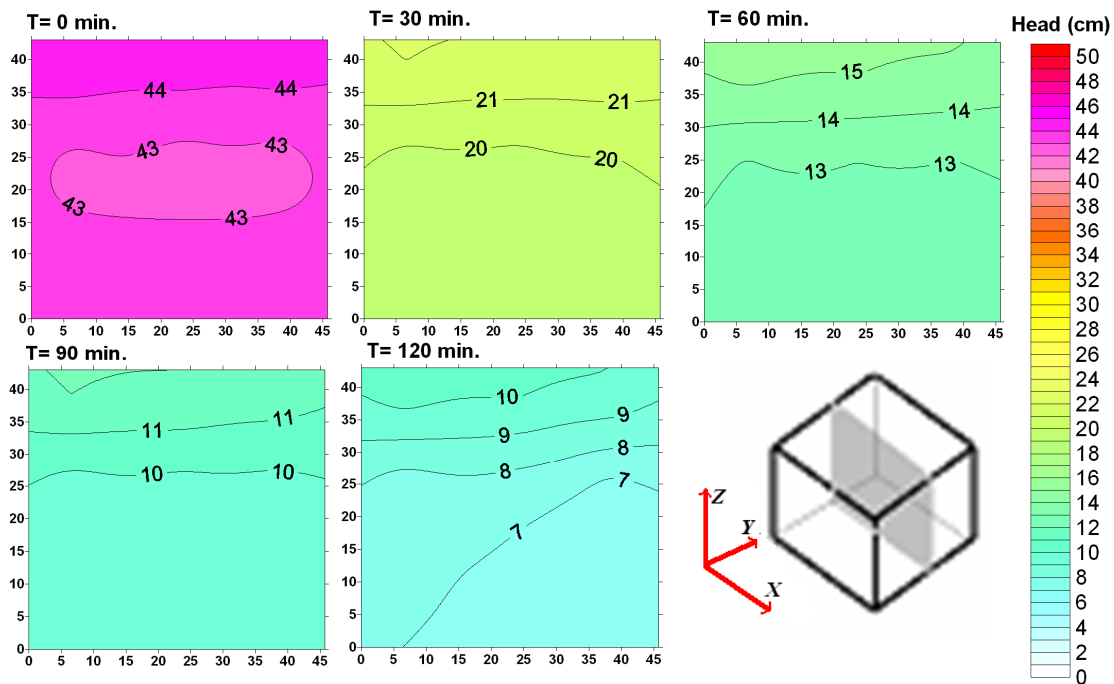
Figure 4-5 Spatial distribution of total hydraulic heads in a XZ plane for drainage experiments under controlled temperature (closed system) without light at 0, 30, 60, 90, and 120 minutes after the beginning of the experiment.

Similar drainage behavior is observed for the drainage experiments conducted in an open system at room temperatures (Figure 4 6, Figure 4 8, and Figure 4 9). Under these conditions, however, the hydraulic heads remain higher than under controlled (closed system) conditions. This behavior is attributed to the lower temperature in the open system. Hydraulic heads and flow patterns are not uniform and reflect SoilBed heterogeneities in boundary conditions and hydraulic, flow, and physical properties. Figure 4-7 shows the variation in hydraulic heads in the horizontal plane (XY) near the center of the SoilBed for drainage conditions in a closed system exposed to and not exposed to light. It shows horizontal variation in hydraulic heads and reflects possible preferential flow zones. This is attributed to local variations in water contents and potential spatial irregularities on the boundary conditions.

99
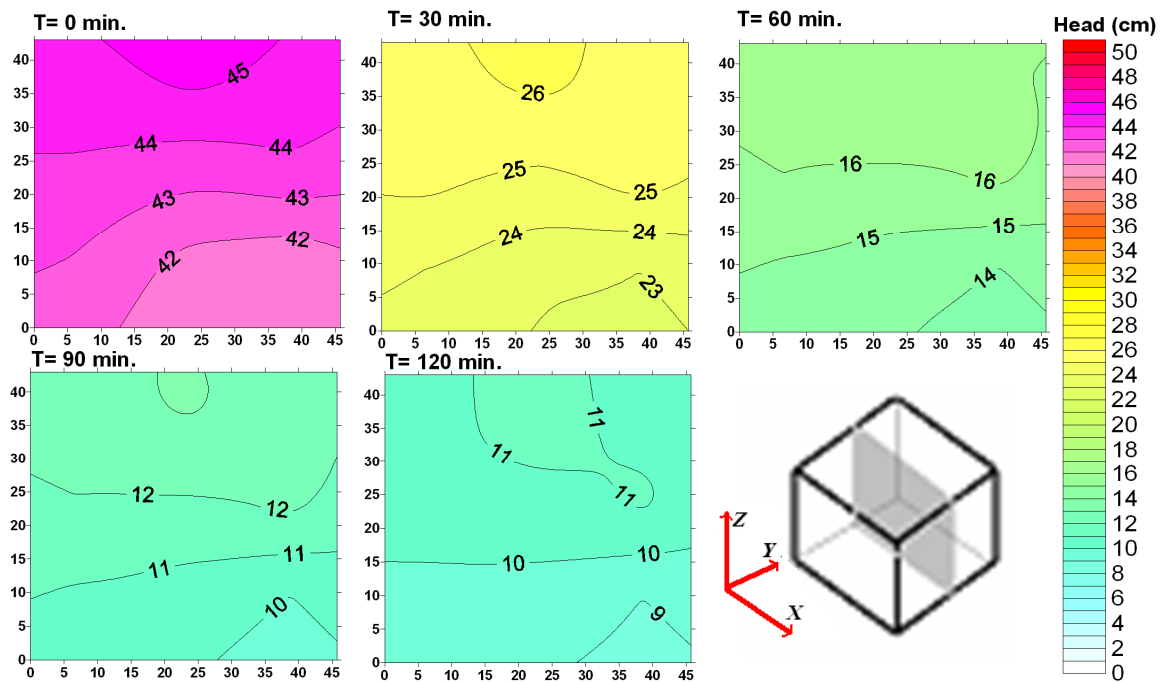
Figure 4-6 Spatial distribution of total hydraulic heads in a XZ plane for drainage experiments under room temperature (open system) with light at 0, 30, 60, 90, and 120 minutes after the beginning of the experiment.
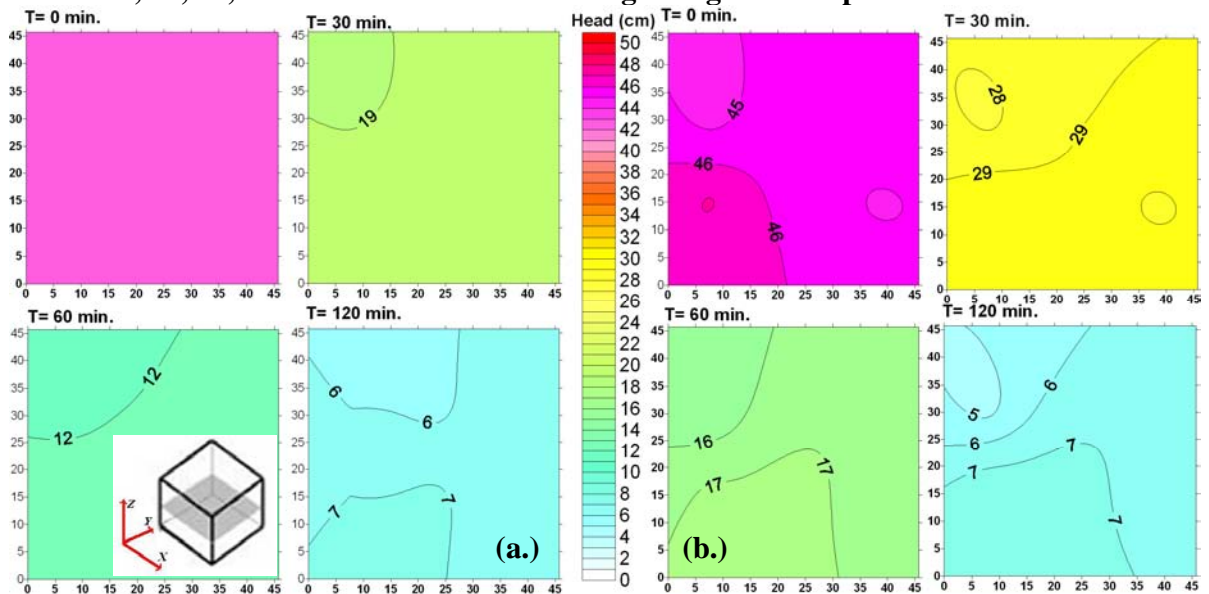
Figure 4-7 Spatial distribution of total hydraulic heads in a XY plane for drainage experiments under controlled temperature (closed system) without light (a) and with light (b) at 0, 30, 60, 90, and 120 minutes after the beginning of the experiment.

100
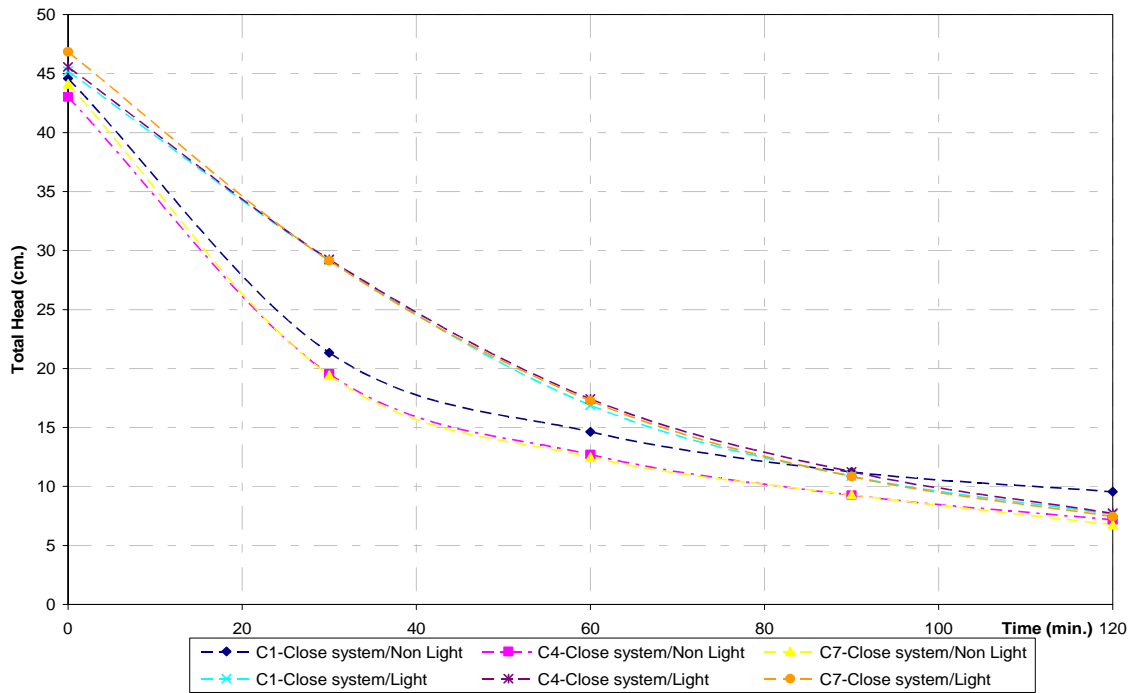
Figure 4-8 Temporal total head variation in draining events by light exposure
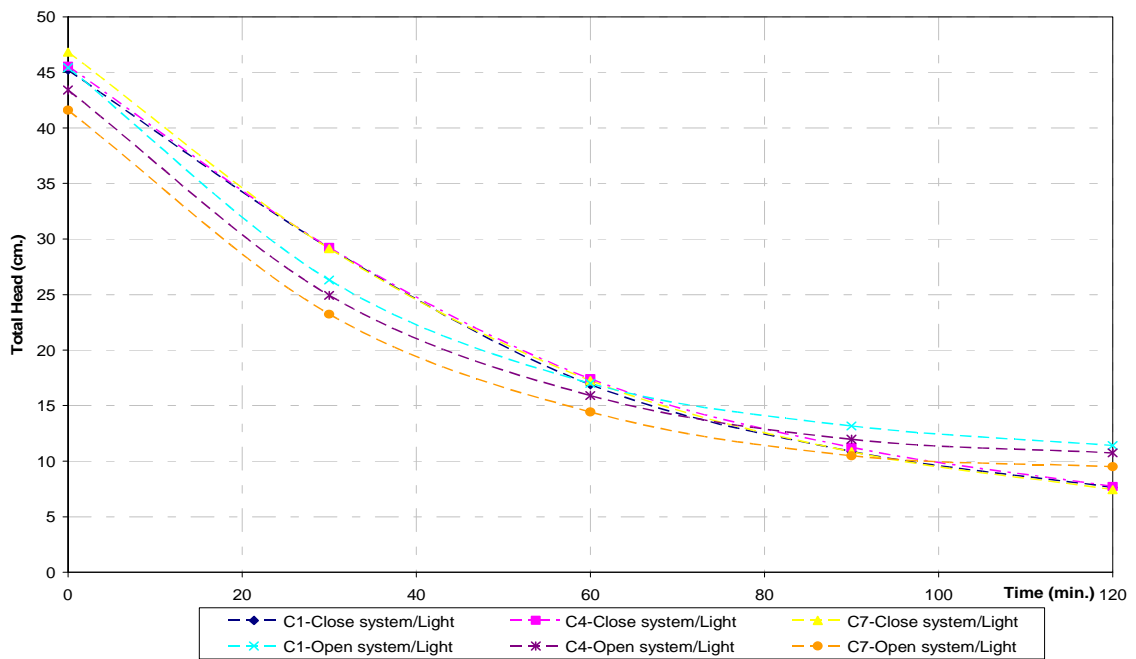
Figure 4-9 Temporal total head variation in draining events by system confinement

101

4.2.2   *Infiltration experiments*

Spatial and temporal hydraulic heads during infiltration experiments show increasing hydraulic heads as the soil becomes wet (Figure 4-10, and Figure 4 -11). Initial hydraulic head in the experiments vary spatially but ranged between -22 and 23 cm for the experiments not exposed to light, and between -24 to 20 cm for the ones with light exposure. This is expected as the soil-water tension decrease with increasing water contents increases during infiltration events. The distribution of hydraulic heads on a XZ plane for infiltration experiments under controlled (closed system) temperatures in the presence and absence of light show higher heads under light exposure conditions (Figure 4-11). This behavior reflects, not only the light and temperature effects heads and drainage, but also the effects of initial conditions. The hydraulic heads for the infiltration experiment indicate that the soil without light is initially dryer (shows lower heads), this results in lower heads than the one exposed to light throughout the experiment.
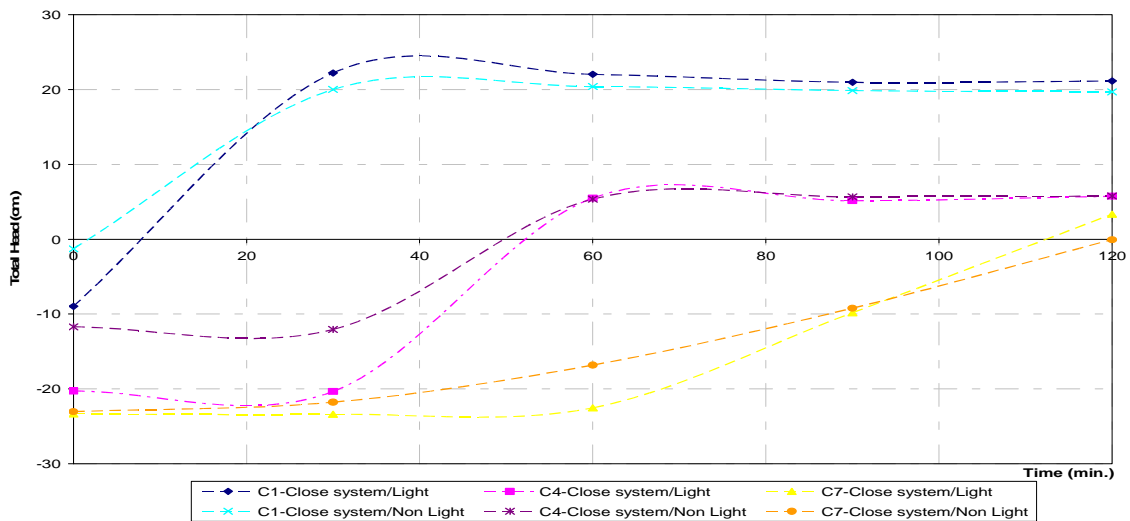
Figure 4-10 Total head variation in infiltration events by light exposure

102
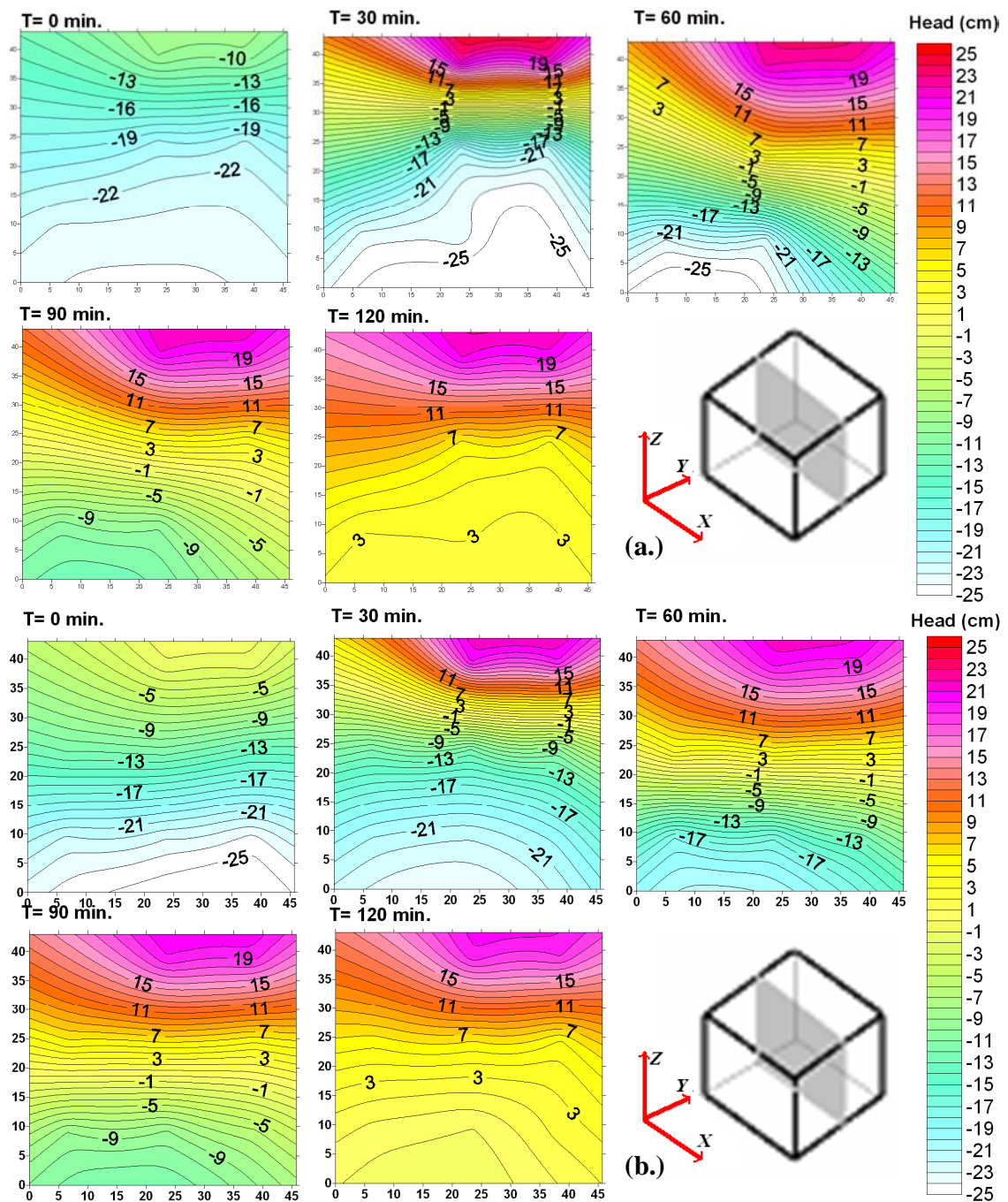
Figure 4-11 Spatial distribution of total hydraulic heads in a XZ plane for infiltration experiments under controlled temperature (closed system) without light (a) and with light (b) at 0, 30, 60, 90, and 120 minutes after the beginning of experiment.

Temporal and vertical effects of infiltration on total heads reflect that light and temperature effects on water and solute transport are also influenced by thermal gradients within the soil (Figure 4 12).   At the onset of infiltration, the lower heads at the top indicate that soil at the top is dryer than the soil at the bottom. Hydraulic heads also show that, for this experiment, the soil with no light had lower initial heads thus was dryer, than the soil with light exposure. As water infiltrates, soil-water pressure increase. Initial response in seen in the top samplers, but it is later seen in the bottom samplers. At the end of the experiment, higher heads are observed for the experiments without light, indicating higher water absorption characteristics at the top, but not at the bottom. This is attributed to the cooler temperatures near the soil surface. Table 3-3 shows the target atmospheric temperature. Measured atmospheric and soil temperatures are described later in this chapter.
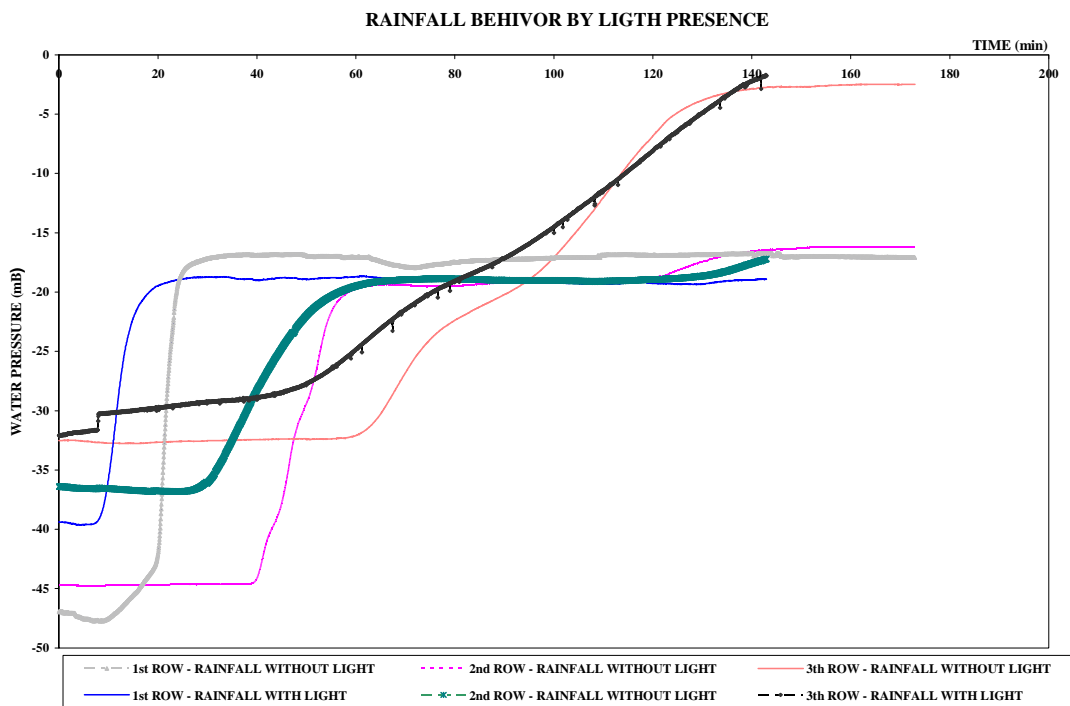
Figure 4-12 Water pressure response at each row of pressure transducers.

104

4.2.3   *Transport Experiments of ERCs*

Flow patterns were determined from spatial and temporal variations in soil water pressures and NaCl concentration distributions, as it is assumed that NaCl behaves as a conservative tracer. The ID and position of each sampling cluster is shown in

Figure **3-5**. Both sets of data indicate the existence of preferential flow paths. Generally, it was observed that pressure heads increased during rainfall and infiltration events and decreased during periods of no rainfall (Figure 4-13). Pressure variations were greater near the surface, reflecting greater influence of the precipitation boundary. Pressures near the soil surface (10 cm from soil surface) increased to maximum values of approximately -15 mbars during rainfall periods and decreased to minimum values of about -40 mbars during the evaporation periods. Pressures at greater depths (~20 cm below the surface) reflected wetter conditions during the evaporation periods (i.e., minimum pressure values greater than -40 mbars.

Water pressure reflected lower influence of precipitation boundary conditions and more influence of 3D water redistribution processes. At greater depths (~35 cm below soil surface), the conditions reflected wetter conditions, with maximum pressures near 0 mbars and minimum values near -25 and -30 mbars. This behavior reflects a greater influence of the drainage boundary condition imposed on the bottom. Preferential flow path are noted in pressure variations and lateral gradients can be observed (red ovals in Figure 4-13).
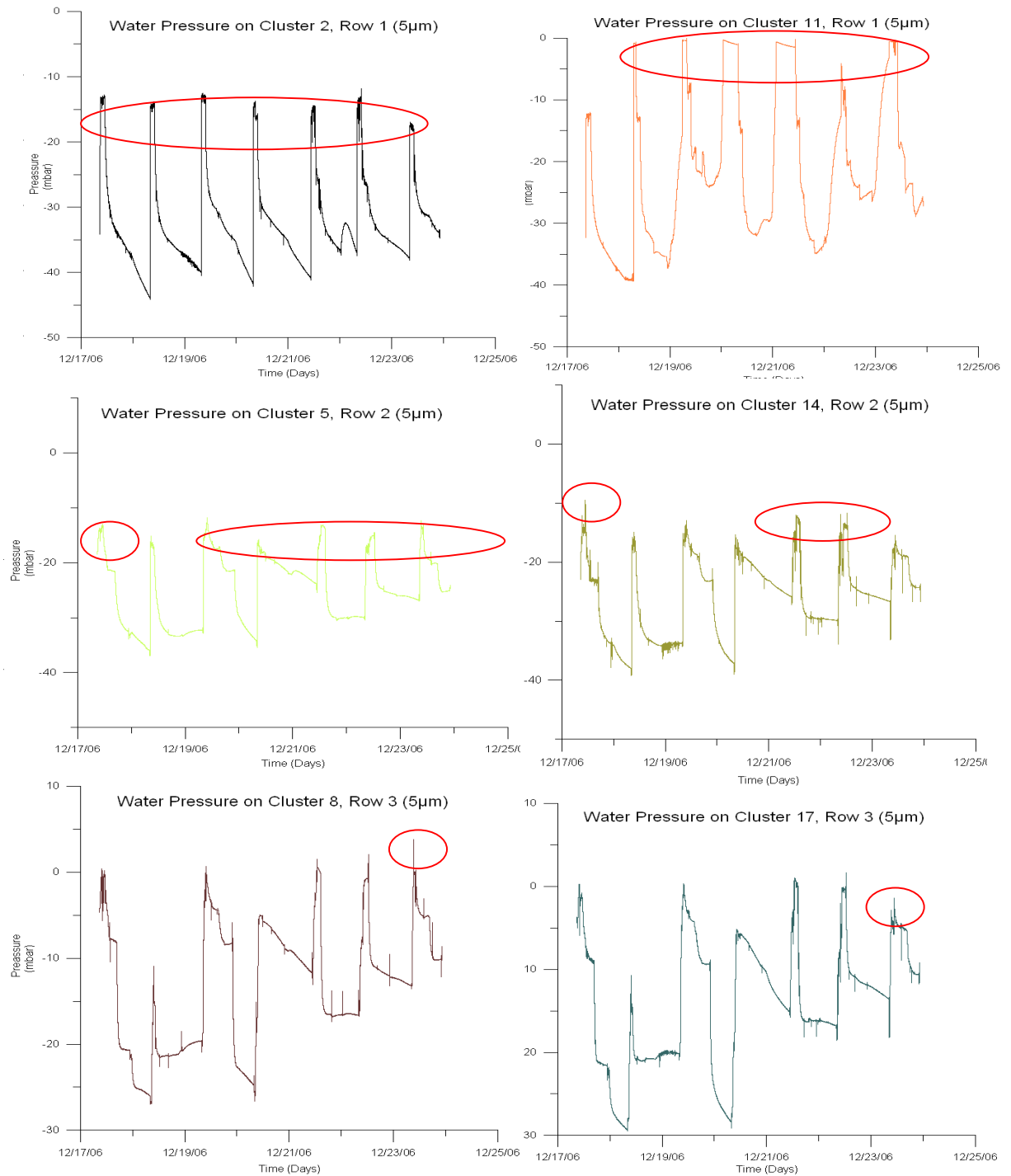
Figure 4-13 Soil-water pressure time series, TE-1

106

Temporal and spatial analyses of total hydraulic heads and gradients in the sampler volumes show the dimension and heterogeneous behavior of water flow in the system (Figures 4-14 to 4-20). These Figures show preferential flow paths and hydraulic gradients with magnitude and direction that are influenced by experimental conditions.

Time series of total head in the central vertical (y-z) plane of sampling clusters (clusters 2, 11, 5, 14, 8, and 17) show cycle variation in heads corresponding to periods with and without rainfall. Total heads generally increased during rainfall events and decreased during drainage periods and evaporation. Variation in head response between pressure sensor at same horizontal plane (e.q., between clusters 2 and 11, Figure 4-14) indicate that water flux is not only vertical and that flow is multidimensional.

Spatial total head distributions at different times after onset of initial rainfall event during transport experiments (Table 3-4) are shown on the right hand side of Figures 4-14 to 4-20. All spatial models of energy distribution can be seen in the appendixes section. The caption of each distribution models describes the experiment number (EN), cycle day (DN), and sample number (SN). The sample number range from 1 to 8, and correspond to samplers taken at 0 (1), 0.5 (2), 1.0 (3), 1.5 (4), 2.0 (5), 4.0 (6), 8.0 (7), and 14.0 (8) hours after the onset of the daily rainfall cycle. The daily rainfall periods stars at t=0 for each day and last 2

hours. As an exampled, total head distribution for sample time No. 5 (2 hours after daily rainfall onset), four day 6 of experiment 1 could be coded as E1.D6.S5.

Time series showed a non-stationary trend in some of the experiments. Experiment TE2-ERC shows two trends: one during the first four days, the highest, and a second one during the last ten days. Similar behavior is observed in experiment TE3-ERC. Experiment TE4-ERC shows lower heads during the first two days, intermediate heads during the following eight days, and higher heads during the last four days. Total heads time series for each cluster and each experiment can be seen in the appendixes (Figures A1.1 to A1.41).

Total head spatial distributions generally show higher heads near the soil surface (upper sampling row), and then decreasing with depth for periods near rainfall events (Figure 4-14 through Figure 4-20). Total heads and hydraulic gradients generally indicate downward flow patterns in most experiments, except in experiment with no radiation conditions (TE-6 ERC), which show slightly upward gradients.

Initial condition in experiment TE-3 ERC, also reflect upward gradients. This is attributed to the trailing effect of evaporation before the rainfall events. Because the upper row is initially sampled at the onset (t=0), the infiltration front may not have reached the sampling location (z=6 cm below the surface). After longer time, the gradient is re-established in the downward direction. Gradients suggest that flow tends toward preferential flow zone exiting around y = 30 cm, x = 15 cm.
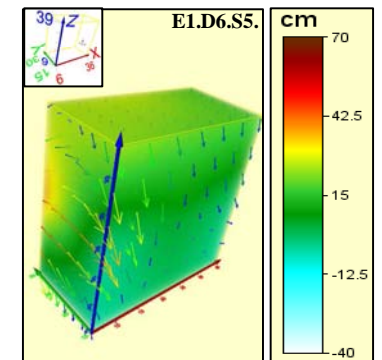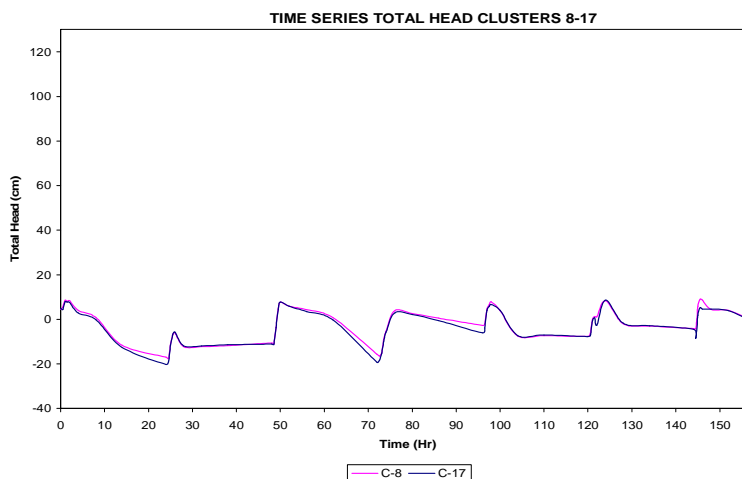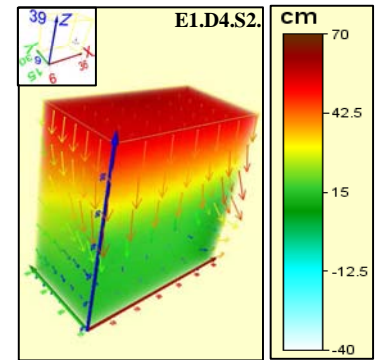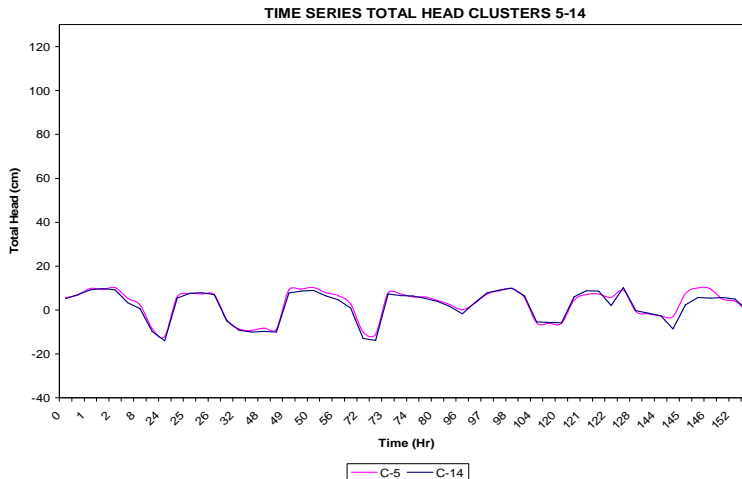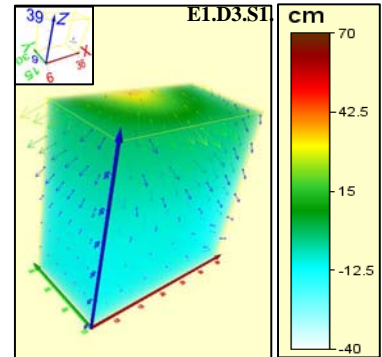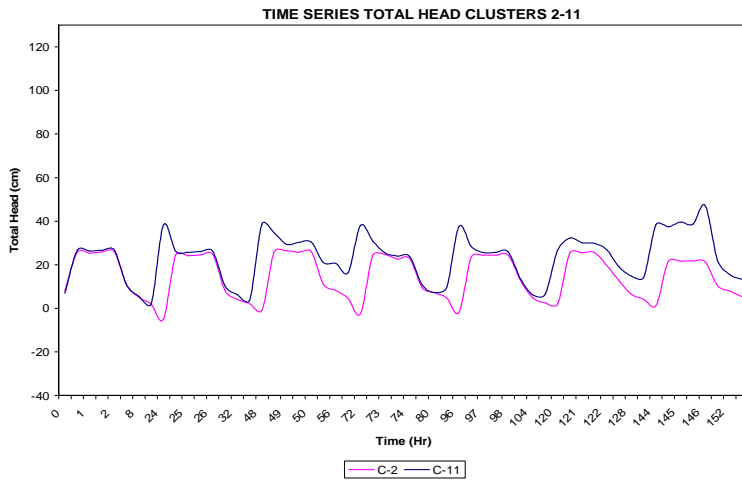
Figure 4-14 Time series (central clusters) and spatial models for total head in experiment TE-1 ERC: draining, with light, close system
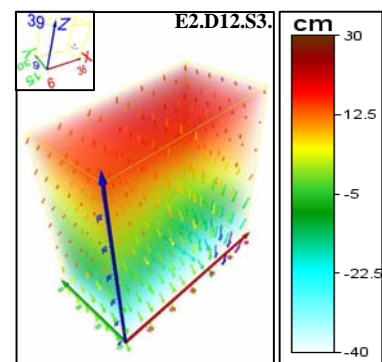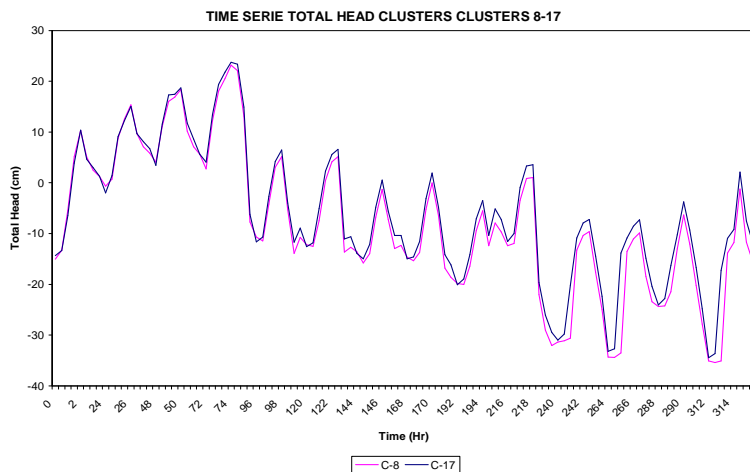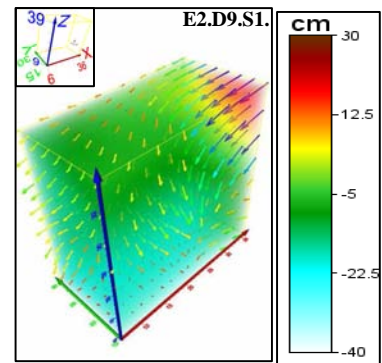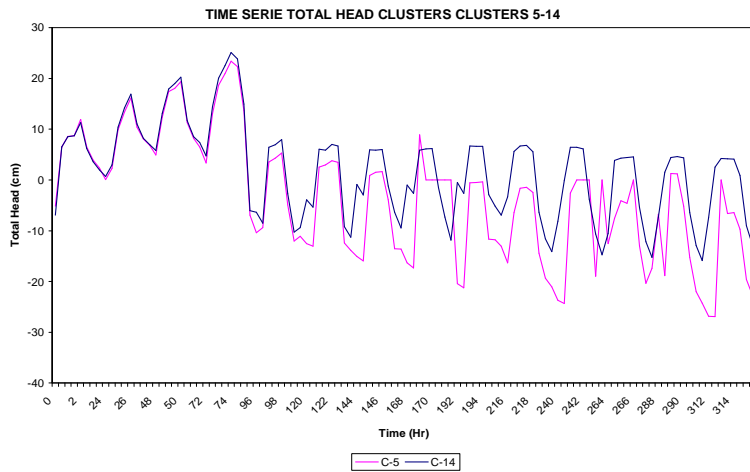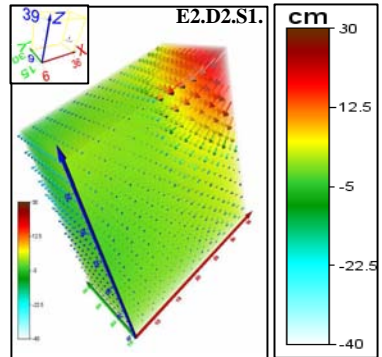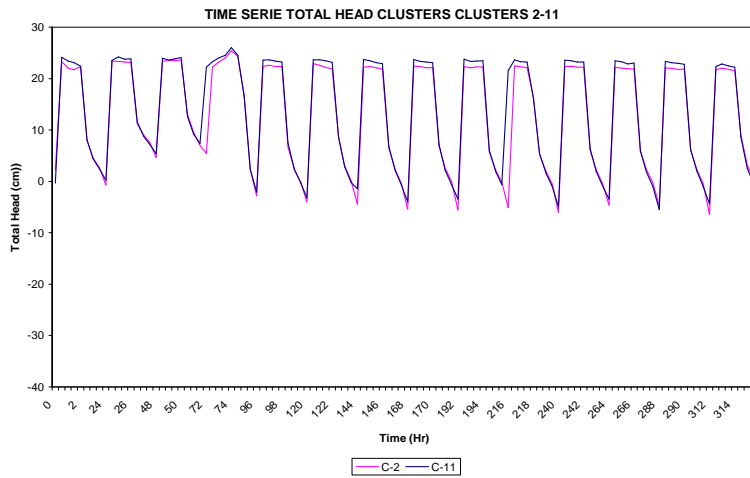
Figure 4-15 Time series (central clusters) and spatial models for total head in experiment TE-2 ERC: draining, with light, close system

110
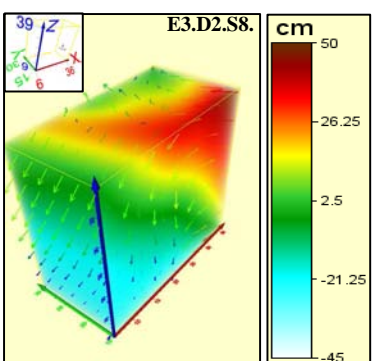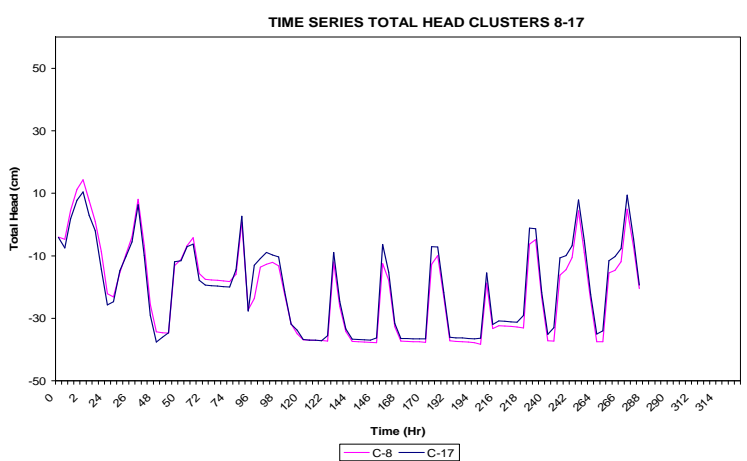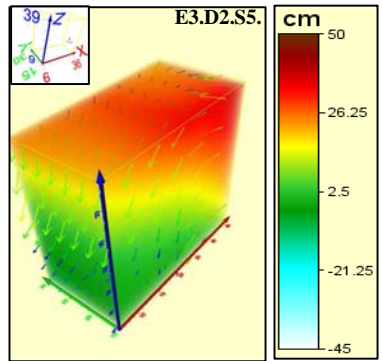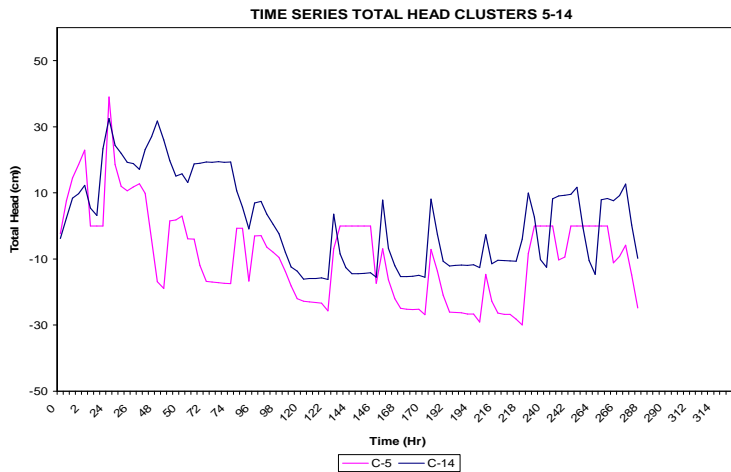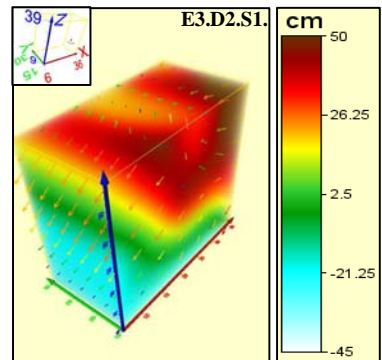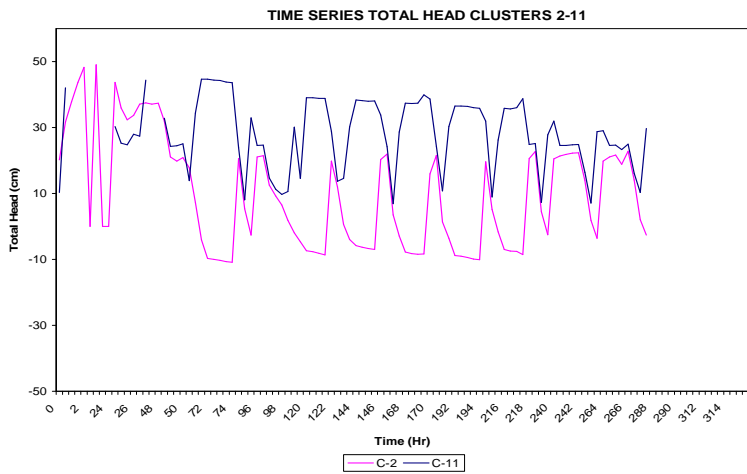
Figure 4-16 Time series (central clusters) and spatial models for total head in experiment TE-3 ERC: draining, with light, close system

111
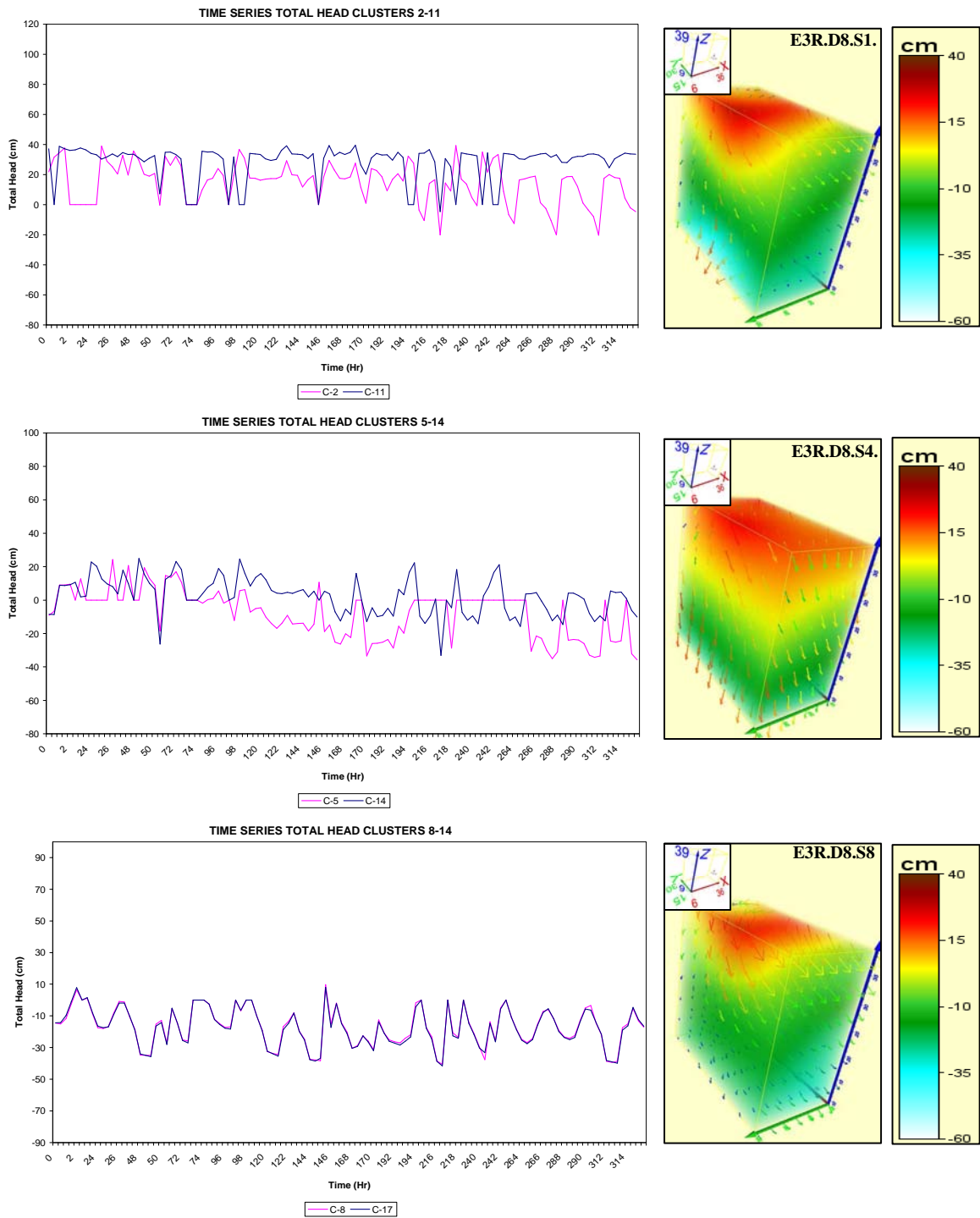
Figure 4-17 Time series (central clusters) and spatial models for total head in experiment TE-3R ERC: draining, with light, close system, replicate

112
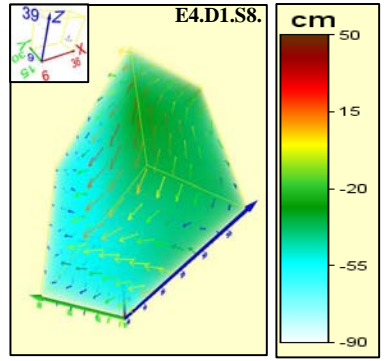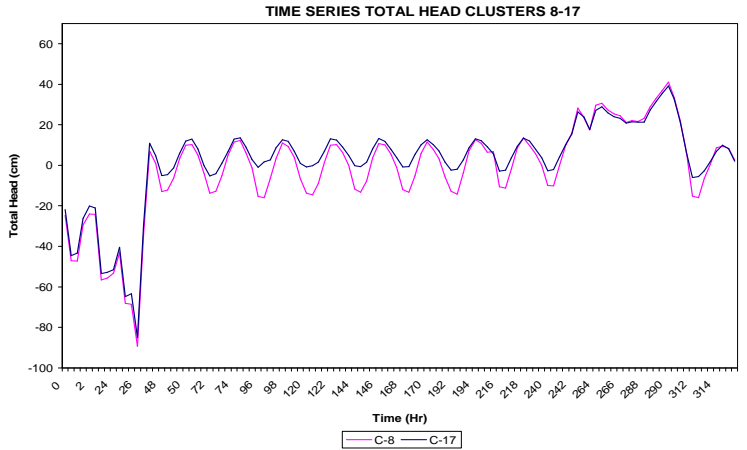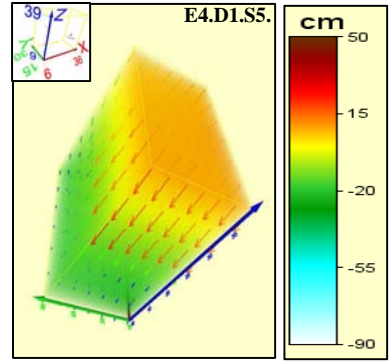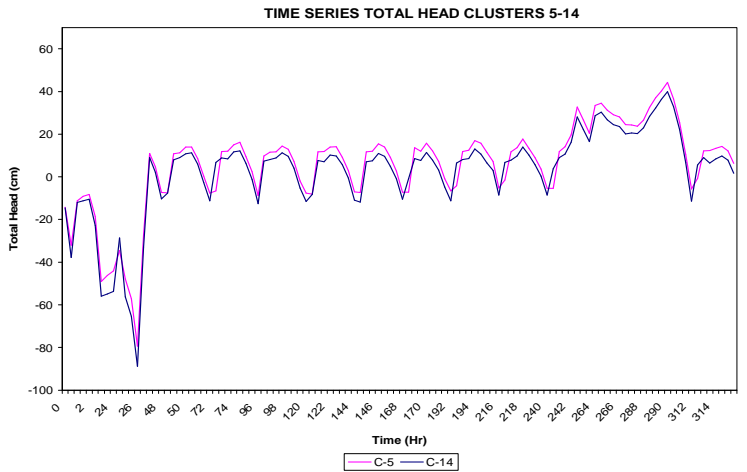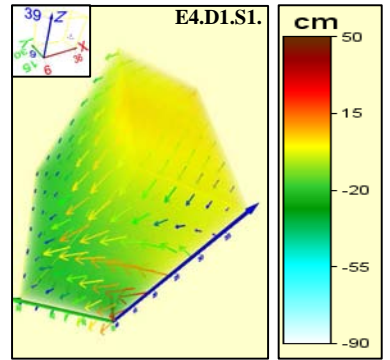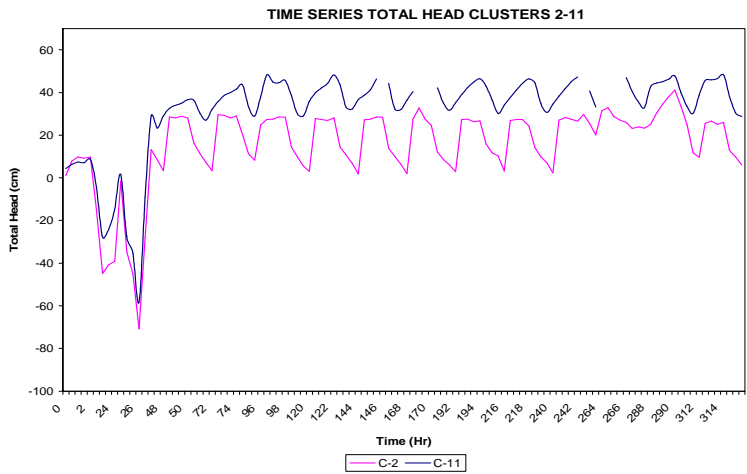
Figure 4-18 Time series (central clusters) and spatial models for total head in experiment TE-4 ERC: draining, with light, close system
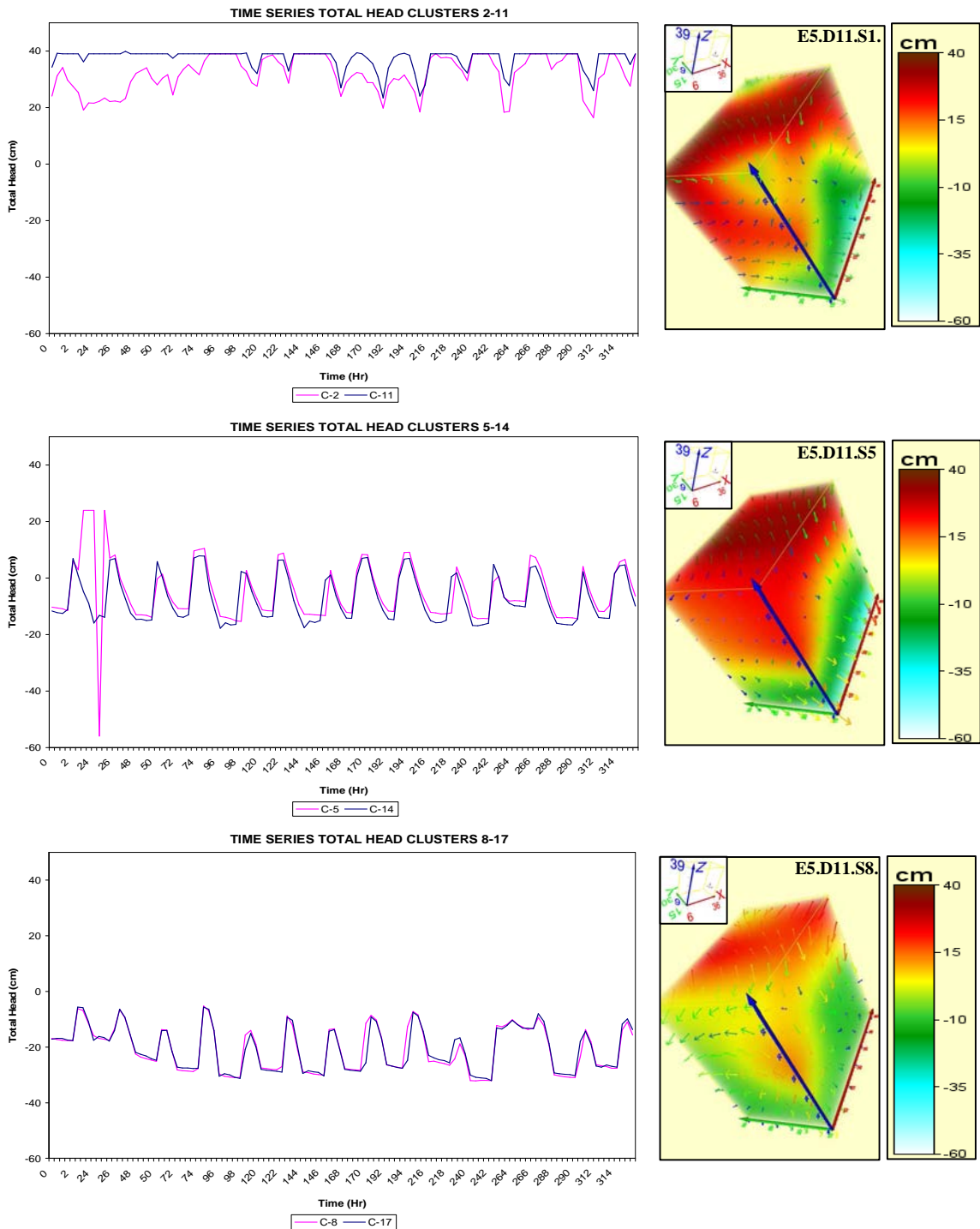
Figure 4-19 Time series (central clusters) and spatial models for total head in experiment TE-5 ERC: draining, with light, close system

114
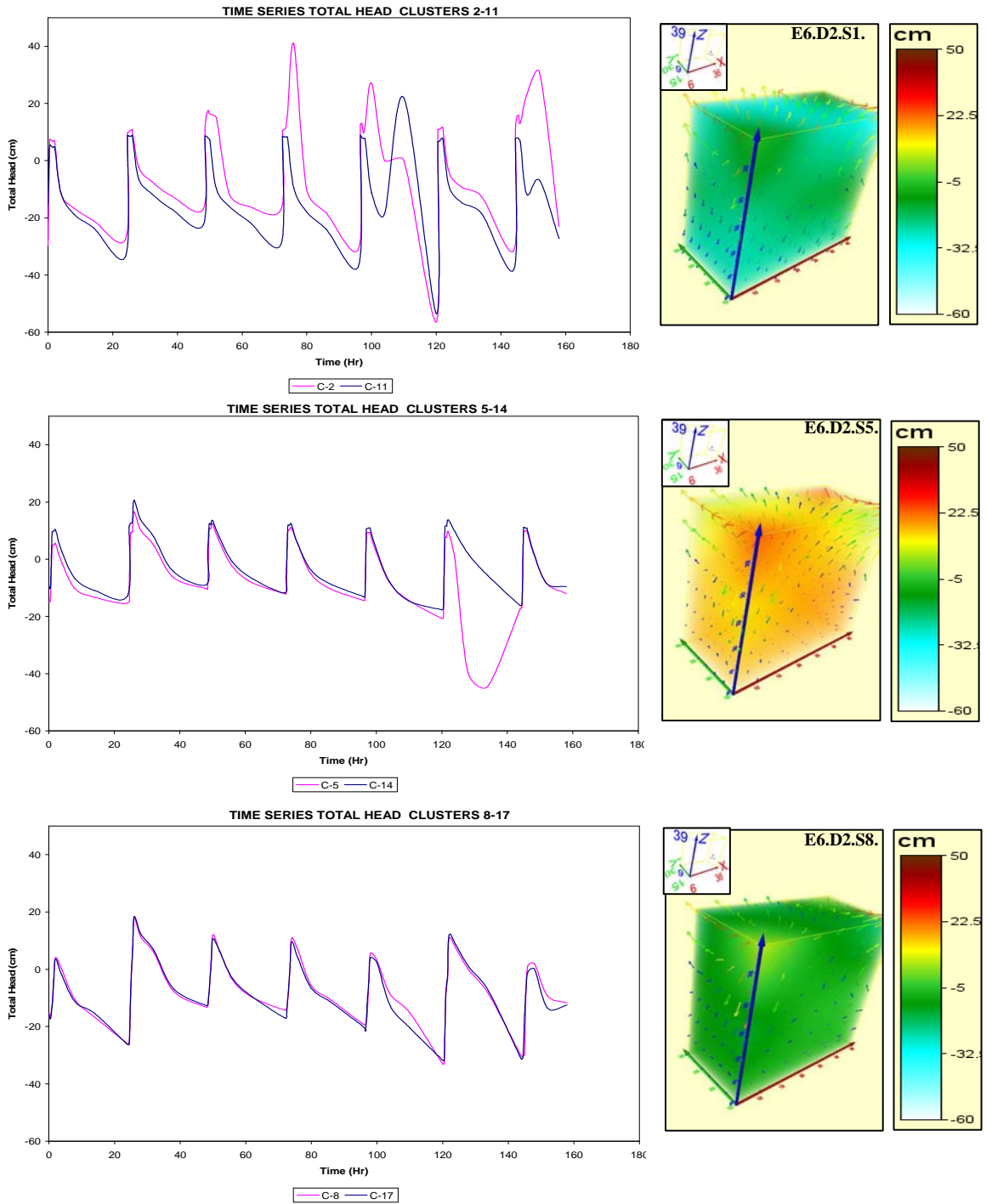
Figure 4-20 Time series (central clusters) and spatial for total head in experiment TE-6 ERC: draining, without light, close system

Total head spatial distributions models indicate the presence of preferential planes of flow. In general, experiments TE-1 and TE-3 ERC present a preferential plane of flow with inclinations between 30°-45° in direction Y=30 to X=15. Experiments TE- 2 and -4 ERC show preferential flow toward Y=30, X=25-30. TE-5 and -6 show no particular preferential flow exit path. Horizontal and vertical average gradients show that the highest gradients occur under the environmental conditions obtained for experiment TE-3 ERC (highest atmospheric temperatures). The lowest vertical gradients occur in experiment TE-6 ERC (no radiation at 25 ^{o}C). The lowest horizontal gradients are observed un TE-5 and -6 ERC (lower rainfall and no radiation respectively). Higher gradients for higher temperatures is attributed to changes in capillary pressure and hydraulic properties (e.q., hydraulic conductivities), inducing greater downward flow. Lower gradients for low rainfall and continuous radiation are attributed to the influence of evaporation and re-distribution process at these conditions. Table 4-3 and **Table 4-4** show the values for vertical and horizontal average gradients for experiments TE-3 ERC and its replicate (TE-3R ERC). Similar gradients in both experiments show good reproducibility of the experiment.

Table 4-3 Magnitude of vertical gradients of total hydraulic head

EXP.	MAGNITUDE OF VERTICAL ENERGY GRADIENT											
	DH/DZ (C1-C7)/ STDEV		DH/DZ (C12-C18) / STDEV		DH/DZ (C2-C8) / STDEV		DH/DZ (C11-C17) / STDEV		DH/DZ (C3-C9) / STDEV		DH/DZ (C10-C16) / STDEV	
TE-1 ERC	0.58	±0.08	0.58	±0.09	0.55	±0.08	0.87	±0.10	0.57	±0.11	0.53	±0.09
TE-2 ERC	0.62	±0.11	0.45	±0.10	0.69	±0.12	0.66	±0.08	0.73	±0.19	0.73	±0.11
TE-3 ERC	**0.84**	±0.07	**1.13**	±0.13	**1.03**	±0.08	**1.61**	±0.12	**1.82**	±0.11	**0.80**	±0.05
TE-3R ERC	0.97	±0.12	1.04	±0.05	1.17	±0.07	2.21	±0.35	1.44	±0.01	1.09	±0.07
TE-4 ERC	0.78	±0.09	0.51	±0.17	0.57	±0.13	0.98	±0.05	0.74	±0.13	0.41	±0.14
TE-5 ERC	1.00	±0.11	0.88	±0.12	1.76	±0.06	1.20	±0.21	1.97	±0.18	0.98	±0.14
TE-6 ERC	0.75	±0.10	0.04	±0.07	0.29	±0.20	0.07	±0.13	0.29	±0.03	0.71	±0.09

Table 4-4 Magnitude of horizontal gradients of total hydraulic head energy

EXP.	MAGNITUDE OF HORIZONTAL ENERGY GRADIENTS (VERTICAL CENTRAL PLANE)					
	DH/DX Row 1 (C2, C11) / STDEV		DH/DX Row 2 (C5, C14) / STDEV		DH/DX (Row 3) (C8, C17) / STDEV	
TE-1 ERC	0.57	±0.77	0.05	±0.11	0.06	±0.09
TE-2 ERC	0.06	±0.20	0.36	±0.42	0.13	±0.18
TE-3 ERC	1.36	±1.39	0.92	±0.74	0.06	±0.18
TE-3R ERC	1.15	±0.81	1.01	±0.76	0.03	±0.05
TE-4 ERC	1.17	±0.56	0.21	±0.23	0.26	±0.29
TE-5 ERC	0.36	±0.33	0.16	±0.55	0.01	±0.15
TE-6 ERC	0.47	±0.71	0.28	±0.52	0.01	±0.17

The response to maximum total head in the samples is influenced by the rainfall event and experimental conditions. Temporal distributions of total heads in the sampling volume (Figure 4-21) show that experiments conducted at 25 ^{o}C with rainfall intensity of 5 cm/hr (experiments TE -1, -2, and -6 ERC) reach a maximum hydraulic head near the end of the rainfall event (2 hours).
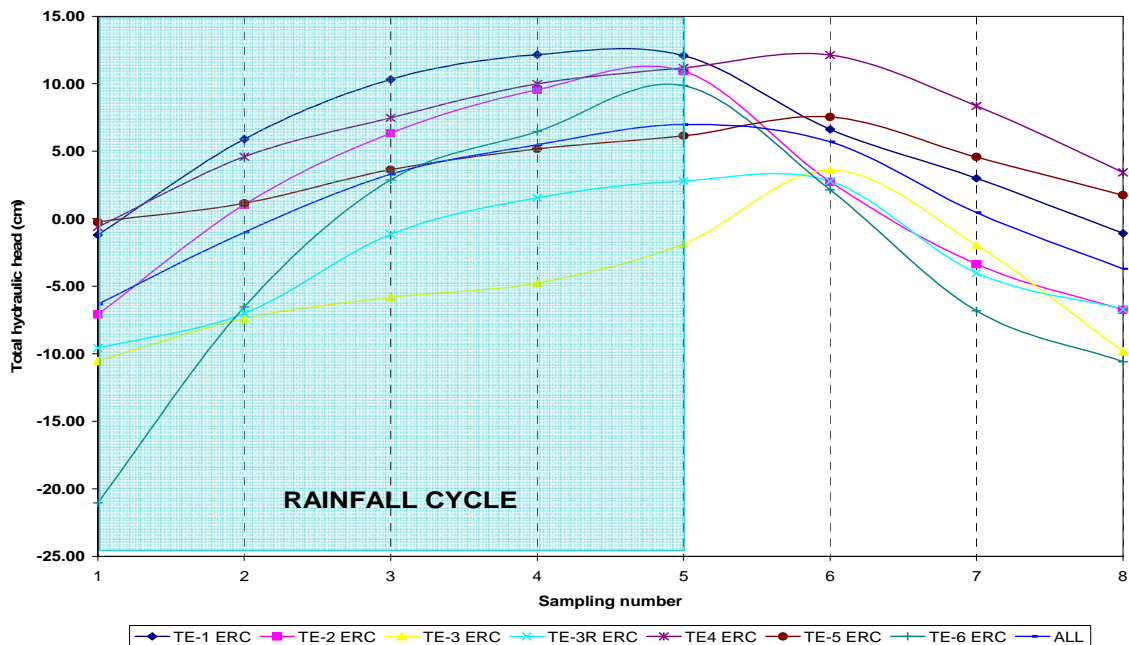
Figure 4-21 Temporal distribution of total head in the sampling volume

Maximum hydraulic heads for experiments with high and low temperatures (exp. TE-3, -3R, and 4 ERC) and low rainfall intensity (TE-5 ERC) occur within 2 hours after the end of the rainfall. The lag in maximum total heads is attributed to greater influence of redistribution pressures. Greater time lag is observed at cluster of row (TE-3 and -4 ERC).

Special variation of average total head in the sampling volume can be observed in the Figure 4-22. Experiments TE-5, -3, and -4 ERC have the highest average energy values, in this order, particularly at clusters 3 and 11. Experiments TE-2 and -6 ERC show the highest average energy values in cluster 10. Total heads gradients controlling water flow and some advective and dispersive processes indicate a strong response of the gradients to environmental conditions, like rainfall (duration, intensity), temperature (atmospheric temperature), and solar radiation. The hydraulic gradients, however, are not the only components controlling water flow. Soil-water contents and hydraulic conductivities also have strong effect on water flow and other fate and transport processes.

4.3 Soil Water Content

The average effective saturation (Se; equation 2-13) of the soil during the experiments was estimated from average soil-water suction using the van Genuchten water characteristic function equation (equations 2-13) and the van Genuchten parameters estimated with Rosetta (Table 4-2).
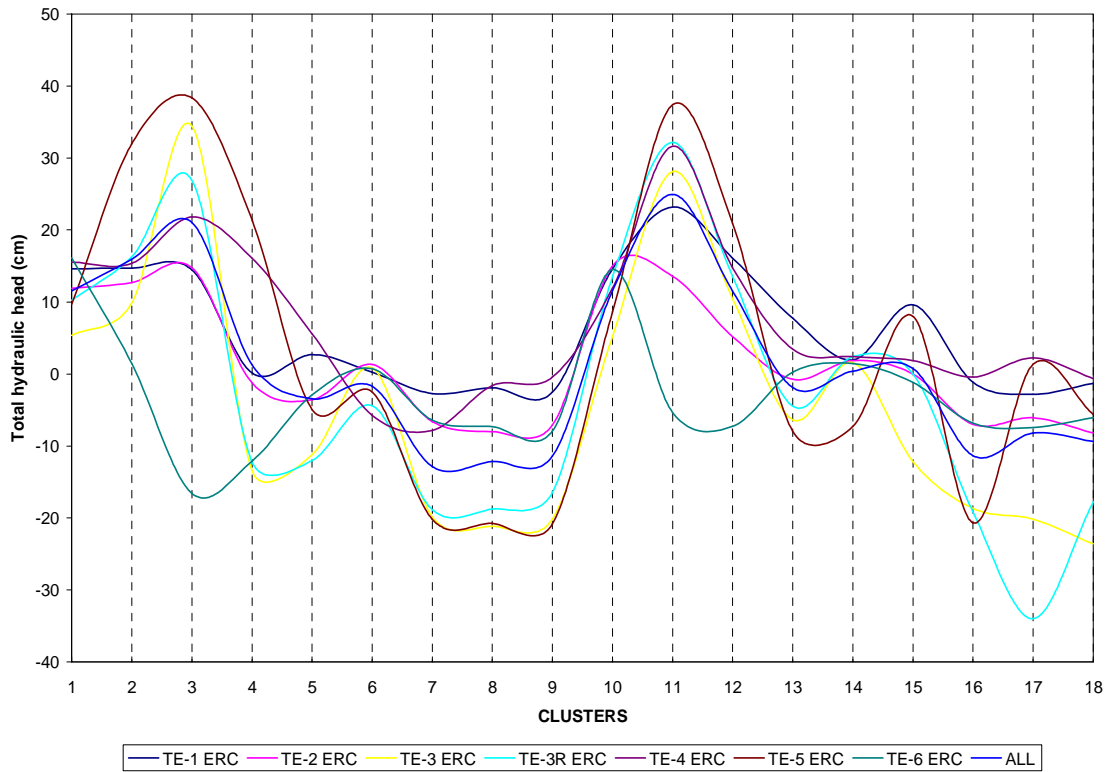
Figure 4-22 Variation of average total head by cluster

Average effective saturation for the experiments (Figure 4-23) show that, as expected, water contents increase during rainfall events. Similar to total hydraulic heads (Figure 4-21), which are also calculated from measured soil-water pressure, maximum saturation is obtained about 2 hours after the beginning of the rainfall events (at end of rainfall event) in experiments TE-1, -2, and -6 ERC. Average maximum saturation is obtained after the end of the rainfall event. Variations in effective saturation by clusters show the presence of preferential flow paths in the system (Figure 4-24).
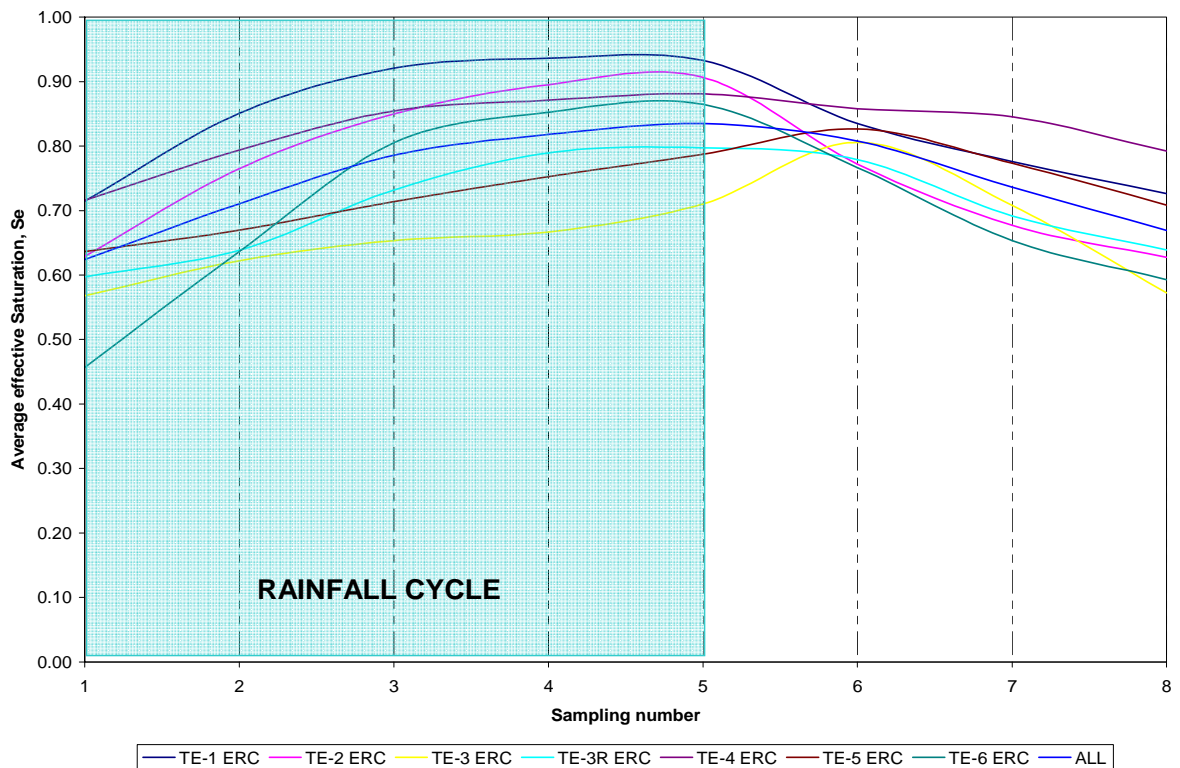
Figure 4-23 Variation of average effective saturation by sampling time

Preferential paths vary for different environmental conditions. Differences in spatial Se within horizontal planes (X,Y) for given depth indicate particular zones of potential preferential flows. For example, higher saturation are observed in the upper-row cluster 3 and 11 for all experiments except experiments TE-6 and -2 ERC (higher temperature). Clusters at the medium level plane (4, 5, 6, 13, 14, and 15) behave as a water transition zone (4, 5, 6). Values in clusters 13, 14 and 15 are, however, higher than their opposite's clusters. At the bottom plane (clusters 7, 8, 9, 16, 17, and 18), water contents are generally higher than in the middle term clusters in most conditions except in experiments TE-3 and -3R ERC (highest temperatures).

120
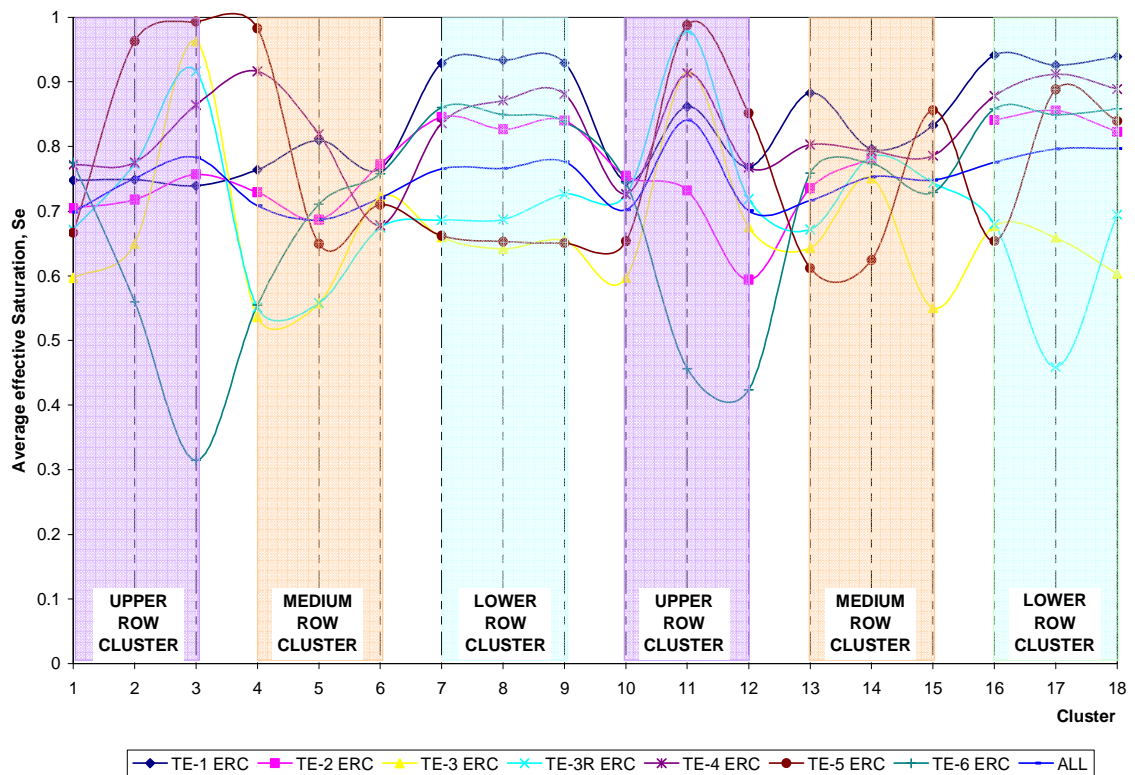
Figure 4-24 Variation of average effective saturation by Cluster

Long-term behavior of soil-water saturation is shown in Figure 4-25 and 4-26. Average effective saturation range between 60 and 90% for almost all experiments, except experiment TE-4 ERC. Careful evaluations of soil saturation at cluster planes (Figure 4-24; Table 4-5), indicate that, generally, experiments having high average saturation at the top tend to have low saturation at the bottom places(e.g., experiments TE -3, -3R, -5 ERC). Experiments with lowest average saturation at the top, tend to have lower average saturation at the bottom. This is attributed to variations in water storage distribution within the sampling volume. Higher soil-water saturation at the bottom, for instance, is indicative of draining conditions at the top. Accumulation at the bottom, is associated with higher rainfall rates, lower temperatures, and continuous radiation exposure (Table 3-4).

121
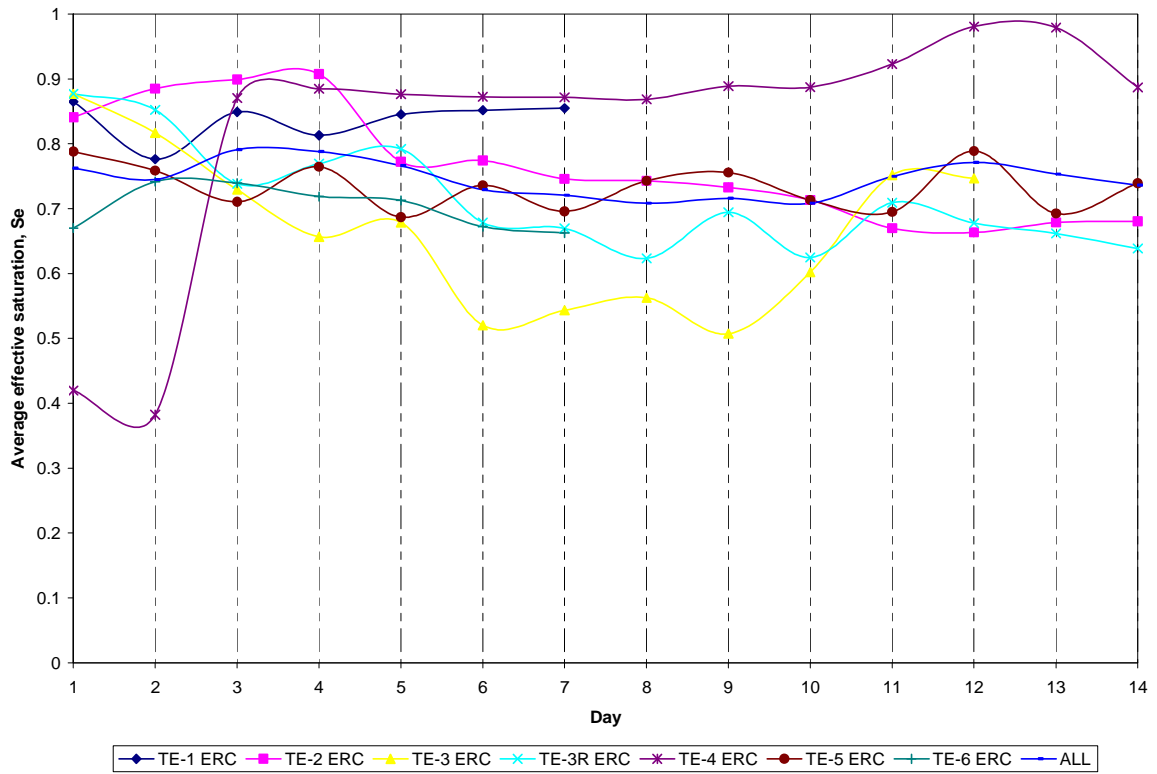
Figure 4-25 Average effective saturation, Se vs. experimental day

	PLANE XZ Y=15			PLANE XZ Y=30		
	Top	**Interm.**	**Bottom**	**Top**	**Interm.**	**Bottom**
High saturation	3, 3R, 5		1, 2, 4, 6	3, 3R, 4, 5		1, 4, 6, 5
Intermed. saturation	1, 3, 4					
Low saturation	6		3, 3R, 5	6, 2		3, 3R

Table 4-5 Soil-water saturation levels in experiments per cluster planes
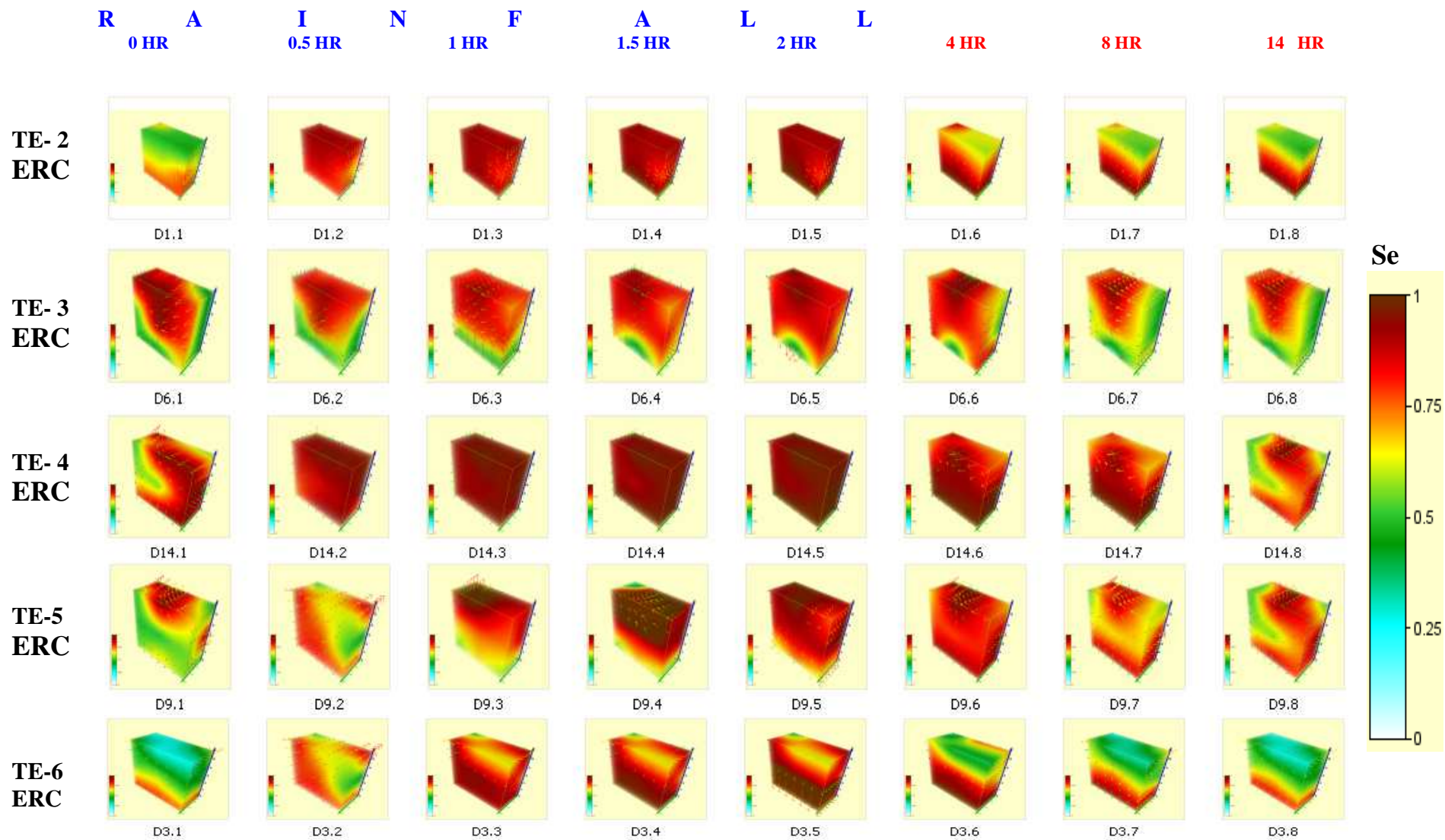
Figure 4-26 Spatial distribution of effective saturation, Se for experiment TE- 3, 4, 5, and 6

Conditions that force water storage at the top of the SoilBed included low rainfall rates (TE-5 ERC), high temperatures (TE-3, and -3R ERC). These experiments also show the highest vertical gradients (Table 4-3).

Overall, saturation was cyclic, but showed a slight tendency to decrease with time (Figure 4-25), depending on the experimental condition. Lowest saturations is observed for experiments with highest temperatures (TE-3, and -3R ERC), and no radiation (TE-6 ERC). Highest saturation was obtained for the experiment with lowest temperature (TE-4 ERC), even through it had the lowest initial water saturation. The effect of temperature on water saturation is attributed to changes in hydraulic conditions. Higher temperatures results in lower water density and lower water viscosity, generally producing higher hydraulic conductivities. Higher temperatures results in lower air-water superficial tension, and lower capillary tension, inducing drainage and water flux.

Figure 4-26 shows the effect of environmental conditions on the spatial and temporal saturation distribution. Generally, infiltrated rainwater reaches the bottom of the sampling volume quickly and then it is distributed laterally. Higher temperatures conditions (TE-3 ERC) induce quick water flux and draining processes. Lower temperature cause greater water retention and higher saturation levels. Lower rainfall rates result in greater heterogeneous water saturation distribution during the initial period after the onset of the rainfall event, and at later times after the ending of the event. At low rainfall intensity, water is initially taken up as hygroscopic water before downward water flux due to gravitational water is induced.

Consequently, it results in slight permeation porous and high water retention by the soil. No solar radiation (TE-6 ERC) seems to cause a more homogeneous water front distribution, with lower water contents at the top and higher saturation at the bottom.

4.4 Environmental Setting Conditions

Atmospheric temperature and relative humidity data were taken for all hydraulic response and transport experiment. Temporal variables in these parameters were analyzed and related to soil hydro-physical characteristics and fate and transport processes.

4.4.1   Temperature

Measured atmospheric temperature above the SoilBed during the hydraulic response experiments (Table 3-3) indicate that initial temperatures range between 22.8 and 25.5 °C with an average of 24.5 (±1) °C (Figure 4-27). Generally, temperatures under drainage conditions were higher at later times than under infiltrating conditions (Figure 4-27). Temperatures show a tendency to increase through time for drainage conditions under controlled temperature (closed system) and room temperature (open system), and for infiltrating conditions exposed to light under controlled (closed system) conditions. Temperatures tend toward lower values for infiltrating, no radiatiion conditions in a temperature-controlled (closed) system and, for infiltrating water exposed to visible light in an open system. These results reflect the effect of water and heat exchange on heat

dissipation. Lower temperatures under infiltrating conditions result from the cooling effect of water in the system. The presence of light induces increasing temperatures in the atmosphere above the SoilBed for a closed system, but not for an open system. Higher temperatures are obtained for closed systems because of the difficulty of exchanging heat with external systems (greenhouse effect).
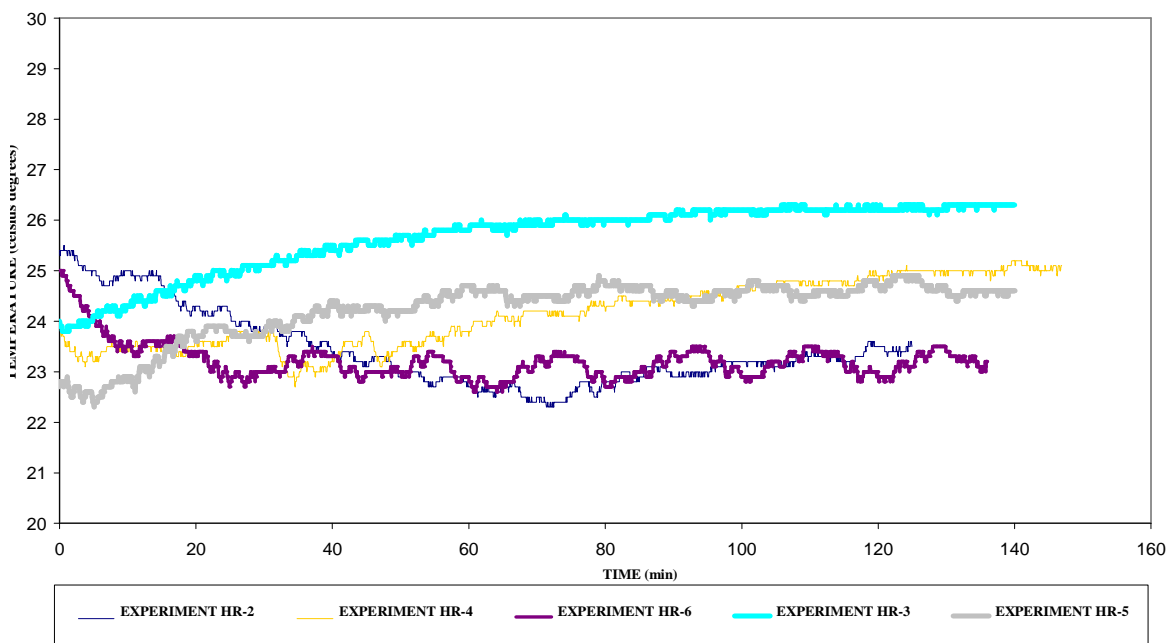
Figure 4-27 Measured temperature above the SoilBed during the hydraulic response experiments

Temporal atmospheric temperatures show cyclic variations reflecting experimental temperatures setting (Table 3-4) and cyclic variations in rainfall and radiation events (Figure 4-28 and 4-29; Table 4-6). Experimental settings were set at 3 different temperatures: 15 ^{o}C, 25 ^{o}C, and 35 ^{o}C (Table 3-4).

126
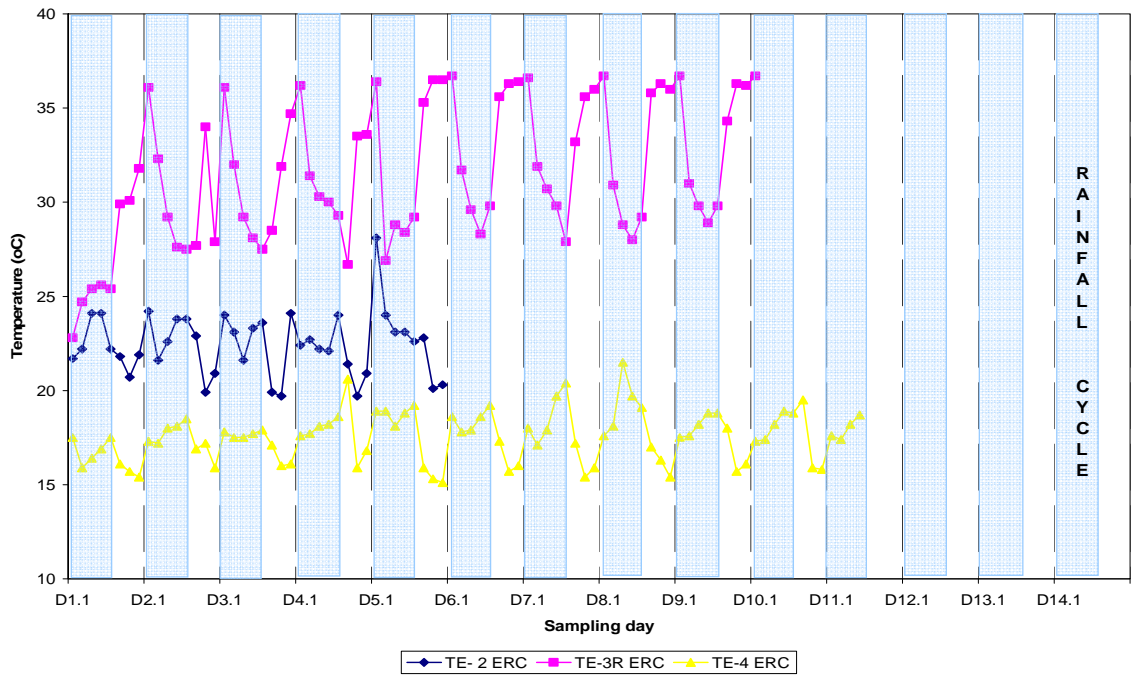
Figure 4-28 Atmospheric temperature in transport experiments TE-2, -3, and -4 ERC
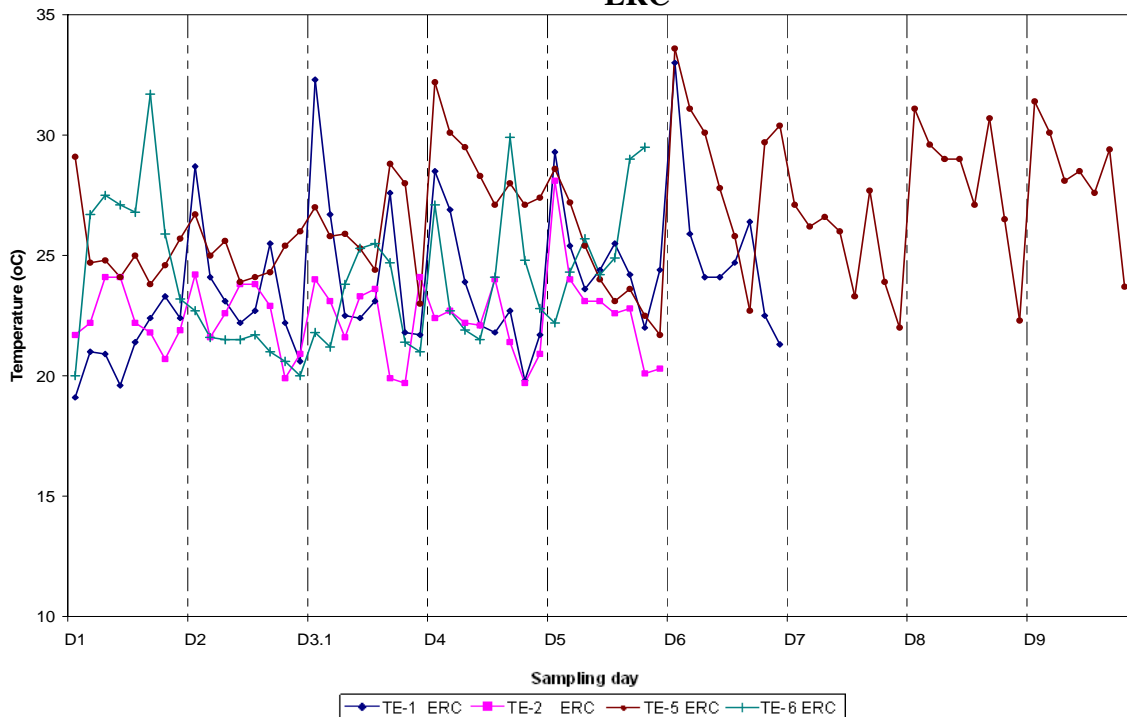
Figure 4-29 Atmospheric temperature in transport experiments TE-1, -2, -5 and -6 ERC

127

Table 4-6 Statistical parameters time series of temperature

EXP.	AVERAGE TEMPERATURES (^{o}C)	STDEV	CHAMBER TEMP. ^{o}C	% SIMILITUDE
1	23.57	2.88	25	94.27
2	22.48	1.65	25	89.94
3r	31.54	3.65	35	90.12
3f	32.21	3.79	35	92.03
4	17.35	1.18	15	84.32
5	26.03	2.19	25	95.89
6	24.07	2.96	25	96.29

Table 4-6 shows a high correlation between temperature configured in the chamber and the average temperature given by experiments results. As reflected average temperatures (Table 4-6), measured atmospheric temperature were mostly below the setting for experiments calculated at 35 ^{o}C (TE- 3 and -3R ERC) and 25 ^{o}C with high rainfall rate (TE-1 and -2 ERC). Measured atmospheric temperatures for experiment conducted at 15 ^{o}C (TE-4 ERC) and 25 ^{o}C with low rainfall rates (TE-5 ERC) were generally higher than the temperature settings (Figure 4-28; Table 4-6). Temperatures for experiments conduced at 25 ^{o}C with no radiation (TE-6 ERC) fluctuated between 20 ^{o}C and above 30 ^{o}C (Figure 4-29).

Differences in atmospheric temperatures and those at settings are attributed to atmospheric configuration (i.e., radiation, rainfall), rain water temperature, and NaCl exchange mechanisms. At high temperatures settings (35 ^{o}), atmospheric temperatures decrease after the onset of rainfall events. This decrease is attributed to cooler rainwater temperature an cooling effects of evaporation. A daily minimum is observed toward the end of rainfall event, and rise then after toward the setting temperature. Higher measured than setting temperatures

at the onset of the rainfall events result from increased thermal energy resulting from radiation. Similar temporal temperature patterns are observed for experiments conduced at 25 ^{o}C and high rainfall rates, but with lower temperature variations than at 35 ^{o}C (Table 4-6). Atmospheric temperatures at low temperatures setting were generally above the established setting, as reflected in their averages (Table 4-6). Temperatures generally increase during rainfall events, and then decease toward the set temperatures (15 ^{o}C). This is attributed to temperature differences between the warmer rainwater and the cooler environmental settings. Temperatures reach a minimum in no radiation events (sample number 7 and 8; 8 and 14 hours after onset of rainfall).

Atmospheric temperatures for low rainfall rates at 25 ^{o}C (TE-5 ERC) show cyclic variations mostly above the set temperatures (Figure 4-29: Table 4-6). This is attributed to lower rainfall volumes, which can absorb energy and buffer temperature changes. Consequently, radiation energy results in greater temperatures increase. Temperatures tend to decrease during rainfall events, and increase thereafter during the radiation cycle.

4.4.2   *Relative Humidity*

Initial relative humidity above the SoilBed for the hydraulic response experiments (Table 3-3) range between 68 and 83% initially, but changed temporally depending on the experimental conditions imposed (Figure 4-30). Relative humidity tends to increase to 100% when the system was subjected to rainfall in closed systems, but remains constant (on average) when

the system is open to the environment. Cyclic variations of relative humidity in the open system are due to variations in the environment. When subject to light, relative humidity increases sharply when subjected to rainfall in a closed environment, but more gradual in the absence of light.
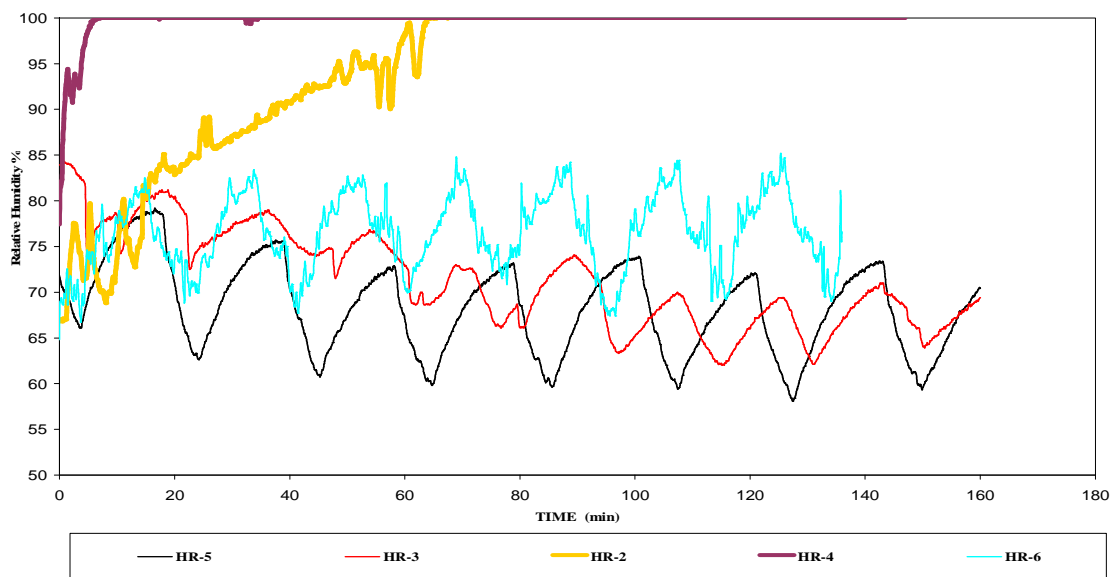
Figure 4-30 Measured relative humidity above the SoilBed during the experiments

Relative humidity is generally lower for draining conditions because these are periods of no rainfall, and were lower when the atmosphere was open to the external environment, facilitating the exchange of water vapor with the external system. Figures 4-31 and 4-32 show the time series of relative humidity for the transport experiments (Table 3-4). These series show cyclic variation in relative humidity, which were influence by temperature, rainfall, solar radiation, and soil water saturation.

Differences between experiments TE-1 and -2 ERC. For low temperature condition (TE-4 ERC), relative humidity increase during rainfall events, and then decrease (Figure 4-31) to a daily minimum before the onset of solar radiation and rainfall. Low temperatures condition show higher relative humidity than other temperatures. This is attributed to high water saturation in the soil (Figure 4-25). At high temperatures condition (TE-3R ERC), relative humidity were lower and generally constant except for some peaks after the end of the rainfall events. These peaks coincide with high water saturation (Figure 4-31 and 4-32). Relative humidity for high rainfall rates at 25 ^{o}C (TE-2 ERC) tend to be lower then those at higher temperatures (Figure 4-31), lower rainfall rates (TE-5 ERC) and no radiation (TE-6 ERC) (Figure 4-32).

Higher humidity for lower rainfall rates is attributed to higher soil water saturation obtained during the experiments (Figure 4-25). The strong relationship between relative humidity and spatial distribution of effective saturation, suggest evaporation processes that carry out humidity from soil matrix, especially at upper levels, to soil-atmospheric boundary layer. Measured relative humidity for experiment TE-1 ERC, show high range because, the humidity sensor was in a different and wetter location than the others experiments.

131
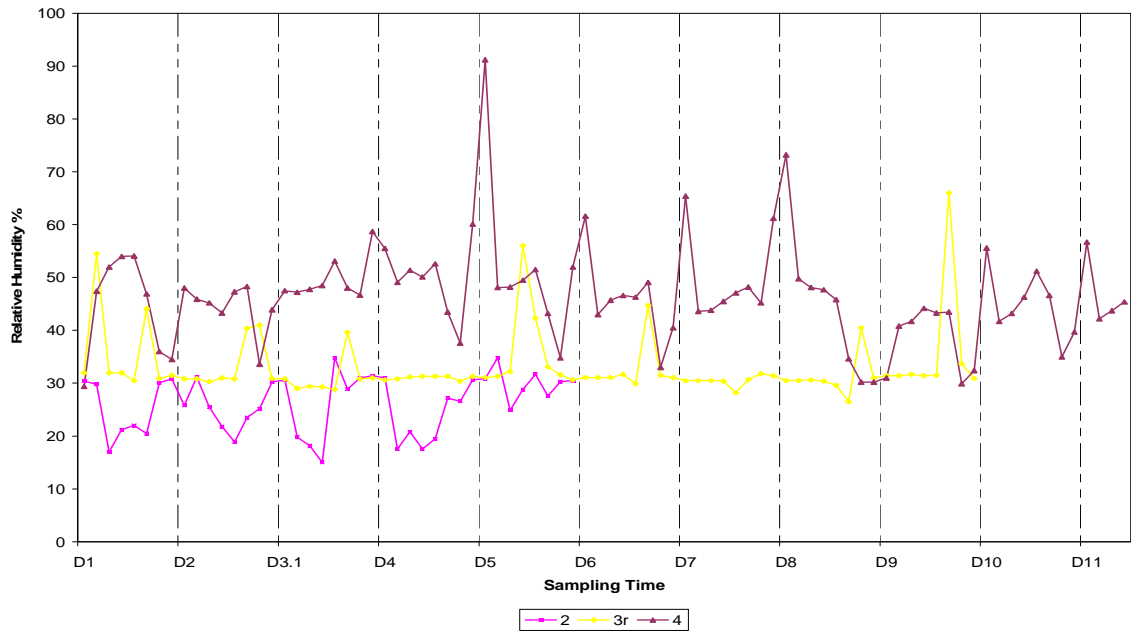
Figure 4-31 Relative humidity in the transport experiments TE-2, -3, and -4 ERC
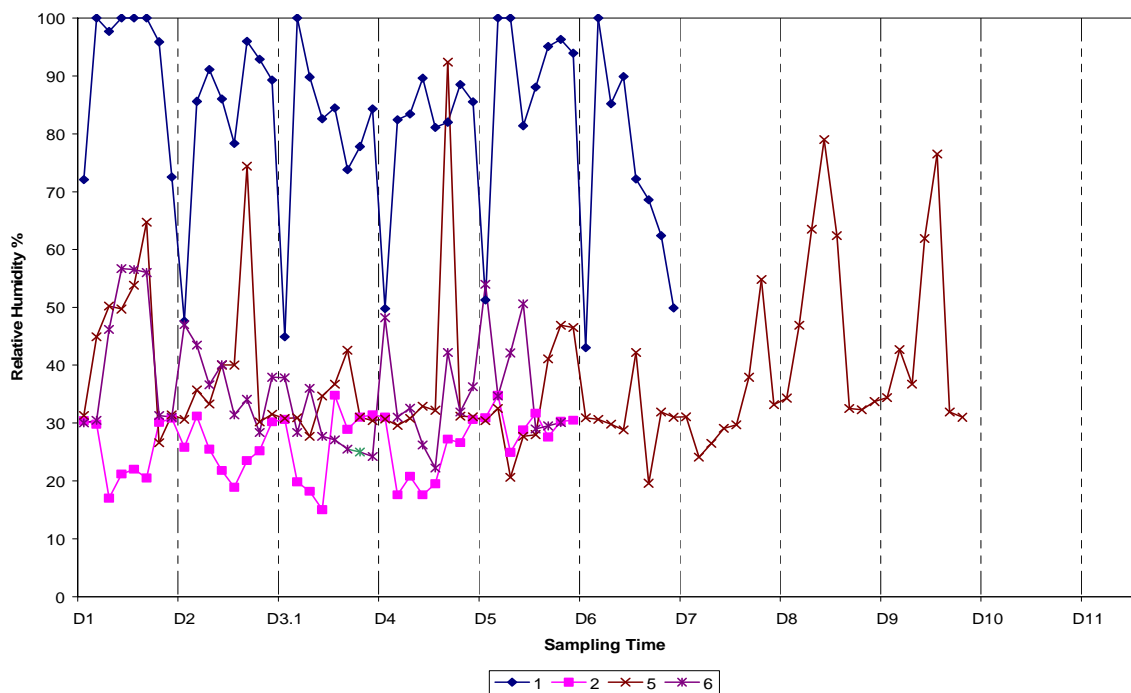
Figure 4-32 Relative humidity in the transport experiments TE-1, -2, -5 and -6 ERC

132

4.4.3   Soil Temperature

Soil temperature was measured for experiments TE-3 through -6 ERC at a depth of approximately 4 cm below foil surface. Measured values (Figures 4-33, 4-34, 4-35, 4-36) show a low variability in the time series ($\pm$ 0.7 ^{o}C for experiment TE-3 ERC, $\pm$ 0.5 ^{o}C for experiment TE-4 ERC, and $\pm$ 0.3 ^{o}C for experiment TE-5 ERC). Generally, soil temperature increased during radiation event, reaching a maximum before the rainfall even for experiments at low (15 ^{o}C) and mid-range (25 ^{o}C) temperatures. In general, soil temperatures decreased during rainfall events, and then declines sharp, after the end of the radiation event (Figure 4-36). Soil temperatures showed the lowest variability in high temperature experiments (35 ^{o}C).
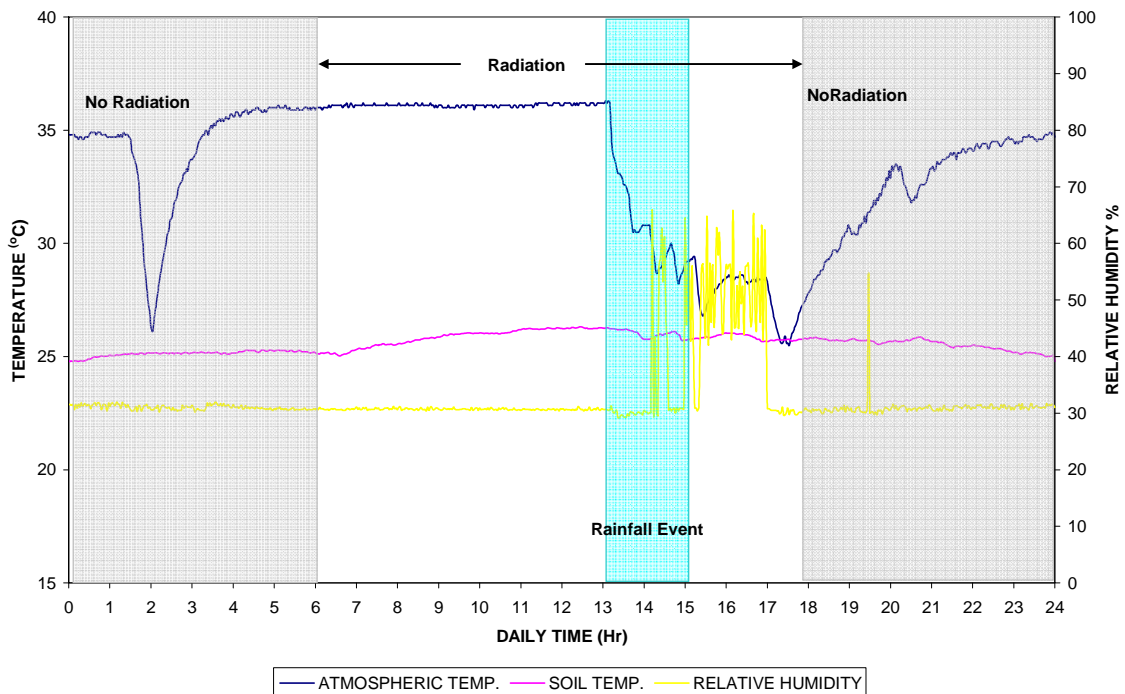
Figure 4-33 Soil-atmospheric variables time series – TE-3R ERC

133
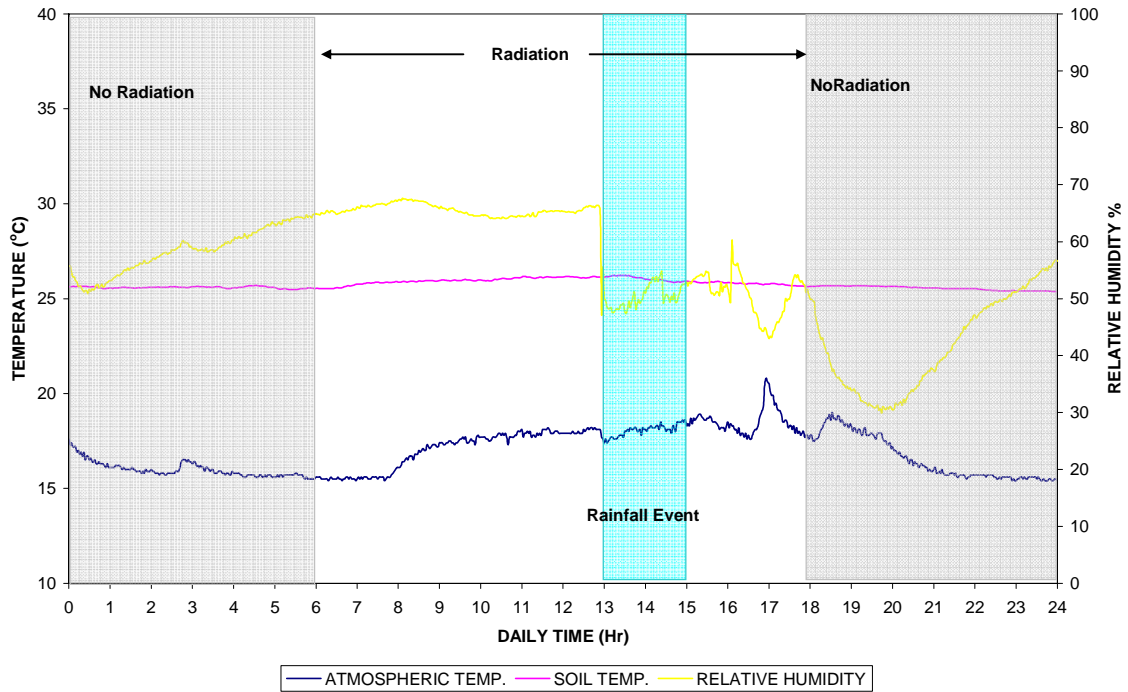
Figure 4-34 Soil-atmospheric variables time series - TE-4 ERC
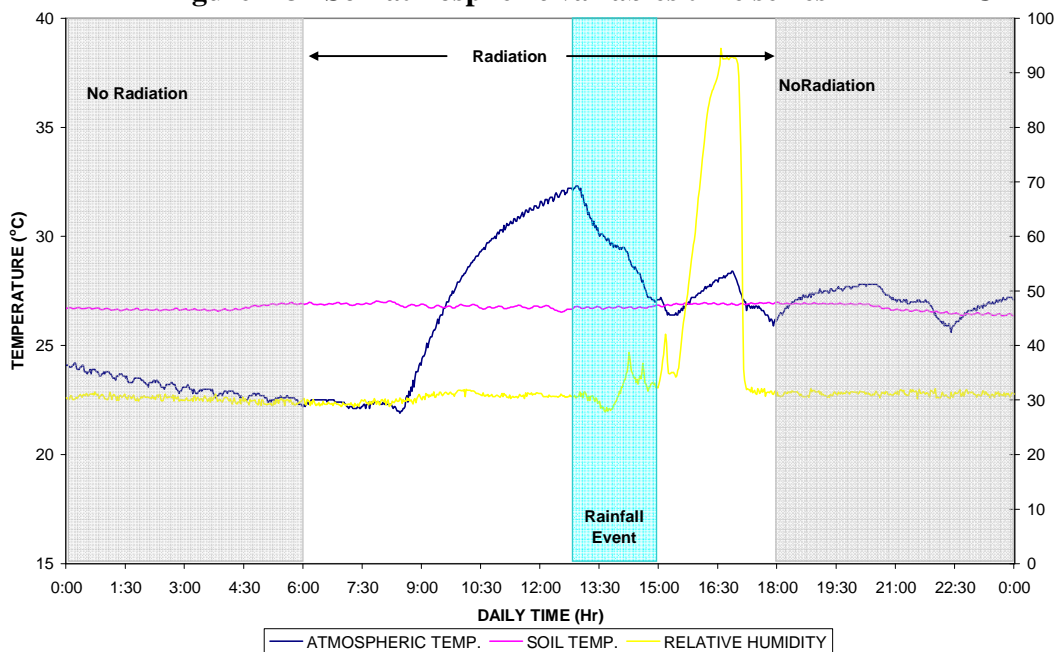
Figure 4-35 Soil-atmospheric variables time series - TE-5 ERC

134
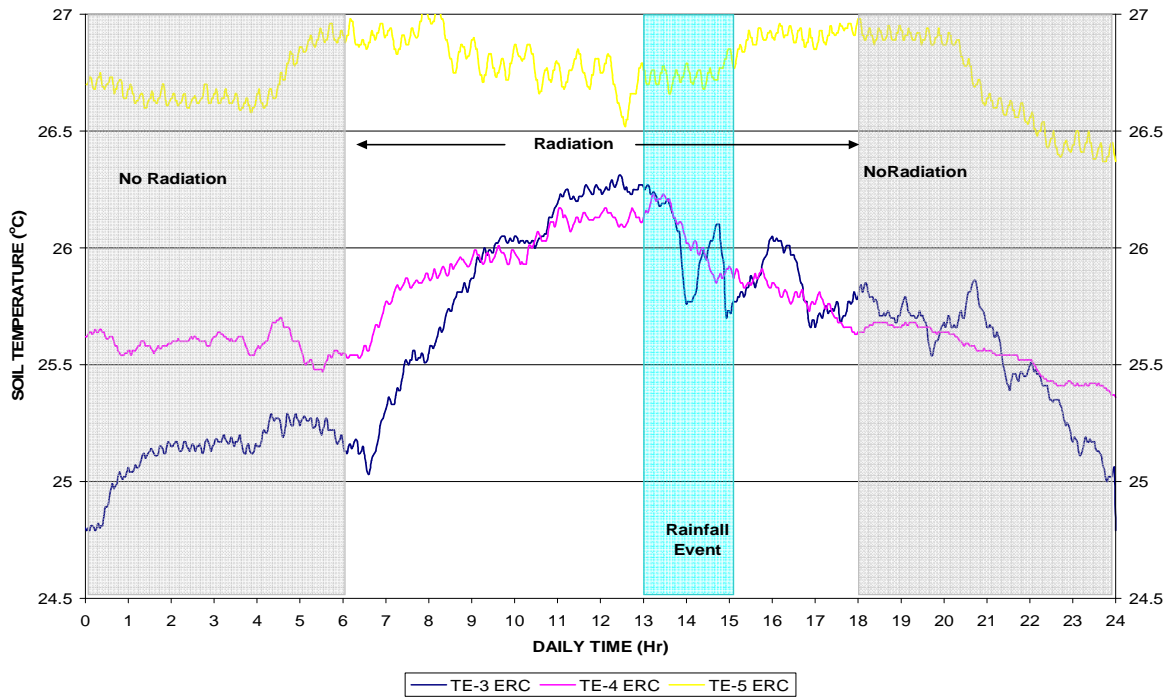
Figure 4-36 Temporal soil temperature for experiments TE 3, -4, -5 ERC

4.5 Breakthrough Curves (BTCs) and Spatial Distribution Models

Temporal and spatial distributions of NaCl (salt), TNT, DNT and related chemicals were analyzed to determine the effect of variable environmental conditions on the fate, transport and detection of ERCs near soil-atmospheric surfaces. Temporal concentration distributions, also known as breakthrough curves (BTCs), were plot and analyzed for all sampled clusters. Spatial concentration distributions were developed with Surfer[TM] and Voxler[TM] for all available sampling times. NaCl concentrations distributions were used to asses the effect of variable environmental conditions on advective and dispersive hydrodynamic transport.

135

Concentration distributions of TNT, DNT, and other related chemicals near analyzed to determine the effect of environmental variables on partitioning, mobility, reactive transport, and detection of these chemicals

4.5.1   NaCl Conservative Tracer

NaCl concentration measurements were taken for the open hydraulic responses experiments under infiltration (wetting) conditions (H.R-6; Table 3-3) and for all transport experiments (Table 3-4). In the hydraulic response experiment, NaCl(s) was placed over the soil surface at the center of the SoilBed. The experiments were designed to assess the dissolution and transport of NaCl solute with infiltrating water. In transport experiments, dissolved NaCl (20 mM) in the rainwater was applied over the surface.

4.5.1.1 Conservative Solute Transport – Hydraulic Response

The concentration distribution of NaCl for infiltration conditions under light exposure in an open system (room temperature) show that, as expected, the solute front moves downward with the infiltrating water as a solute pulse (Figure 4-37). Figure 4-37 shows a progressive downward pulse of NaCl, and increasing concentrations at the bottom of tank. This behavior is attributed to dissolution of NaCl crystals located at surface.

The temporal and spatial distributions also show preferential transport of NaCl. This preferential transport of NaCl coincides with the preferential flow pattern observed from hydraulic head distributions (Figures 4-4 through 4-8).
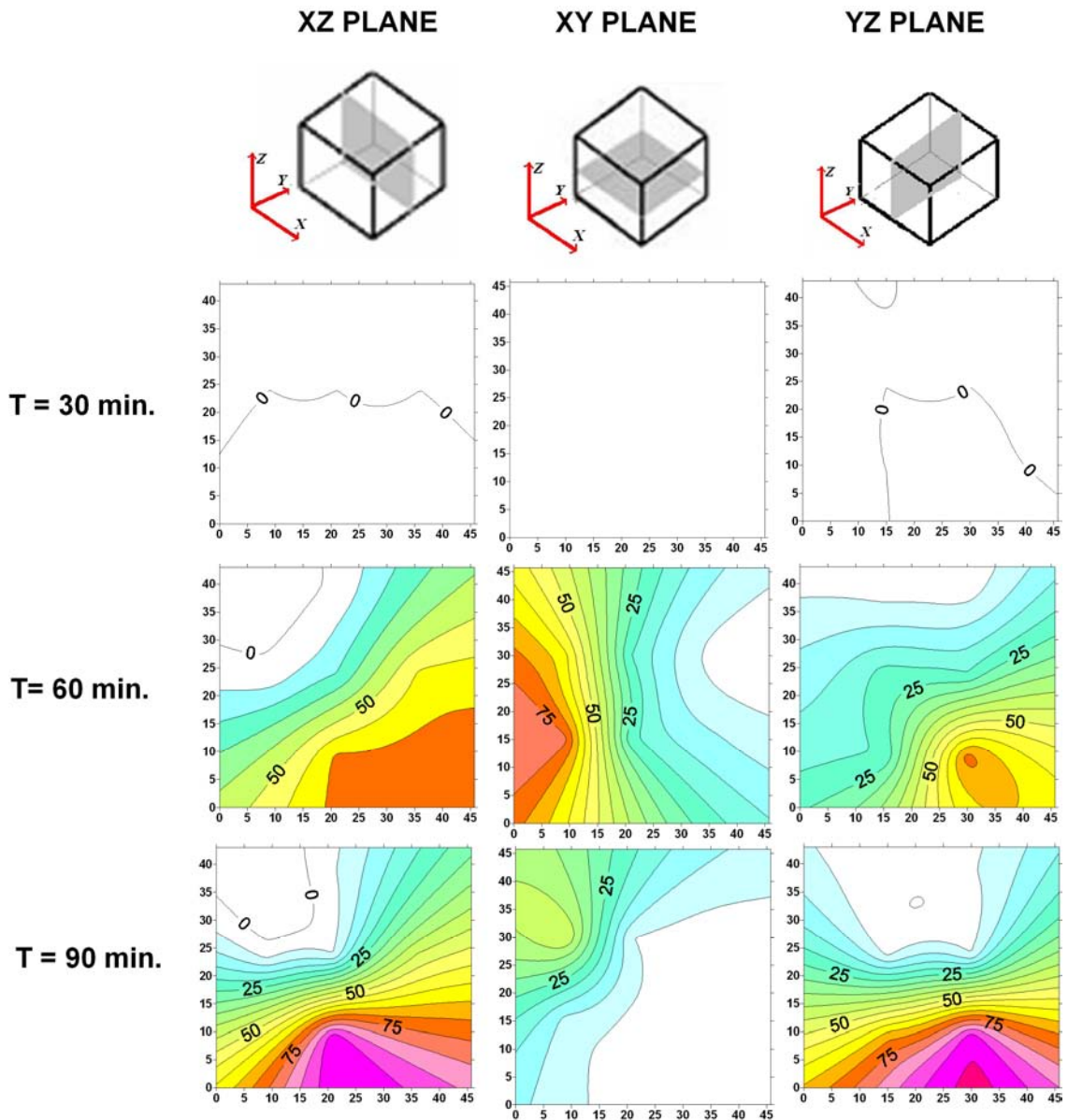
Figure 4-37 NaCl concentration [mM] distribution in a XZ (a) and YZ (b) and XY (c) planes.

4.5.1.2 Conservative Solute Transport –ERC Transport Experiments

Conservative tracer transport experiments were conduced by applying rainwater with NaCl concentration of 20 mM. Results were analyzed to characterize hydrodynamic transport processes and identify flow patterns. It was assumed that NaCl behaved as a conservative solute and, thus, moved advectively as water.

Solute concentration measurements were limited by soil-water saturation and flow. Generally, greater number of water samples were taken during and near rainfall events (Figure 4-38), which increase advective transport and dissolution processes, and was higher for conditions with higher saturation (Figure 4-23). Lower sampling number (e.g., TE-5 ERC) coincided with low water saturation and flow caused by high temperature and low rainfall rates. The number of water samples withdrawn generally increased after the onset of the rainfall event, peaked near the end of the rainfall period (sample No 4 and 5), and then decreased after the end of the rainfall (Figure 4-38). Lower numbers of samples after rainfall indicate low flow conditions.

Low sampling density in sampling clusters 12 and 15 (Figure 4-39) indicate the presence of low water-flow zones, as cluster 15 is located below cluster 12. this is supported by soil water saturation and head distributions (Figure 4-26).
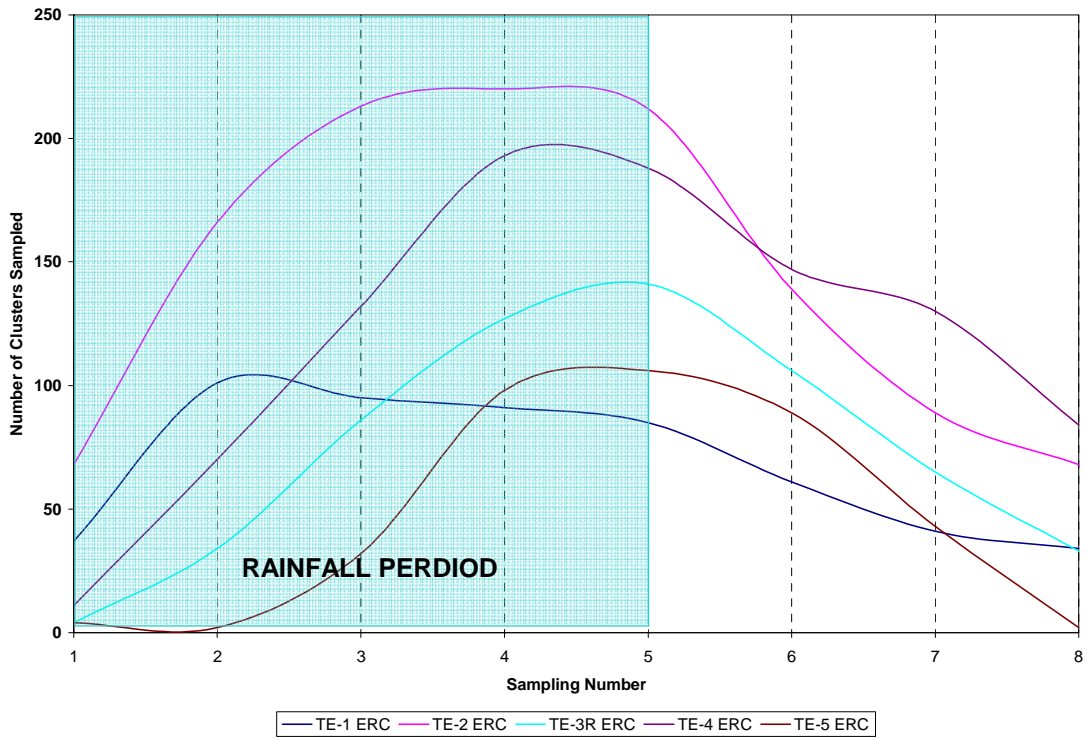
Figure 4-38 Number of clusters sampled over time
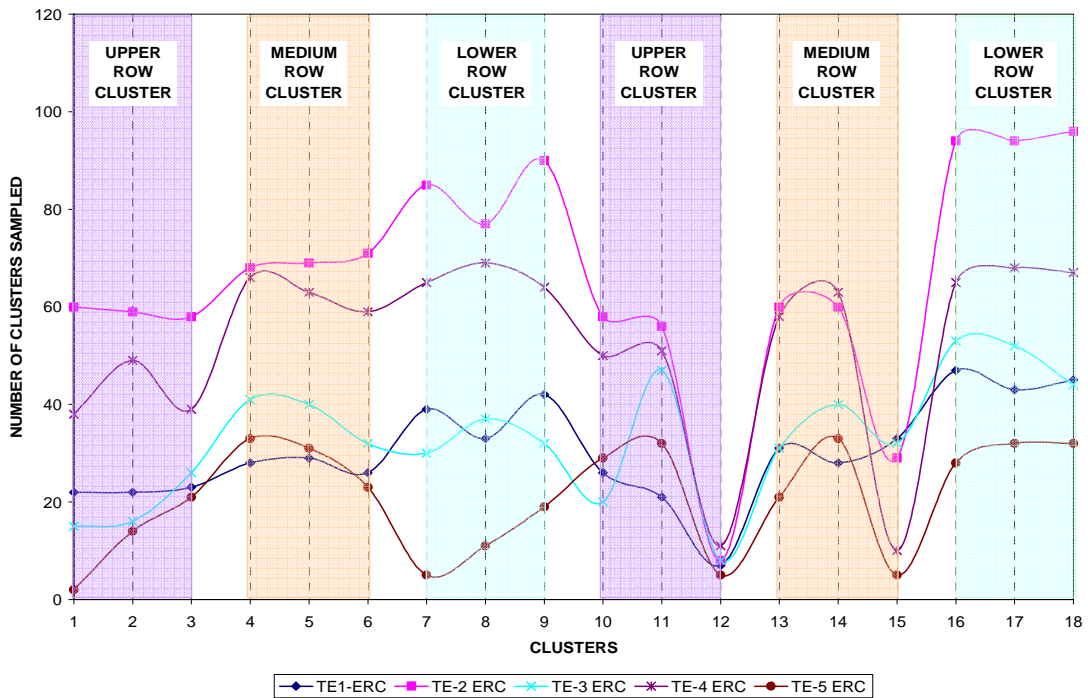
Figure 4-39 Sampling density per cluster

139

Average NaCl concentration over sampling time (Figure 4-40) show a range of concentration around 20 ± 2 mM. Variations in salt concentrations can occur due to evaporation, accumulation, and different amounts of soil water limiting dissolution and advection transport.

Average NaCl concentration distribution by sampling clusters (Figure 4-41) indicate that low concentrations for low temperature conditions are associated with low samples density (Figure 4-39). This is attributed to low flow zones around these clusters, causing low advecting transport influenced by slow mass transfer between mobile and immobile regions. Other variation are attributed to solute transport and accumulation processes during infiltration and evaporation processes.
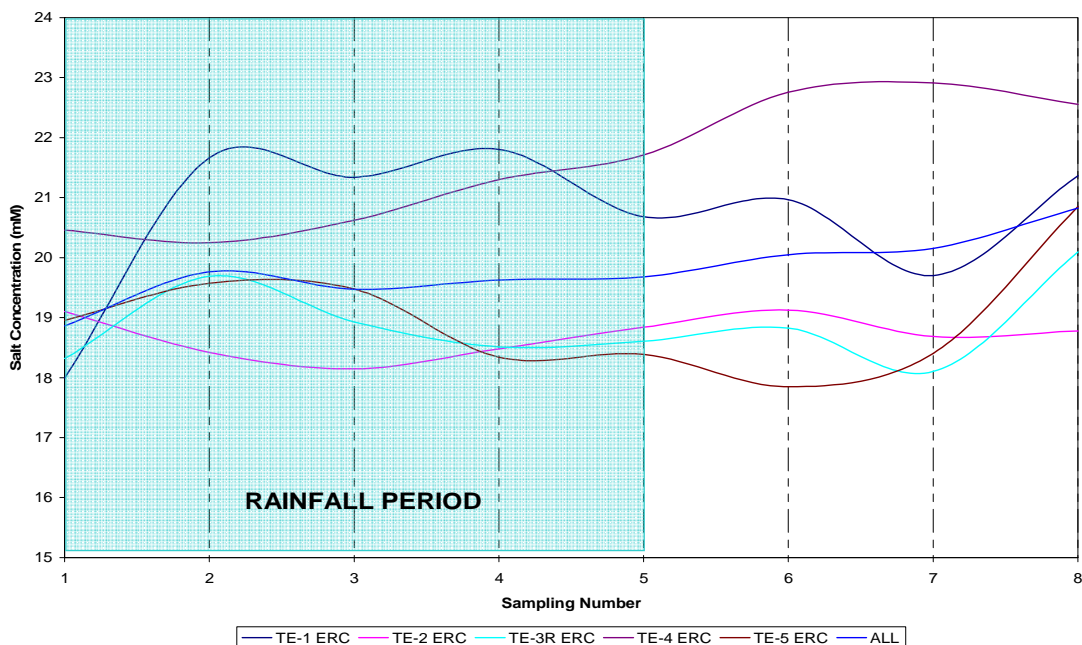
Figure 4-40 Average NaCl concentration in measured over the daily sampling period
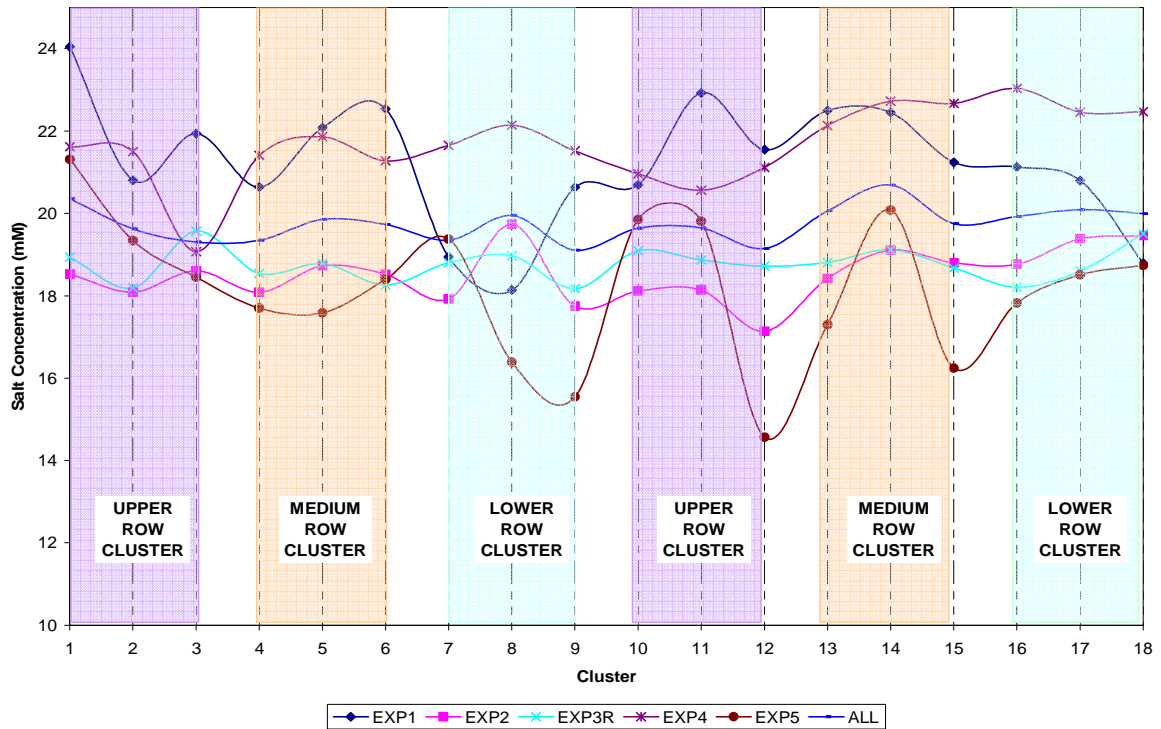
Figure 4-41 Average NaCl concentration by clusters

Average NaCl concentrations gradients (Tables 4-7 and 4-8) indicate low vertical and horizontal concentrations gradients for low rainfall conditions (TE-5 ERC) and high temperatures (TE-3 ERC). Cyclic transport behavior of NaCl solutes under infiltration and evaporation events have been reported by Gutierrez (2008). Lower gradients indicate more uniform concentration distribution, and seem to be related to low water saturation. Highest vertical gradients correspond to high rainfall rates (TE-2 ERC), lower temperatures (TE-4 ERC), and water saturation. This behavior indicates low vertical uniformity at greater flow rates, and suggests vertical preferential flow and grater mechanical dispersion. Higher temperatures can induce evaporation processes decreasing soil water content, and increasing NaCl concentrations. Low gradient and higher uniformity behavior is associated with low

141

water contents conditions, but with saturation mostly distributed over the soil surface. These conditions enhance evaporation, and may contribute to more uniform solute distribution as they are transported downward during infiltration and upward during evaporation.

Table 4-7 Magnitude of horizontal gradients of NaCl

EXP.	MAGNITUDE OF [NaCl] HORIZONTAL GRADIENTS (VERTICAL CENTRAL PLANE)		
	DH/DX Row 1 (C2, C11)	DH/DX Row 2 (C5, C14)	DH/DX (Row 3) (C8, C17)
TE-1 ERC	0.57	0.05	0.06
TE-2 ERC	0.06	0.36	0.13
TE-3R ERC	1.15	1.01	0.03
TE-4 ERC	1.17	0.21	0.26
TE-5 ERC	0.36	0.16	0.01

Table 4-8 Magnitude of vertical gradients of NaCl

EXP.	MAGNITUDE OF [NaCl] HORIZONTAL GRADIENTS (VERTICAL CENTRAL PLANE)		
	DC/DX Row1 (C2, C11)	DC/DX Row 2 (C5, C14)	DC/DX Row 3) (C8, C17)
TE-1 ERC	0.0283	0.0140	0.3521
TE-2 ERC	0.0307	0.0868	0.1690
TE-3R ERC	0.3545	0.0079	0.1580
TE-4 ERC	0.0029	0.0323	0.0003
TE-5 ERC	0.2161	0.0699	0.2452

Spatial and temporal NaCl concentrations for experiment TE-1 ERC (Figure 4-42) show heterogeneous distributions during the first 3 days of the experiments. After the third day, concentrations tend toward a constant value of similar characteristics as the source (20 mM). NaCl concentrations higher than the inlet concentration are initially observed in certain regions of the sampling volume, indicating zones of preferential flow paths and solute accumulation. The transport behavior of NaCl observed in this experiment is similar to that

observed for a similar experiment, where NaCl was placed as a point source (Anaya and Padilla, 2006).

Breakthrough curves for experiment TE-2 ERC (central clusters, Figure 4-42) show high NaCl concentrations during the 5th and 7th experimental day, suggesting solute accumulation. This may be caused by an increase in temperature (Figures 4-28) after day 5, potentially inducing higher evaporation rates enhancing solute accumulation.

NaCl BTCs times series and spatial models for experiment TE-3 ERC (Figure 4-44) show a rapid breakthrough to background concentration values of 20 mM, and the lowest deviation value around the geometric mean of all experiments. The spatial model shows a preferential flow path during rainfall event influenced by advection transport. The experiment TE-4 ERC, show a high dispersion in their breakthrough curves (Figure 4-45) with an increasing trend after the seventh day of the experiment.

Breakthrough curves for experiment TE-5 ERC (Figure 4-46) show a slow increase of NaCl concentrations that tend to equilibrate after the sixth day around the input concentration of 20 mM. The spatial models show poor dispersion into the volume of control due the lowest soil water contents, limiting, and advection transport. NaCl relation with others environmental variables (hydraulic head and soil saturation) are shown in Figure 4-47 where a specific day is showed for the three variables in the experiment TE-3 ERC.

143
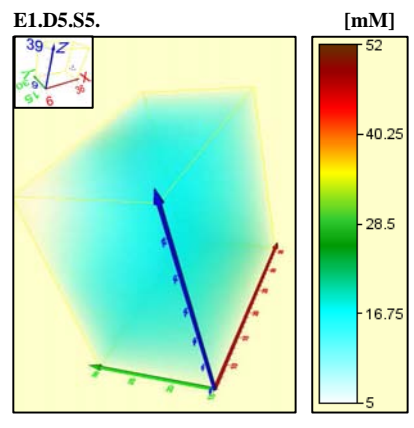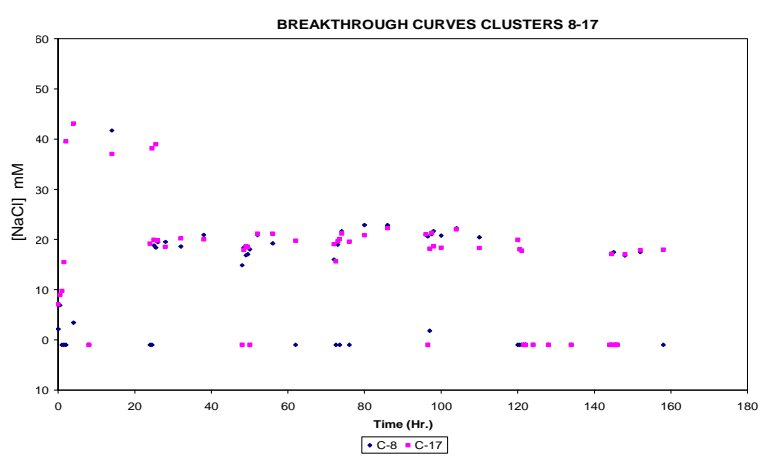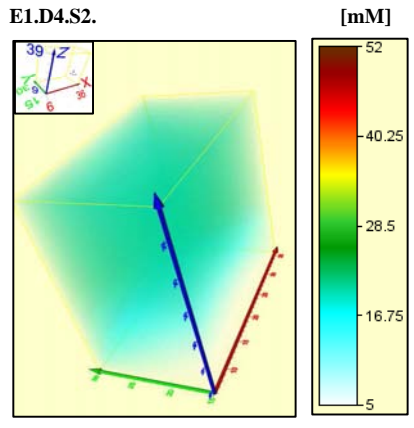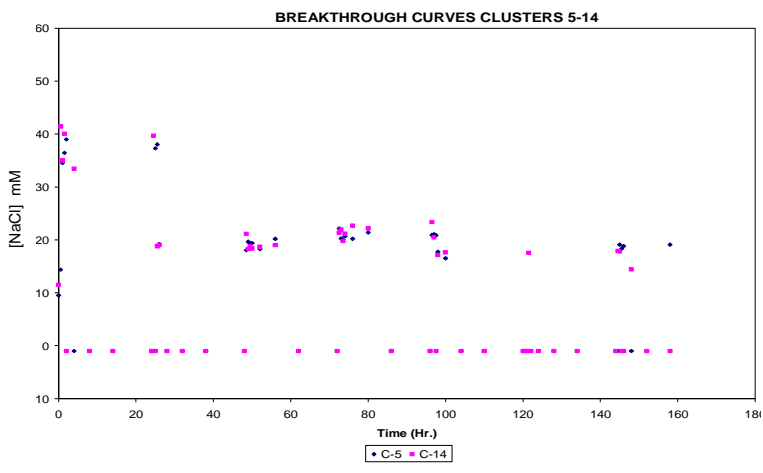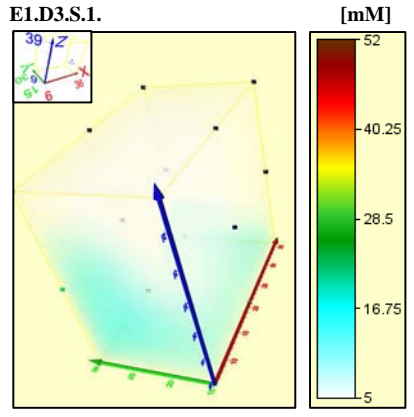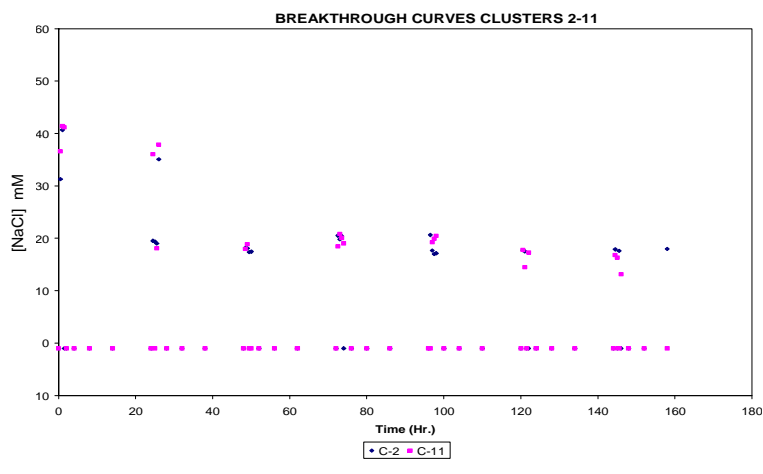
Figure 4-42 Temporal and spatial NaCl concentration distribution – TE-1 ERC

144
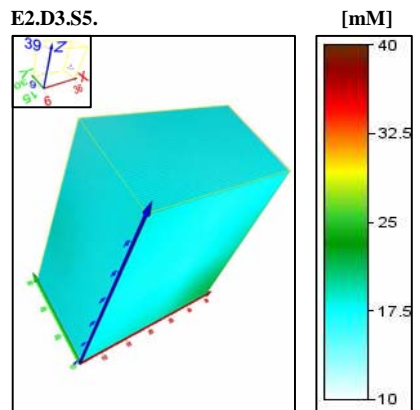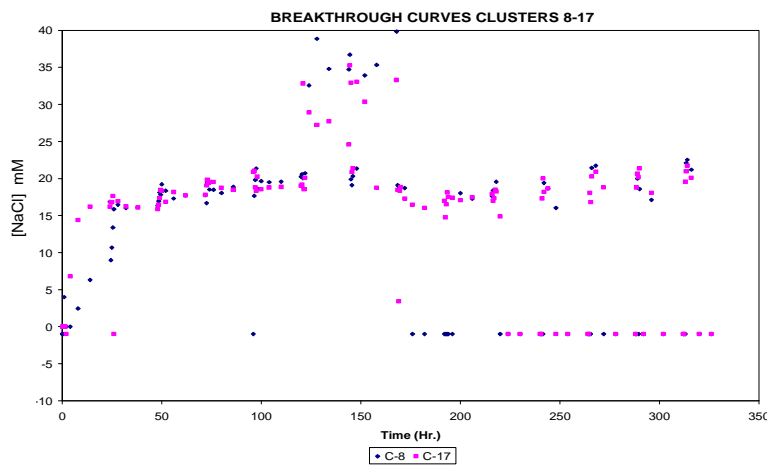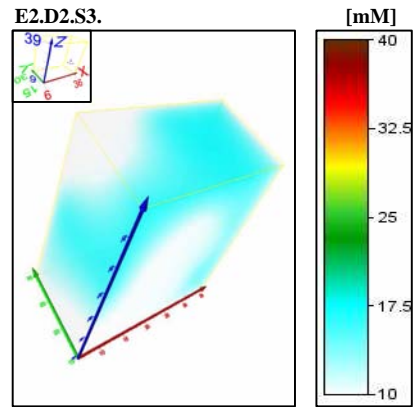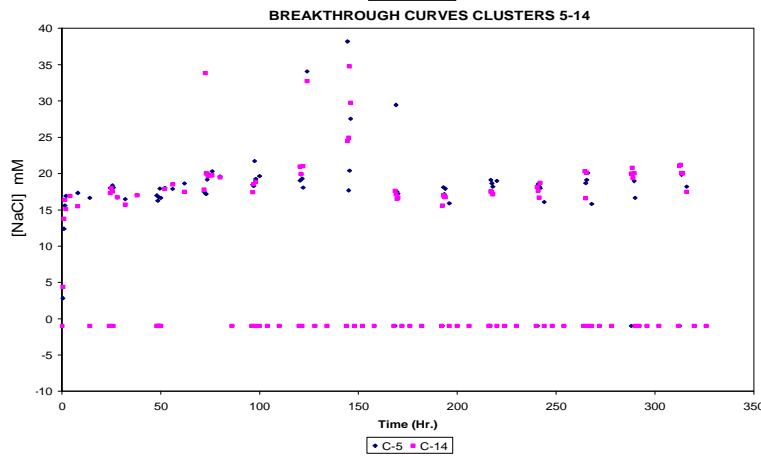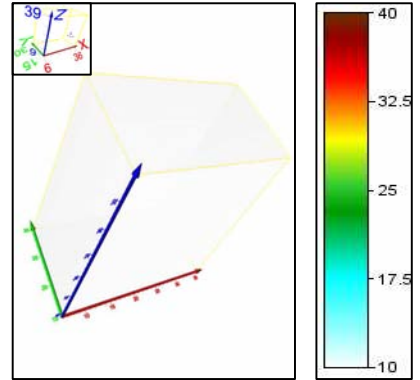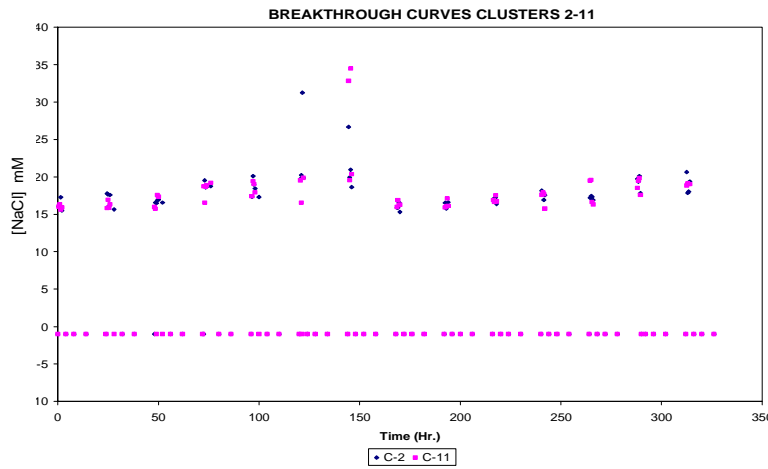
Figure 4-43 Temporal and spatial NaCl concentration distribution – TE-2 ERC

E2.D1.S1.   [mM]
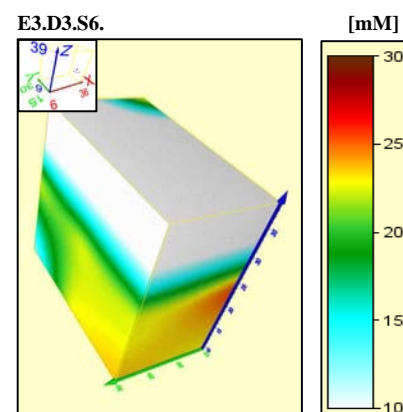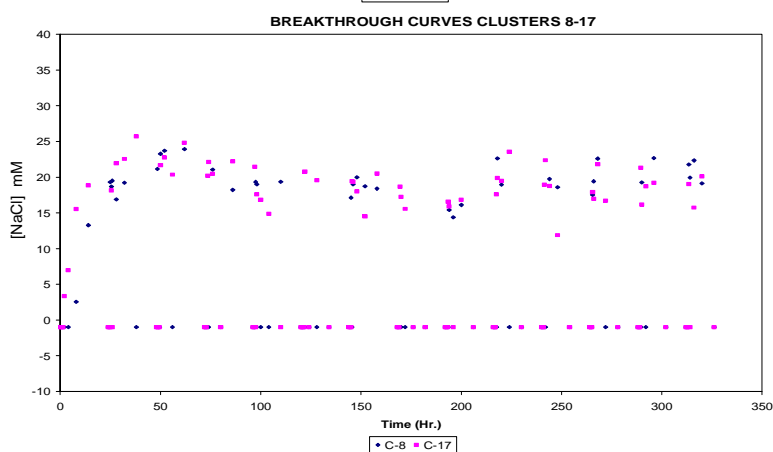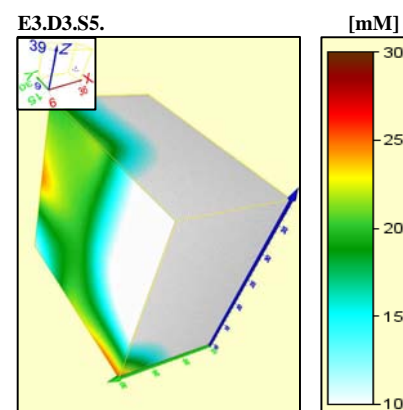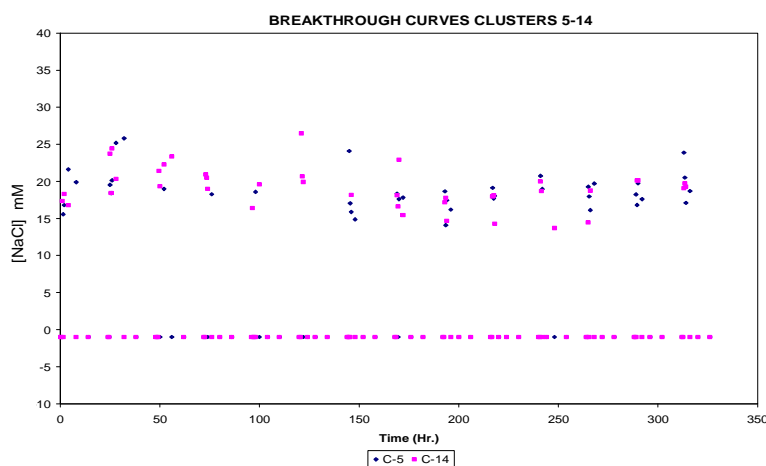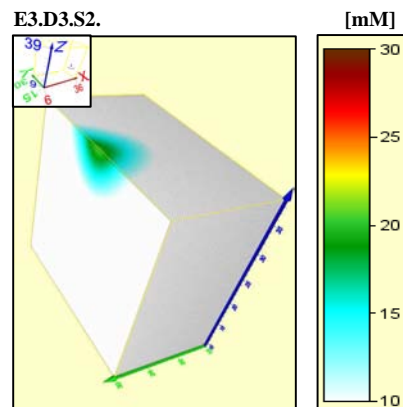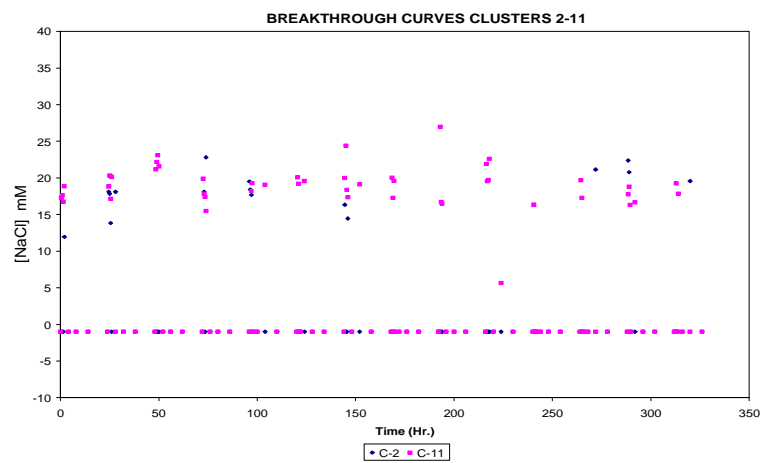
Figure 4-44 Temporal and spatial NaCl concentration distribution –TE-3R ERC
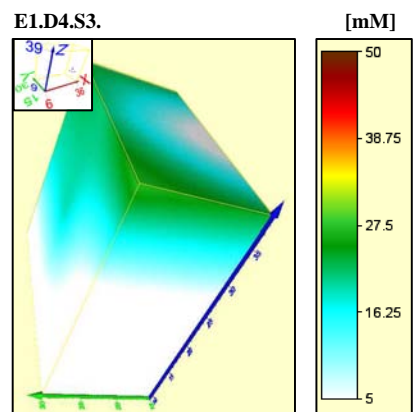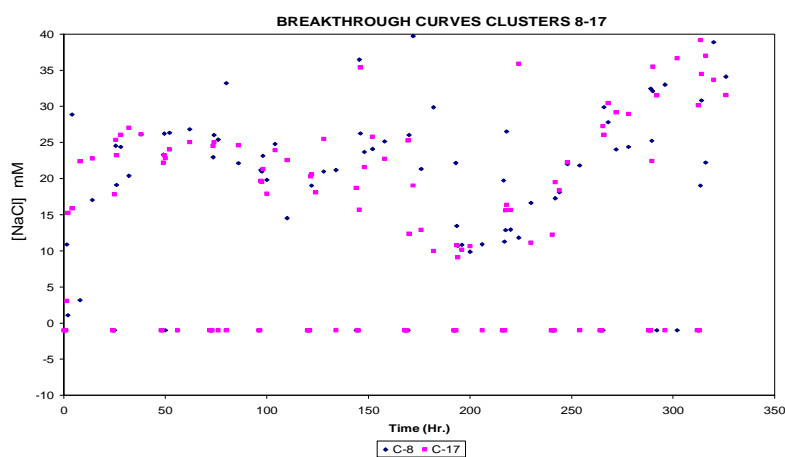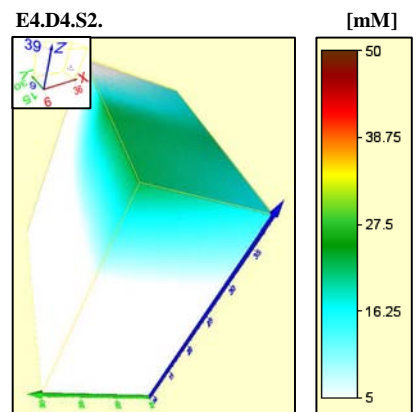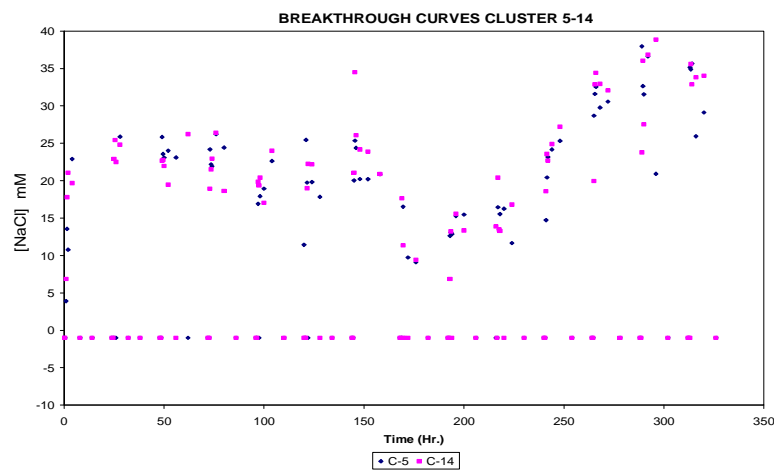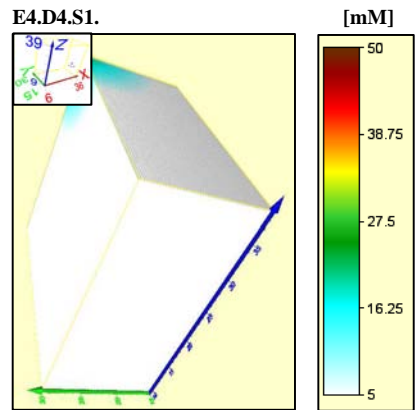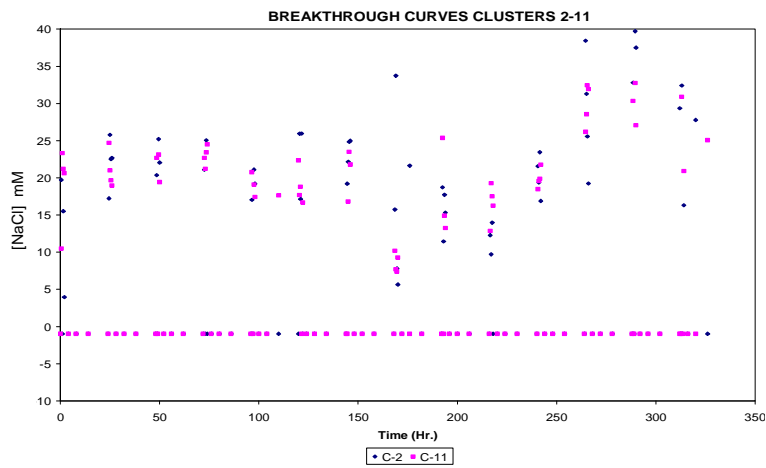
Figure 4-45 Temporal and spatial NaCl concentration distribution – TE-4 ERC

147
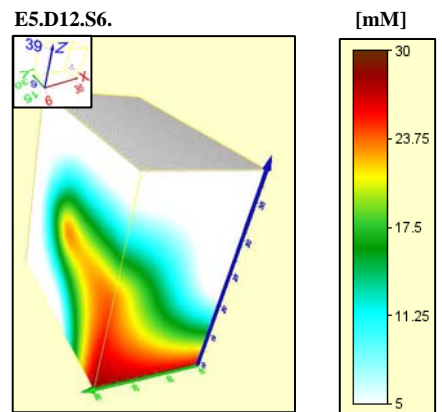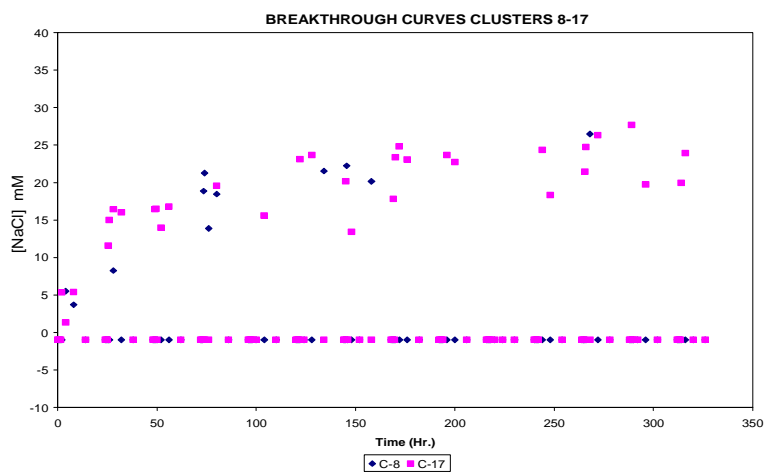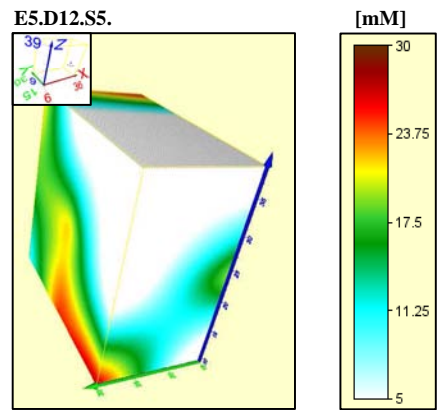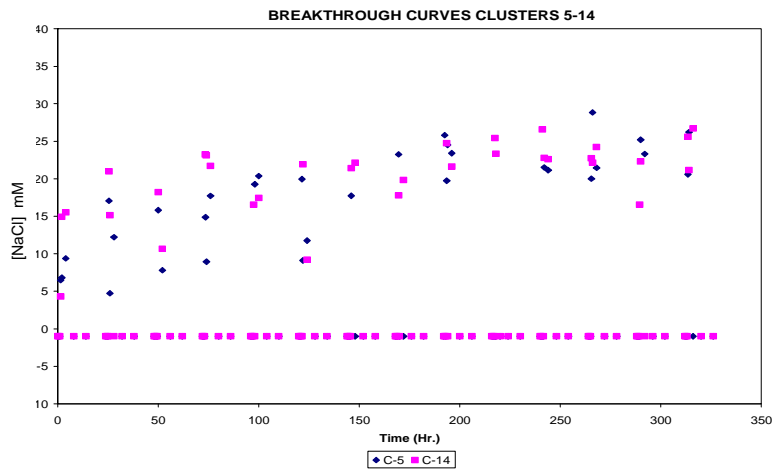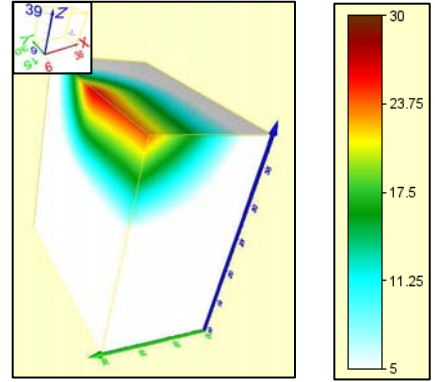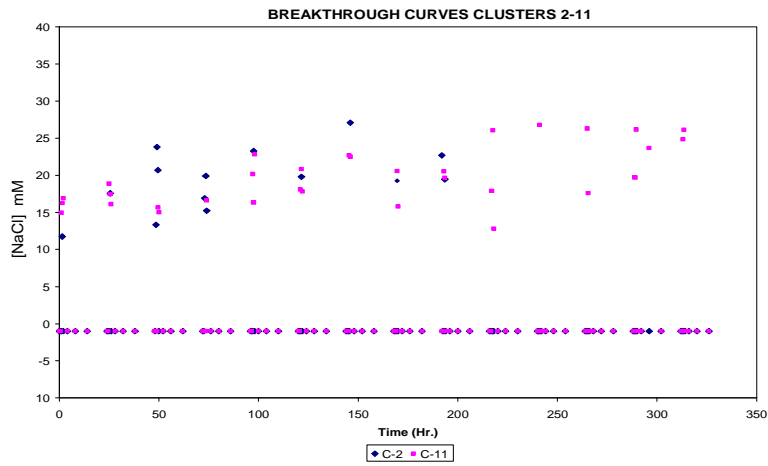
Figure 4-46 Temporal and spatial NaCl concentration distribution – TE-5 ERC

148

E5.D12.S3.   [mM]
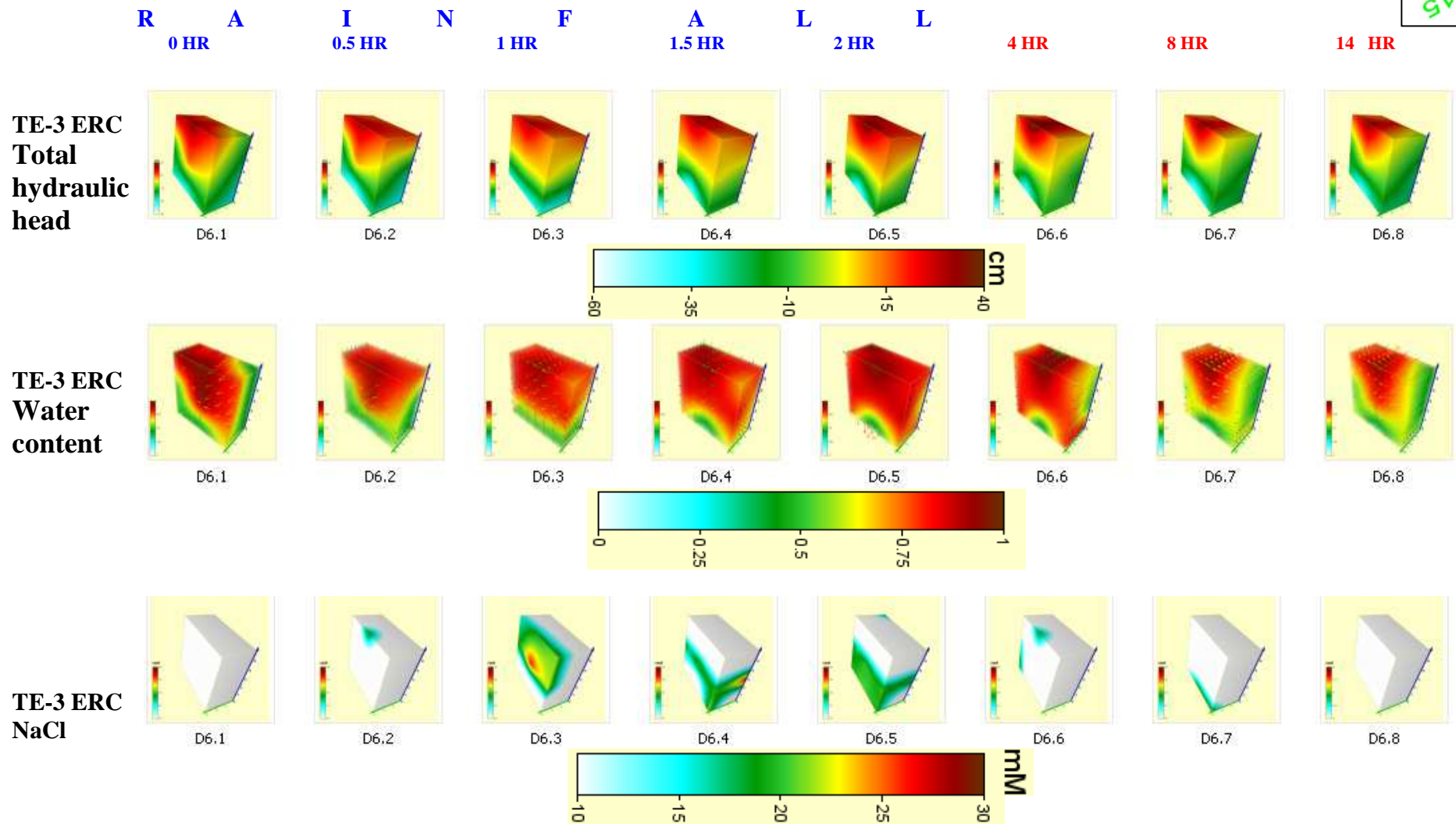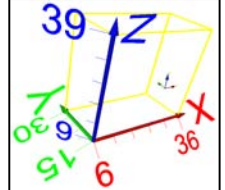
Figure 4-47 Spatial and temporal relations between NaCl concentration, total hydraulic head, and soil saturation for TE- 3R ERC

The breakthrough NaCl analysis was used to estimate time of travel values for each experimental day and cluster. This travel time is defined as the time it takes for a parcel or packet of water, contaminant, or tracer from one point to another. In this case travel time was quantified from the soil surface, where solute infiltration occurs and the solute enter to the system, to a given depth point. A travel time was defined as the time it took to reach a 50% of the inlet concentration ($0.5 \, C_o$). All travel times values are presented in Tables 4-9, 4-10 ad Figures 4-48 and 4-49:

Table 4-9 Average travel time (hr) given by cluster

EXP.	CLUSTER																	
	1	2	3	4	5	6	7	8	9	10	11	12	13	14	15	16	17	18
TE-1 ERC	0.4	0.2	0.3	0.6	0.4	0.2	0.6	1.9	1.0	0.4	0.3	2.1	0.2	0.4	0.2	0.1	0.3	0.5
TE-2 ERC	0.3	0.3	0.3	0.6	0.5	0.6	3.1	2.2	2.1	0.3	0.3	1.0	0.7	0.5	0.6	1.0	0.7	1.7
TE-3R ERC	2.8	1.9	0.8	1.0	1.2	1.4	2.9	2.4	1.6	1.0	0.4	1.2	1.4	0.9	0.9	1.8	1.6	1.4
TE-4 ERC	0.4	0.2	0.4	0.9	0.9	0.8	1.1	1.1	1.0	0.5	0.3	0.6	0.8	0.8	2.6	1.2	1.0	1.2
TE-5 ERC	3.9	1.0	1.2	1.6	1.6	1.9	2.0	4.4	3.0	1.0	0.9	1.8	1.9	1.3	3.2	2.5	2.3	3.5

Table 4-10 Average travel time (hr) given by experimental day

EXP.	DAY													
	1	2	3	4	5	6	7	8	9	10	11	12	13	14
TE-5 ERC	3.4	2.0	1.7	2.2	2.4	2.1	2.0	1.3	1.6	1.2	2.2	1.5	1.6	1.2
TE-4 ERC	1.2	0.9	0.8	0.8	0.7	0.7	0.6	0.9	0.9	0.7	1.1	0.8	1.0	0.8
TE-3R ERC	3.1	0.8	1.4	1.4	1.2	1.1	1.0	1.0	1.1	2.0	1.4	1.3	1.2	1.6
TE-2 ERC	7.0	0.5	0.3	0.2	0.3	0.4	0.2	0.4	0.8	0.4	0.8	0.7	0.3	0.7
TE-1 ERC	1.1	0.2	0.6	0.3	0.2	0.4	0.8							

Generally, Table 4-9 and Figure 4-48 show that superficial (top) sampling cluster, respond faster, than cluster in the med-level and bottom clusters planes. Faster response is observed for experiments TE-1, -2, and -4 ERC, having travel times lower than 30 minutes for the

upper cluster plane, and increasing its value with deeper planes. Experiments TE-5 and -3 ERC show higher travel times (Figures 4-48 and 4-49). Experiment TE-5 ERC presents, in general, the highest travel times. The highest values in the experiment TE-5 ERC is attributed to low soil saturation, which result in higher velocities for similar water flux. lower travel times are associated with higher water contents. Patterns with different average behavior (travel velocity increase with depth) can indicate high probability of preferential flow or low transport near these clusters. The lowest travel times correspond to experiments 1 and 2 with a average value less than 1 hour.
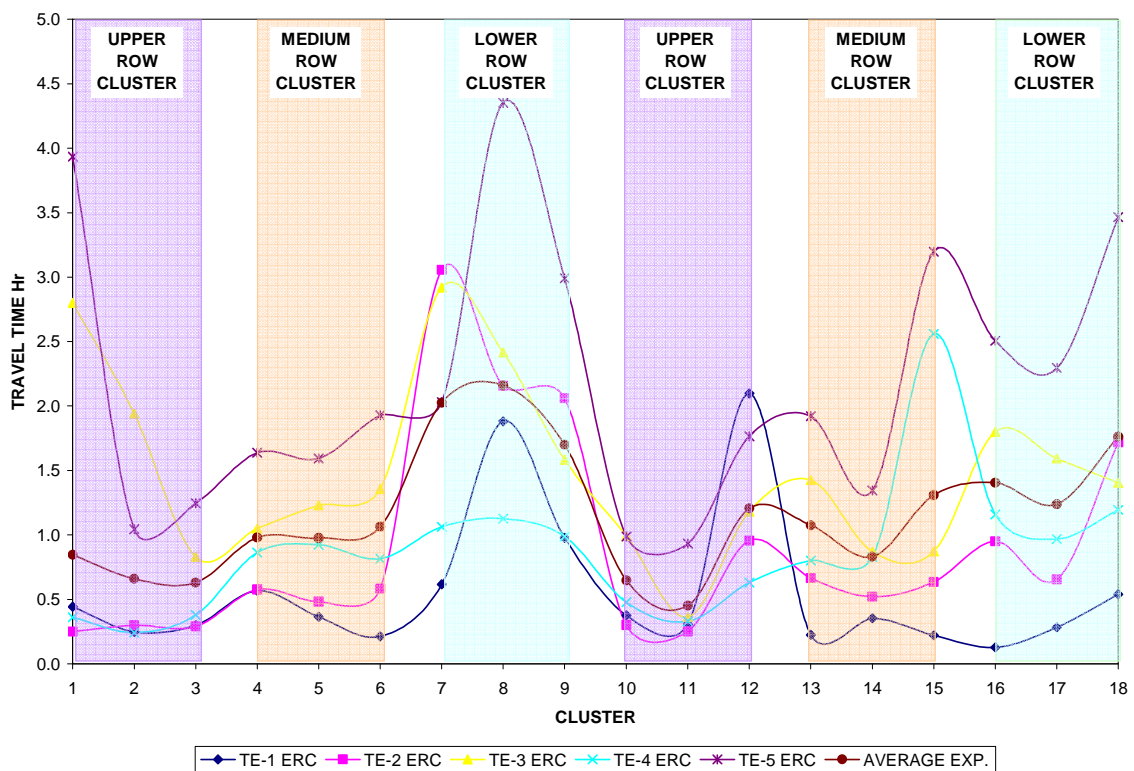
Figure 4-48 Average travel time by sampling cluster

Average travel time for each experimental day indicate higher values at the beginning of all experiments, especially for experimental day 1.

151
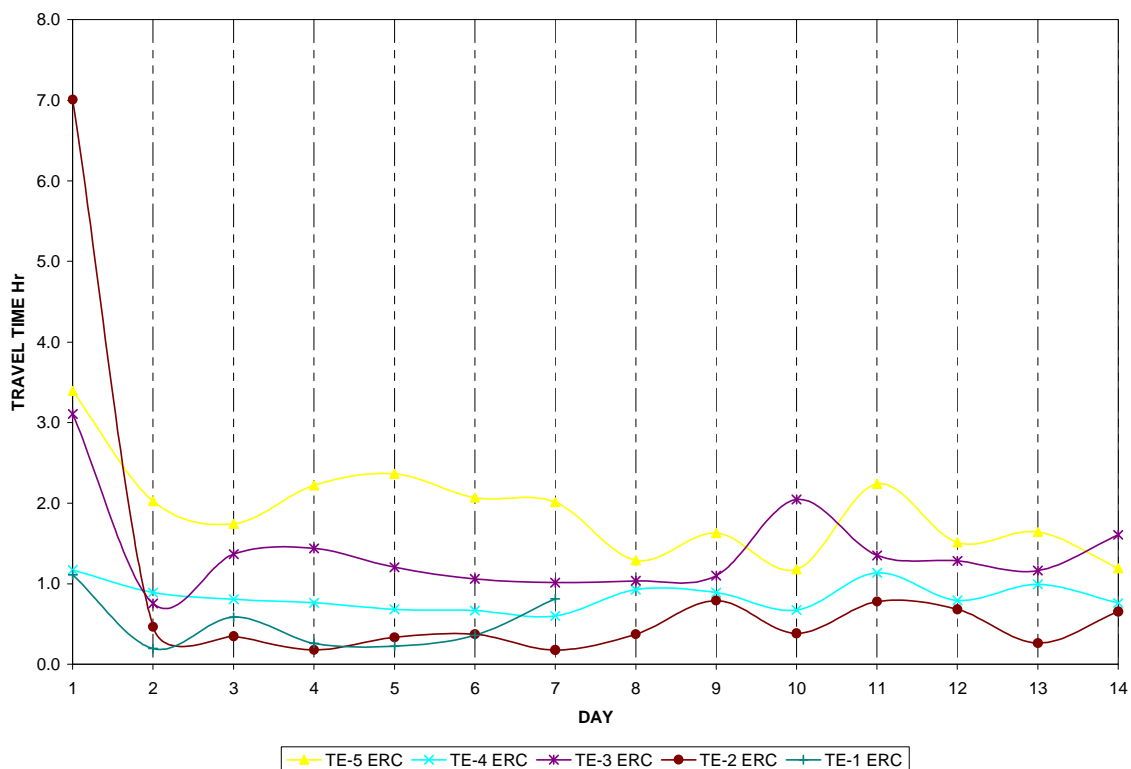
Figure 4-49 Average travel Times by experimental day

4.5.2 TNT and DNT concentration distributions

TNT and DNT transport experiments involved burying a point source of these chemicals under the soil surface, and applying cyclic rainfall and radiation events under different atmospheric temperatures. Concentration distributions of 2, 4, 6 TNT and 2, 4 DNT and other related chemical were analyzed to determine the effect of variable environmental condition on the partitioning behavior, mobility, reactive transport, and detection of these chemicals. It is assumed that these chemicals are subjected the same hydrodynamic transport processes as NaCl.

Chemical analysis of TNT crystals used in the simulated landmines show that the TNT source was not pure, and contained 2, 4 DNT impurities. This can be seen in a chromatogram the TNT source (Figure 4-50). The chromatogram shows an initial solvent (methanol) peak, followed by a TNT peak, around 5.5 minutes, and a DNT peak around 6.1 minutes. The presence of DNT, thus, did not necessarily indicate TNT degradation. TNT and DNT fate and transport processes were analyzed simultaneously.
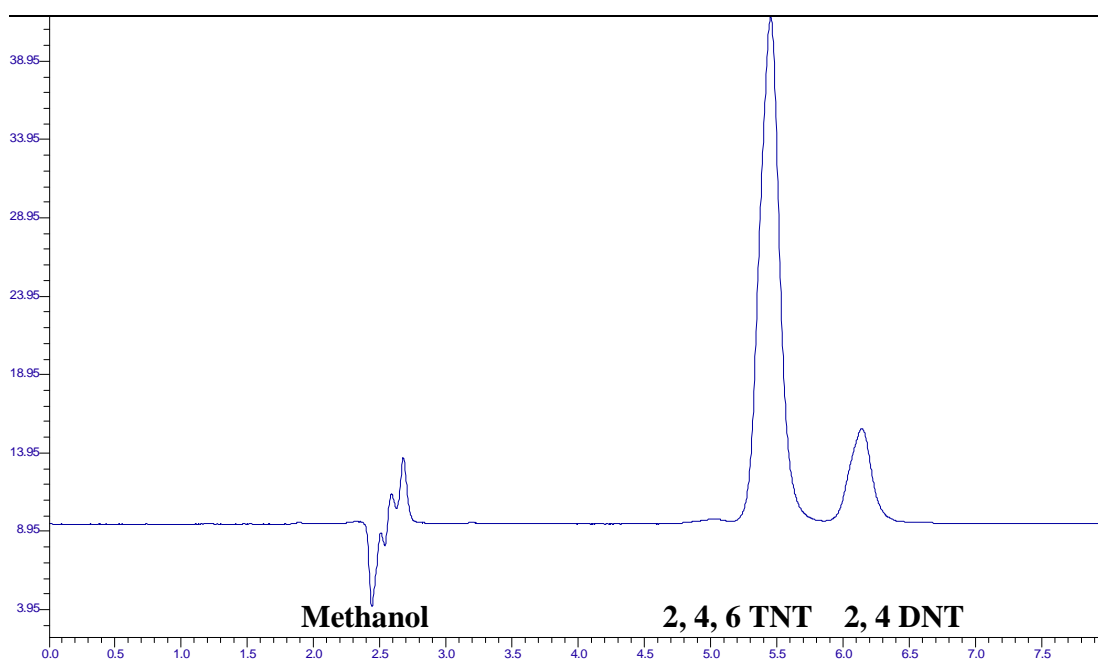
Figure 4-50 Chromatogram of solid crystal of TNT used in landmine sources

4.5.2.1 TNT and DNT in the aqueous phase

Experimental results indicate that TNT detection density (number of samples with detected TNT solutes) and concentration are strongly influenced by variability in environmental conditions (Figure 4-51 and 4-52). TNT detection density tends to increase during the rainfall period for high soil-saturation conditions (TE-2 and -6 ERC) at 25 ^{o}C.

153
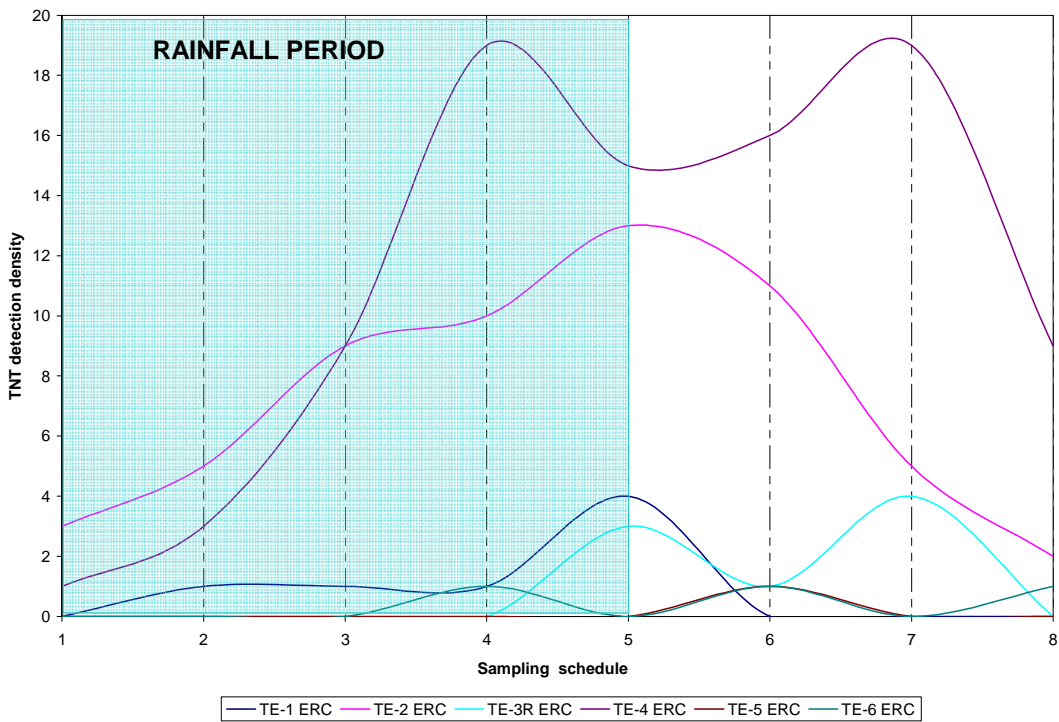
Figure 4-51 TNT detections over the sampling schedule
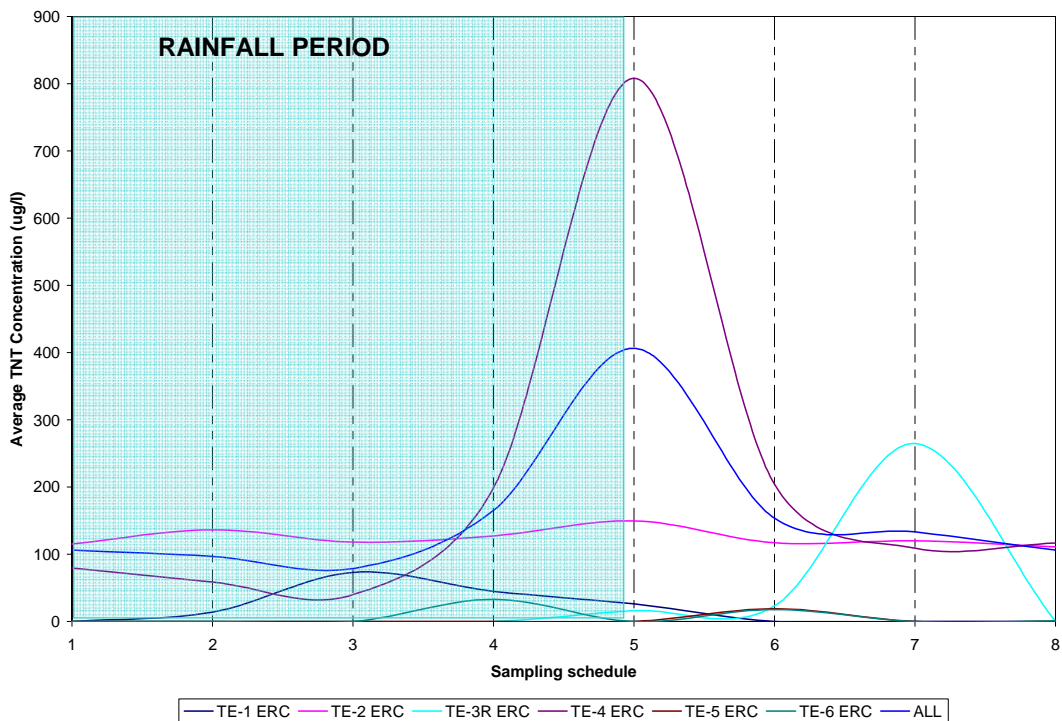
Figure 4-52 Average TNT solute concentration (μg/l) over the sampling schedule

154

Detection density for conditions of lower saturation (TE-3R,-5, and -6 ERC) is lower than at higher saturations. Maximum detection density occurs generally near the end of the rainfall periods, depending on environmental conditions, but seem to also be influenced by radiation events (Figure 4-51). High detection density is also associated with the beginning of the no-radiation period after the rainfall event, for low (15 ^{0}C, TE-4) and high (35 ^{0}C; TE-3R) temperature conditions. Low rainfall (TE-5) and no radiation resulted in very low TNT detection density, with peaks before and after the end of the rainfall period (Figure 4-51). The low detection density obtained for experiment TE-1 ERC, which is similar to experiment TE-2 ERC, is attributed to the smaller source size in TE-1 ERC. It is also controlled to the shorter length of the experiment. It is, expected that the number of samples with TNT detection increases for sources buried for longer period and subjected to cyclic environmental variations.

Higher TNT solute concentration are generally observed during rainfall period (Figure 4-52), except for high temperature conditions (TE-3R ERC). Higher concentrations are observed for the high saturation conditions obtained at high rainfall rates for low (15 ^{0}C) and mid-range (25 ^{0}C) temperatures (TE-4 and -2 ERC, respectively). Very low concentrations are measured for low saturation experiments induced by low rainfall rates (TE-5 ERC) and no radiation (TE-6 ERC). TNT average solute concentrations at high atmosphere concentrations (TE-3R ERC) are influenced by water saturation and temperature. Low relative saturation results in lower concentrations that under higher saturation conditions (TE-4 and -2 ERC).

Concentrations are, however, higher than lower temperature conditions (25^0C) for similar soil water saturation (experiments TE-5 and -6 ERC).

Average TNT solute concentration under variable conditions indicate that soil-water saturation and flux rates strongly influenced TNT detection density and concentration near the TNT source. This is attributed to greater dissolution capacity at higher water saturation, and lower partioning into the gas phase at low temperatures. Although higher dissolution rates and concentrations are expected for higher temperatures, these are limited by the lower water- saturation conditions attained at higher temperatures. Higher temperatures also induce higher partitioning into gas phase (as given by K_H, Table 2-3) and degradation rates, thus reducing concentrations in the aqueous phase. Potential degradation of TNT is supported by increase detection of potential by-products, as later discussed in this chapter.

Spatial analysis of TNT detection (Figure 4-53) an average solute concentration (Figure 4-54) by cluster indicate higher detection and concentrations near the SoilBed bottom, and above bottom clusters No. 8, 17, and 19 (Figure 4-53). This is attributed to preferential flow paths that carry dissolved TNT solute to the bottom, where it accumulates. The location of higher TNT detection density and concentration correspond to zones of low NaCl travel times (Figure 4-48).
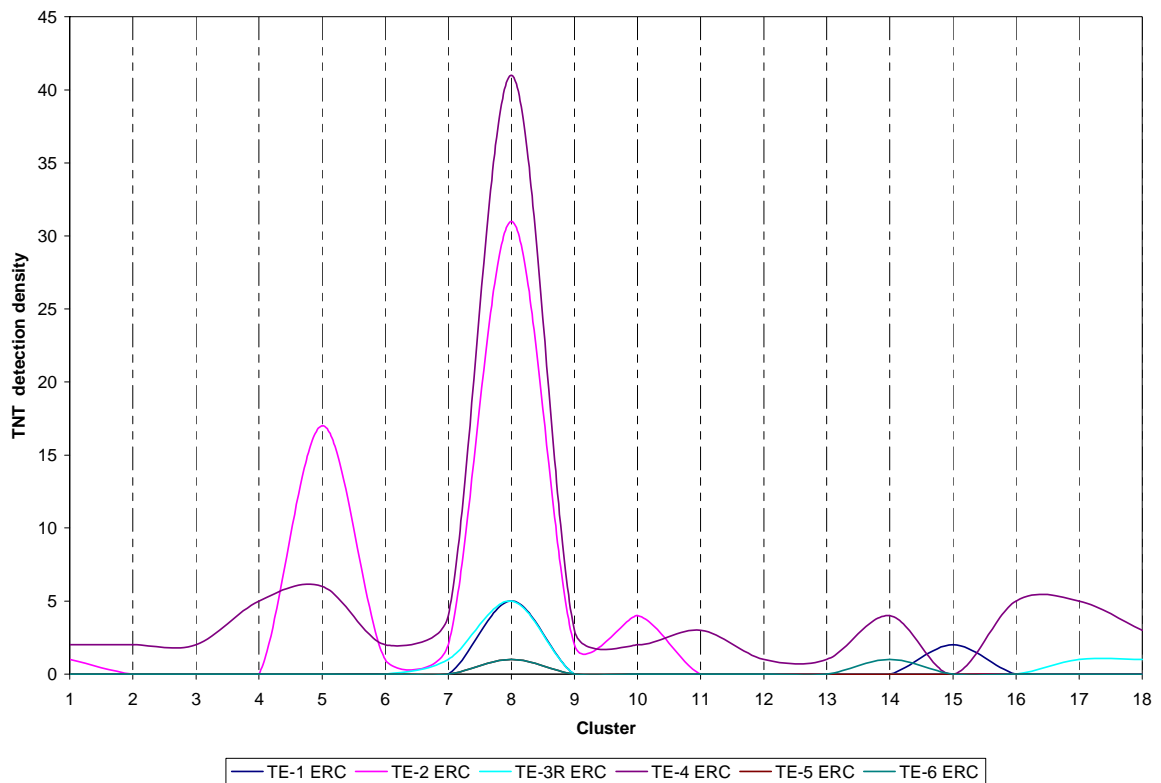
Figure 4-53 TNT detection in sampling clusters

Temporal distributions of TNT detection density and average solute concentrations show higher initial values with a tendency to decrease over time (Figures 4-55 and 4-56). This is attributed to higher initial dissolution rates, and the influence of greater partition into the gas and soil phases and degradation at later times.

Detection densities tend to increase to as maximum near the first 4 days. TNT solute concentrations tend to decrease over time for higher saturation conditions (TE-4 ERC and -2 ERC), but increase to a peak concentration and then decrease for lower saturation conditions (Figure 4-56). Similar results have been observed in dissolution experiments of TNT and DNT. The time and magnitude of peak detection and concentration depends on

157

environmental conditions. Earlier peak detection is associated with conditions that enhance drainage (e.g., high temperature). Higher TNT detection density and concentrations are associated with high saturation and temperature conditions. This is attributed to higher initial dissolution rates at these conditions. Higher TNT and DNT dissolution rates at higher water-contents also have been reported by other researchers (Gutierrez, 2008; Torres, 2008).
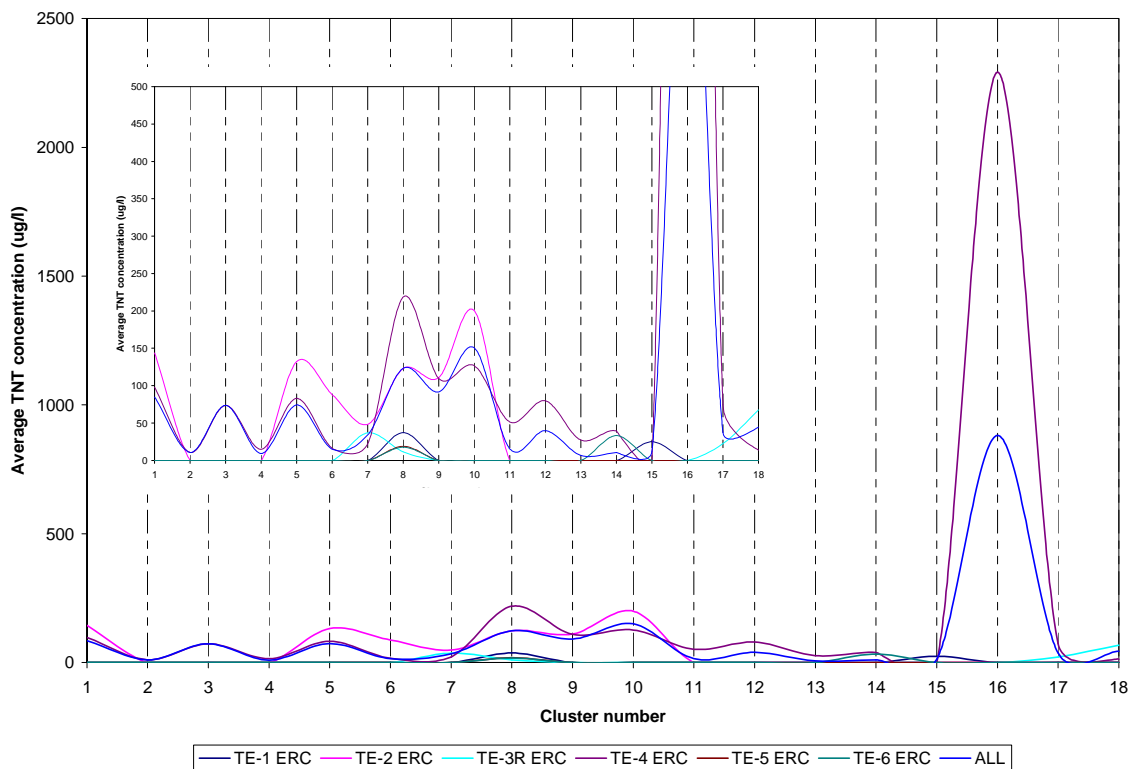
Figure 4-54 Average concentration of TNT solute by cluster

Maximum DNT detention density data generally occurs near the end of rainfall events, exept for the experiment TE-5 ERC, which shows greater density six hours after the end of water precipitation (Figure 4-57).

158
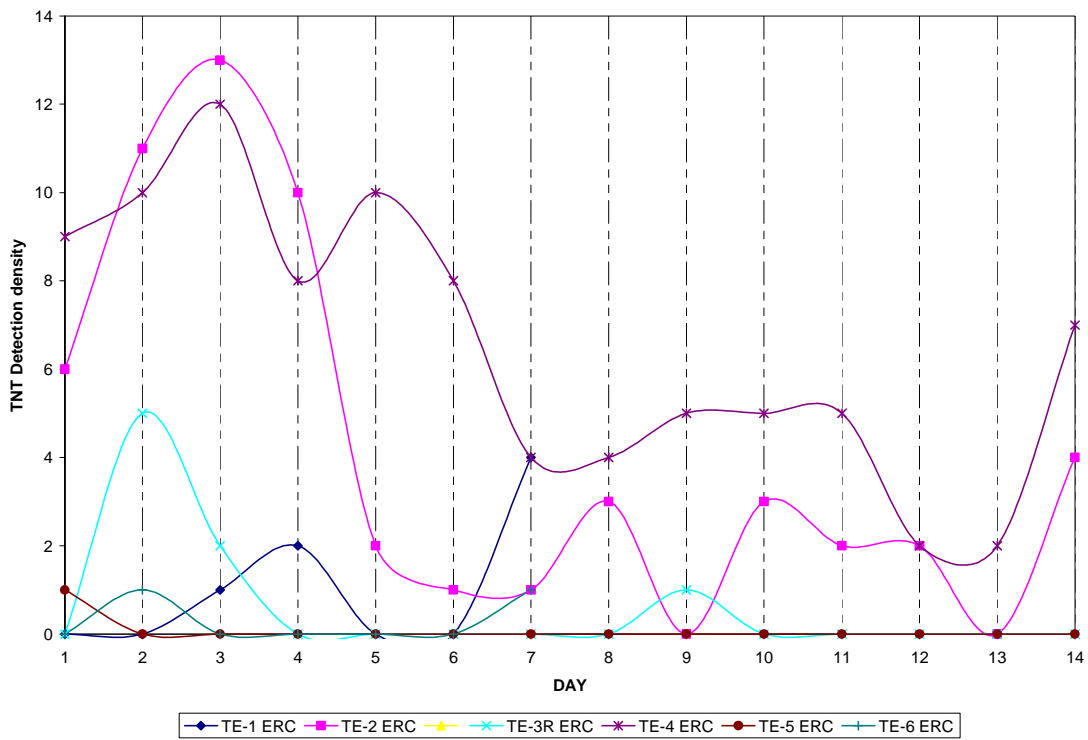
Figure 4-55 TNT detection density over time
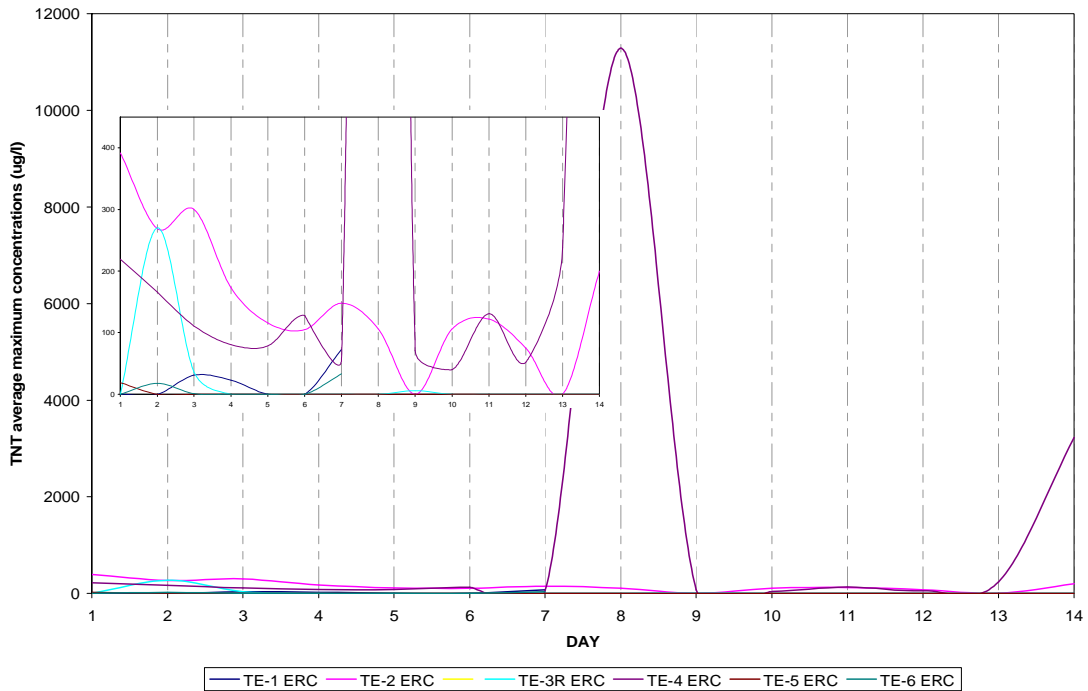
Figure 4-56 TNT average maximum concentrations over time

159
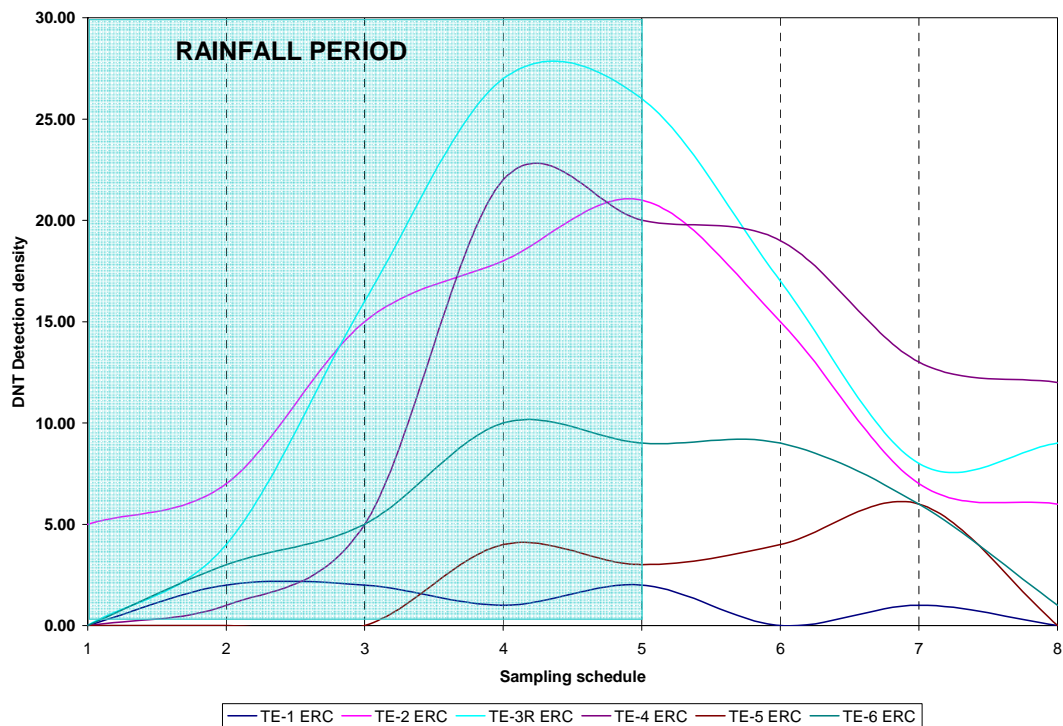
Figure 4-57 DNT data density vs. sampling time

In contrast with TNT (Figure 4-51), DNT shows higher detection density at high temperature conditions (TE-3 ERC) than at conditions of higher soil-water saturation (TE-2 and -4 ERC) (Figure 4-58). DNT also shows higher detection density for all experiments, (Figure 4-57), than TNT (Figure 4-51), except for experiment TE-1 ERC. Significant increase in DNT over TNT detection density is observed for no radiation conditions (experiment TE-6 ERC), showing a tenfold increased detection of DNT over TNT. Over a six fold increase on DNT detection density over that of TNT is observed for high temperatures, which also show the highest DNT detection temperature. A slight increase of DNT detection over that of for TNT is observed for the lower temperature conditions having high rainfall rates and soil-water saturation (TE-2 and 4 ERC). No increase in detection was observed for DNT in experiment TE-1 ERC.

160
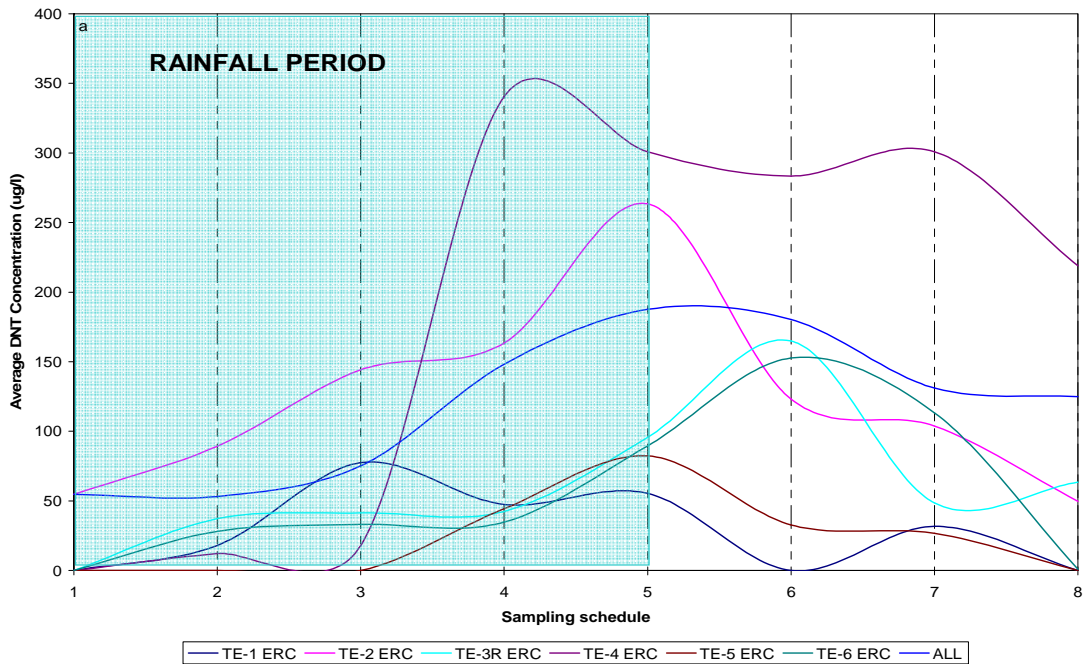
Figure 4-58 Average DNT concentration (µg/l) vs. sampling time

Average DNT solute concentrations tend to increase during rainfall events, reach a maximum concentration, and then decrease slowly after rainfall events (Figure 4-58). Similar to TNT (Figure 4-52), the magnitude and peak times of average DNT concentrations are influenced by environmental conditions (Figure 4-58). Unlike TNT, which generally shows normal pulse-like sampling distribution (Figure-4-52), average DNT generally shows sampling distribution with strong tailing (Figure 4-58). Higher average DNT concentrations, like TNT, are associated with higher soil-water saturation conditions. Lower maximum concentrations are observed for DNT over TNT for no radiation (TE-6) and low and high rainfall (TE-5) conditions at 25 ^{0}C. Higher maximum DNT concentration are observed for low (15 ^{0}C, TE-4) and high (35 ^{0}C, TE-6) temperature conditions. Higher detection density of DNT suggest degradation processes acting on TNT. Higher DNT detection at higher temperatures, and low rainfall and soil-water saturation, indicate that these conditions promote degradation. Highest

161

relative increase under cyclic radiation conditions suggest enhanced photodegradation near the soil-atmospheric surface. Concentration distributions for TNT and DNT sampling (Figure 4-52 and 4-58), also indicate potential degradation of TNT to DNT. These distribution show that TNT solute concentrations increase to a maximum and then decrease relatively sharply, where as DNT's distribution increases for a maximum but do not decrease as sharply. This behavior is observed even for experiment TE-1, which did not have DNT crystals in its source. Generally, higher DNT solute detection and concentrations are expected because of its higher solubility and lower sorption capacity. Greater vapor pressure and henry's constant for DNT (Table 2-3), however, would favor partitioning into the gaseous phase, thus potentially decreasing the total relative mass in the water phase. Higher TNT average concentration peak under given conditions (low temperature TE-4 ERC, high temperature TE-3R ERC, no radiation TE-6 ERC, low rainfall TE-5 ERC) suggest some retention mechanisms associated with sorption.

Spatial analysis of DNT detection density (Figure 4-59) shows increasing values toward the bottom of the solid bed. Higher detention density is observed in sampling clusters and 8, which are located at and above the XZ plane at Y=15 (Figure 3-5). This is attributed to preferential flow patterns that dissolve the source and transport the solute in this zone. Similar behavior is also observed for TNT (Figure 4-56), but there is a greater number of DNT detection in clusters of all planes. This suggest higher mobility and dissolution of DNT and TNT.

162
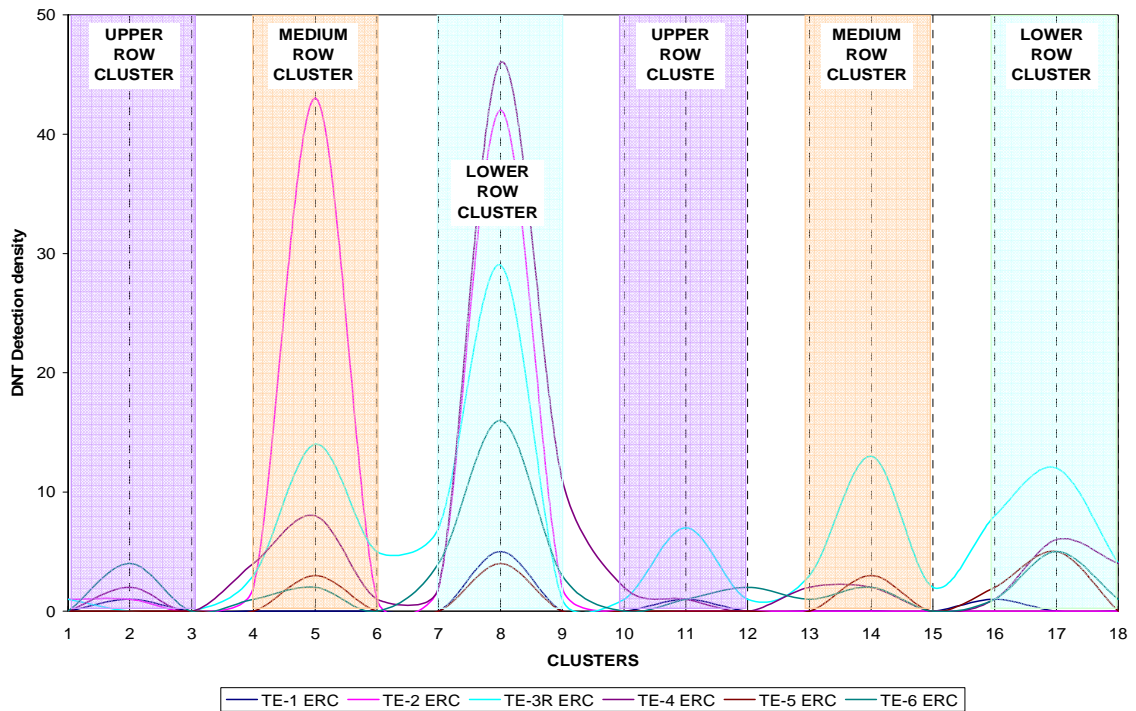
Figure 4-59 DNT presence vs. cluster

Higher DNT detection density is observed in zones of preferential flow for conditions of higher saturation (TE-4 and 2 ERC). In other zones, DNT is detected to a higher extend for high temperature (TE 3), low rainfall (TE-5), and no radiation conditions (Figure 60), whereas TNT detection is very limited (Figure 4-53). For high temperatures and low rainfall conditions, DNT is detected in approximately 95% and 30% of the sampling volume, whereas TNT is only detected in less than 16% of the clusters.

Higher DNT solute concentrations generally increase toward the bottom of the SoilBed (Figure 4-60). Higher concentrations are associated to the preferential flow path near clusters 5 and 8 at higher soil-water saturation conditions (TE-2 ERC and TE-4 ERC). High DNT

concentrations are also observed at cluster 16 (bottom) and 10 (top). Average DNT concentration are generally higher than TNT in all clusters, except cluster 16.

Average daily detection of DNT is initially higher for condition of low soil-water saturation under high temperatures (TE-3R ERC), low rainfall rates (TE-5 ERC), and no radiation (TE-6 ERC). Detection remains high for low rainfall, but tends to decrease with time for high temperature and no radiation. At the higher saturation regime (TE-2 ERC and TE-4 ERC), DNT detection density increases toward day 4, and then increases with time for conditions at 25 ^{o}C, but tends to increase for low temperature conditions.
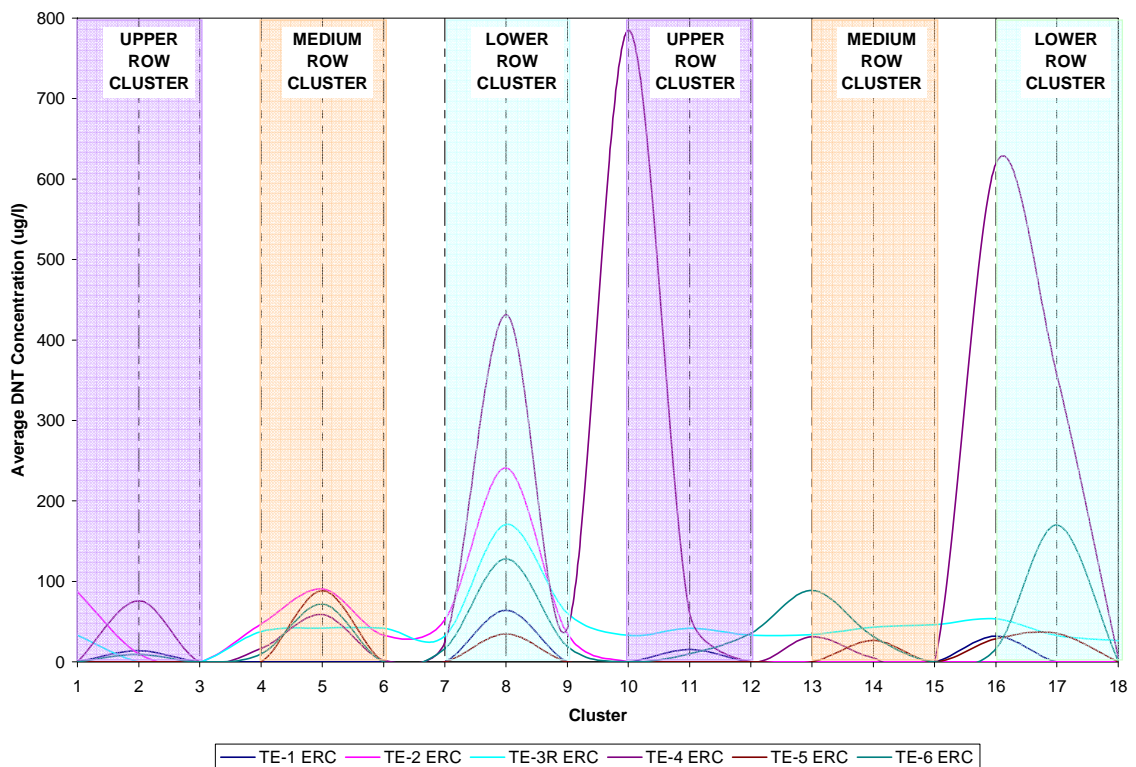
Figure 4-60 Average DNT concentration vs. cluster
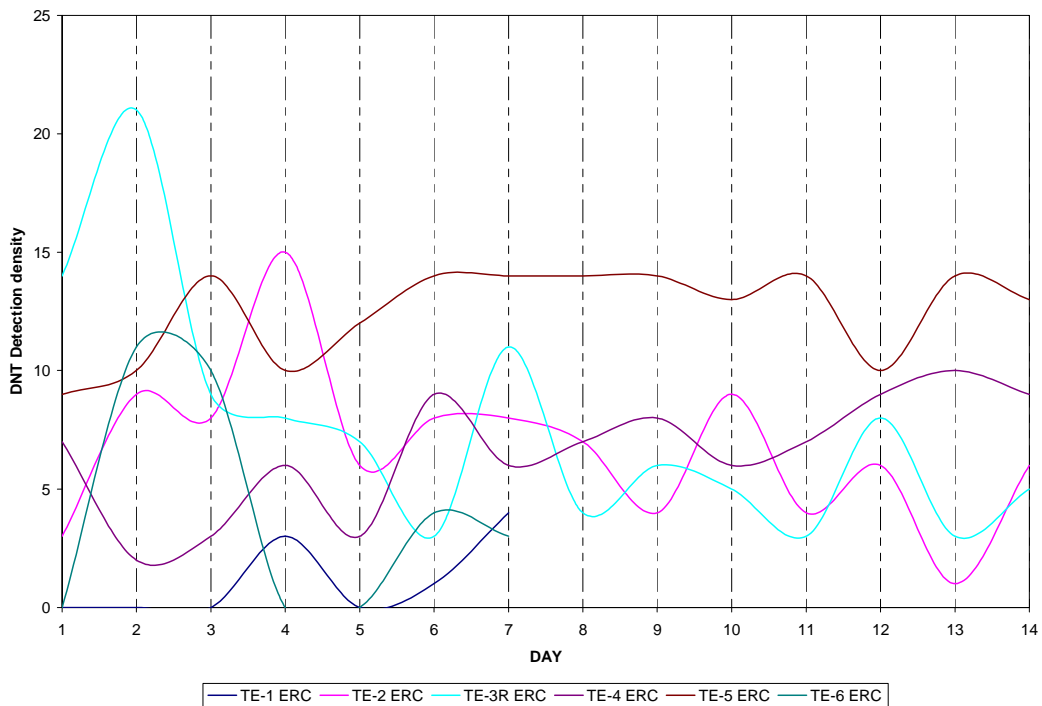
Figure 4-61 DNT data density vs. experimental day

DNT detection density is initially lower than TNT for conditions of low temperature (TE-4 ERC), but is higher after day 6. It is always lower than TNT for high soil-water saturation at 25 ^{o}C (TE-2 ERC). Daily DNT detection is always higher than TNT at high temperatures (TE-3R ERC), no radiation (TE-6 ERC), and low rainfall rates (TE-5 ER) conditions (Figure 4-61). Average daily DNT solute concentrations over the experimental period (Figure 4-62) tend to increase initially to a maximum and then decrease toward a constant average ($\pm$ daily variations), except for conditions of higher soil-water saturation (TE- 2 and – 4 ERC). At higher saturation, DNT concentrations tend to increase toward the end of the experiment. Where TNT shows high initial concentrations within the first 2 days (Figure 4-56), DNT concentrations are low during the first 2 days, and begin to increase in the third day. Initial peak concentrations are observed for conditions of high temperature (TE-3 ERC) followed b

conditions of high saturation (TE-2 ERC). Daily DNT concentrations are higher than TNT at all detection times for high temperatures, no radiation and low rainfall conditions. At higher saturation, DNT concentrations (Figure 4-62) are initially lower than TNT, but becomes higher than TNT after day 8 (Figure 4-56). Average TNT and DNT spatial analysis show higher DNT detection and concentration for high temperature and low rainfall conditions, indicating potential enhanced degradation of TNT to DNT under this condition. Spatial analysis shows that TNT and DNT detention and concentration are higher in preferential flow paths for high soil-water saturation conditions. For low-saturation conditions under high temperatures, and low rainfall, which permit TNT degradation and sorption, DNT shows higher detection and concentration in all other areas.

An interrelation between the highest density of occurrences (Figure 4-61) and the highest DNT concentration can be established on experiments TE-1, TE-2, TE-3, TE-4, and -6 ERC. Generally highest density of data occur the same day than the days of highest DNT concentration. Figures 4-63 and 4-64 show TNT and DNT spatial concentration distribution for days at which maximum concentration was detected. In these Figures, the day and sampling time when the maximum concentration occur is below each spatial model. For experiment 1, TNT and DNT maximum concentration occurs the same day at the same time because the landmine source was built only with TNT crystals. Spatial distributions of TNT and DNT (Figures 4-63 and 4-64) maximum concentration are shown in conjunction with spatial distribution of NaCl concentrations, total hydraulic heads, and soil water saturation for the same time at which the maximum concentration occurs, greater TNT maximum
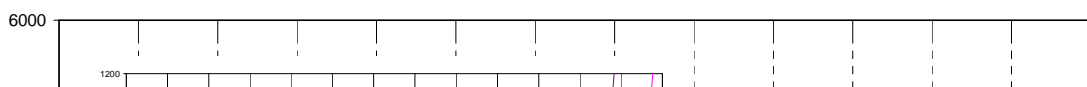
concentration distribution is observed toward the SoilBed bottom for conditions that promote drainage (TE-3 and -5 ERC). Conditions which promote higher water storage and saturation (TE-2 and TE -4 ERC) show maximum concentration distribution in the redistribution zones with SoilBed (zone between the infiltration and drainage zones near the top and bottom boundaries). Highest TNT maximum concentration distribution is observed for high rainfall conditions at 25 $^\circ$C with cyclic radiation, followed by conditions which promote drainage and advective movement of dissolved TNT toward the bottom. Conditions with no radiation show TNT maximum concentration distribution near the redistributing zone, but a lower maximum concentrations. Lowest TNT maximum concentration distribution is observed for low temperatures conditions. Generally, TNT maximum concentration occurs during the first week of burial. Higher TNT maximum concentrations are observed with the first 2 days for conditions that promote drainage and source dissolution (TE-3, -5 and -2 ERC).
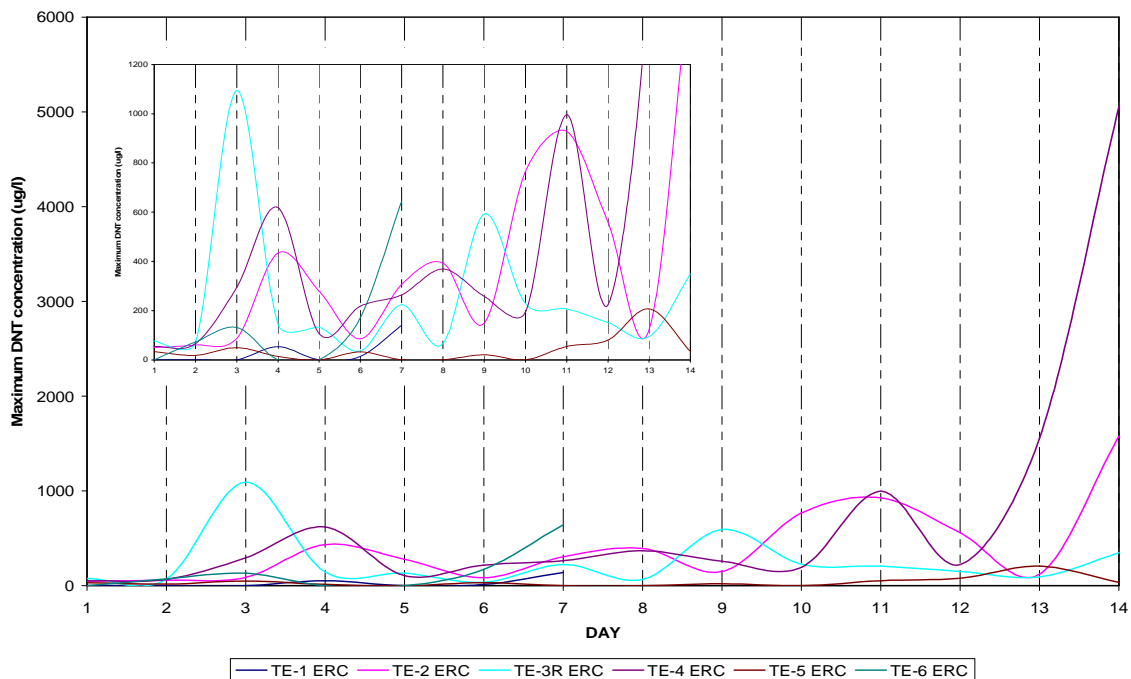
Figure 4-62 Maximum DNT concentration vs. experimental day

167
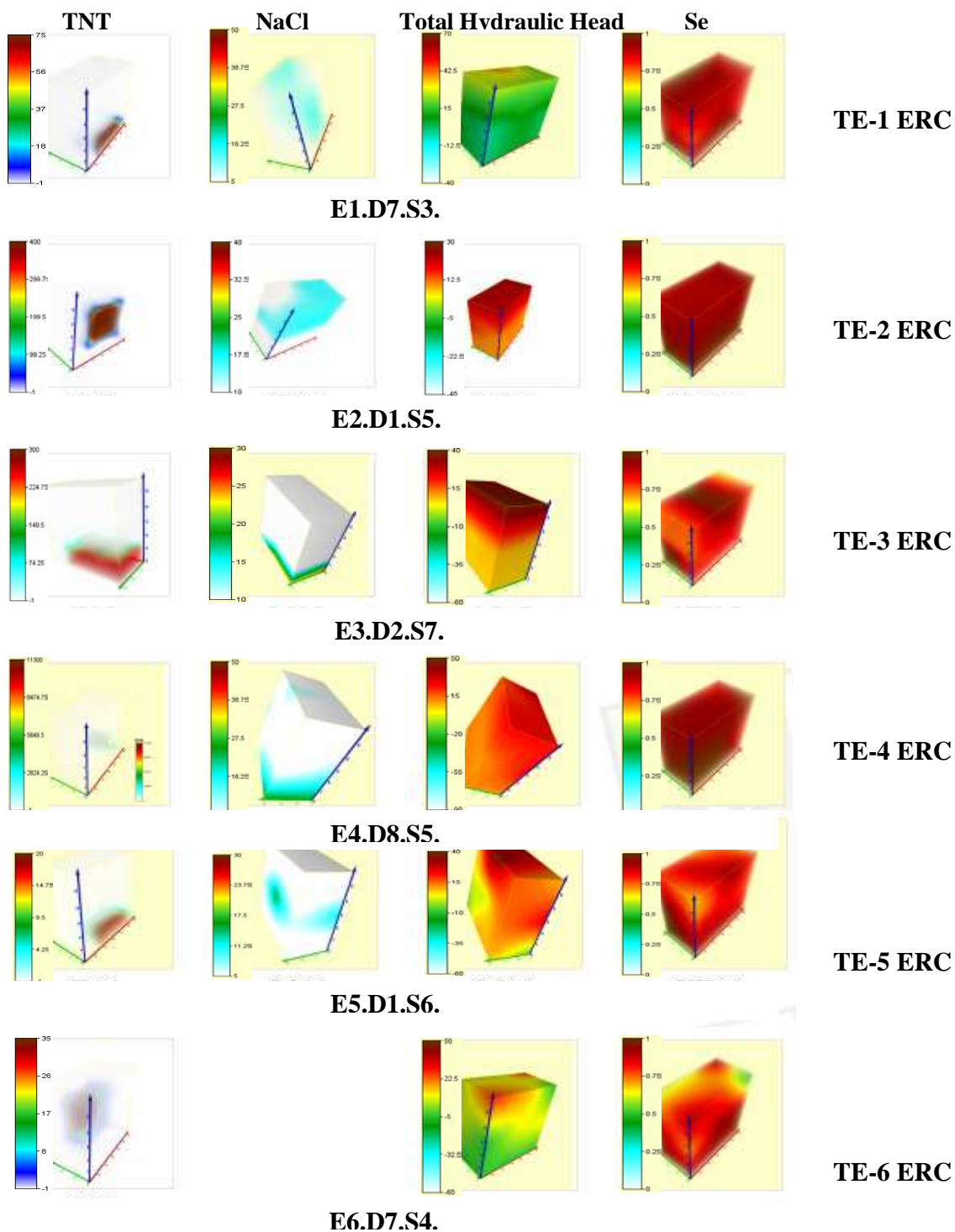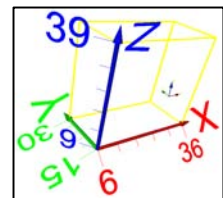
Figure 4-63 Spatial distribution of TNT maximum concentration, NaCl concentration, soil-water saturation, and hydraulic total head

DNT	NaCl	Total Hydraulic Head	Se	
				TE-1 ERC

E1.D7.S3.

| | | | | **TE-2 ERC** |

E2.D14.S5.

| | | | | **TE-3 ERC** |

E3.D3.S6.

| | | | | **TE-4 ERC** |

E4.D14.S4.

| | | | | **TE-5 ERC** |

E5.D13.S5.

| | | | | **TE-6 ERC** |

E6.D7.S6.
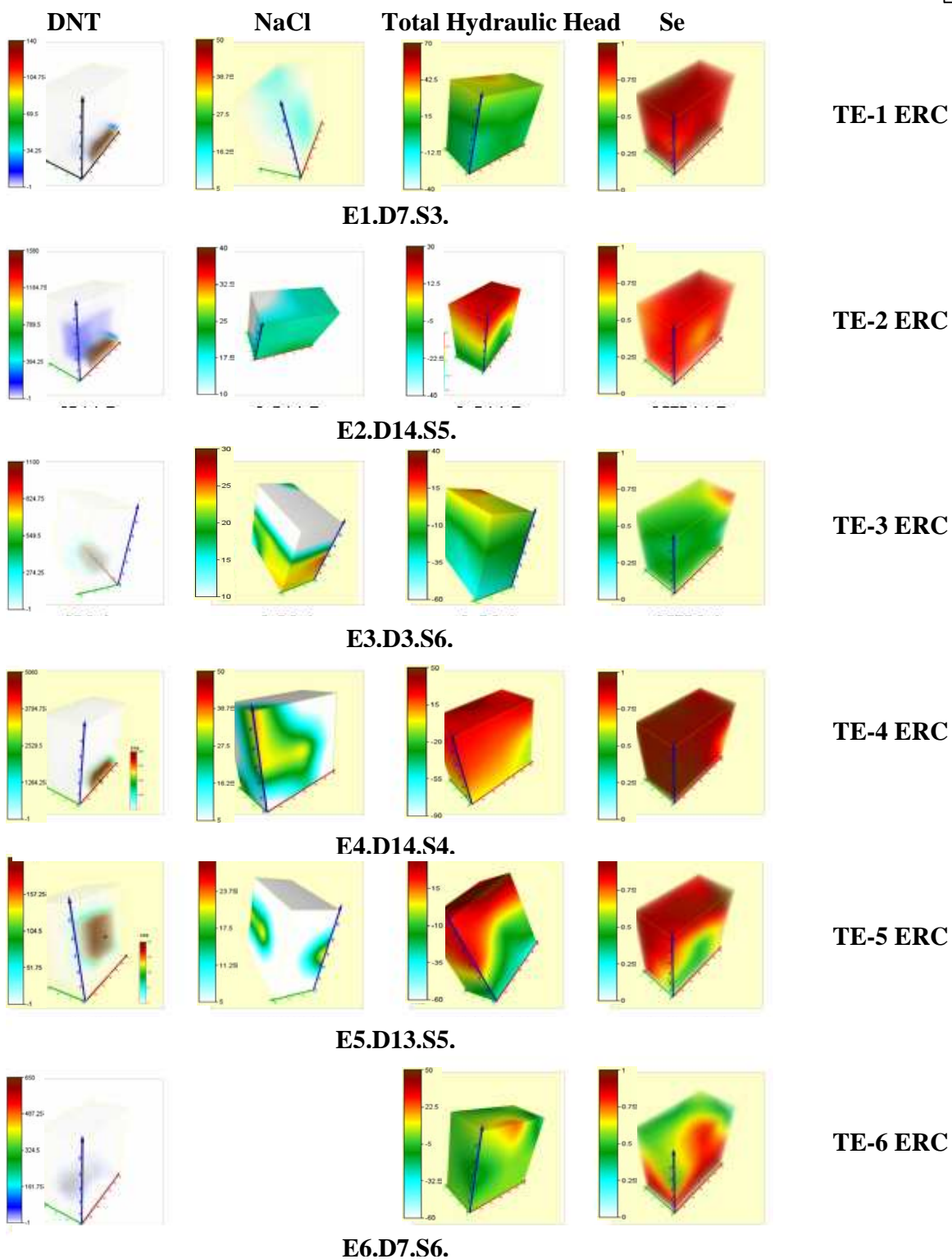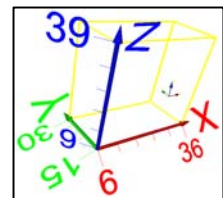
Figure 4-64 Spatial distribution of DNT maximum concentration, NaCl concentration, soil-water saturation, and hydraulic total head

169

TNT and DNT maximum concentration tend to coincide with high NaCl concentrations and hydraulic gradients (Figure 4-63 and -64). This indicates that preferential flow influenced by hydraulic gradients heterogeneities influence significantly the transport and concentrations of TNT and DNT solutes. Results have previously shown that soil-water saturation influence TNT and DNT concentrations and detection. The effect of Se spatial distribution on TNT and DNT maximum concentrations is, however, not as easily discerned. On an average maximum TNT and DNT concentrations are associated with high Se (Figure 4-65)
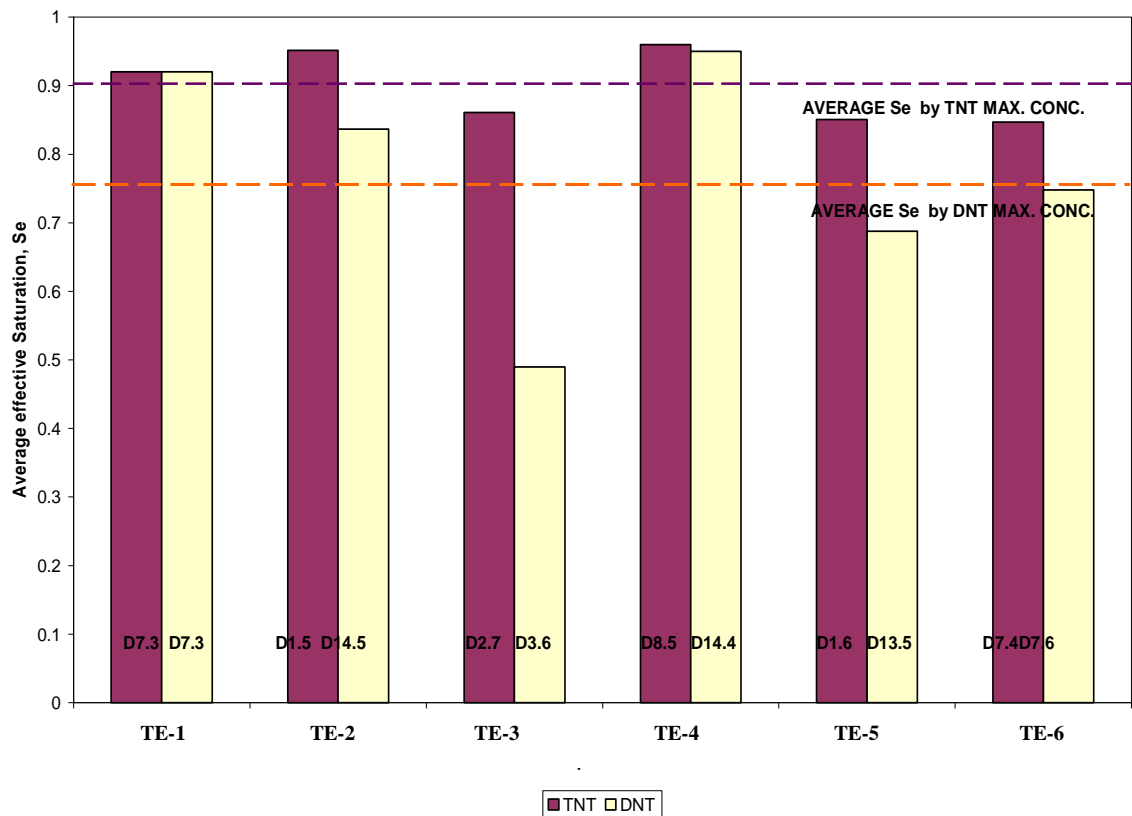
Figure 4-65 Average Se by the sampling time of maximum concentration

4.5.2.2 ERC's in Gas Phase

The effect of environmental variables on the detection of TNT, DNT and other related chemicals in the gas phase was analyzed using detection frequency data. The analysis served to assess the effect on fate and transport processes under variable environmental conditions. Gas phase analyzes was conducted for experiments TE- 2 – 3 , and 6 ERC.

Daily TNT detection density in the gas-phase (Figure 4-66) is higher for high temperatures (35 ^{o}C, TE-3), and tends to decrease with time for cyclic radiation conditions (TE-2 and TE-3). Under no radiation, TNT in the gas phase is detected after the 2nd day, peaks at about the 5th, and decreases to no detection at the 7th day.
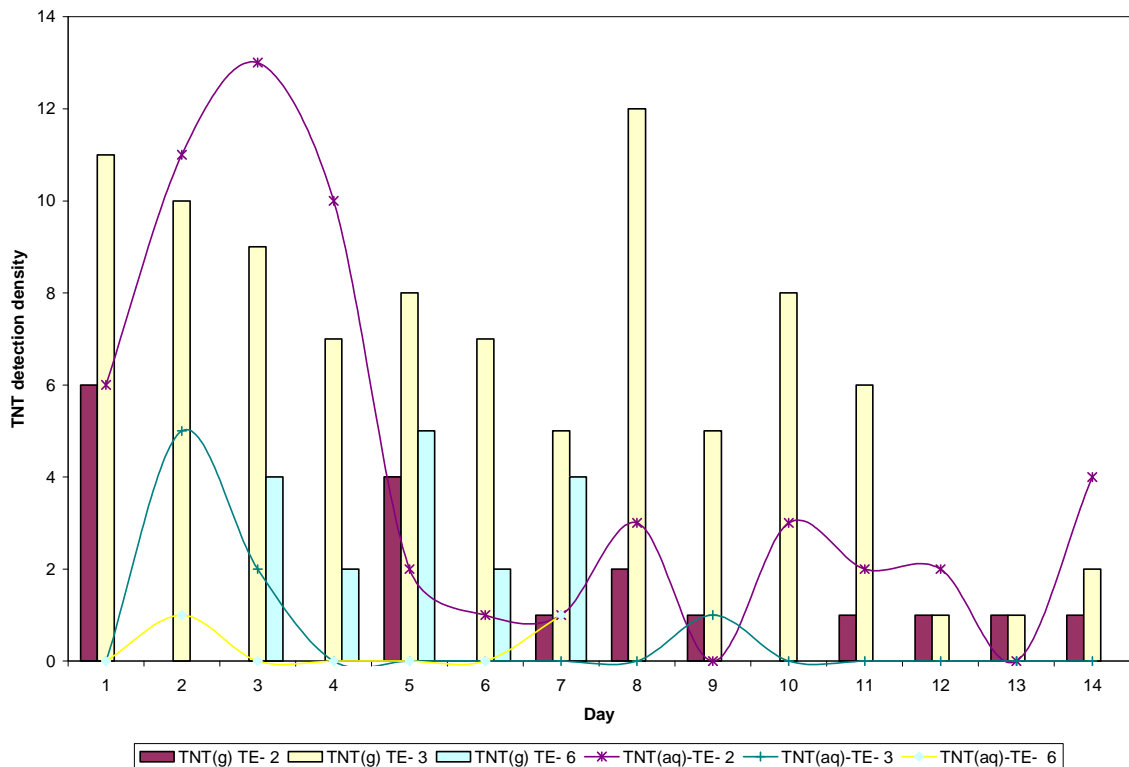
Figure 4-66 Daily detection density of TNT in the gas phase

171

Detection density of TNT in the gas phase tends to follow a similar general pattern as these in the water-phase (Figure 4-66). High and low peak density in the aqueous TNT generally precede those in the gas phase by about 1 day. For cyclic and no radiation conditions at 25 $^{\circ}$C, a higher TNT detection density is observed in the gas-phase than in the aqueous phase. For higher temperatures conditions, the number of samples with TNT detection in the water phase is about the same on higher than in the gas-phase.

Daily detection of DNT in the gas phase tends to increase initially with time reach a peak after 10 days, and then decrease (Figure 4-67), for high temperatures (TE-3 ERC) and cyclic radiation correlations at 25 $^{\circ}$C (TE-2 ERC). Under no radiation (TE-6 ERC), DNT detection in the gas phase shows similar behavior as that for TNT (Figure 4-66), which is only detected between days 3 and 7 (Figure 4-67). DNT detection in the gas phase tends to be lower than in the aqueous phase initially, until when peak detection occurs in the aqueous has. Thereafter detention density is similar in both phases. All detection peaks in the gas phase lag these in the water phase.

The detection behaviors of TNT and DNT in the gas and water phases suggest close average interaction of these ERCs among phases. The temporal response lag of TNT and DNT in the gas phase indicates partition from the water into the gas phase. Higher detection in the gas than the water phase suggest other processes acting on the desorbed phases. For instance, higher TNT detection in the gas phase at higher temperatures conditions suggest higher sorption into solid phase and / or higher degradation. Higher sorption is attributed to lower

water contents at these conditions. For higher water saturation condition (TE-2 ERC), TNT detection in the gas phase is controlled by detection and concentration in the water phase. Lower DNT detection in the gas than in the water-phase, suggest that DNT detection in the gas phase is mostly controlled by detection and concentration in the water phase.

DNT is detected to a greater than TNT extent in the gas phase for no radiation(TE-6 ERC) and cyclic (TE-2 ERC) radiation at 25 ^{o}C. This is attributed to potential degradation of TNT to DNT under these conditions. DNT is detected to a lower extent than TNT at higher temperatures (TE-3 ERC). This is potentially caused by degradation of DNT. This is supported by the presence of an unidentified chemical, presumably smaller than DNT (since it came out earlier than DNT in the chromatographic analyzes). This chemical was present in 79 gas samples taken a high temperature conditions.
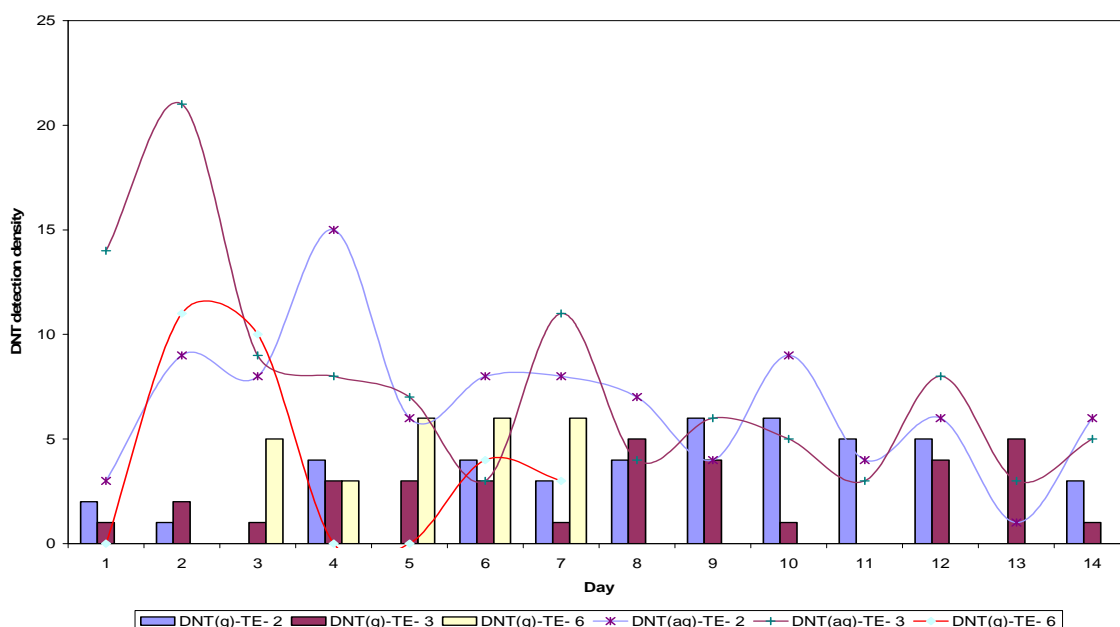
Figure 4-67 Daily detection density of DNT in the gas phase

173

Spatial detection of TNT and DNT in the gas phase are shown by clusters in Figures 4-68 and 4-69. TNT and DNT show strong gas-phase detection at the soil surface and the first row of air samplers (4 cm below the soil surface), whereas high dissolved (water) detection is observed in the bottom clusters.

DNT shows greater spatial presence than TNT in the gas phase. Highest DNT detection in the gas-phase corresponds to high rainfall rates at 25 $^{\circ}$C for cyclic radiation events (TE-2 ERC), which also shows highest DNT detection in the water phase at the bottom clusters.
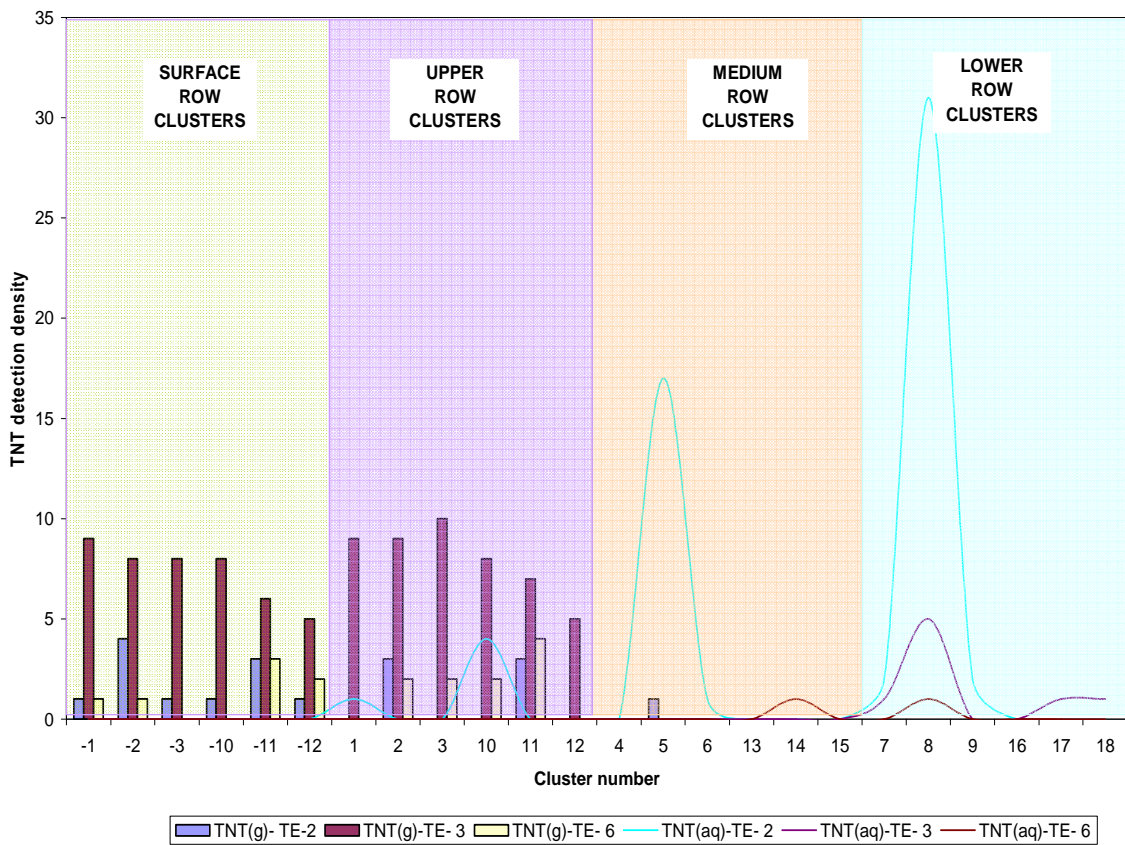
Figure 4-68 Detection of TNT in the gas-phase by cluster. Negative cluster number refer to gas samplers at the soil surface
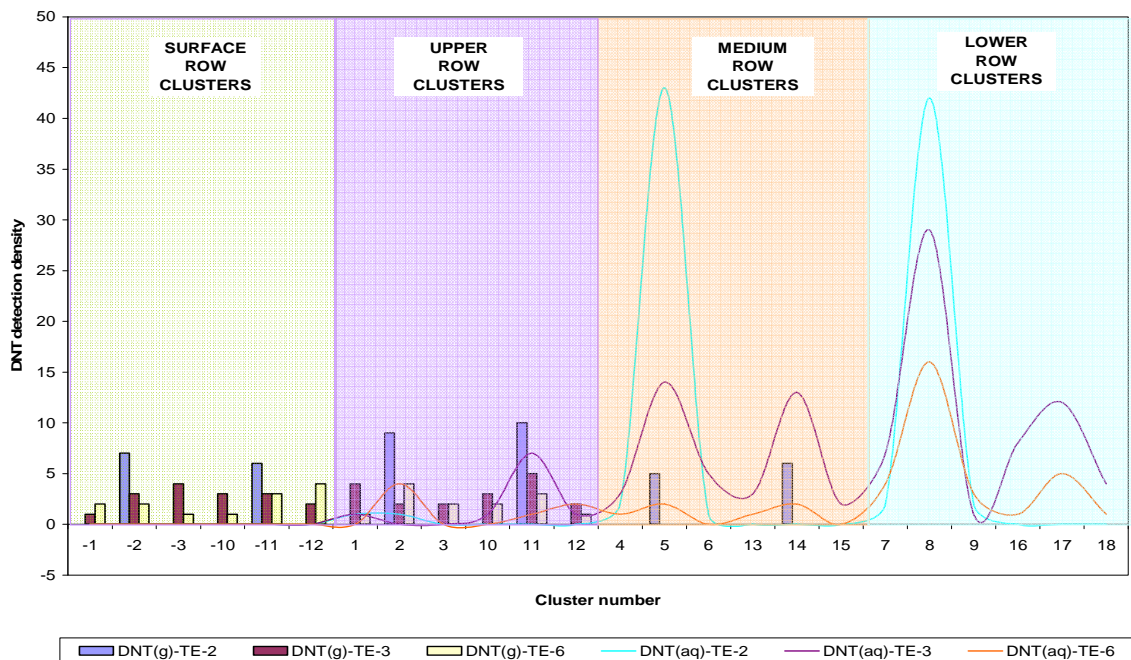
Figure 4-69 Detection of DNT in the gas-phase by cluster. Negative cluster number refer to gas samplers at the soil surface

Highest TNT gas-phase detection occurred for high temperatures conditions (TE-3 ERC) under the soil surface, principally at clusters 1, 2, 3. No dissolved TNT was, however, detected at these locations. This suggests fast mpvement of dissolve TNT in water due high hydraulic conditions, and the presence of up-ward transport due to thermal gradients and evaporation processes.

Daily spatial distribution (Figure 4-70 and 4-71) show that TNT in the gas phase is initially higher near the soil-atmospheric surface, and then decreases with time. DNT is also higher near the surface, but tends to increase with time.
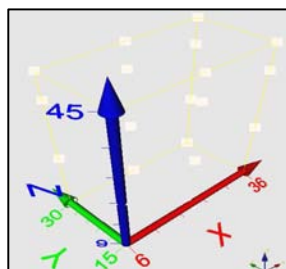
TNT (g)
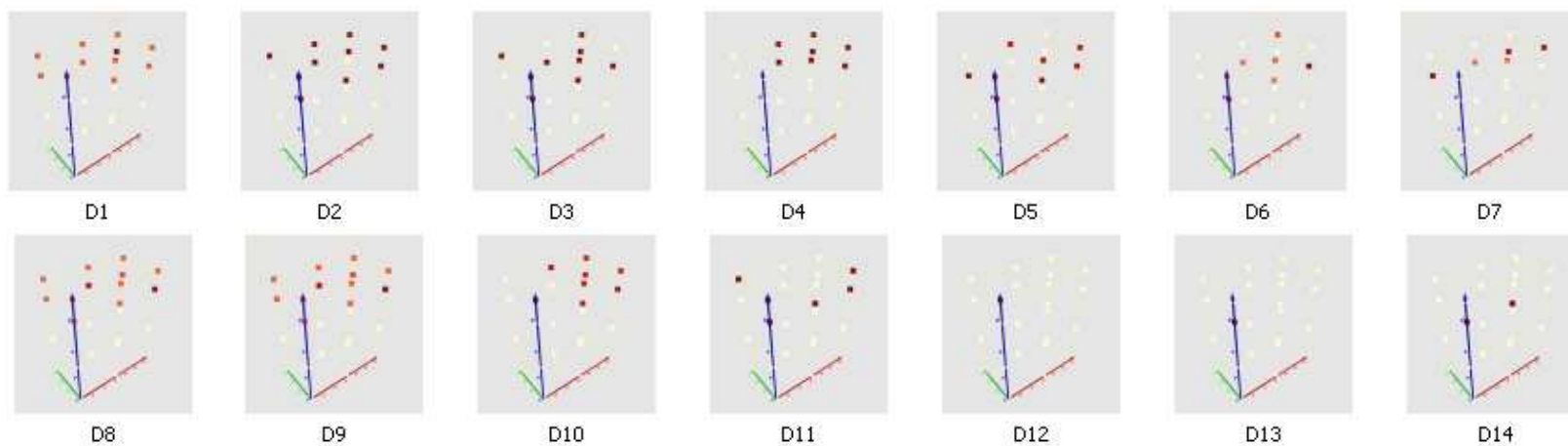
Figure 4-70 Daily spatial distribution of TNT in the gas phase for high temperature conditions -TE-3R. Red point indicate TNT presence
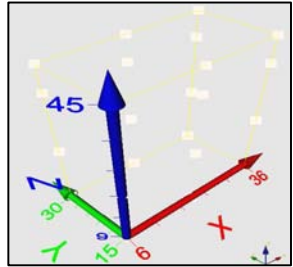
DNT (g)
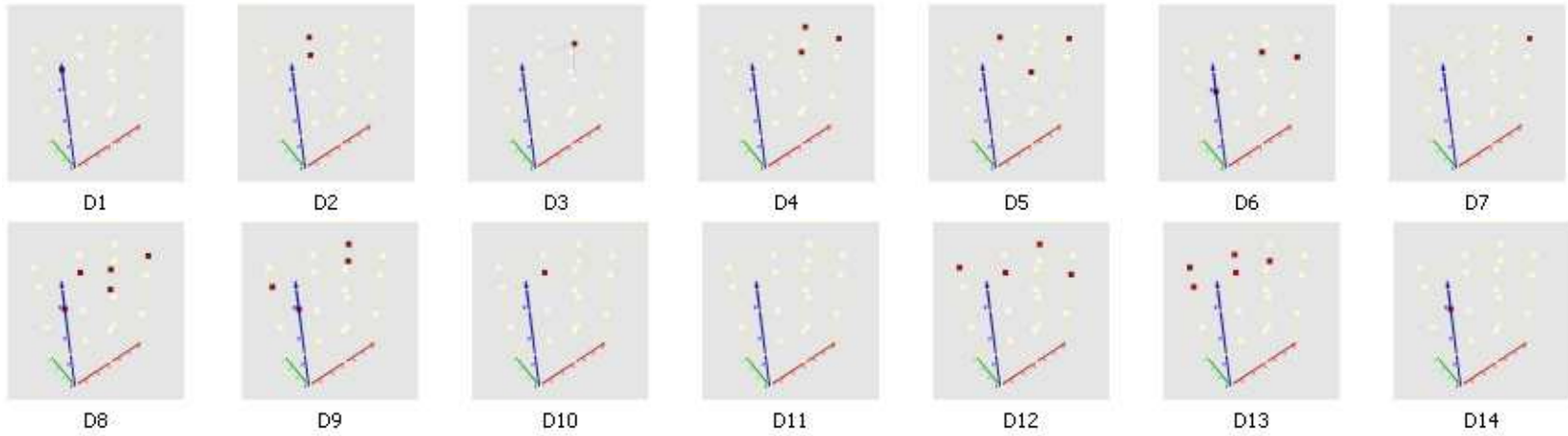
Figure 4-71 Daily spatial distribution of DNT in the gas phase for high temperature conditions -TE-3R. Red point indicate DNT presence

4.6 Statistical Model

A generalized linear mixed statistical model (GLMM) has been applied to quantify the effect of environmental conditions on TNT and DNT detection and concentrations. GLMMs represent a class of fixed and random effects regression models for several types of dependent variables (i.e., continuous, dichotomous, counts, binary). They are applicable to experimental data having binary outcomes, unbalanced models, and non-normal error distributions (See Chapter 2, for more information on those models). The data collected and analyzed show some of these characteristics (see **Table 4-1**). The GLIMMIX Procedure, nested in SAS™ Software, was applied to the experimental data to assess the effect of environmental parameters on detection and concentration distribution. The models used binary response distribution for all distribution, logit type, diagonal matrix of variances, and maximum likehood estimation.

The statistical analysis indicates that rainfall events and related water contents are the most influential factors affecting the presence and concentrations of ERCs in the aqueous and gaseous phase. Solar radiation, and related heat flux, is the second most influential parameter. Although atmospheric temperature influences the presence and concentration of ERCs in soils, it is the least influential parameter.

4.6.1 Description of the Analysis

Statistical simulations were run to quantify the effect of soil-environmental effects on detection of TNT and DNT (in aqueous phase and gas phase) and TNT/DNT concentrations in aqueous phase. Thirty-eight simulations were run for TNT presence analysis, 50 for DNT presence, 41 for DNT concentration, 41 for TNT concentration, 8 for TNT air concentration and 8 for DNT gaseous-phase concentration. The input and outcome variables used in the simulations (Table 4-11) show a wide variety of input and outcome data type including: categorical, nominal, and numerical ranges, and binary data (some categorical data, such as, concentrations were converted to binary data using dummies variables).

4.6.2 Inferential Analysis

Tables 4-11 to Table 4-17 show the summary of the simulations for each outcome variable. The first column refers to the simulation identification (with this name SAS output files are referenced at appendixes B). The second column refers to the analyzed outcome variable (dependent variable). The probability of detecting DNT/TNT in different phases under the influence of single or combination of soil environmental effects (independent variables) or the probability of measuring DNT/TNT concentrations at specified space ranges. The third column refers to the effect (single or combination) of independent variable(s) on dependent variable, as described in Table 4-11. The fourth column corresponds to the experiments TE - ERC (Table 3-4) from which data were used in the simulations. When analyzing experimental data different temporal range like some experiments have different temporal range, TE-1 and 6 have a duration of 7 days, TE-2, 3, 4, and 5 have a duration of 14 days.

179

Table 4-11 Summary of input and output variables used in the GLMM.

Effect on outcome variable	Description Effect	Values
CLUSTER	Spatial location of water/air sampler	1 to 18
COD TEMP	Atmospheric Temperature classification	1: $15<T<20$ 2: $20<=T<25$ 3: $25<=T<30$ 4: $T>=30$
COD2 TEMP	Atmospheric Temperature classification	1: $15<T<22$ 2: $22<=T<29$ 3: $T>=29$
COD3 TEMP	Atmospheric Temperature classification	1: $15<T<21$ 2: $21<=T<27$ 3: $T>=27$
COD4 TEMP	Atmospheric Temperature classification	1: $15<T<20$ 2: $20<=T<25$ 3: $T>=25$
COD5 TEMP	Atmospheric Temperature classification	1: $15<T<25$ 2: $T>=25$
CODSE1	Water Content Classification - Effective Saturation	1:0-25% 2:25-50% 3:50-75% 4:>75% 0:NULL
DAY	Experimental Day	1 to 7 by exp. 1 and 6 1 to 14 by exp. 2 to 5
RAINFALL	Rainfall intensity Classification	0.5: 0.5 in/hr 2: 2 in/hr
SAMPLING	Sampling Time classification	1 to 8
SOLAR LIGHT	Presence Solar Radiation	O: non presence 1: presence
TEMP1	Atmospheric Temperature classification	1: $15<T<22$ 2: $22<=T<29$ 3: $T>=29$
TEMPERATURE	Atmospheric Temperature classification fixed by exp.	15: Exp. 3 25: Exp. 2,5,6 35: Exp. 3
W. CONT.-CODSE1	Water Content Classification - Effective Saturation	1:0-25% 2:25-50% 3:50-75% 4:>75% 0:NULL
CLUSTER / RAINFALL	Effect on outcome variable due variations in Cluster and Rainfall values	Combinations of individual values of each effect
CLUSTER / SAMPLING	Effect on outcome variable due variations in Cluster and Sampling time values	Combinations of individual values of each effect
CLUSTER/ COD2 TEMP	Effect on outcome variable due variations in Cluster and COD2 TEMP values	Combinations of individual values of each effect
RAINFALL / COD2 TEMP	Effect on outcome variable due variations in Rainfall and COD2 TEMP values	Combinations of individual values of each effect
SAMPLING/COD2 TEMP	Effect on outcome variable due variations in Sampling times and COD2 TEMP values	Combinations of individual values of each effect
SAMPLING/CODSE1	Effect on outcome variable due variations in Sampling and Codse1 values	Combinations of individual values of each effect
SAMPLING/RAINFALL	Effect on outcome variable due variations in Sampling times and Rainfall values	Combinations of individual values of each effect
SAMPLING/SOLAR LIGHT	Effect on outcome variable due variations in Solar light and Sampling values	Combinations of individual values of each effect
SOLAR LIGHT / RAINFALL	Effect on outcome variable due variations in Solar light and Rainfall values	Combinations of individual values of each effect
SOLAR LIGHT / COD2 TEMP	Effect on outcome variable due variations in Solar light and cod2 temp values	Combinations of individual values of each effect
DNT PRESENCE	Outcome variable: Assets presence of DNT(aq)	0: Presence 1: non Presence
DNT1 CONC.	Outcome variable: Assets concentration of DNT(aq)	0: [DNT] > 100 $\mu g/l$ 1: [DNT] <= 100 $\mu g/l$
DNT2 CONC.	Outcome variable: Assets concentration of DNT(aq)	0: [DNT] < 100 $\mu g/l$ or [DNT] > 1000 $\mu g/l$
DNT3 CONC.	Outcome variable: Assets concentration of DNT(aq)	0: [DNT] < 1000 $\mu g/l$ 1: [DNT] >= 1000 $\mu g/l$
TNT PRESENCE	Outcome variable: Assets presence of TNT(aq)	0: Presence 1: non Presence
TNT1 CONC.	Outcome variable: Assets concentration of TNT(aq)	0: [DNT] > 100 $\mu g/l$ 1: [DNT] <= 100 $\mu g/l$
TNT2 CONC.	Outcome variable: Assets concentration of TNT(aq)	0: [DNT] < 100 $\mu g/l$ or [DNT] > 1000 $\mu g/l$
TNT3 CONC.	Outcome variable: Assets concentration of TNT(aq)	0: [DNT] < 1000 $\mu g/l$ 1: [DNT] >= 1000 $\mu g/l$

The temporal duration was fixed to 7 days or was analyzed unbalanced. One of the characteristics of GLIMMIX procedure is that it supports unbalanced and mixed models. The sixth and seventh column in Table 4-12 to Table 4-17 refers to the validation of the test

hypothesis. Column 6 indicates whether the effect is significant at 95% based on values on P values in column 5. For confidence limits of 95% and α values of 0.05, values lower than 0.05 indicates a significance of the effects tested on the outcome variable due changes in the values of the independent variables. If variation is significant, a nominal value of YES appears in the seventh column.

The presence of significance in the simulations with combination of single effects, does not imply an existence of significance by all possible combinations (e.g., Cluster and Rainfall, Cluster and Sampling time, Cluster and COD2 TEMP, Rainfall and COD2 TEMP, Sampling times and COD2 TEMP, Sampling and Codse1, Sampling times and Rainfall, Solar light and Sampling, Solar light, Rainfall and Solar light and cod2 temp). Diffogram and least squares differences let establish which combinations are or not significant.

Odd ratios analysis (later described in this chapter) allows to quantify the change of soil environmental effects on the predictive variable. It indicates the probability of increasing or decreasing the dependent variable (e.g., presence, concentration) from changes in the independent variable. Values less than one indicate a decrease in a factor equal to one minus the odd ratio value in the probability of success of the outcome variable. Odd ratios greater than one indicate an increase in a factor equal to the odd ratio value minus one. Significance or non-significance are evaluated in function of α values established the confidence limits. Knowledge of the nature of data and characteristics of the outcome variable research, is used to decide levels of significance by a model.

Table 4-12 GLMM statistical analysis on the effect of independent variables on TNT solute (aq) detection

No	Output Parameter	Independent Variable	Experiment No.	Pr>F	95% CL?
1	TNT PRESENCE	SOLAR LIGHT	2,6	<.0001	YES
1.1	TNT PRESENCE	SOLAR LIGHT	2,6 Fixed7	<.0001	YES
2	TNT PRESENCE	RAINFALL	2,5	<.0001	YES
3	TNT PRESENCE	COD2 TEMP	2,3,4	0.1216	NO
4	TNT PRESENCE	WATER CONT.-CODSE1	2,3,4	<.0001	YES
5	TNT PRESENCE	WATER CONT.-CODSE1	2,5	<.0001	YES
6	TNT PRESENCE	WATER CONT.-CODSE1	2,6 Fixed7	<.0001	YES
7	TNT PRESENCE	WATER CONT.-CODSE1	3	<.0001	YES
8	TNT PRESENCE	WATER CONT.-CODSE1	4	0.4199	NO
9	TNT PRESENCE	WATER CONT.-CODSE1	2	0.9747	N0
10	TNT PRESENCE	WATER CONT.-CODSE1	5	0.9816	NO
11	TNT PRESENCE	WATER CONT.-CODSE1	6	0.9805	NO
12	TNT PRESENCE	SAMPLING	2,3,4	<.0001	YES
13	TNT PRESENCE	SAMPLING	2,3,4,5	<.0001	YES
14	TNT PRESENCE	SAMPLING	2,3,4,5,6	<.0001	YES
15	TNT PRESENCE	SAMPLING	2	0.051	YES
16	TNT PRESENCE	SAMPLING	3	0.0007	YES
17	TNT PRESENCE	SAMPLING	4	0.0022	YES
18	TNT PRESENCE	SAMPLING	5	0.9595	NO
19	TNT PRESENCE	SAMPLING	6	0.9994	NO
20	TNT PRESENCE	DAY	2,3,4	<.0001	YES
21	TNT PRESENCE	DAY	2,3,4,5	<.0001	YES
22	TNT PRESENCE	DAY	6	1	NO
23	TNT PRESENCE	DAY	1	0.9356	NO
24	TNT PRESENCE	CLUSTER	2,3,4	<.0001	YES
25	TNT PRESENCE	CLUSTER	2,3,4,5	<.0001	YES
26	TNT PRESENCE	CLUSTER	2,3,4,5,6	<.0001	YES
27	TNT PRESENCE	SOLAR LIGHT / RAINFALL	2,5	<.0001	YES
28	TNT PRESENCE	SOLAR LIGHT / RAINFALL	5,6 Fixed7	-	
29	TNT PRESENCE	RAINFALL / COD2 TEMP	2,3,4,5	<.0001	YES
30	TNT PRESENCE	SOLAR LIGHT / COD2 TEMP	3,6 Fixed	<.0001	YES
31	TNT PRESENCE	SOLAR LIGHT / COD2 TEMP	4,6 Fixed7	-	
32	TNT PRESENCE	SAMPLING/RAINFALL	2,5	0.9651	NO
33	TNT PRESENCE	SAMPLING/SOLAR LIGHT	2,6 Fixed7	1	NO
34	TNT PRESENCE	SAMPLING/COD2 TEMP	2,3,4	0.6408	NO
35	TNT PRESENCE	SAMPLING/CODSE1	2,3,4	0.7401	NO
36	TNT PRESENCE	CLUSTER / SAMPLING	2,3,4,5	1	NO
37	TNT PRESENCE	CLUSTER / RAINFALL	2,5	1	NO
38	TNT PRESENCE	CLUSTER/ COD2 TEMP	2,3,4	0.2243	NO

Table 4-13 GLMM statistical analysis on the effect of independent variables on DNT solute (aq) detection

No	Output Parameter	Independent Variable	Experiment No.	Pr>F	95% CL?
1	DNT PRESENCE	SOLAR LIGHT	2,6	0.0298	YES
2	DNT PRESENCE	RAINFALL	2,5	<.0001	YES
3	DNT PRESENCE	TEMPERATURE	2,3,4	0.3151	NO
4	DNT PRESENCE	TEMPERATURE	2,3,4,5	<.0001	YES
5	DNT PRESENCE	TEMPERATURE	2,3,4,5,6	<.0001	YES
6	DNT PRESENCE	TEMPERATURE	2,4	0.8807	NO
7	DNT PRESENCE	TEMPERATURE	2,3	0.2235	NO
8	DNT PRESENCE	TEMPERATURE	3,4	0.1719	NO
9	DNT PRESENCE	COD TEMP	2,3,4	0.0782	NO
10	DNT PRESENCE	COD2 TEMP	2,3,4	0.0011	YES
11	DNT PRESENCE	COD3 TEMP	2,3,4	0.2269	NO
12	DNT PRESENCE	COD4 TEMP	2,3,4	0.1504	NO
13	DNT PRESENCE	COD5 TEMP	2,3,4	0.1304	NO
13.1	DNT PRESENCE	WATER CONT.-CODSE	2,3,4	<.0001	YES
13.2	DNT PRESENCE	WATER CONT.-CODSE1	2,3,4	<.0001	YES
13.3	DNT PRESENCE	WATER CONT.-CODSE1	2,5	<.0001	YES
13.4	DNT PRESENCE	WATER CONT.-CODSE1	2,6 Fixed7	0.3114	NO
13.5	DNT PRESENCE	WATER CONT.-CODSE1	3	0.3114	NO
13.6	DNT PRESENCE	WATER CONT.-CODSE1	4	0.1545	NO
13.7	DNT PRESENCE	WATER CONT.-CODSE1	2	<.0001	YES
13.8	DNT PRESENCE	WATER CONT.-CODSE1	5	0.389	NO
13.9	DNT PRESENCE	WATER CONT.-CODSE1	6	0.3684	NO
14	DNT PRESENCE	SAMPLING	2,3,4	<.0001	YES
15	DNT PRESENCE	SAMPLING	2,3,4,5	<.0001	YES
16	DNT PRESENCE	SAMPLING	2,3,4,5,6	<.0001	YES
17	DNT PRESENCE	SAMPLING	2,3,4,5,6	<.0001	YES
17.1	DNT PRESENCE	SAMPLING	2	0.0027	YES
17.2	DNT PRESENCE	SAMPLING	3	0.0007	YES
17.3	DNT PRESENCE	SAMPLING	4	0.0041	YES
17.4	DNT PRESENCE	SAMPLING	5	0.0041	YES
17.5	DNT PRESENCE	SAMPLING	6	0.22	N0
18	DNT PRESENCE	DAY	2,3,4	0.0528	YES
19	DNT PRESENCE	DAY	2,3,4,5	0.0496	YES
20	DNT PRESENCE	DAY	6	0.0909	YES
21	DNT PRESENCE	DAY	1	0.95	NO
22	DNT PRESENCE	CLUSTER	2,3,4	<.0001	YES
23	DNT PRESENCE	CLUSTER	2,3,4,5	<.0001	YES
24	DNT PRESENCE	CLUSTER	2,3,4,5,6	<.0001	YES
25	DNT PRESENCE	SOLAR LIGHT / RAINFALL	2,5	0.0342	YES
26	DNT PRESENCE	SOLAR LIGHT / RAINFALL	5,6 Fixed7	-	-
27	DNT PRESENCE	RAINFALL / COD2 TEMP	2,3,4,5	<.0001	YES
28	DNT PRESENCE	SOLAR LIGHT / COD2 TEMP	3,6 Fixed7	0.0193	YES
29	DNT PRESENCE	SOLAR LIGHT / COD2 TEMP	4,6 Fixed7	-	NO
30	DNT PRESENCE	SAMPLING/RAINFALL	2,5	0.5831	NO
31	DNT PRESENCE	SAMPLING/SOLAR LIGHT	2,6 Fixed7	0.9884	NO
32	DNT PRESENCE	SAMPLING/COD2 TEMP	2,3,4	0.4999	NO
32.1	DNT PRESENCE	SAMPLING/CODSE1	2,3,4	0.0947	YES
33	DNT PRESENCE	CLUSTER / SAMPLING	2,3,4,5	0.9997	NO
34	DNT PRESENCE	CLUSTER / RAINFALL	2,5	1	NO
35	DNT PRESENCE	CLUSTER/ COD2 TEMP	2,3,4	<.0001	YES

Table 4-14 GLMM statistical analysis on the effect of independent variables on TNT solute (aq) concentration

No	Output Parameter	Independent Variable	Experiment No.	Pr>F	95% CL?
1.1	TNT2 CONC.	SOLAR LIGHT	2,6 Fixed7	<.0001	YES
1.2	TNT3 CONC.	SOLAR LIGHT	2,6 Fixed7	ND	
2	TNT1 CONC.	RAINFALL	2,5	0.0024	YES
2.1	TNT2 CONC.	RAINFALL	2,5	<.0001	YES
2.2	TNT3 CONC.	RAINFALL	2,5	ND	
2.3	TNT3 CONC.	RAINFALL	2,3,4,5	<.0001	YES
3	TNT1 CONC.	COD2 TEMP	2,3,4	<.0001	YES
3.1	TNT2 CONC.	COD2 TEMP	2,3,4	<.0001	YES
3.2	TNT3 CONC.	COD2 TEMP	2,3,4	0.949	NO
4	TNT1 CONC.	WATER CONT.-CODSE1	2,3,4	<.0001	YES
4.1	TNT2 CONC.	WATER CONT.-CODSE1	2,3,4	0.0152	YES
4.2	TNT3 CONC.	WATER CONT.-CODSE1	2,3,4	0.9708	NO
5	TNT1 CONC.	WATER CONT.-CODSE1	2,5	<.0001	YES
5.1	TNT2 CONC.	WATER CONT.-CODSE1	2,5	<.0001	YES
5.2	TNT3 CONC.	WATER CONT.-CODSE1	2,5	-	
6	TNT1 CONC.	WATER CONT.-CODSE1	2,6 Fixed7	<.0001	YES
6.1	TNT2 CONC.	WATER CONT.-CODSE1	2,6 Fixed7	1	NO
6.2	TNT3 CONC.	WATER CONT.-CODSE1	2,6 Fixed7	-	
7	TNT1 CONC.	SAMPLING	2,3,4	0.0004	YES
7.1	TNT2 CONC.	SAMPLING	2,3,4	0.2543	NO
7.2	TNT3 CONC.	SAMPLING	2,3,4	1	NO
8	TNT1 CONC.	SAMPLING	2,3,4,5	0.0003	YES
8.1	TNT2 CONC.	SAMPLING	2,3,4,5	0.2555	NO
8.2	TNT3 CONC.	SAMPLING	2,3,4,5	1	NO
9	TNT1 CONC.	SAMPLING	2,3,4,5,6	0.0002	YES
9.1	TNT2 CONC.	SAMPLING	2,3,4,5,6	0.256	NO
9.2	TNT3 CONC.	SAMPLING	2,3,4,5,6	1	NO
10	TNT1 CONC.	DAY	2,3,4	0.0081	YES
10.1	TNT2 CONC.	DAY	2,3,4	0.0016	YES
10.2	TNT3 CONC.	DAY	2,3,4	0.3402	NO
11	TNT1 CONC.	DAY	2,3,4,5	0.0093	YES
11.1	TNT2 CONC.	DAY	2,3,4,5	0.0016	YES
11.2	TNT3 CONC.	DAY	2,3,4,5	0.3405	NO
12	TNT1 CONC.	CLUSTER	2,3,4	<.0001	YES
12.1	TNT2 CONC.	CLUSTER	2,3,4	<.0001	YES
12.2	TNT3 CONC.	CLUSTER	2,3,4	0.6314	NO
13	TNT1 CONC.	CLUSTER	2,3,4,5	<.0001	YES
13.1	TNT2 CONC.	CLUSTER	2,3,4,5	<.0001	YES
13.2	TNT3 CONC.	CLUSTER	2,3,4,5	0.6311	NO
14	TNT1 CONC.	CLUSTER	2,3,4,5,6	0.6311	
14.1	TNT2 CONC.	CLUSTER	2,3,4,5,6	0.6311	NO
14.2	TNT3 CONC.	CLUSTER	2,3,4,5,6	0.6311	NO

**Table 4-15 GLMM statistical analysis on the effect of
independent variables on DNT solute (aq) concentration**

No	Output Parameter	Independent Variable	Experiment No.	Pr>F	95% CL?
1	DNT1 CONC.	SOLAR LIGHT	2,6 Fixed7	0.2041	NO
1.1	DNT2 CONC.	SOLAR LIGHT	2,6 Fixed7	0.3392	NO
1.2	DNT3 CONC.	SOLAR LIGHT	2,6 Fixed7	--	
2	DNT1 CONC.	RAINFALL	2,5	<.0001	YES
2.1	DNT2 CONC.	RAINFALL	2,5	0.0004	YES
2.2	DNT3 CONC.	RAINFALL	2,5	<.0001	YES
2.3	DNT3 CONC.	RAINFALL	2,3,4,5	<.0001	YES
3	DNT1 CONC.	COD2 TEMP	2,3,4	0.003	YES
3.1	DNT2 CONC.	COD2 TEMP	2,3,4	<.0001	YES
3.2	DNT3 CONC.	COD2 TEMP	2,3,4	0.6088	NO
4	DNT1 CONC.	WATER CONT.-CODSE1	2,3,4	0.0001	YES
4.1	DNT2 CONC.	WATER CONT.-CODSE1	2,3,4	0.0015	YES
4.2	DNT3 CONC.	WATER CONT.-CODSE1	2,3,4	0.7395	NO
5	DNT1 CONC.	WATER CONT.-CODSE1	2,5	<.0001	YES
5.1	DNT2 CONC.	WATER CONT.-CODSE1	2,5	0.0291	YES
5.2	DNT3 CONC.	WATER CONT.-CODSE1	2,5	0.9763	NO
6	DNT1 CONC.	WATER CONT.-CODSE1	2,6 Fixed7	0.7052	NO
6.1	DNT2 CONC.	WATER CONT.-CODSE1	2,6 Fixed7	0.3408	NO
6.2	DNT3 CONC.	WATER CONT.-CODSE1	2,6 Fixed7	--	
7	DNT1 CONC.	SAMPLING	2,3,4	<.0001	YES
7.1	DNT2 CONC.	SAMPLING	2,3,4	0.0002	YES
7.2	DNT3 CONC.	SAMPLING	2,3,4	0.8168	
8	DNT1 CONC.	SAMPLING	2,3,4,5	<.0001	NO
8.1	DNT2 CONC.	SAMPLING	2,3,4,5	0.0001	YES
8.2	DNT3 CONC.	SAMPLING	2,3,4,5	0.8166	NO
9	DNT1 CONC.	SAMPLING	2,3,4,5,6	<.0001	NO
9.1	DNT2 CONC.	SAMPLING	2,3,4,5,6	<.0001	NO
9.2	DNT3 CONC.	SAMPLING	2,3,4,5,6	0.8164	NO
10	DNT1 CONC.	DAY	2,3,4	<.0001	YES
10.1	DNT2 CONC.	DAY	2,3,4	0.2338	NO
10.2	DNT3 CONC.	DAY	2,3,4	0.2759	NO
11	DNT1 CONC.	DAY	2,3,4,5	<.0001	YES
11.1	DNT2 CONC.	DAY	2,3,4,5	0.2856	
11.2	DNT3 CONC.	DAY	2,3,4,5	0.2763	NO
12	DNT1 CONC.	CLUSTER	2,3,4	<.0001	NO
12.1	DNT2 CONC.	CLUSTER	2,3,4	<.0001	YES
12.2	DNT3 CONC.	CLUSTER	2,3,4	0.3347	NO
13	DNT1 CONC.	CLUSTER	2,3,4,5	<.0001	YES
13.1	DNT2 CONC.	CLUSTER	2,3,4,5	<.0001	YES
13.2	DNT3 CONC.	CLUSTER	2,3,4,5	0.3352	NO
14	DNT1 CONC.	CLUSTER	2,3,4,5,6	<.0001	YES
14.1	DNT2 CONC.	CLUSTER	2,3,4,5,6	<.0001	YES
14.2	DNT3 CONC.	CLUSTER	2,3,4,5,6	0.3353	NO

Table 4-16 GLMM statistical analysis on the effect of independent variables in TNT detection in gas-phase.

No	Output Parameter	Independent Variable	Experiment No.	Pr>F	95% CL?
1	TNT	TEMP1	2,3,6	<.0001	YES
2	TNT	TEMP1	2,3,6 Fixed7	<.0001	YES
3	TNT	CLUSTER	2,3,6	0.7896	NO
4	TNT	CLUSTER	2,3,6 Fixed7	0.9606	NO
5	TNT	DAY	2,3,6	0.0192	YES
6	TNT	DAY	2,3,6 Fixed7	0.284	NO
7	TNT	CODSE1	2,3,6	0.0679	YES
8	TNT	CODSE1	2,3,6 Fixed7	0.2931	NO

Table 4-17 GLMM statistical analysis on the effect of independent variables in DNT detection in gas-phase.

No	Output Parameter	Independent Variable	Experiment No.	Pr>F	95% CL?
1	DNT	TEMP1	2,3,6	0.2121	NO
2	DNT	TEMP1	2,3,6 Fixed7	0.0906	YES
3	DNT	CLUSTER	2,3,6	0.004	YES
4	DNT	CLUSTER	2,3,6 Fixed7	0.6984	NO
5	DNT	DAY	2,3,6	0.138	NO
6	DNT	DAY	2,3,6 Fixed7	0.1664	NO
7	DNT	CODSE1	2,3,6	0.9912	NO
8	DNT	CODSE1	2,3,6 Fixed7	0.9978	NO

4.6.3   Description of GLMM Simulation Outcomes

Table 4-12 to Table 4-17 show simulations run in SAS[TM]. Simulation properties are shown in appendixes B as identified by the simulation ID. Output files contain model information, characteristics of the data used, optimization information, fit statistics of the error control, information of the parameter estimates, information about significance level reach and odd ratios information. When combinations of effects are simulated, the output file also contains information about odd ratios of combination of effects, least square mean differences, and diffograms information. Two output files are explained below: the first one corresponds to a single variable, and the second one to the assessment of a combination of effects.

4.6.3.1 Single Effect Outcomes

This example corresponds to simulation 2 on DNT detection. This run quantifies the

influence of rainfall intensity on detection of DNT. Initially, the output file show information

about information of the SAS statistical procedure:

The SAS System   The GLIMMIX Procedure

Table 4-18, shows information on the characteristics of the generalized linear mixed model

and the input matrix data:

Table 4-18 GLMM Model Information

Model Information	
Data Set	WORK.ANGELFILTER
Response Variable	DNTOUTPUT
Response Distribution	Binary
Link Function	Logit
Variance Function	Default
Variance Matrix	Diagonal
Estimation Technique	Maximum Likelihood
Degrees of Freedom Method	Residual

Class Level Information		
Class	Levels	Values
SOLAR_RADIATION	2	1 0
RAINFALL__IN_HR_	2	0.5 2
TEMP___C_	1	25
COD_ATM_TEMP	3	4 3 2

Table 4-19 shows all input data present in the data matrix its names, and the levels of information; this simulation was run with data of experiments TE-2 and TE-5, which have identical environmental conditions, except for the rainfall intensity. Both experiments have a 14-day duration (Table 3.5) with a total amount data of 4032 records, 2016 for each experiment.

Table 4-19 GLMM data information

Number of Observations Read	4032
Number of Observations Used	4032

Table 4-20 shows the number of values with the DNT presence condition, 111 of 4032. It indicates simulation was modeling the probability of DNTOUTPUT (outcome variable) being 0 (probability of DNT presence).

Table 4-20 GLMM response profile information

Response Profile		
Ordered Value	**DNTOUTPUT**	**Total Frequency**
1	**0**	111
2	**1**	3921
The GLIMMIX procedure is modeling the probability that DNTOUTPUT='0'.		

For binary and multinomial data, the "Response Profile" Table displays the Ordered Value from which the GLIMMIX procedure determines:

• the probability being modeled as binary data

• the ordering of categories for ordinal data

• the reference category for generalized logit models.

Table 4-21 refer to optimization processes to guarantee the convergence criteria.

Table 4-21 GLMM optimization and iteration history

Dimensions	
Columns in X	3
Columns in Z	0
Subjects (Blocks in V)	1
Max Obs per Subject	4032

Optimization Information	
Optimization Technique	Newton-Raphson
Parameters in Optimization	2
Lower Boundaries	0
Upper Boundaries	0
Fixed Effects	Not Profiled

Iteration History					
Iteration	**Restarts**	**Evaluations**	**Objective Function**	**Change**	**Max Gradient**
0	**0**	4	635.33262646	.	258.241
1	**0**	3	507.65930126	127.67332521	72.06794
2	**0**	3	482.12711498	25.53218628	16.36728

189

Table 4-21 GLMM optimization and Iteration History - continued

Dimensions					
3	**0**	3	478.26820557	3.85890941	2.8603
4	**0**	3	478.05317042	0.21503515	0.192559
5	**0**	3	478.05207881	0.00109162	0.001065
6	**0**	3	478.05207877	0.00000003	3.308E-8
Convergence criterion (GCONV=1E-8) satisfied.					

After convergence, statistics parameters are shown in Table 4-22.

Table 4-22 GLMM fit statistics

Fit Statistics	
-2 Log Likelihood	956.10
AIC (smaller is better)	960.10
AICC (smaller is better)	960.11
BIC (smaller is better)	972.71
CAIC (smaller is better)	974.71
HQIC (smaller is better)	964.57
Pearson Chi-Square	4032.00
Pearson Chi-Square / DF	1.00

-2l + 2d

-2l + 2dn*/(n*-d-1)

-2l –d*log(n)

-2l –d*log(n + 1)

2l –d*log((log(n))

Missing data can be forced to non-convergence conditions. The "gradient" is derived from the first partial derivatives with respect to the parameters and should be small numbers if the estimates are good (Demidenko, 2004). The AIC (Akaike's information criteria), AICC (small sample bias corrected version of AIC), BIC (Bayesian inference criterion), CAIC (consistent Akaike's information criterion), and HQIC (Hannan Quinn information criteria)

fit statistics reported by the GLIMMIX procedure. The calculations above are from SAS, where l denotes the log likelihood (which may be restricted and a pseudo or quasi likelihood), d is the dimension of the model, and n or n* reflects the size of the data. These values vary for different options, methods, and restrictions. Once convergence criteria is reached, the output file (Table 4-23) shows the parameters estimates by the regression model and its significance level within the model.

Table 4-23 GLMM parameter estimates

Parameter Estimates						
Effect	**RAINFALL (IN/HR)**	**Estimate**	**Standard Error**	**DF**	**t Value**	**Pr > |t|**
Intercept		-3.0178	0.1056	4030	-28.57	<.0001
RAINFALL__IN_HR_	**0.5**	-1.7494	0.2655	4030	-6.59	<.0001
RAINFALL__IN_HR_	**2**	0	.	.	.	.

DF = degree of freedom

Type III test of fixed effects (Table 4-24) contains hypothesis tests for the significance of each of the fixed effects specified in the model statement. If Pr > F greater than 0.05 (By confidence limits of 95%), the effect analyzed is not significant. For this simulation, the effect of rainfall intensity is highly significant within confidence limits greater of 99.9%.

Table 4-24 GLMM fixed effects

Type III Tests of Fixed Effects				
Effect	**Num DF**	**Den DF**	**F Value**	**Pr > F**
RAINFALL__IN_HR_	1	4030	43.42	<.0001

Odds ratios estimates provide information that allow quantifying the effect. It is known that rainfall effect is highly significant, but for how much. Odd ratio estimates for rainfall intensity compares probability of the outcome variable, DNT presence, for each level of the independent variable. This relation is shown by the odd ratio estimate. In this example, the odd ratio value shows that the probability of finding DNT in aqueous phase decreases 82.6% if the rainfall intensity decreases from 2 inches per hour to 0.5 inch per hour (Table 4-25).

Table 4-25 GLMM odds ratio estimates

Odds Ratio Estimates					
RAINFALL (IN/HR)	RAINFALL (IN/HR)	Estimate	DF	95% Confidence Limits	
0.5	**2**	0.174	4030	0.103	0.293

An uncertainty level decreases the significance and validation of analysis if the confidence limits vary between values lower than 1 and values greater than 1.

4.6.3.2 Combination of Single Effects

The following example shows the output file of simulation No.25 for determining the probability of presence due to a combination of two singles independent variables: Rainfall intensity and Solar radiation. The data used corresponds to experiments TE-2 and TE-5 ERC. On this simulation, there are two effects each one with two levels: 0.5 and 2 for rainfall and 0 and 1 for solar radiation. The analysis evaluates the change probability on DNT (aq) detection under changes in all possible combinations of the independent variables levels (Table 4-26 to 4-32).

Table 4-26 GLMM model information (mixed effects)

Model Information	
Data Set	WORK.ANGELFILTER
Response Variable	DNTOUTPUT
Response Distribution	Binary
Link Function	Logit
Variance Function	Default
Variance Matrix	Diagonal
Estimation Technique	Maximum Likelihood
Degrees of Freedom Method	Residual

Class Level Information		
Class	**Levels**	**Values**
CLUSTER	18	1 2 3 4 5 6 7 8 9 10 11 12 13 14 15 16 17 18
DAY	14	1 2 3 4 5 6 7 8 9 10 11 12 13 14
SOLAR RADIATION	2	1 0
RAINFALL__IN_HR_	2	0.5 2
TEMP___C_	1	25
COD_ATM_TEMP	3	4 3 2
COD2_ATM_TEMP	3	3 2 1
COD3_ATM_TEMP	3	3 2 1
COD4_ATM_TEMP	2	3 2
COD5_ATM_TEMP	2	2 1
SAMPLING	8	1 2 3 4 5 6 7 8

193

Table 4-27 GLMM response profile (mixed effects)

Number of Observations Read	4032
Number of Observations Used	4032

Response Profile		
Ordered Value	DNTOUTPUT	Total Frequency
1	0	111
2	1	3921
The GLIMMIX procedure is modeling the probability that DNTOUTPUT='0'.		

Table 4-28 GLMM dimensions and optimization (mixed effects)

Dimensions	
Columns in X	9
Columns in Z	0
Subjects (Blocks in V)	1
Max Obs per Subject	4032

Optimization Information	
Optimization Technique	Newton-Raphson
Parameters in Optimization	4
Lower Boundaries	0
Upper Boundaries	0
Fixed Effects	Not Profiled

Table 4-29 GLMM iteration history (mixed effects)

			Iteration History		
Iteration	**Restarts**	**Evaluations**	**Objective Function**	**Change**	**Max Gradient**
0	**0**	4	634.18503659	.	258.4911
1	**0**	3	504.79142954	129.39360704	72.75175
2	**0**	3	478.24129303	26.55013651	16.98165
3	**0**	3	474.16049001	4.08080302	2.999478
4	**0**	3	473.90363575	0.25685426	0.225918
5	**0**	3	473.90162304	0.00201271	0.001959
6	**0**	3	473.90162287	0.00000017	1.695E-7

Convergence criterion (GCONV=1E-8) satisfied.

Table 4-30 GLMM fit statistics (mixed effects)

Fit Statistics	
-2 Log Likelihood	947.80
AIC (smaller is better)	955.80
AICC (smaller is better)	955.81
BIC (smaller is better)	981.01
CAIC (smaller is better)	985.01
HQIC (smaller is better)	964.74
Pearson Chi-Square	4032.00
Pearson Chi-Square / DF	1.00

Table 4-31 GLMM parameter estimates (mixed effects)

Parameter Estimates							
Effect	**LUZ SOLAR**	**RAINFALL (IN/HR)**	**Estimate**	**Standard Error**	**DF**	**t Value**	**Pr > |t|**
Intercept			-3.6315	0.2810	4028	-12.92	<.0001
SOLAR_RADIATION	1		0.7598	0.3033	4028	2.50	0.0123
SOLAR_RADIATION	0		0	.	.	.	.
RAINFALL__IN_HR_		0.5	-0.7873	0.4976	4028	-1.58	0.1137
RAINFALL__IN_HR_		2	0	.	.	.	.
SOLAR_RADIATION*RAINFALL__	1	0.5	-1.2570	0.5935	4028	-2.12	0.0342
SOLAR_RADIATION*RAINFALL__	1	2	0	.	.	.	.
SOLAR_RADIATION*RAINFALL__	0	0.5	0	.	.	.	.
SOLAR_RADIATION*RAINFALL__	0	2	0	.	.	.	.

Table 4-32 GLMM fixed effects (mixed effects)

Type III Tests of Fixed Effects				
Effect	**Num DF**	**Den DF**	**F Value**	**Pr > F**
SOLAR_RADIATION	1	4028	0.20	0.6581
RAINFALL__IN_HR_	1	4028	22.76	<.0001
SOLAR_RADIATION*RAINFALL__	1	4028	4.49	0.0342

The analysis indicates high significance effect on DNT presence by rainfall intensity (see the previous example), but no no-significance effects caused. The analysis also shows that the mixture effect of both single variables has a significant effect. This behavior can be attributed to the high significance of rainfall intensity.

Odds ratio estimates must be analyzed under researcher criteria based in the knowledge of the data. For example, the odds ratio for solar radiation effects indicates an increase of 14% on probability of DNT (aq) presence if solar radiation conditions are present. The type III test to fixed effects, however, indicate a low confidence limit for this variable (about 35%). Also the confidence limits reported by the odds ratio estimates suggest uncertainty on this presumption. For rainfall intensity, the odd ratios suggest that the probability of finding DNT in aqueous phase decrease 75.7% if the rainfall intensity decreases from 2 inches per hour to 0.5 inch per hour (Table 4-33).

Table 4-33 GLMM odd ratio estimates (mixed effects)

Odds Ratio Estimates							
SOLAR RADIATION	RAINFALL (IN/HR)	LUZ SOLAR	RAINFALL (IN/HR)	Estimate	DF	95% Confidence Limits	
1		0		1.140	4028	0.637	2.040
	0.5		2	0.243	4028	0.136	0.434

When the simulations involve a combination of effects the option LSMEANS statement were added to the code. It computes the least-squares means (LS-means) of fixed effects and estimates the marginal means over a balanced population. LS-means for each single effect and combination of them are shown in the next Table. It shows the least squares means for the effect of solar radiation (Table 4-34).

197

Table 4-34 GLMM least squares means (mixed effects)

SOLAR_RADIATION Least Squares Means					
SOLAR_RADIATION	**Estimate**	**Standard Error**	**DF**	**t Value**	**Pr > |t|**
1	-3.8938	0.1617	4028	-24.08	<.0001
0	-4.0252	0.2488	4028	-16.18	<.0001

Information in this analysis is used to construct differences graphics or diffograms. The Diffogram is a graphical display of least-squares means related analyses. It is comprised of plots of all pairwise differences and plots of differences against a control level (the dashed line in the Figure 4-72). The number of pairwises comparisons among the least-squares means depend on the amount of levels, L, analyzed by LS-means by a factor L (L-1)/2. The solar radiation Diffogram contains 1 line rotated by 45 degrees counter clockwise, and a reference line (dashed 45 degree line). The (x, y) coordinate for the center of each line corresponds to the two least-squares means being compared and then estimates values determinate the location in the plane. The lowest estimate is the X value and the highest the Y value, then the center of the line segment analyzed is placed at (-4.0252, -3.8938).

The length of the line segment for the comparison between means corresponds to the width of the confidence interval for the difference between the estimates. This length is adjusted for the rotation in the plot. Consequently, comparisons whose confidence interval covers zero cross the 45 degree reference line. These are the non-significant comparisons. Lines associated with significant comparisons do not touch or cross the reference line. Since these data are balanced, the estimated standard errors of all pairwise comparisons are identical, and

the widths of the line segments are the same. Diffogram for solar radiation is shown in the Figure 4-72.
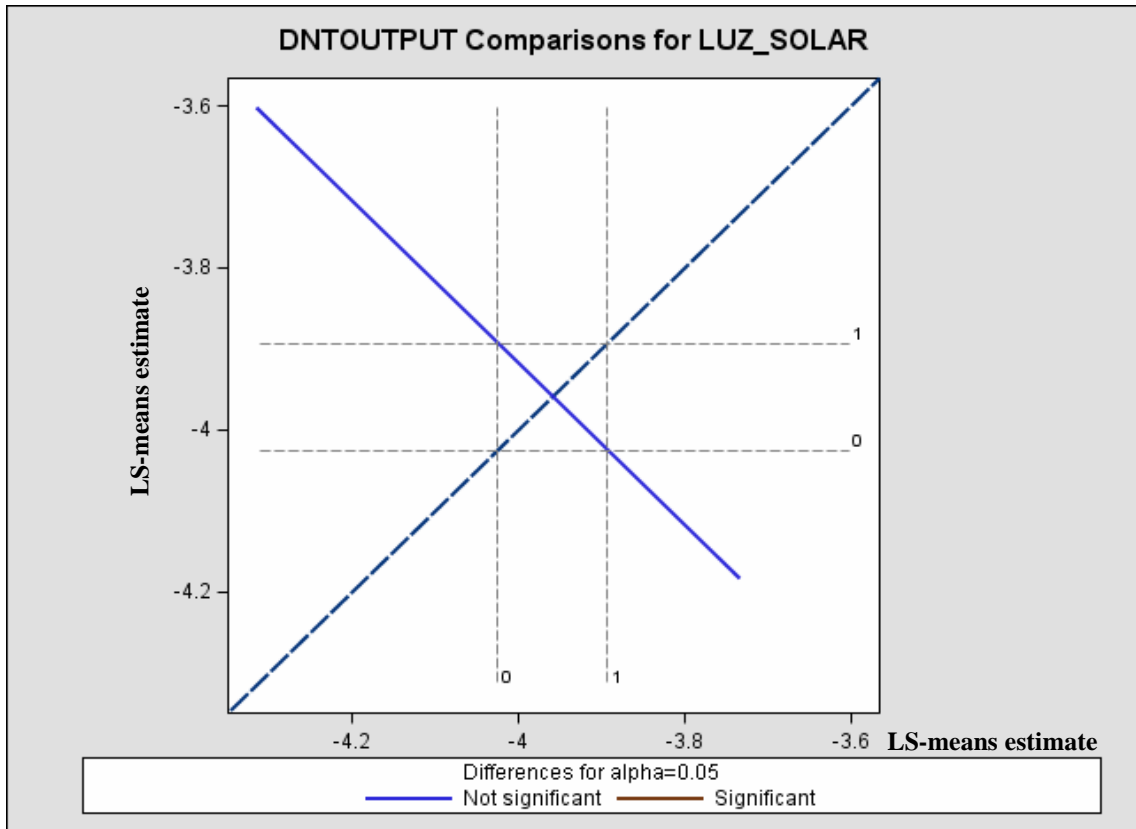
Figure 4-72 GLMM diffogram for radiation for DNT (mixed effects)

The T grouping for effect analyzed by LS-means sort all possible combinations by significance grade and assigns a letter to each level or combination of levels; levels with the same letter are not significantly different by this classification (Table 4-35 and 4-36).

Table 4-35 GLMM T-grouping (mixed effects)

T Grouping for SOLAR_RADIATION Least Squares Means		
LS-means with the same letter are not significantly different.		
LUZ SOLAR	**Estimate**	
1	-3.8938	A
		A
0	-4.0252	A

Table 4-36 GLMM least squares means (mixed effects)

RAINFALL__IN_HR_ Least Squares Means					
RAINFALL (IN/HR)	**Estimate**	**Standard Error**	**DF**	**t Value**	**Pr > |t|**
0.5	-4.6674	0.2551	4028	-18.30	<.0001
2	-3.2516	0.1517	4028	-21.44	<.0001

LS-means by rainfall intensity show a highly significant effect by both levels: 0,5 and 2 inches / hour. The number of levels condition only one line of differences in the diffogram. The center of the line segment analyzed is placed at (-4.6674, -3.2516) and the line does not cut the 45 degree reference line. This means that changes between levels produce significant changes in the probability of the outcome variable (Figure 4-73).
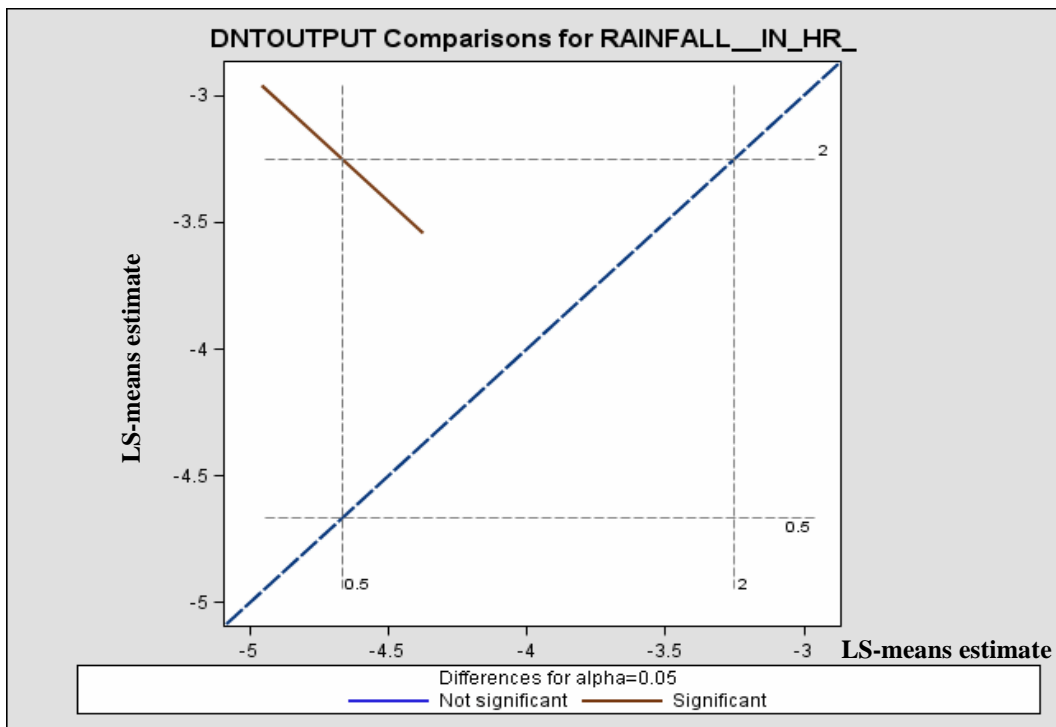
Figure 4-73 GLMM diffogram for rainfall for DNT (mixed effects)

T grouping for rainfall intensity shows a high significance at all levels of the effect analyzed

by LS-means (Table 4-37 and Table 4-38).

Table 4-37 GLMM T-grouping for rainfall (mixed effects)

T Grouping for RAINFALL__IN_HR_ Least Squares Means		
LS-means with the same letter are not significantly different.		
RAINFALL (IN/HR)	Estimate	
2	-3.2516	A
0.5	-4.6674	B

Table 4-38 GLMM least squares means (mixed effects)

LUZ SOLAR	RAINFALL (IN/HR)	Estimate	Standard Error	DF	t Value	Pr > |t|
1	0.5	-4.9160	0.3026	4028	-16.25	<.0001
1	2	-2.8717	0.1142	4028	-25.14	<.0001
0	0.5	-4.4188	0.4107	4028	-10.76	<.0001
0	2	-3.6315	0.2810	4028	-12.92	<.0001

The diffogram produced by combination of levels shows 6 lines (this number is given by 4(4-1)/2, where 4 is the number of combinations given by the levels analyzed). Figure 4-74 indicates that by pairwise [1 2] presence of solar radiation at maximum intensity is significant, as seen by the three brown lines at the highest horizontal dashed line.
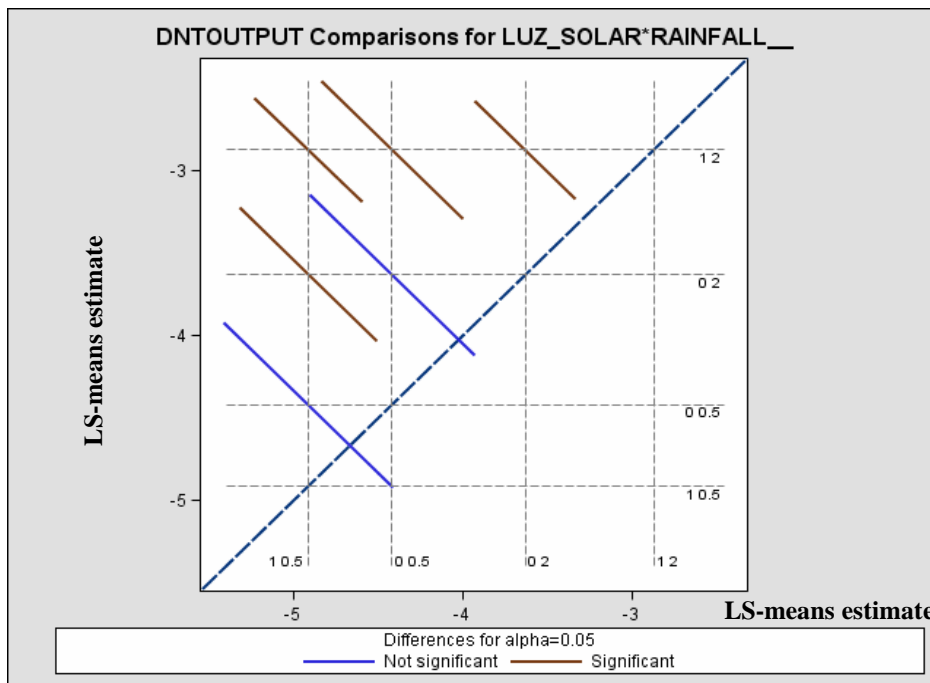
Figure 4-74 GLMM diffogram for DNT (mixed effects)

T grouping confirms the hypothesis suggested by the diffogram; that is, the only significant different pairwise correspond to rainfall intensities of 2 in/hour during events of solar radiation (Table 4-39).

Table 4-39 GLMM T grouping for radiation - rainfall

T Grouping for SOLAR_RADIATION*RAINFALL__ Least Squares Means				
LS-means with the same letter are not significantly different.				
LUZ SOLAR	RAINFALL (IN/HR)	Estimate		
1	2	-2.8717		A
0	2	-3.6315		B
				B
0	0.5	-4.4188	C	B
			C	
1	0.5	-4.9160	C	

With this considerations Odd ratios tables by mixture effects that changes in solar radiation under high rainfall intensities and changes in rainfall intensity under presence or solar radiation are significantly different. For example, with high rainfall intensities the probability of finding DNT (aq) in samples increases 114% if solar radiation conditions is presented over no solar radiation. Similarly, with solar radiation events, the probability of detecting DNT (aq) decrease 87.1 % if sampling is collected under rainfall intensities of 0.5 in/hr and not under rainfall intensities of 2 in/hr (Table 4-40).

203

Table 4-40 GLMM simple effect comparisons by mixed effects

Simple Effect Comparisons of SOLAR_RADIATION*RAINFALL__ Least Squares Means By RAINFALL__IN_HR_									
Simple Effect Level	LUZ SOLAR	LUZ SOLAR	Estimate	Standard Error	DF	t Value	Pr > |t|	Adj P	Odds Ratio
RAINFALL__IN_HR_ 0.5	1	0	-0.4972	0.5101	4028	-0.97	0.3299	0.3299	0.608
RAINFALL__IN_HR_ 2	1	0	0.7598	0.3033	4028	2.50	0.0123	0.0123	2.138
Simple Effect Comparisons of SOLAR_RADIATION*RAINFALL__ Least Squares Means By SOLAR_RADIATION									
Simple Effect Level	RAINFALL (IN/HR)	RAINFALL (IN/HR)	Estimate	Standard Error	DF	t Value	Pr > |t|	Adj P	Odds Ratio
SOLAR_RADIATION 1	0.5	2	-2.0443	0.3234	4028	-6.32	<.0001	<.0001	0.129
SOLAR_RADIATION 0	0.5	2	-0.7873	0.4976	4028	-1.58	0.1137	0.1137	0.455

For the other combination levels, odd ratios Table 4-40 show confidence levels lower than 95% (these factor are filled in red). The magnitude of confidence range and knowledge of the input data allow the assessment of the statistical results. For this example, pairwise labeled as non-significantly different, changes in rainfall intensities during events with presence of solar radiation, can be assumed as valid. Since the event has a confidence limits close to 89%, this indicates that under non-radiation events, the probability of DNT detection (aq) decrease by 54% if sampling is collected under rainfall intensities of 0.5 in/hr over intensities rainfall of 2 in/hr.

5 INTEGRATION OF RESULTS

A three-dimensional laboratory-scale SoilBed system has been designed and developed to assess the influence of environmental parameters in the flow patterns and transport of TNT and DNT. Experimental work to determine the effect of visible and UV light, temperature, and rainfall conditions indicate that water and solute transport is highly influenced by interrelated environmental and boundary conditions (Figures 4-38, 4-39, 4-40, 4-41; Table 4-8). The presence of light and higher system temperatures induces greater water drainage (Figures 4-11, 4-12, 4-23, 4-24, 4-25 and Table 4-3) and solute fluxes (Figures 4-37, 4-40, 4-41, and Tables 4-3, 4-9, 4-10.

During infiltration, hydraulic heads increase at faster rates under no light exposure suggesting greater water and solute retention then when the surface is exposed to radiation of visible light (Figure 4-12). Water and solute transport is also influenced by boundary conditions and thermal gradient (Figure 4-26, 4-27, Figure 4-51, Figure 4-55, Figure 4-66, Figure 4-67, and Table 4-4).

Transport of conservative solutes closely follows water flow patterns, and reflects the influence of variable and interrelated environmental factors on spatial and temporal concentration distribution (Figure 4-26, 4-37, 4-47, 4-64, 4-65, 4-73, 4-74). Experiments demonstrate that non-reactive and reactive ERCs solutes are highly influenced by variation in hydraulic and advective processes induced by changes in environmental conditions. Fate and

transport is affected by variations in sorptive, gas transport, and degradation processes (Figures 4-67, 4-68, 4-69, 4-70, and 4-71), which are also influenced by environmental conditions.

The number of samples in which TNT, DNT, and other related chemicals (UI) were detected during the experiment. Experiments are summarized in Table 5-1.

EXP.	SAMPLES CHEMICAL Total ERC Sample (Max conc. (μg/l) –sampling day)					
	DNT (l)	TNT (l)	UI ERC (l)	DNT (G)	TNT (G)	UI ERC (G)
1 *(7d)*	*8 (140-d7.3)*	*7 (73-d7.3)*	*12 (* - d7.3)*			
2 *(14d)*	*94 (1577-d14.5)*	*58(392-d1.5)*	***	*Morning:47 Evening:43*	*Morning:10 Evening:18*	*Morning:*** Evening:****
(7d)	*57 (306-d7.5) (434-d4.7)*	*44(392-d1.5)*		*Morning:10 Evening:14*	*Morning:2 Evening:11*	*Morning:*** Evening:****
3 *(14d)*						
3 REP *(14d)*	*107 (1093-d3.6)*	*8(270 –d2.7)*	***	*Evening: 34(174-d13)*	*Evening: 92(728-d6)*	*Evening: 79**(d13)*
4 *(14d)*	*92 (5058-d14.4)*	*91(11284-d8.5)*	***			
5 *(14d)*	*17 (207-d13.5)*	*1(19-d1.6)*	***			
6 *(7d)*	*43(644-d7.6)*	*2(33-d7.4)*	***	*Evening: 26(89-d3) (75-d7)*	*Evening: 17(83-d4) (73-d7)*	*Evening: 0*

Table 5-1 Summarize ERCs detections in the transport experiments conduced

*OVER 100 μg/l AS TNT concentration, ERC identified like 4A-2,6DNT.
** ERC less heavier than DNT, non quantified
*** Non analyzed

In general the results show that::

- Daily TNT solute detection tends to increase during rainfall periods for high saturation. At lower saturation conditions, peak detection occurs after rainfall events. Daily DNT detection tends to increase during rainfall periods for all conditions. This is attributed to enhanced distribution during rainfall periods. Greater dissolution occur at higher water saturation and flux. Lower water flux, higher potential sorption and greater gas phase partitioning contribute to the delayed TNT solute transport at lower water saturation conditions.

- TNT and DNT solute concentrations are below solubility limits. Daily TNT and DNT concentration tend to increase to a maximum value, and then decrease. Higher concentrations are initially observed for high Se. At later times, high concentrations are observed at high temperatures conditions. DNT concentrations are also observed at later times for no radiation condition. This is attributed to rate limited dissolution processes. Higher dissolution at higher water saturation results in higher initial concentration. Higher concentrations at later times for no radiation are attributed to low water-saturation in these conditions.

- TNT solute detection and concentration tends to decrease over long time. DNT solute detection tends to reach a constant value. DNT concentration increase to a maximum and then decrease over time for low saturation conditions. Initial DNT solute peak occurs for high temperature conditions. At high saturation, concentrations increase significantly toward the end of the 14th day period. These long-term temporal effects indicate high initial dissolution rates. Similar results were reported by (Padilla et al, 2007). These results also suggest potential degradation of TNT to DNT, and potential

rate limited sorption. Rate limited sorption of TNT and DNT has been reported by Torres (2008).

- TNT and DNT solute detection and concentration are higher with depth, and near preferential flow paths having low travel times (high velocity). Maximum TNT and DNT concentration in preferential flow patterns coincide with high NaCl concentrations and hydrodynamic gradients. Generally, higher TNT and DNT detection density in zones of preferential flow occurs for high saturation conditions. In other zones, DNT detection is higher for high temperatures, low rainfall, and cyclic radiation, whereas detection of TNT is limited. Higher accumulation at the bottom is attributed to the advective transport of dissolved TNT and DNT toward the bottom.

- TNT and DNT solute detection and concentration are higher for high soil-water saturation. In fact, aqueous maximum TNT and DNT concentrations increase for high soil water contents. This is attributed to greater dissolution of TNT/DNT source.

- TNT and DNT detection and concentrations are generally higher for higher rainfall rates. TNT concentrations are lower for low rainfall event. Solute detection is high at low rainfall for DNT, but very low for TNT. Higher rainfall rates generally contribute to higher water saturation and flux, which induce greater dissolution, higher advective transport, and lower sorption. Low rainfall limits dissolution and transport, and induce low water content and subsequent higher sorption.

- Higher temperature increase TNT detection and concentration after rainfall events. DNT solute detention is significantly increased at higher temperatures, showing highest detection under highest temperatures conditions. TNT and DNT solute

detection and concentration are influenced to a greater degree by saturation than temperature. The higher detection and concentration generally observed for lower temperature result for the higher saturation condition (higher dissolution), and lower potential degradation and volatilization at low temperature. Higher solute detection and concentration at higher temperature is attributed to greater dissolution rates and water drainage, but is limited by water saturation. High DNT solute detection and concentration at high temperature also result from potential degradation of TNT to DNT.

- Radiation, high temperature, and low rainfall cause a significant increase in DNT solute detection. This is attributed to degradation and volatilization of TNT into DNT under these conditions.

- TNT and DNT maximum solute detection density is earlier for conditions that induce draining. This is attributed to greater water flux under drainage conditions.

- TNT solute detection is somewhat influenced by radiation, whereas DNT detection is significantly increased. TNT and DNT concentrations are, however, low under no radiation. Increased DNT solute detection at radiation is attributed to TNT degradation to DNT. Presence of an unidentified compound (potentially as 4A-2,6DNT (aq)) shows that degradation products are being formed to a higher degree in the presence of radiation. Low TNT and DNT concentration at no radiation is attributed to low saturation (low dissolution) and lower volatilization and degradation.

- TNT solute detection and concentration are lower for sources of smaller size. This is caused by lower dissolution area.

- TNT solute concentrations are always at higher saturation, but DNT concentrations are higher than TNT for conditions of low soil-water saturation under no radiation, high temperature, and low rainfall. Higher TNT concentrations at high saturation are attributed to lower TNT degradation, volatilization, and sorption. Higher DNT concentration at low water saturation is attributed to greater TNT degradation, volatilization, and sorption.

- Aqueous DNT is detected at higher frequencies than TNT, even if the source only contains TNT Exp. TE-1 ERC, Table 5-1). This is attributed to: (1) DNT presence in the TNT source, (2) degradation of TNT to DNT, and (3) higher solubility and vapor pressure of DNT.

- TNT and DNT detection in the gas phase is concentrated near the soil-surfaces and near preferential flow paths after rainfall events. Higher gas-phase detection near the surface is associated with lower saturation, inducing greater volatilization.

- TNT detection density in the gas phase is generally higher than in the water phase. TNT gas phase detection follows a similar pattern as that in the water phase, but lagged by a day or two. It tends to decrease over time. The similarity with advection patterns in the water phase indicates that vapor concentrations are controlled by aqueous concentrations. Similar results have been reported by Gutierrez (2008). The lagged phase in gas phase detection is attributed to mass-transfer limitations between the water and gas phases.

211

- DNT detection in the gas phase is generally lower than in the water phase, but it tends to increase with time. Greater DNT detection with time is attributed to TNT degradation to DNT and DNT volatilization.

- TNT detection in the gas phase is highest for high temperatures. High detection at radiation occurs within the 1st week after burial. DNT in the gas phase is detected to a greater extent at 25 ^{o}C than at higher temperatures. Greater TNT detection at higher temperatures is attributed to higher gas-phases partitioning. The lower DNT detection at high temperatures is attributed to enhance DNT degradation at higher temperatures. This is supported by a high number of unidentified ERCs (g) of lower weight than DNT (g) found under high temperatures.

- TNT in the gas-phase is detected to a higher extent than DNT at early times under high temperatures and cyclic radiation at 25 ^{o}C, but not at later times. DNT is detected to a greater extent for no radiation conditions. This is attributed to TNT degradation over time.

5.1 Temporal-Spatial Effects on Presence/Concentration of ERCs

Odd ratios information generated by the SAS modeling show a direct influence of soil atmospheric effects on the presence and concentrations of TNT and DNT. Soil-water content related to rainfall events have a particular strong influence, as shown by the odd ratios calculated for daily detection and concentration values (Figure 5-1). This Figure shows the

changes (increasing-decreasing) in probability of detecting TNT/DNT in the aqueous phase

for concentrations lower than 1 mg/l. It shows that the highest probabilities to detect

TNT/DNT at higher concentrations is close to the time of maximum water saturation during

rainfall events. Results show a confidence limits above 95% except for TNT concentrations

between 100 μg/l and 1000 μg/l, where confidence limits is around 75%. A lower effect is

caused in the absence of radiation. There is a higher probability, however, of finding TNT

during the no-radiation period after rainfall event than DNT. There is a higher probability of

detecting DNT at the end of the rainfall events. Similarly, probabilities to detect low and

medium TNT concentrations are higher than DNT probabilities.
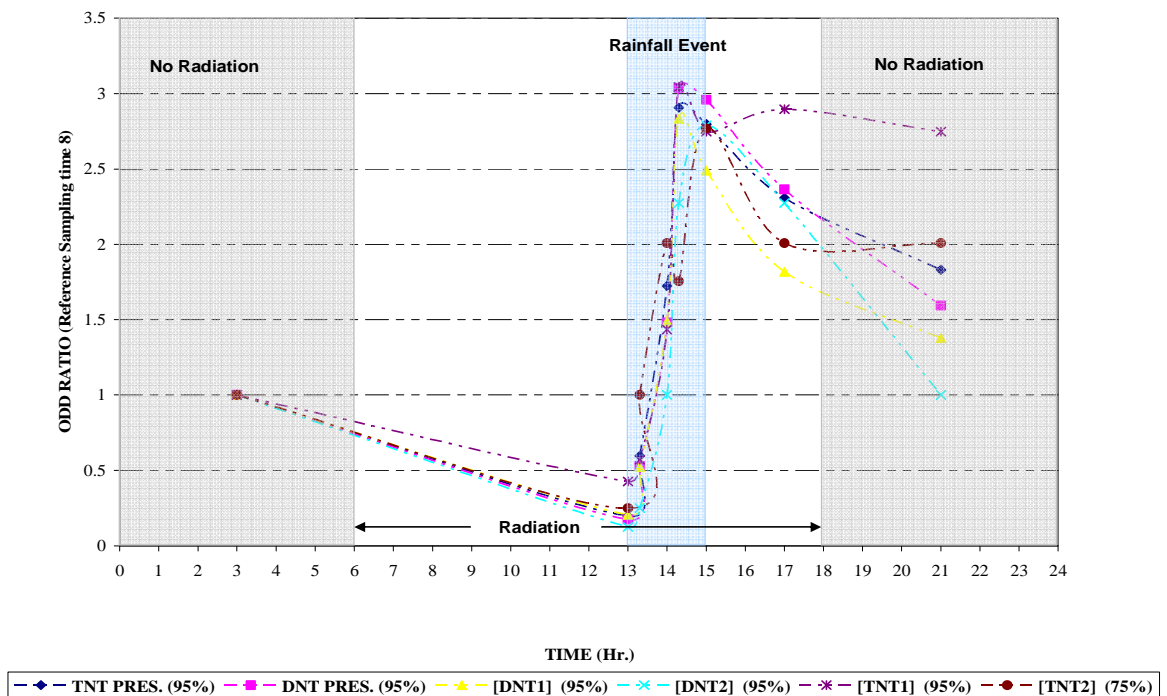
Figure 5-1 Daily probability in presence / concentration of DNT/TNT (aq)

Long-term analysis (Figure 5-2) indicates a higher probability to detect TNT (aq) in the first three days of the experiments by a factor of three times higher than TNT (aq) detection in the last experimental days. DNT (aq) probability tends to be constant during all simulation time. DNT concentrations probabilities indicate a decrease with time for low concentrations ranges, in contrast with medium DNT concentrations probabilities. In contrast, with the detection probability of DNT (g) increases with time. TNT(g) detection probabilities present a high variability, with an increasing tendency for the first half of the experiment, and a decrease tendency for the second half.

Spatial analysis (Figure 5-3) shows existence of preferential clusters in each sampling plane, where probability in detection and concentration of TNT-DNT are higher than others in the same plane. Figure 5-3 indicates that clusters 2 and 11 in the top plane, 5 and 14 in the med-level plane, and 8 and 17 in the lowest plane have preferential detection. It also demonstrates higher vertical transport gradients patterns.

Deeper clusters present the highest probability for both, detection and concentration. These behaviors suggest accumulation processes at the bottom of the sampling volume. The probabilities to detect TNT (aq) is lower than DNT (aq) at the top , whereas there is a higher probability for DNT (aq) in the bottom ones.
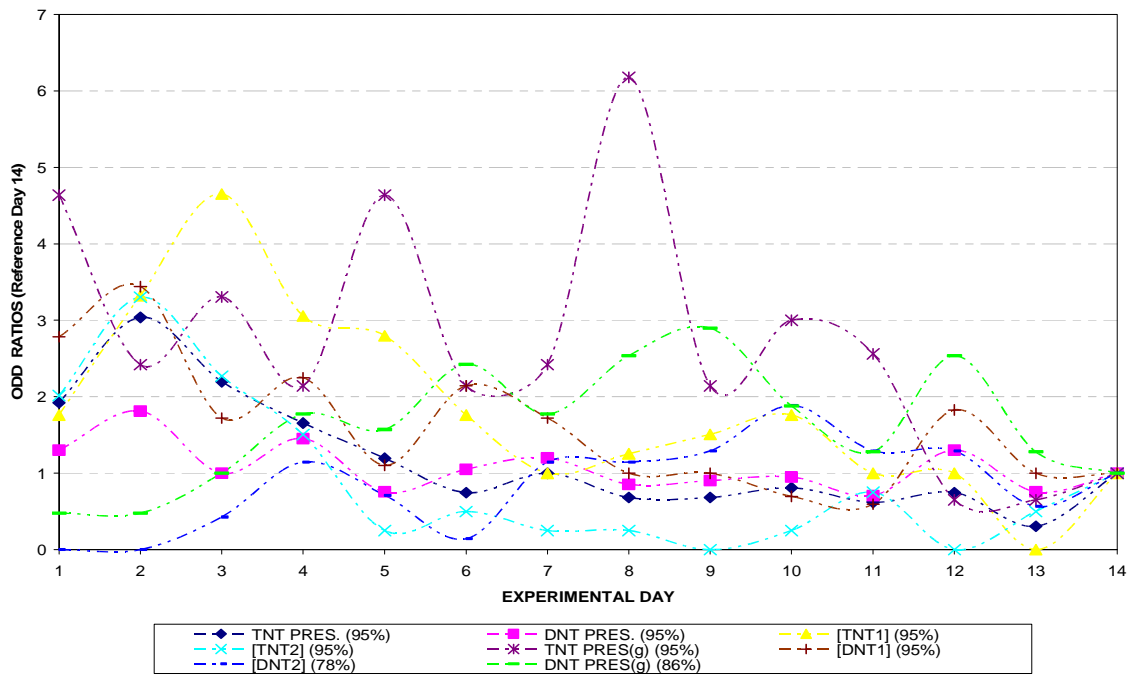
Figure 5-2 Detection/Concentration probability of ERC (aq/g) - long-term scale
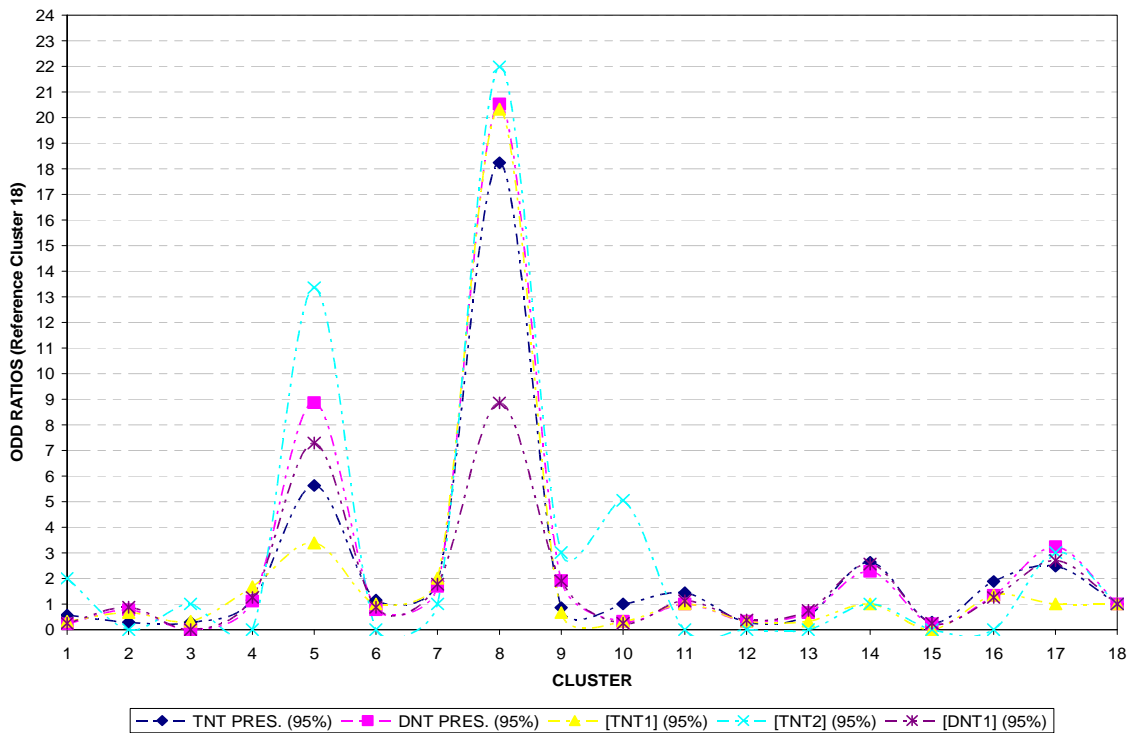
Figure 5-3 Detection/Concentration probability of ERC (aq) - spatial distribution

215

5.2 Soil-environmental Single Effects on Detection-concentration of ERCs

Several scenarios were simulated using the GLIMMIX (GLMM model) procedure provided by SAS software to determine the significance of environmental factors on the presence and concentration of TNT and DNT. This can then be related to the processes controlling the fate and transport of these chemicals. Table 5-2 summarize the results obtained: the <u>output</u> refer to the variable being tested; the <u>variable</u> refers to the environmental condition tested for effects; the phase refers to the phase where the chemical was measured; the P value must be less than 0.05 to be a significant variable within the 95% confidence interval (95% CL). If significant, the odd ratio indicates the level of significance based on comparison of S1 to S2. "Est." refers to odd ratio estimation; "DF" refers to the degree freedom of modeling and depends of amount of data and the number of levels.

Table 5-2 Odd ratios analysis - GLMM statistical results

Output	Variable	Exp	Phase	Pr>F	95% CL?	Odd Ratios Analysis					
						S1	S2	Est.	DF	95% CL	
DNT PRES.	SOLAR LIGHT	2,6	W	0.0298	YES	1	0	1.47	3022	1.0	2.1
TNT PRES.	SOLAR LIGHT	2,6	W	<.0001	YES	1	0	5.83	3022	2.9	11.9
DNT1 CONC.	SOLAR LIGHT	2,6 FIXED 7	W	0.2041	NO	1	0	1.34	2014	0.9	2.1
DNT2 CONC.	SOLAR LIGHT	2,6 FIXED 7	W	0.3392	NO	1	0	1.52	2014	0.6	3.6
TNT1 CONC.	SOLAR LIGHT	2,6 FIXED 7	W	0.0274	YES	1	0	3.37	2014	1.1	9.9
TNT2 CONC.	SOLAR LIGHT	2,6 FIXED 7	W	<.0001	YES	1	0	11.6	2014	4.1	33.4
DNT PRES.	RAINFALL	2,5	W	<.0001	YES	0.5	2	0.17	4030	0.1	0.3
TNT PRES.	RAINFALL	2,5	W	<.0001	YES	0.5	2	0.02	4030	0.0	0.1
DNT1 CONC.	RAINFALL	2,5	W	<.0001	YES	0.5	2	0.27	4030	0.2	0.5

216

Table 5-2 Odd ratios analysis – GLMM statistical results -   continued

Output	Variable	Exp	Phase	Pr>F	95% CL?	Odd Ratios Analysis					
						S1	S2	Est.	DF	95% CL	
DNT2 CONC.	RAINFALL	2,5	W	0.0004	YES	0.5	2	0.03	4030	0.0	0.2
DNT3 CONC.	RAINFALL	2,5	W	<.0001	YES	0.5	2	<0.001	4030	.	.
DNT3 CONC.	RAINFALL	2,3,4,5	W	<.0001	YES	0.5	2	<0.001	8062	.	.
TNT1 CONC.	RAINFALL	2,5	W	0.0024	YES	0.5	2	0.05	4030	0.0	0.3
TNT2 CONC.	RAINFALL	2,5	W	<.0001	YES	0.5	2	<0.001	4030	.	
TNT3 CONC.	RAINFALL	2,3,4,5	W	<.0001	YES	0.5	2	<0.001	8062	.	.
DNT PRES.	TEMPERATURE	2,3,4	W	0.0011	YES	1	2	0.6	6045	0.5	0.8
						3	2	0.72	6045	0.5	1.0
TNT PRES.	TEMPERATURE	2,3,4	W	0.1216	NO	1	2	0.77	6045	0.6	1.1
						3	2	1.01	6045	0.7	1.4
DNT1 CONC.	TEMPERATURE	2,3,4	W	0.003	YES	1	2	0.6	6045	0.4	0.8
						3	2	1	6045	0.7	1.4
DNT2 CONC.	TEMPERATURE	2,3,4	W	<.0001	YES	1	2	0.57	6045	0.4	0.9
						3	2	0.18	6045	0.1	0.4
DNT3 CONC.	TEMPERATURE	2,3,4	W	0.6088	NO	1	2	2.18	6045	0.2	19.6
						3	2	0.86	6045	0.1	13.7
DNT PRES.	TEMPERATURE	2,3,6	G	0.2121	NO	1	2	0.8	837	0.5	1.4
						3	2	0.62	837	0.4	1.1
DNT PRES.	TEMPERATURE	2,3,6 FIXED 7	G	0.0906	YES	1	2	0.5	669	0.2	1.0
						3	2	0.62	669	0.4	1.1
TNT	TEMPERATURE	2,3,6	G	<.0001	YES	1	2	0.5	837	0.3	1.0
						3	2	3.35	837	1.9	5.8
TNT	TEMPERATURE	2,3,6 FIXED 7	G	<.0001	YES	1	2	0.62	501	0.3	1.4
						3	2	4.56	501	2.5	8.3
DNT PRES.	WATER CONTENT	2,3,4	W	<.0001	YES	2	4	0.29	5588	0.2	0.5
						3	4	0.37	5588	0.2	0.6
						1	4	0.15	5588	0.0	1.1
DNT PRES.	WATER CONTENT	2,5	W	<.0001	YES	2	1	438	3565	<0.001	>999.999
						4	1	>999.999	3565	<0.001	>999.999
						3	1	904	3565	<0.001	>999.999
DNT PRES.	WATER CONTENT	2,6 FIXED 7	W	0.3114	NO	2	1	1.13	1878	0.2	5.2
						3	1	0.73	1878	0.2	3.3
						4	1	1.31	1878	0.3	5.5
TNT PRES.	WATER CONTENT	2,3,4	W	<.0001	YES	2	4	0.33	5588	0.2	0.6
						3	4	0.35	5588	0.2	0.5
						1	4	1.25	5588	0.6	2.7

Table 5-2 Odd ratios analysis – GLMM statistical results   - continued

Table 5-2 Odd ratios analysis – GLMM statistical results   - continued

Output	Variable	Exp	Phase	Pr>F	95% CL?	Odd Ratios Analysis					
						S1	S2	Est.	DF	95% CL	
TNT PRES.	WATER CONTENT	2,5	W	<.0001	YES	2	1	0.2	3565	.	.
						4	1	>999.999	3565	.	.
						3	1	0.18	3565	.	.
TNT PRES.	WATER CONTENT	2,6 FIXED 7	W	<.0001	YES	2	1	0.93	1878	<0.001	>999.999
						3	1	>999.999	1878	>999.999	>999.999
						4	1	>999.999	1878	.	.
DNT1 CONC.	WATER CONTENT	2,5	W	<.0001	YES	2	1	0.01	3565	<0.001	>999.999
						4	1	>999.999	3565	>999.999	>999.999
						3	1	>999.999	3565	.	.
DNT2 CONC.	WATER CONTENT	2,5	W	0.0291	YES	2	1	438	3565	<0.001	>999.999
						4	1	>999.999	3565	<0.001	>999.999
						3	1	400	3565	<0.001	>999.999
DNT3 CONC.	WATER CONTENT	2,5	W	0.9763	NO	2	1	0.24	3565	.	.
						4	1	>999.999	3565	<0.001	>999.999
						3	1	0.23	3565	.	.
DNT1 CONC.	WATER CONTENT	2,3,4	W	0.0001	YES	2	4	0.4	5588	0.2	0.7
						3	4	0.44	5588	0.3	0.7
						1	4	0.23	5588	0.0	1.6
DNT2 CONC.	WATER CONTENT	2,3,4	W	0.0015	YES	2	4	0.08	5588	0.0	0.6
						3	4	0.24	5588	0.1	0.6
						1	4	<0.001	5588	.	.
DNT3 CONC.	WATER CONTENT	2,3,4	W	0.7395	NO	2	4	<0.001	5588	.	.
						3	4	0.69	5588	0.1	6.2
						1	4	<0.001	5588	.	.
TNT1 CONC.	WATER CONTENT	2,3,4	W	<.0001	YES	2	4	0.23	5588	0.1	0.7
						3	4	0.32	5588	0.1	0.7
						1	4	3.25	5588	1.4	7.7
TNT2 CONC.	WATER CONTENT	2,3,4	W	0.0152	YES	2	4	0.13	5588	0.0	0.9
						3	4	0.15	5588	0.0	0.6
						1	4	0.87	5588	0.1	6.4
TNT3 CONC.	WATER CONTENT	2,3,4	W	0.9708	NO	2	4	<0.001	5588	.	.
						3	4	<0.001	5588	<0.001	>999.999

Table 5-2 Odd ratios analysis – GLMM statistical results   - continued

Table 5-2 Odd ratios analysis – GLMM statistical results   - continued

Output	Variable	Exp	Phase	Pr>F	95% CL?	Odd Ratios Analysis				95% CL	
						S1	S2	Est.	DF		
						1	4	<0.001	5588	.	.
TNT1 CONC.	WATER CONTENT	2,5	W	<.0001	YES	2	1	0.2	3565	.	.
						4	1	>999.999	3565	.	.
						3	1	0.18	3565	.	.
TNT2 CONC.	WATER CONTENT	2,5	W	<.0001	YES	2	1	0.2	3565	.	.
						4	1	>999.999	3565	.	.
						3	1	0.18	3565	.	.
TNT	WATER CONTENT	2,3,6	G	0.0679	YES	4	1	>999.999	836	.	.
						3	1	>999.999	836	.	.
						2	1	>999.999	836	.	.
DNT	WATER CONTENT	2,3,6	G	0.9912	NO	4	1	>999.999	836	.	.
						3	1	>999.999	836	.	.
						2	1	>999.999	836	.	.

In Table 5-2, the variables are defined as:

Solar Light: (1) Presence (0) Non presence

 Rainfall: (0.5) Intensity of 0.5 in/hr (2) Intensity 1 in/hr.

Temp: (1) $15<T<21^oC$ (2)$21<T<29^oC$ (3) $T>29^oC$.

Water Cont. : (1) WC<25% (2) 25<WC50% (3)50<WC<75% (4)WC> 75%.

The statistical analyses for single effects indicate that:

• Solar radiation enhances the presence of DNT and TNT in the system by 47% and 580%, respectively. Solar radiation also enhances the probability of finding higher concentrations of TNT/DNT. The probability of finding TNT (aq) concentrations lower than 100 μg/l increases by 337%, and between a range of 110 to 1000 μg/l increasing by a factor of 11.

- Lower rainfall reduces the presence of DNT and TNT by 83% and 98%, respectively. It also reduces the measured concentrations. Low (concentrations lower than 100 µg/l), medium (concentrations between 100 and 1000 µg/l) and high (concentrations higher than 1000 µg/l) NT (aq) concentrations are reduced by 83%, 97% and 99.99%, respectively. Low and medium TNT (aq) concentrations are reduced by factors of 95% and 99.99%, respectively.

- DNT (aq) detections under low temperatures (lower than 22 ^{o}C) is 40% lower than detections under medium temperatures (22 ^{o}C < T < 29 ^{o}C). Medium DNT (aq) concentrations are reduced by a factor of 43% at low temperatures instead of medium (25 ^{0}C) temperatures, and are reduced by a factor of 82% at high temperatures.

- High temperatures induce high thermal and hydraulic gradients, faster water drainages, and low water saturation below saturations of about 10%, the DNT vapor mass fraction show a significant decrease in detection by a factor about 105. Lower water contents generally, reduce the detection and concentration of DNT and TNT, in both the water and gas phases. This is attributed to lower dissolution rates and greater sorption and degradation at lower water content. Consequently, higher temperature reduces significantly the presence of DNT on water by 40%.

- At low temperatures, DNT detection in the gas phase decreases by 50% instead of medium range temperatures. TNT detection increase by 335% relative to medium range temperatures

- In the water phase, DNT presence probability decrease by 71% under medium soil water content conditions (25% < Se < 50%), 43% under medium high conditions (50% < Se < 75%), and > 71% for low conditions (Se < 25%) instead of high conditions (75% < Se < 100%). TNT (aq) presence probability decreases 67% under medium soil water content conditions and, 65% under medium high conditions related to high saturation. A behavior at low conditions can not be defined due limits of confidence.

- In the water phase, DNT low and medium concentrations probability decrease 60 % and 92% under medium soil water content conditions (25% < Se < 50%), decrease 56% and 76% under medium high conditions (50% < Se < 75%) and decrease 77% and 99.99% by low conditions (Se < 25%) relative to high saturation (75% < Se < 100 %).

- In the water phase, TNT low and medium concentrations probability decrease 77 % and 87%, respectively, under medium soil water content conditions (25% < Se < 50%), and 68% and 85% under medium high conditions (50% < Se < 75%) relative to high saturation. Low concentrations increase 325% over medium concentrations with low conditions (Se < 25%). Medium concentrations decrease 13% with low conditions instead of high soil water content conditions.

5.3 Soil Environmental Mixture Effects

The previous section analyzed single effects of soil environmental variables on presence and concentration or ERCs. However fate and transport processes of ERCs are highly non-linear. For this reason a series of simulations were run to evaluate mixture effects. After evaluating different pairs of variables, the followings pairs were evaluated for significant different through statistical validation tools provided at SAS, such as diffograms and T Grouping test:

- Mixture effect of solar radiation and rainfall intensity on TNT (aq) presence probability.(M1)

- Mixture effect of solar radiation and Temperature on TNT (aq) presence probability. (M2)

- Mixture effect of solar radiation and Rainfall intensity on DNT (aq) presence probability. (M3)

- Mixture effect of Rainfall intensity and Temperature on DNT (aq) presence probability. (M4)

- Mixture effect of solar radiation and Temperature on DNT (aq) presence probability. (M5)

Figures 5-5 through 5-8 show the diffograms for each mixture effects simulation. Tables 5-3 through 5-7 present T grouping Tables (evaluation of pairs significantly different). Table 5-8 presents odd ratios analysis where, quantification of mixture effects are shown.
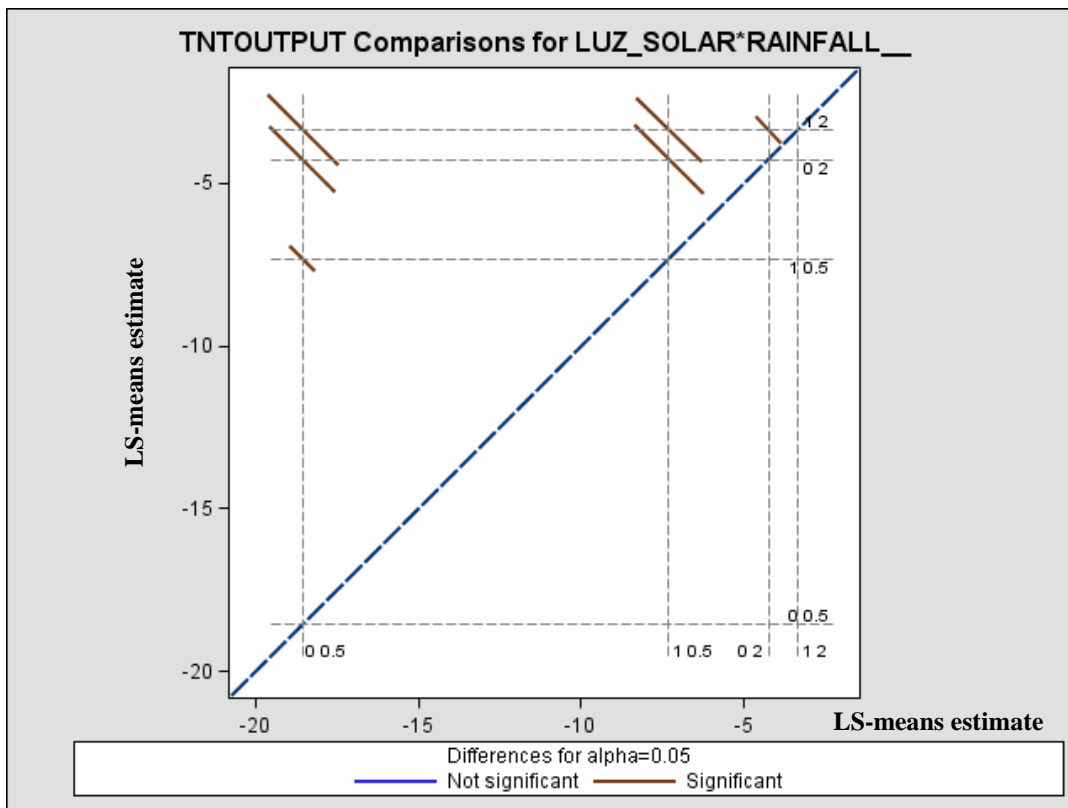
Figure 5-4 Diffogram mixture effect of solar radiation and rainfall intensity on TNT (aq)

Table 5-3 T Grouping for mixture effect of solar radiation and rainfall intensity on TNT (aq)

T Grouping for SOLAR_RADIATION*RAINFALL__ Least Squares Means			
LUZ SOLAR	**RAINFALL (IN/HR)**	**Estimate**	
1	2	-3.3551	A
0	2	-4.2627	B
1	0.5	-7.3205	C
0	0.5	-18.5661	D

223
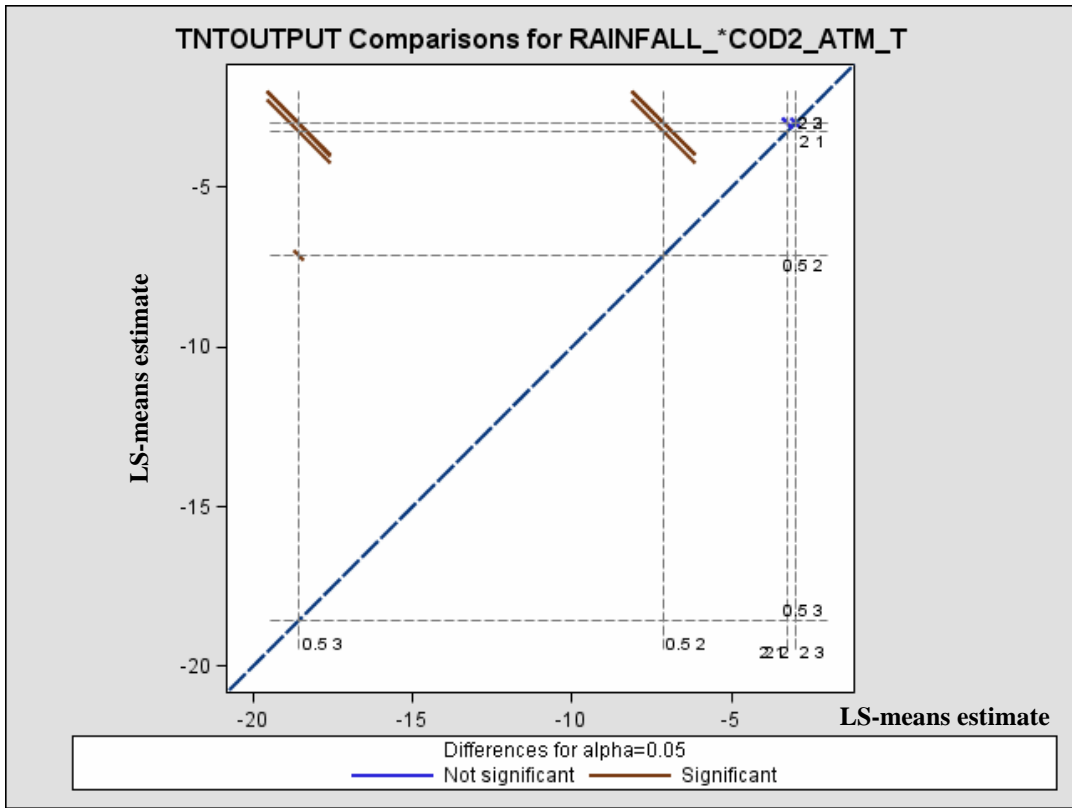
Figure 5-5 Diffogram mixture effect of solar radiation and temperature on TNT (aq)

Table 5-4 T Grouping for mixture effect of solar radiation and temperature on TNT (aq)

T Grouping for RAINFALL_*COD2_ATM_T Least Squares Means			
RAINFALL (IN/HR)	COD2 ATM TEMP	Estimate	
2	3	-2.9833	A
2	2	-2.9957	A
2	1	-3.2547	A
0.5	2	-7.1381	B
0.5	3	-18.5661	C
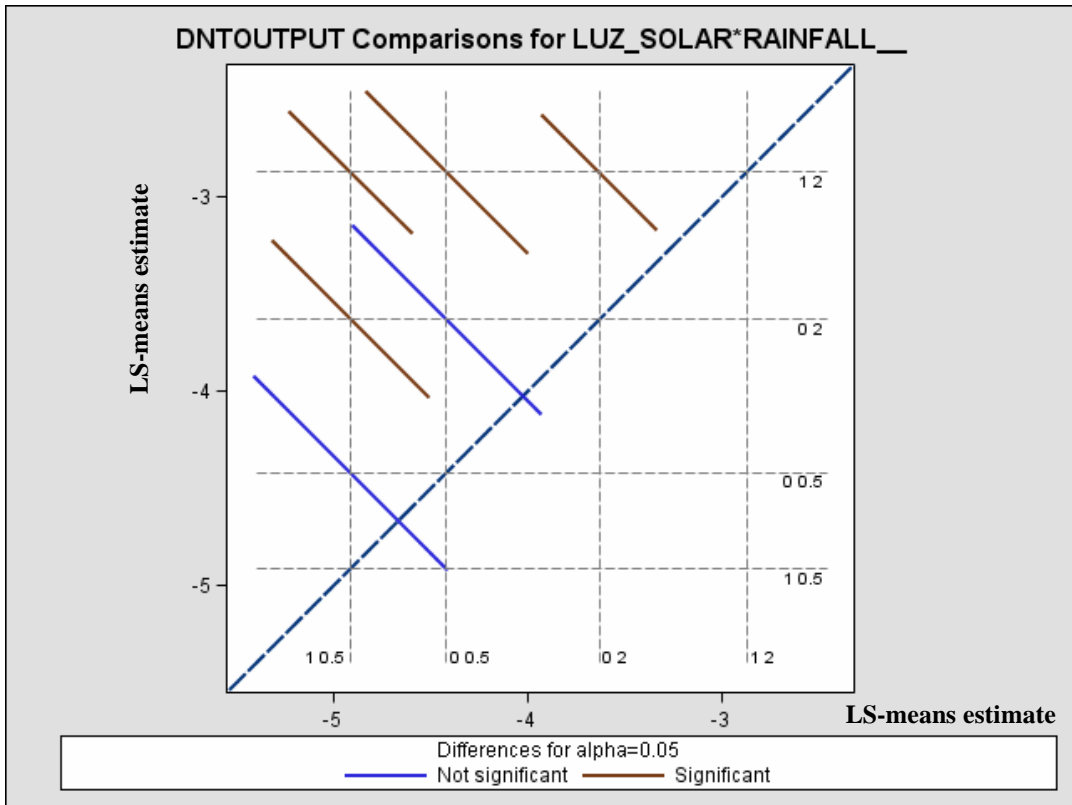
Figure 5-6 Diffogram mixture effect of solar radiation and rainfall intensity on DNT (aq)

Table 5-5 T Grouping for mixture effect of solar radiation and rainfall intensity DNT(aq)

T Grouping for SOLAR_RADIATION*RAINFALL__ Least Squares Means				
LUZ SOLAR	**RAINFALL (IN/HR)**	**Estimate**		
1	2	-2.8717		A
0	2	-3.6315		B
0	0.5	-4.4188	C	B
1	0.5	-4.9160	C	

225
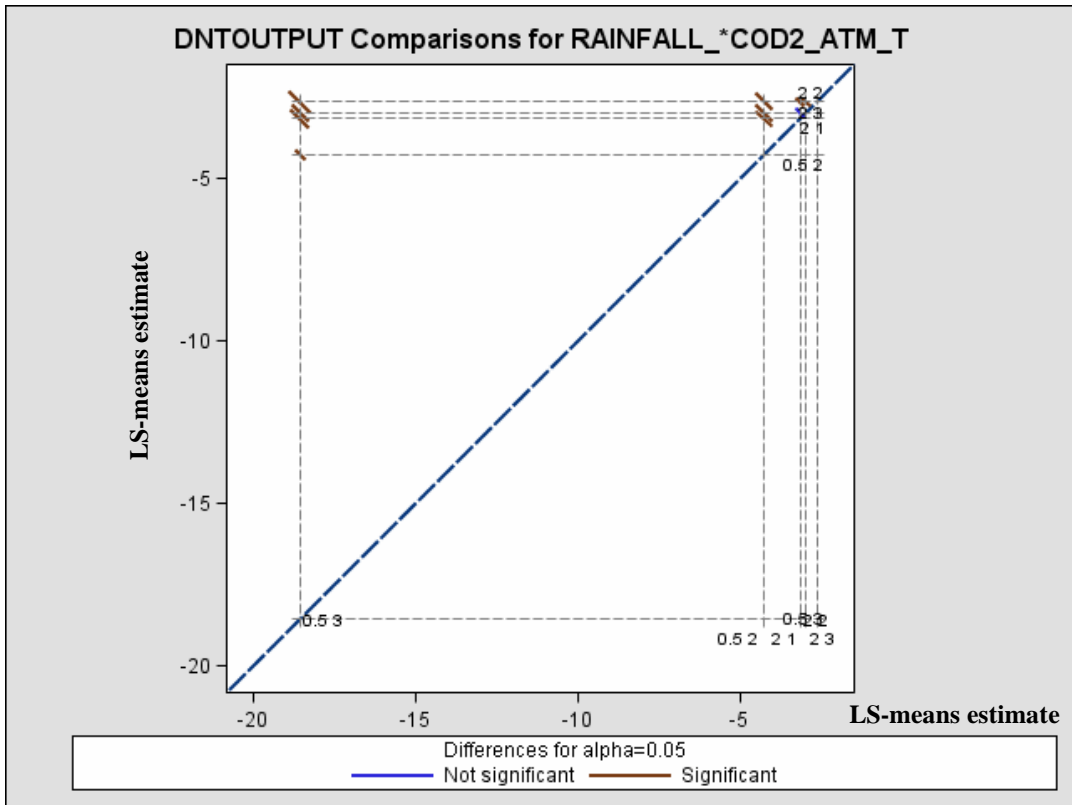
Figure 5-7 Diffogram mixture effect of rainfall intensity and temperature on DNT (aq)

Table 5-6 T Grouping for mixture effect of rainfall intensity and temperature on DNT (aq)

T Grouping for RAINFALL_*COD2_ATM_T Least Squares Means			
RAINFALL (IN/HR)	**COD2 ATM TEMP**	**Estimate**	
2	**2**	-2.6476	A
2	**3**	-2.9833	B
2	**1**	-3.1676	B
0.5	**2**	-4.2921	C
0.5	**3**	-18.5661	D

226
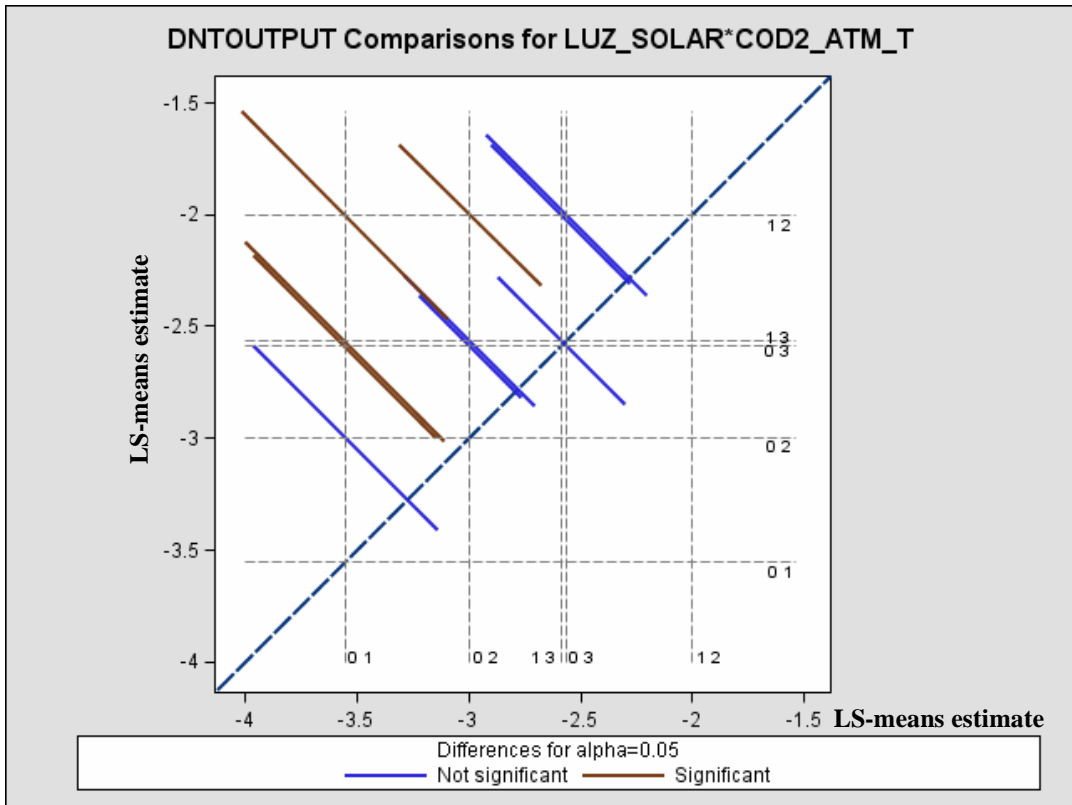
Figure 5-8 Diffogram mixture effect of solar radiation and temperature on DNT (aq)

Table 5-7 T Grouping for mixture effect of solar radiation and temperature on DNT (aq)

T Grouping for SOLAR_RADIATION*COD2_ATM_T Least Squares Means				
LUZ SOLAR	**COD2 ATM TEMP**	**Estimate**		
1	2	-2.0015		A
0	3	-2.5649	B	A
1	3	-2.5891	B	A
0	2	-2.9957	B	C
0	1	-3.5553		C

227

Table 5-8 Odd ratios analysis by mixture of effects analyzed on TNT/ DNT

Simple Effect Comparisons of RADIATION*RAINFALL__ Least Squares Means By RAINFALL__IN_HR_ -M1									
Simple Effect Level	RADIATION	RADIAT ION	Estimate	Standard Error	DF	t Value	Pr > |t|	Adj P	Odds Ratio
RAINFALL__IN_HR_ 0.5	1	0	11.2455	0.4064	4028	27.67	<.0001	<.0001	>999.999
RAINFALL__IN_HR_ 2	1	0	0.9076	0.4064	4028	2.23	0.0256	0.0256	2.478
Simple Effect Comparisons of RAINFALL_*COD2_ATM_T Least Squares Means By COD2_ATM_TEMP – M2									
Simple Effect Level	RAINFALL (IN/HR)	RAINFALL (IN/HR)	Estimate	Standard Error	DF	t Value	Pr > |t|	Adj P	Odds Ratio
COD2_ATM_TEMP 3	0.5	2	-15.5828	1.0077	8059	-15.46	<.0001	<.0001	<0.001
COD2_ATM_TEMP 2	0.5	2	-4.1423	1.0077	8059	-4.11	<.0001	<.0001	0.016
Simple Effect Comparisons of RADIATION *RAINFALL__ Least Squares Means By RADIATION –M3									
Simple Effect Level	RAINFALL (IN/HR)	RAINFALL (IN/HR)	Estimate	Standard Error	DF	t Value	Pr > |t|	Adj P	Odds Ratio
RADIATION 1	0.5	2	-2.0443	0.3234	4028	-6.32	<.0001	<.0001	0.129
RADIATION 0	0.5	2	-0.7873	0.4976	4028	-1.58	0.1137	0.1137	0.455

Table 5-8 Odd ratios analysis by mixture of effects analyzed on TNT/DNT   -   continued

Simple Effect Comparisons of RAINFALL_*COD2_ATM_T Least Squares Means By COD2_ATM_TEMP – M4									
Simple Effect Level	RAINFALL (IN/HR)	RAINFALL (IN/HR)	Estimate	Standard Error	DF	t Value	Pr > |t|	Adj P	Odds Ratio
COD2_ATM_TEMP 3	0.5	2	-15.5828	0.2652	8059	-58.76	<.0001	<.0001	<0.001
COD2_ATM_TEMP 2	0.5	2	-1.6445	0.2652	8059	-6.20	<.0001	<.0001	0.193

Simple Effect Comparisons of RADIATION *COD2_ATM_T Least Squares Means By COD2_ATM_TEMP - M5									
Simple Effect Level	RADIATION	RADIATION	Estimate	Standard Error	DF	t Value	Pr > |t|	Adj P	Odds Ratio
COD2_ATM_TEMP 3	1	0	-0.02418	0.2903	2011	-0.08	0.9336	0.9336	0.976
COD2_ATM_TEMP 2	1	0	0.9943	0.3238	2011	3.07	0.0022	0.0022	2.703

The statistical analyses for single effects indicate that:

- For mixture effect of solar radiation and rainfall intensity on TNT (aq) presence probability (M1), all combination of levels are significantly different. Under low rainfall intensities, the probability to detect TNT (aq) increases significantly (non-quantifiable) if solar radiations conditions are present instead of no-solar radiation. Under high rainfall intensities, the probability to detect TNT (aq) increases 248% if solar radiations conditions are presented instead of non-solar radiation presence.

- For mixture effect of solar radiation and temperature on TNT (aq) presence probability (M2), only two pairs of all combination of levels are significantly different. Under high temperatures, the probability to detect TNT (aq) decreases significantly close to 99.99% if low rainfall intensities conditions are present instead of high rainfall intensities. Under medium temperatures conditions, the probability to detect TNT (aq) decreases 98%, if low rainfall intensities conditions are presented instead high rainfall intensities conditions.

- For mixture effect of solar radiation and rainfall intensity on DNT (aq) presence probability (M3), only one pair of all combination of levels is significantly different. Under solar radiation presence, the probability to detect DNT (aq) decreases 87% if low rainfall intensities conditions are presented instead of high rainfall intensities. Under no radiation presence, the probabilities to detect DNT (aq) decreases 54% if low rainfall intensities are present instead of high rainfall intensities.

- For mixture effect of rainfall intensity and temperature on DNT (aq) presence probability (M4), only three pairs of all combination of levels are significantly different. Under high temperatures, the probability to detect DNT (aq) decreases significantly close to 99.99% if low rainfall intensities conditions are presented instead of high rainfall intensities. Under medium temperatures conditions, the probability to detect DNT (aq) decreases 80.7% if low rainfall intensities conditions are present instead of high rainfall intensities.

- For mixture effect of solar radiation and temperature on DNT (aq) presence probability (M5), there is no pairs significantly different. Under high temperatures, the probability to detect DNT (aq) decreases significantly close 2.4 % if solar radiation conditions are presented instead non presence of solar radiation conditions. Also under medium temperatures conditions, the probability to detect DNT (aq) increases 270%, if solar radiation are presented instead of no solar radiation conditions.

6 CONCLUSIONS

Results from transport experiments conducted to determine and quantify the effect of spatially and temporally variable environmental factors on fate and transport of TNT and DNT near soil-atmospheric surfaces indicate that the mobility and persistence of these ERCs is highly influenced by water contents, flow conditions, and thermal and light radiations.

A three-dimensional soil-atmospheric system (3D SoilBed System) was developed, which could simulate and monitor the fate and transport behavior of TNT, and DNT near soil surfaces exposed to variable soil-atmospheric conditions. Physical model shows consistent flow results under the same soil environmental settings. It demonstrated a high duplicity of these results. Results from experimental data and statistical modeling permit the inference of the following conclusions:

- Rainfall events tend to enhance TNT and DNT detection and concentration in the aqueous phase. Generally, detection and concentration are higher for higher rainfall rates, and lower for lower rainfall rates. Because detection in gas phase follows similar, but lagged, detection patterns as that in the aqueous phase, it is concluded that rainfall also enhances TNT detection in the gas phase.

Rainfall-enhanced detection and concentrations are attributed to higher soil water contents and flux, which induce enhanced dissolution of the source, higher advective transport, and lower sorption. Lower water flux, higher potential for sorption, and degradation, and greater volatilization contribute to lower detection and concentration at low soil water contents. In fact, results indicate a strong relationship between the daily maximum soil-water contents and the highest concentrations and detections of TNT and DNT. In a well-drainage sandy soil, higher water contents are generally, found near rainfall periods, depending of boundary conditions.

Lower range solubility concentrations and decreasing solute detection and concentration over time indicate rate limiting dissolution processes and potential degradation losses. Increasing DNT detection and concentration over time suggest potential degradation of TNT to DNT.

- Higher temperatures increase the detection of DNT in the water phase, but not that of TNT. TNT aqueous concentration are, however, higher at high temperatures, whereas DNT's are not. Higher detection of DNT at higher temperatures is attributed to greater dissolution rates and water drainage, and TNT degradation to DNT. High TNT and DNT frequencies at lower temperatures are attributed to higher water contents, and slower degradation and volatilization rates. Greater TNT detection in the gas phase is attributed to higher partitioning. Lower DNT detection in the gas phase is attribute to enhanced DNT degradation at higher temperatures. This is

233

suggested by the presence of potential DNT degradation by products on the gas phase at high temperatures.

At high temperatures, TNT in the gas phase show higher initial detection, whereas DNT detection is higher at later times. This is attributed to rate-limited TNT degradation, volatilization, and sorption. TNT degradation to DNT and partitioning into the gas phase contribute to the high detection of DNT at later times.

Higher TNT and DNT solute detection and concentrations at low temperatures is attributed to higher water saturation, which induce greater dissolution and lower sorption, and lower degradation and volatilization. Higher saturation at low temperatures is attribute to changes in hydraulic conditions due to higher water viscosity and air-water surface tension, which result in higher water retention.

- DNT detection in the water phase is slightly increased during radiation periods, whereas TNT is influenced to a higher degree. Increased DNT solute detection at radiation is attributed to TNT degradation on DNT. Presence of an unidentified compound (potentially as 4A-2,6DNT (aq)) shows that degradation products are being formed to a higher degree in the presence of radiation. Low TNT and DNT concentration at no radiation conditions are attributed to low saturation (low dissolution), and lower volatilization and degradation.

- TNT and DNT solute detection, concentration, and gas-phase detection are higher near preferential flow paths having high velocities for high saturation conditions. This is attributed to preferential transport of dissolved TNT and DNT and high concentrations caused by higher dissolution rates. For low saturation conditions, DNT detection was higher in diffuse flow (not preferential flow) zones at high temperatures, low rainfall, and no radiation. These results indicate that at high water saturation, source dissolution and advective transport dominates other diffuse flow, degradation, sorption, volatilization, and contribute to solute dispersion.

- Higher TNT and DNT solute detection and concentration with depth, and, higher gas-phase detection toward the surface show strong influence of flow and atmospheric boundary conditions. For high saturation, high advective transport is accumulated at the bottom as water accumulating due to the imposed boundary conditions. Higher gas-phase detection near the surface is associated with lower saturation, inducing greater volatilization.

- TNT solute concentrations are always higher at higher saturation, but DNT concentrations are higher than TNT for conditions of low soil-water saturation under no radiation, high temperature, and low rainfall. Higher TNT concentrations at high saturation are attributed to lower TNT degradation, volatilization, and sorption. Higher DNT concentration at low water saturation is attributed to greater TNT degradation, volatilization, and sorption.

- Higher detection of TNT in the gas-phase than in water suggest high gas-phase partioning and low gas-phase degradation. Similar temporal patterns between TNT and water phases indicate that vapor dilution is controlled by TNT presence in the water phase. The thermal lag in the gas – phase is attribute to mass-transfer limitation between the water and gas-phases.

- DNT detection in the gas phase is generally lower than in the water phase, but it tends to increase with time. Greater DNT detection with time is attributed to TNT degradation to DNT, and DNT volatilization.

Conclusions of the statistical analysis using GLMM indicate that:
- Standard errors evaluated by LS means analysis indicate that the data used in statistical models are unbalanced. It shows more confidence in the use of GLINMIX procedure instead of ANOVA analysis.

- Rainfall events and related water content are the most influential factors affecting the presence and concentration of TNT and DNT in aqueous-and-gas phases near soil-atmospheric environments. Solar radiation is the second most influential parameter. Although atmospheric temperatures influence their presence and concentrations, it is the lest influential and most variable factor.

- Higher rainfall increases the presence and concentration of DNT and TNT.

236

- Solar radiation enhances the presence of DNT and TNT in the system.

- Higher soil water contents increase TNT and DNT detection and concentration.

- Temperature has variable effects in detection and concentration of TNT and DNT.

- In gas phase TNT - DNT detection probability decrease under lower temperatures condition instead of medium conditions. TNT increase 335% under high temperatures instead of medium temperatures.

- For mixture effect of solar radiation and rainfall intensity on TNT (aq) presence probability, all combination of levels are significantly different. Under low rainfall intensities, the probability to detect TNT (aq) increase significantly (non-quantifiable) if solar radiations conditions are presented instead of non-solar radiation presence. Also under high rainfall intensities, the probabilities to detect TNT (aq) increase significantly if solar radiations conditions are presented instead of no-solar radiation.

- For mixture effect of solar radiation and temperature on TNT (aq) presence probability only two pairs of all combination of levels are significantly different. Under high and medium temperatures, the probability to detect TNT (aq) decreases significantly for low rainfall intensities, instead of high rainfall intensities conditions.

- For mixture effect of solar radiation and rainfall intensity on DNT (aq) presence probability, only one pair of all combination of levels are significantly different. Under solar radiation presence, the probability to detect DNT (aq) decrease for low rainfall intensities instead of high rainfall intensities. Also for no radiation, the probability to detect DNT (aq) decreases if low rainfall intensities are presented instead of high rainfall intensities.

- For mixture effect of rainfall intensity and temperature on DNT (aq) presence probability, only three pairs of all combination of levels are significantly different. Under high and medium temperatures, the probability to detect DNT (aq) decreases significantly for low rainfall intensities.

- For mixture effect of solar radiation and temperature on DNT (aq) presence probability, there is no pairs significantly different. Under high temperatures, the probability to detect DNT (aq) decreases significantly if solar radiation is presented instead of no solar radiation. Also under medium temperatures conditions, the probabilities to detect DNT (aq) increase, if solar radiation is presented instead of no radiation.

In general, results indicate:

- Higher TNT and DNT detection and concentration at higher rainfall rates and soil water saturation, this is attributed to higher dissolution an transport rates, and lower sorption and degradation.

- Solar radiation influences soil temperature and heat fluxes, and enhance TNT/DNT dissolution, transport and degradation. It significantly enhances DNT detection.

- Higher temperatures induce water drainage, lower water contents and higher sorption, degradation, and gas-phase partitioning. Lower temperatures have the opposite effect. The effect of temperature on DNT and TNT detection is highly variable and is influenced by interrelated factors.

The best environmental and soil conditions for the detection of ERCs in the aqueous phase in the vadoze zone are the following: soil water contents higher than 10% provided by rainfall with high intensities (TNT and DNT), and high temperatures (DNT) provided by high atmospheric temperatures and the presence of solar radiation (TNT and DNT). SuiTable moments for better detection in the soil surface are during times near the end of high rainfall intensities occurring under solar radiation (TNT and DNT).

The best environmental and soil conditions for the detection of ERCs in the gas phase in the vadoze zone are the following: for TNT at soil surface in the initial after source burial and for DNT at later times. for both TNT-DNT, soil water content should be higher than 10% and lower than 90%.

7 RECOMMENDATIONS

The following recommendations are suggested to further advances in the description and quantification of soil-atmospheric effects affecting the fate and transport of ERCs in sandy soils:

- Measure and monitor temporal and spatial soil temperatures to characterize water evaporation flux.
- Determine and quantify the porous cups efficiencies at the same distance from the source and use those that have similar efficiencies.
- Conduced experimental work to identify water content curves by the sandy soil used in the experiments.
- Develop a numerical model to compare the soil environmental effects on fate and transport of ERCs, with statistical modeling and field results.
- Expand the scope of the research to work with other types of soils, temperatures, relative humidity, boundary conditions, and water contents (above the soil field capacity).
- Increase sampling times especially under non-solar radiation conditions and before starting of rainfall events.
- Develop experimental work to get replicates of soil environmental conditions simulates, to increase the reliability of the data collected. SAS statistical procedure used in the modeling allow work with random effects due non-lineal behavior of fate and transport processes.
- Evaluate biological and photo degradation effects on fate of ERCs used in the experimental work.

REFERENCES

Acevedo d., Padilla I., Torres P., Torres A., and Anaya, A., 2007, Vapor Sampling of ERCs for Environmental Assessment in Atmospheric and Soil Settings. Proc. of SPIE on Detection and Remediation Technologies for Mines and Minelike Targets XII, SPIE Defense and Security Symposium, April 10-14 2007 in Orlando, FL, Vol. 6553, Pags. 1-10.

Amrhein M., Srinivasan, B., Bonvin, d., Schumacher, M.M., Behringer, M.H., Grifoll, J., and Cohen, Y., 1996, Contaminant Migration in the Unsaturated Soil Zone: the Effect of Rainfall and Evapotranspiration. Journal of Contaminant Hydrology, No. 23. Pags. 185-211.

Anaya A., and Padilla I.Y. 2006, 3D Laboratory-Scale SoilBed for Assessment of Fate and Transport of Explosive-Related Compounds in Soils under Variable Environmental Conditions, Paper Number: 6217-77, Proc. of SPIE on Detection and Remediation Technologies for Mines and Minelike Targets XI, SPIE Defense and Security Symposium, April 17-21 2006 in Orlando, FL, Volume 6217, 62171U, Pags. 1-10.

Anaya A., Padilla, I.Y., and Hwang, S. 2007, Influence Of Environmental Conditions in Fate and Transport of Ercs in a 3D SoilBed Model: Spatial and Temporal Assessment in a Sandy Soil, Proc. of SPIE on Detection and Remediation Technologies for Mines and Minelike Targets XII, SPIE Defense and Security Symposium, April 10-14 2007 in Orlando, FL, Vol. 6553, Pags. 1-8.

Armstrong J.E., Frind, E.O., and McClellan, R.d., 1994, Non Equilibrium Mass Transfer between the Vapor, Aqueous, and Solid Phases in Unsaturated Soils during Vapor Extraction. Water Resources Research. No. 30. Pags. 355-368.

Arya, S.P., 1988, Introduction to Micrometeorology, Academic Press, San diego.

ATSDR (Agency for Toxic Substances and Disease Registry) 1995. Toxicological Profile for 2,4,6-Trinitrotoluene. http://www.atsdr.cdc.gov/toxprofiles/tp81.html. Last accessed on June, 2008.

ATSDR (Agency for Toxic Substances and Disease Registry) 1998. Toxicological Profile for 2,4- and 2,6-Dinitrotoluene. http://www.atsdr.cdc.gov/toxprofiles/tp109.pdf. Last accessed on June, 2008.

Auer L.H., Rosenberg, N.d., Birdsell, K.H., and Whitney, E.M., 1996, The Effects of Barometric Pumping on Contaminant Transport, Journal of Contaminant Hydrology, Vol. 24. Pags. 145-156.

Bachmann J., Horton, R., Grant, S.A., and R.R. an der Ploeg, R.R., 2002, Temperature Dependence of Water Retention Curves for WetTable and Water-Repellent Soils. Soil Science Society of America Journal, No. 66. Pags. 44-52.

Bajracharya K., and Barry, d.A., 1997, Nonequilibrium Solute Transport Parameters and their Physical Significance: Numerical and Experimental Results. Journal of Contaminant Hydrology. No. 24 :(3-4). Pags. 185-204.

Bear, J., 1972, Dynamics of Fluids in Porous Media. New York. American Elseiver publishing Company. 764 pags.

Bender, E.A., Hogan, A., Leggett, d., Miskolczy, G., and Macdonald, S., 1992, Surface Contamination by TNT, Journal of Forensic Sciences, No. 37(6), Pags.1673-1678.

Best, E. P., and Sprecher, S. L., 1996, Phytoremediation of Explosives Contaminated Groundwater Using Constructed Wetlands. Phase I report: Plant Screening Study Submerged Plant Species. Draft Letter Report for Army Environmental Center, U.S Army Engineer Waterways Experiment Station, Vicksburg, MS.

Bonsor, K., 2002, How Landmines Work. 19 June 2001. HowStuffWorks.com. <http://science.howstuffworks.com/landmine.htm> Last access: 05 June 2009.

Box, G.E., and Cox, D.R., 1964, An Analysis of Transformations. Journal of the Royal Statistical Society. Series B. No. 26. Pags. 211-252.

Brannon, M.J., Deliman, P., Ruiz C., Price, C., Qasim, M., Gerald, J.A., Hayes, C. and Yost, S. 1999. Conceptual Model and Process Descriptor Formulations for Fate and Transport of UXO. US Army Corps of Engineers Waterways Experimental Station Technical Report No. IRRP-99-1.

Breslow, N.R., and Clyton, d.G., 1993, Approximate Inference on Generalized Linear Mixed Models . Journal of Statistical American Association. No. 88. Pags. 8-25.

Brooks, R. H., and Corey, A. t., 1996, Properties of Porous Media Affecting Fluid Flow. Proceedings American Society of Civil Engineers. Irrigation and Drainage Division 92. No. IRC. Pags. 61-87.

Brown, T.L., H.E. LeMay, and B.E. Bursten (2000). Chemistry, The Central Science. 8th ed., *Prentice Hall*, NJ.

Burlinson, M.B., 1980, Fate of TNT in an Aquatic Environment: Photodecomposition vs. Biotransformation, Tech. Rep. 79-445. Naval Surface Weapons Center. Silverspring, Md.

Campbell, G.S., and Norman, J.M., 1998, an Introduction to Environmental Biophysics. 2nd Edition, Springer-Verlag, New York.

Cattaneo, M.V., Pennington, J.C., Brannon, J.M., Gunnison, d., Harrelson, D.W and Zikikhani, M., 2000, Natural Attenuation of Explosives, in Remediation Engineering of Contaminated Soils. Wise, L.J., ed, Pags. 949-970. New York, Marcel decker Press.

Cerrito, P., 2005, From GLM to GLIMMIX-Which Model to Choose?. Workshop, Southeast SAS Users Group Conference.

Chambers, W.B., Rodacy, P. J., Jones, E. E., Gomez B. J., and Woodfin, R. L., 1998, Chemical Sensing System for Classification of Mine-like Objects by Explosives Detection.

Coats, K.H., and Smith, B.D., 1964, Dead End Pore Volume and Dispersion on Porous Media. Society of Petroleum Engineering Journal. No. 4. Pags. 73-84.

Comfort, S.D., P.J. Shea, L.S. Hundal, Z. Li, B. L. Woodbury, J.L. Martin, and W.P Powers., 1995, TNT Transport and Fate in Contaminated Soil, Journal of Environmental Quality. Vol. 24, Pags. 1174-1182.

Cumming C. J., Aker, C., Fisher, M., Fox, M., La Grone, M. J., Reust, d., Rockley, M. G., Swager, T. M., Towers E., and Williams, V., 2001,Using Novel Fluorescent Polymers as Sensory Materials for Above-Ground Sensing of Chemical Signature Compounds Emanating from Buried Landmines. IEEE Transactions on Geosciences and Remote Sensing, No. 39, Vol. 6, Pags. 1119-1128.

Costanza, M.S. and Brusseau, M.L., 2000, Contaminant Vapor Adsorption at the Gas-Water Interface of Soils. Environmental Science and Technology, Vol. 34, Issue 1, Pages 1-11.

Dellour, J. W., 1999, The Handbook of Groundwater Engineering. CRC Press. 940 p.

Demidenko, E., 2004, Mixed Models. Theory and Applications. John Wiley & Sons, 1st Edition.

Dillert, R., Brandt, M., Fornefett, I., Siebers, U and Bahnemann, d., 1995. Photo Catalytic Degradation of TNT and other Nitroaromatic Compounds. Chemosphere, Vol. 30, Issue 12, Pags. 2333-2341

Dubey, A.C., Harvey, J.F. and Broach, J.T. (eds), Proceedings of the SPIE 12th Annual International Symposium on Aerospace/defense Sensing, Simulation and Controls,

detection and Remediation Technologies for Mines and Minelike Targets III, April 13-17.

Ericksson, J. and Skyllberg, U., 2001, Binding of 2,4,6-Trinitrotoluene and its Degradation Products in a Soil Organic Matter Two-Phase System. Journal of Environmental Quality, Volume 30, Pages 2053-2061.

Fetter, C.W., 1999, Contaminant Hydrogeology, Prentice Hall Inc., New Jersey, 500 pags.

Fitzmaurice, G and Lard, N., 1993, A Likelihood-based Method for Analysing Longitudinal Binary Responses. Biometrika. No. 80(1). Pags.141–51.

Frezee, R. A., and Cherry, J. A., 1979, Groundater. Englewood Cliffs. NJ. Pretince Hall Publishing Company . 64 p.

George V.,. Jenkins, T.F., Leggett, D.C., J.H. Cragin, D.C., Phelan, J., Oxley, J., and Pennington, J., 1999, Progress on Determining the Vapor Signature of a Buried Landmine, Proceedings of the SPIE, Detection and Remediation Technologies for Mines and Minelike Targets IV, No. 3710(2): Pags. 258-269.

Goldstein, H., 2003, Software for Multilevel Modeling, Resources and Further developments. Technical report. Published by Hodder Arnold.

Grant, C. L., Jenkins, T. F., and Golden, S. M., 1993, Experimental Assessment of Analytical Holding Times for Nitroaromatic and Nitramine Explosives in Soil, U.S. Army Cold Regions Research and Engineering Laboratory Special Report 93-11, Hanover, New Hampshire, June.

Grant S.A., and Salehzadeh, A., 1996, Calculations of Temperature Effects on Wetting Coefficients of Porous Solids and their Capillary Pressure Functions. Water Resources Research. No. 32. Pags. 261-270.

Grifoll, J., Gasto, J.M. and Cohen, Y., 2005, Non-isothermal Soil Water Transport and Vaporation. Advances in Water Resources. No. 28(11). Pags.1254-1266.

Gutierrez, J., 2008, Effects of Flow Reversal on Two-dimensional Transport of Explosive Chemicals in Soils. , Department of Civil Engineering, University of Puerto Rico at Mayaguez.

Havis R.N., Smith, R.E and Adrian, D.D., 1992, Partitioning Solute Transport Between Infiltration and Overland Flow under Rainfall, Department of Civil Engineering, Colorado State University, Fort Collins, Water Resources Research, Vol. 28, Issue 10, Pags. 2569-2580.

Hawari, J., Halasz, A., Groom, C., deschamps, S., Paquet, C., Beaulieu, C., and Corriveau, A., 2002, Photodegradation of RdX in Aqueous Solution: A Mechanistic Probe for Biodegradation with Rhodococcus sp., Journal of Environmental. Science Technology. Vol. 36, Pags. 5117-5123.

Hawari, J., Beaudet, S., Halasz, A., Thibouto, S., and Ampleman, G., 2000, Microbial Degradation of Explosives: Biotransformation versus Mineralization, Applied Microbiology and Biotechnology, Volume 54, Pages 605-618.

Hernández, M.D., I. Santiago, and I.Y. Padilla (2006). Macro-Sorption of 2,4-Dinitrotoluene onto Sandy and Clay Soils. Proceedings of SPIE on Detection and Remediation Technologies for Mines and Minelike Targets, XI SPIE Defense and Security Symposium, Orlando, FL, vol. 6217.

Hillel, d., 1980, Fundamentals of Soil Physics. New York. Academic Press, Inc. 413 pags.

Hogan, A. W., Leggett, d. C., Jenkins, T., and Miyares, P., 1992, Surface Contamination of Depot-Stored Landmines: Results from Preliminary Analyses, Memorandum to defense Advanced Research Projects Agency, 23 June.

Hopmans J.W. and Dane, J.H., 1986, Temperature Dependence of Soil Hydraulic Properties. Journal of Soil Science, Society of America, Vol. 50. Pags. 4-9.

Hussein, E.M.A., and Waller, E.J. 2000, Landmine Detection: The Problem and The Challenge, Applied Radiation and Isotopes, Vol. 53, Pags. 557-563.

Hwang, H,M., Slaughter, S.M., Cook, S.M. and Cui, H., 2000, PhotoChemical and Microbial Degradation of 2,4,6- Trinitrotoluene (TNT) in a Freshwater Environment. Bolletin of Environmental Contamination and Toxicology. No. 65, Pages 228-235.

Hwang S., Batchelor C.J., Davis J.L., and MacMillan D.K., 2005, Sorption of 2,4,6-trinitrotoluene to Natural Soils before and after Hydrogen Peroxide Application. Journal of Environmental Science and Health, Part A-Toxic/Hazardous Substances & Environmental Engineering, Vol. 40, Issue 3, Pags. 581-592.

Hwang S., Felt d.R., Bouwer E.J., Brooks M.C., Larson S.L., and Davis J.L., 2006, Remediation of RDX-contaminated Water using Alkaline Hydrolysis. Journal of Environmental Engineering, ASCE, Vol. 132, Issue 2, Pags. 256-262.

Jackson, R. d., 1964, Water Vapor Diffusion on Relatively Dry Soil. Science Society of America Proccedings, Vol. 28. Pags. 172-176.

Jenkins, F.T., Pennington, C.J., Ranney, A.T., Berry Jr., E.T., Miyares, H.P, Walsh, E.M., Hewitt, D.A., Perron, M.N., Parker, V.L., Hayes, A.C and Wahlgren G.E., 2001,

Characterization of Explosives Contamination at Military Firing Ranges. U.S. Army Corps of Engineers Engineer Research and Development Center Technical Report No. 01-05.

Jenkins, T.F., M.E. Walsh, P.H. Miyares, J.A. Kopczynski, T.A. Ranney, V. George, J.C. Pennington, and T.E. Berry Jr., 2000, Analysis of Explosives-Related Chemical Signatures in Soil Samples Collected Near Buried Land Mines. U.S. Army Corps of Engineers, Cold Regions Research & Engineering Laboratory, Technical Report ERdC TR-00-5.

Jury W.A., and Horton, R., 2004, Soil Physics, 6th edition, John Wiley & Sons, Inc., Pags. 370.

Jury, W.A., Gardner, W.R., and Gardner, W.H., 1991, Soil Physics, 5th Edition, John Wiley and Sons.

Jury, W.A., Russo, d., Streile, G., and Abd, H., 1990, Evaluation of Volatilization by Organic Chemicals Residing below the Surface. Water Resources Research, No. 26 (1). Pags.13-20.

Jury, W.A., Spencer, W.F. and Farmer, W.J., 1983, Behavior Assessment Model for Trace Organics in Soil: I. Model Description. Journal of Environmental Quality, Vol. 12(4). Pags. 558-564.

Kaiser, E. G., and Burlinson, N. E., 1982, Migration of Explosives in Soil. Naval Surface Weapons Center. Report TR 82-566.

Kaplan, D.L. and Kaplan, A.M., 1982, 2,4,6 Trinitrotoluene Surfactant Complexes: Decomposition, Mutagenicity and Soil Leaching Studies. Journal of Environmental Science and Technology. Volume 16, Pages 566-571.

Karimi-Lotfabad, S., M.A Pickard, and M.R. Gray (1996). Reactions of Polynuclear Aromatic Hydrocarbons on Soil. Environ. Sci. Technol., Vol. 30, No.4.

Kaye, S. M., 1980, Encyclopedia of Explosives and Related Items, Volume 9, U.S. Army Armament Research and Development Command, Large Caliber Weapon Systems Laboratory, Dover, New Jersey.

Kossugi, K., 1999, General Model for Unsaturated Hydraulic Conductivity for soils with Lognormal pore-size Distribution. Journal of Soil Science Society. Vol. 63, pags. 270-277.

Landmine monitor report, 2006, http://icbl.org/index.php, last accessed: march, 2008.

Larson, R.A., 2000, Effects of Surfactants on Reduction and Photolysis (>290 nm) of Nitro aromatic Compounds. Journal of Environmental Science and Technology. Vol. 34, Issue 3, Pags. 505-508.

Lee, Y., and Nelder, J., 2004, Conditional and marginal models: Another view. Statistical Science. No. 19(2). Pags. 219–238.

Legget, d. C., Jenkis, T. F., Hogan, A., Ranney, T. A., Miayers, P. H., 2000, External Contamination on Landmines by Organic Nitro Compounds. US Army Engineer Research and Development Center Cold Regions Research and Engineering Laboratory, Technical Report 00-2.

Leggett, D.C., Jenkins, T. F., and Murrmann, R. P., 1977, Composition of Vapors Evolved from Military TNT as Influenced by Temperature, Solid Composition, Age, and Source. U.S. Army Cold Regions Research and Engineering Laboratory, Special Report 77-16.

Littell, R.C., Milliken, G.A., Stroup, W.W., Wolfinger, R.d., Schabenberger, O., 2006, SAS for Mixed Models. Second Edition. SAS Press, Cary NC. 814 p.

Macdonald, J., Lockwood, J. R., McFee, J., Altshuler, T., Broach, T., Carin, L., Rappaport, C., Scott, W.R and Weaver, R., 2003, Alternatives for Landmine Detection, Alternatives for Landmine Detection, RAND, Santa Monica, CA, 336 pags.

Maskerinek, M, P., Mannig, d. L., and Harwey, W, H., 1986, Application of Solid Sorbent Collection Techniques and High Performance Liquid Chromatography with Electrochemical Detection to the Analysis of Explosives on Water Samples. Oak ridge National Laboratory, Oak Ridge, Tennessee, TM-10190

Millington, R.J., and Quirk, J.M., 1961 Permeability of Porous Solids, Transactions of the Faraday Society. Vol. 57. Pags. 1200-1207.

McCarthy, K.A. and Johnson, R.L., 1993, Transport of Volatile Organic Compounds across the Capillary Fringe, Water Resources Research, Vol. 29, Issue 6, Pags. 1675-1683.

Mccullagh, P., and Nelder, J.A, 1989, Generalized Lineal Models. 2nd Edition. Chapman & Hall Press. 511 pags.

McGrath, C.J., 1995, Review of Formulations for Processes Affecting the Subsurface Transport of Explosives. Technical Report IRRP-95-2 US Army Engineering Waterways Experiment Station, Vicksburg, MS.

Molina, G.M., Padilla, I., Pando, M., and Pérez, d., 2006, Field Lysimeters for the Study of Fate and Transport of Explosive Chemical in Soils under Variable Environmental Conditions. Proceedings of SPIE, Vol. 6217-137.

Myers, T.E., and Townsend, D.M., 1996, Recent Developments in Formulating Model Descriptors for Subsurface Transformation and Sorption of Trinitrotoluene. Conference on the Bioremediation of Surface and Subsurface Contaminants, Palm Coast, FL. January 1996.

Nelder, J.A., and Wedderburn, W.M., 1972, Generalized Linear Models. Journal of the Royal Statistical Society. Series A. No. 135. Pags. 370-384.

Nkedy-Kizza, P., Biggar, J.W., Vag Genutchen, M. TH., Wierenga, P.J., Selim, H.M., davinson, J.M., and ielsen, D.R., 1983, Modeling Tritium and Cloride-36 Transport through an Aggregated Oxisol. Water Resources Research. No. 19-3. Pags. 691-700.

Nielsen, d.r., Van Genutchen, M.Th., and Biggar J.W., 1986, Water Flow and Solute Transport Processes in the Unsaturated Zone. Water Resources Research. No. 22-9. Pags. 89S-108S.

Ong, S.K., Culver, T.B., Lion, L.W., and Shoemaker, C.A., 1992, Effects of Soil Moisture and Physical - Chemical Properties of Organic Pollutants on Vapor-Phase Transport in the Vadoze Zone. Journal of . Contaminant. Hydrology. Vol. 11, Pags. 273-290.

Padilla I.Y., Jim Yeh, T.C and Conklin, M.H., 1999, The Effect of Water Content on Solute Transport in Unsaturated Porous Media, Department of Hydrology and Water Resources, University of Arizona, Tucson, Water Resources Research, Vol. 35, Issue 11, Pags. 3303–3313.

Padilla A.C., Padilla, I and Santiago, I., 2006, Multiphase Extraction Sampling of Explosives in Unsaturated Soils, Paper Number: 6217-139, Proc. of SPIE on detection and Remediation Technologies for Mines and Minelike Targets XI, SPIE defense and Security Symposium, April 17-21 2006 in Orlando, FL, Volume 6217, 62173C, Pages 1-11.

Padilla I.Y., Gutiérrez, J.P, Irizarry M.d.L. and Hwang, S., 2007, Transport of Explosive Related chemicals from Point Sources. Proc. of SPIE on Detection and Remediation Technologies for Mines and Minelike Targets XII, SPIE Defense and Security Symposium, April 10-14 2007 in Orlando, FL, Vol. 6553.

Pennington, J.C and Patrick, W.H., 1990, Adsorption and Desorption of 2,4,6-Trinitrotoluene be Soils, Journal of Environmental Quality, Vol. 19, Pags. 559-567.

Pennington J.C., T.F. Jenkins, G. Ampleman, S. Thiboutot, J.M. Brannon, J. Lewis, J.E. deLaney, J. Clausen, A.d. Hewitt, M.A. Hollander, C.A. Hayes, J.A. Stark, A. Marois, S. Bochu, H.Q. dinh, d. Lambert, A. Gagnon, M. Bouchard and Martel, 2003, Distribution and Fate of Energetics on DoD Test and Training Ranges: Interim Report 3. US Army Corps of Engineers, Engineer Research and Development Center, Technical Report ERdC TR-03-2.

Petersen, L.W., Moldrup, P. Y., El-Farhan, H., Jacobsen, O. H., Yamaguchi, T., and Rolston, d. E., 1995, The Effect of Moisture and Soil Texture on the Adsorption of Organic Vapors, Journal of Environmental Quality, Vol. 24, pags. 752-759.

Petersen, L.W.,. Rolston, d.E., Moldrup, P., and Yamaguchi, T., 1994. Volatile Organic Vapor Diffusion and Adsorption in Soils. Journal of Environmental Quality. Vol. 23. Pags. 799-805.

Phelan, J. M., and Barnett, J. L., 2001. Solubility of 2,4-dinitrotoluene and 2,4,6-Trinitrotoluene in Water. Journal of . Chemical . Engineering. No. 46, pags. 375-376.

Phelan, J., and Webb, S.; 2002, Chemical Sensing for Buried Landmines- Fundamental Processes Influencing Trace Chemical Detection, Sandia National Laboratory Report No. SANd2002-0909.

Phelan, J.M., S.W. Webb, M. Gozdor, M.C and Barnett, J.L, 2001, Effect of Soil Wetting and Drying on DNT Vapor Flux – Laboratory Data and T2TNT Model Comparisons. Sandia National Laboratories, Albuquerque.

Phelan J.M., M. Gozdor, S.W and Webb, M.C., 2000, Laboratory data and Model Comparisons of the Transport of Chemical Signatures From Buried Landmines/UXO. Sandia National Laboratories, Albuquerque, NM.

Phelan, J. M., and Webb, S. W., 1997, Environmental Fate and Transport of Chemical Signatures from Buried Landmines – Screening Model Formulation and Initial Simulations. Sandia National Laboratories, SANd97-1426.

Price, C.B., Brannon, J.M., and Hayes, C.A., 1995, Transformation of 2,4,5 Trinitrotoluene under Controlled Eh/pH Conditions. Technical Report IRRP-95-5, US Army Engineer Waterways Experiment Station. Vicksburg, MS.

Ravikrishna, R., Yost, W.H., Price, C.B., Valsaraj, K.T., Brannon, J.M and Miyares, P., 2002, Vapor Phase Transport of Unexploded Ordnance Compounds Through Soils, Environmental Toxicology and Chemistry, Vol. 21, Issue 10, Pags. 2020-2026.

Reichman R., Mahrer, Y., and Wallach, R., 2000, A Combined Soil-Atmosphere Model for Evaluating the Fate of Surface Applied Pesticides 2. The Effect of Varying Environmental Conditions. Environmental Science & Technology. No. 34. Pags. 1321-1330.

Rodriguez, S., Padilla, I and Santiago, I., 2006, Development of a Multi-Scale Packing Methodology for Evaluating Fate and Transport Processes of Explosive-Related Chemicals in Soil Physical Models, Paper Number: 6217-77, Proc. of SPIE on detection and Remediation Technologies for Mines and Minelike Targets XI, SPIE Defense and Security Symposium, April 17-21 2006 in Orlando, FL, Volume 6217, 62171U, Pages 1-10.

SAS Inc. 2004, SAS online documentation: The NLMIXEd PROCEdURE.

Schmelling, d.C., Gray, K.A and Kamat, P.V., 1996, Role of Reduction in the Photo Catalytic Degradation of TNT. Journal of Environmental Science and Technology. Vol. 30, Issue 83, Pags. 2547-2555.

Schaap M.G., F.J. Leij and M.Th. van Genuchten., 2001, ROSETTA: A Computer Program for Estimating Soil Hydraulic Parameters with Hierarchical Pedotransfer Functions. Journal of Hydrology, Vol.251, Pags. 163-176.

Schwarzenbach, R. P., Gschwend, ., P. M., and Imboden d. M., 2003, Environmental Organic Chemistry. 2nd Edition. John Wiley and Sons, Inc. Hoboken, NJ.

Shoemaker, C.A., T.B. Culver, L.W. Lion, and M.G. Peterson (1990). Analytical Models of the Impact of Two Phase Sorption on Subsurface Transport of Volatile Chemicals. Water Resour. Res., Vol. 26, pags. 745-758.

Spain, J.C., 1995, Biodegradation of Nitroaromatic Compounds. Annual Review of Microbiology, Vol. 49, Pags. 523-555.

Spain, J. C., Hughes, J. B., and Knackmuss, H., 2000, Biodegradation of Nitroaromatic Compounds and Explosives, Lewis Publishers, CRC Press, Boca Raton, Florida.

Spangler, G.E.,1974, Physical Model for the Subterranean Movement of Explosive Vapors from Mines, Report MERAdCOM-R-2095, U.S. Army Mobility Equipment Research and Development Center, Fort Belvoir, Virginia.

Spiegel, M.R., 1997, Shaum's Outline of Theory and Problems of statistics, McGraw-Hill, New York.

Šimůnek, J., Šejna, M and van Genuchten, M.Th., 1999, The HYDRUS-2d Software Package for Simulating the Two-dimensional Movement of Water, Heat, and Multiple Solutes in Variably-Saturated Media, Version 2.0, U.S. Salinity Laboratory, Riverside, California.

Snedecor,G.W., and Cochran, W.G., 1989, Statistical Methods. 8th Edition. Ames. Iowa State. University Press.

Spaulding, R. F., and Fulton, J. W., 1988, Groundwater Munition Residues and Nitrate near Grand Island, Nebraska U.S.A. Journal of Contaminant Hydrogeology, Vol. w, Pags. 139-152.

Spitz, K., and Moreno, J., 1996, A Practical Guide to Groundwater and Solute Transport Modeling. Wiley and Sons publications. New York. N.Y. 461 p.

Steel, R.d., and Torrie, J.H., 1980, Principles and Procedures of Statistics. Second Edition. McGrow-Hill Press. New York, NY

Todd, d.K., and Mays, L.W., 2005, Grounwater Hydrology. 3rd Edition. Jhon Wiley & Sons, Inc. 636 pags.

Torres A., Padilla, I., and Hwang, S., 2007, Physical Modeling of 2,4-dNT Gaseous Diffusion through Unsaturated Soil. Proceedings of SPIE, detection and Remediation Technologies for Mines and Minelike Targets XII, SPIE defense and Security Symposium, Orlando, FL., April 9-13, 6553.

Torres, A., 2008, Vapor Phase Transport of Explosive Related Compounds through Unsaturated Sandy Soils, Department of Civil Engineering, University of Puerto Rico at Mayaguez.

Torres, P.A., 2004, Numerical integration: Its Use in glmms. Technical Report, Advanced Topics of Computation Course, Department of Mathematics, University of Puerto Rico at Mayaguez.

U.S. EPA. , 1994, Handbook Nitroaromatics and Nitramines by High Performance Liquid Chromatography (HPLC), September. Report Number: SW-846 Ch 4.3.3.

U.S. EPA. , 2002, Handbook on the Management of Ordnance and Explosives at Closed, Transferring, and Transferred Ranges and Other Sites, February. Interim report.

Van Genuchten, M. TH., 1980, A Closed Form Equation for Predicting the Hydraulic Conductivity of Unsaturated Soils. Soil Science Society of America Journal. No. 44. Pags. 892-898.

Van Genuchten, M.TH., and Wierenga, P.J., 1976, Mass Transfer Studies in Sorbing Porous Media: I. Analytical Solutions. Journal of Soil Science Society of America, No. 40(4), Pags. 473-480.

Van Genuchten, M. TH., Davinson, J. M., and Wierenga, P. J., 1974, An Evaluation of Kinetic and Equilibrium Equations for the Prediction of Pesticide Movement of Porous Soils. Soil Science Society of America Proceedings, No. 38-1. Pags. 29-35.

Vanderborght J., Timmerman, A., and Feyen, J., 2000, Solute Transport for Steady-State and Transient Flow in Soils with and without Macropores. Soil Science Society of America, Vol. 64, Pags. 1305-1317.

Walsh, M. E., Jenkins, T. F., Schnitker, P. S., Elwell, J. W., and Stutz, M. H., 1993, Evaluation of SW846 Method 8330 for characterization of Sites Contaminated with Residues of High Explosives. CRREL Report 93-5, USA Cold Regions Research and Engineering Laboratory, Hanover, NH.

Webb S.W. and Phelan, J.M., 2000, Effect of Diurnal and Seasonal Weather Variations on the Chemical Signatures from Buried Landmines/UXO, Sandia National Laboratories, Albuquerque, NM 87185.

Webb, S.W., Finsterle, S.A., Pruess, K and Phelan., J.M., 1998, Prediction of TNT-Signature from Buried Landmines, Proceeding of the TOUGH Workshop'98, Lawrence Berkeley National Laboratory, Report LBNL-41995, Berkeley, CA.

Webb, S.W., Pruess, K., Phelan, J.M and Finsterle, S.A., 1999, Development of a Mechanistic Model for the Movement of Chemical Signatures from Buried Landmines/UXO., Sandia National Laboratories, Albuquerque, NM 87185.

Wildenschild d. and Jensen, K.H., 1999, Laboratory Investigations of effective Flow Behavior in Unsaturated Heterogeneous Sands, Department of Hydrodynamics and Water Resources, Technical University of Denmark, Lyngby, Water Resources Research, Vol. 35, Issue 1, Pags. 17-27.

Wolfinger, R., and O'Conell, M., 1993, Generalized Linear Models: A Pseudo Likelihood Approach. Journal of Statistical Computation and Simulation. No. 48. Pags. 233-243.

Wood, W.W., Kramer, T.P., and Hem, P.P., 1990, Intergranular Diffusion: An Important Mechanism Influencing Solute Transport in Clastic Aquifers. Science Vol. 247. Pags. 1569-1572.

Woodfin, R. L., 2007, Trace Chemical Sensing of Explosives. 1st Edition. John Wiley and Sons Publication. Hoboken, N.J. 361 pags.

Yoshikawa, K., Masuda, K., Yamamoto, Y., Takamatsu, T., Toku, H., Nagasaki, K., Hotta, E., Yamauchi, K., Ohnishi, M., and Osawa, H., 2002, Research & Development of Technology for Humanitarian Landmine Detection by a Compact IEC Fusion Neutron Source. IC/P6-54, 5th US-Japan Workshop on Inertial Electrostatic Confinement Fusion, U. Wisconsin, Madison.

Xue, S. K., Iskandar, I. K., and Selim, H. M., 1995, Adsorption-Desorption of 2,4,6-Trinitrotoluene and Hexahydro-1,3,5-Trinitro- 1,3,5-Triazine in Soils, Soil Science, Vol. 160 (5).